論文 / 著書情報
Article / Book Information

題目(和文)	ヘテロポリ酸/ブルッカイト複合薄膜の作製とその光触媒活性
Title(English)	Preparation and photocatalytic activity of heteropolyacid/brookite hybrid films
著者(和文)	PruethiarenunKunchaya
Author(English)	KUNCHAYA PRUETHIARENUN
出典(和文)	学位:博士（工学）, 学位授与機関:東京工業大学, 報告番号:甲第9616号, 授与年月日:2014年9月25日, 学位の種別:課程博士, 審査員:中島　章,坂井　悦郎,生駒　俊之,宮内　雅浩,松下　祥子
Citation(English)	Degree:, Conferring organization: Tokyo Institute of Technology, Report number:甲第9616号, Conferred date:2014/9/25, Degree Type:Course doctor, Examiner:,,,,
学位種別(和文)	博士論文
Type(English)	Doctoral Thesis

平成 26 年度 博士論 文

Preparation and photocatalytic activity of heteropolyacid/brookite hybrid films.

ヘテロポリ酸/ブルッカイト複合薄膜の作製とその光触媒活性

Tokyo Institute of Technology
Department of Metallurgy and Ceramics Science

東京工業大学大学院
大学院理工学研究科 材料工学専攻

Kunchaya PRUETHIARENUN

11D51278

Content

CHAPTER 1

Introduction

1.1. Introduction

Titanium dioxide (TiO_2) is a well-known and important photocatalyst used for water and air purification [1]. Because of the strong oxidation power of photogenerated holes from TiO_2, it decomposes almost all organic compounds under UV illumination. However, its quantum yield is not so high because of poor charge separation efficiency and its low Fermi level for O_2 reduction. Therefore, to date, various methods have been used to improve the photocatalytic performance of TiO_2, such as surface modification, morphology control, application of an external field, and a Z-scheme design [1–10].

Additionally, the photoinduced hydrophilicity of a TiO_2 photocatalyst was discovered in 1995 [11]. A highly hydrophilic surface is generated when UV is illuminated onto the TiO_2 surface. This surface exhibits both antifogging and self-cleaning properties. Polycrystalline TiO_2 film coatings have been applied to various industrial items [12]. To date, two mechanisms have been proposed for this intriguing property: photocatalytic decomposition of surface organic contaminants [13–15] and photoinduced surface structural change [16,17].

Heteropolyacids (HPAs) constitute a subclass in a family of polyoxometalates (POMs), which are clusters of metal oxides that have a well-defined structure [18]. Actually, HPAs are metal oxide frameworks called polyanions that include heteroanions. Their total charge is balanced by counter-cations. They are not only acid catalysts because of their exceedingly strong Brønsted acid sites. In fact, HPAs are also

photocatalysts by oxygen-to-metal and ligand-to-metal charge transfer (O→ M LMCT) under UV illumination. Materials of this group enhance the photocatalytic activity of TiO_2 by a Z-scheme [19]. Initially, the systems of HPA(aq)/TiO_2(s) were mainly studied. Recently however, transparent thin films of these hybrid materials have been prepared. Their unique properties such as excellent sustainability of the hydrophilicity after stopping UV illumination have been reported [20]. This chapter presents a review of several recent studies that have examined this hybrid material system for use as a photocatalyst.

1.2. Titanium dioxide (TiO_2)

1.2.1. Three polymorphs

Titanium dioxide (TiO_2) is a well-known material used for various applications because of its abundance, non-toxicity, low cost, and physical and chemical properties. It is commonly used as a white pigment (no light absorption at 350–700 nm), as a cosmetic and sunscreen (high reflective index n_D = 2.5–2.9), and as a source of ferroelectric materials such $BaTiO_3$. This material naturally presents three polymorphs: rutile, anatase, and brookite. Rutile is the most stable phase from a thermodynamical viewpoint. Brookite and anatase transform respectively into rutile at 715 °C and 950 °C [21]. These three polymorphs are TiO_6 octahedra having different alignments and spacing parameters [21, 22]. Crystal structures of these three polymorphs are displayed in Figure 1-1 [23]. Rutile belongs to a tetragonal system of which the [001] direction is lined with an edge shared octahedron. The octahedron chain is linked to the other chain via corner sharing. The study of surface energy on various index of TiO_2 face [24] revealed that the most stable face of rutile is (110), and that (110) and (100) faces

possess remarkably low surface energy. Anatase also belongs to a tetragonal system. Four edges of the octahedron mutually link to form a zigzag chain of the octahedron. Surface energies of (101) and (001) are low. These faces commonly appear in natural anatase crystal **[25, 26]**. Different from rutile and anatase, the crystal system for brookite is orthorhombic. One octahedron shares three edges and corners, sharing an edge along [001] as a back-bone and sharing an edge for cross-linking the back-bone. The most stable face for brookite is (100) **[27]**.

1.2.2. Electronic band structure

Titanium dioxide is a semiconductor with a 3.0–3.2 eV band gap (E_G), which adsorbs photon energy in the UV range. Fujishima and Honda first reported photolysis of water using a TiO_2 electrode under UV illumination in 1972 **[28]**. Its valence band (VB) and conduction band (CB) are composed mainly of O2p and Ti3d orbitals, respectively. This electronic band structure is common among many metal oxide semiconductors because of oxygen's high electronegativity **[29]**. The optical transition for anatase and rutile are generally regarded respectively as an indirect transition (optical transition with a change of crystal momentum) and direct transition (optical transition without a change of crystal momentum). Additionally, although the report showed dissimilar values, the band gap value of anatase is always wider than that of rutile. The commonly reported values for anatase and rutile are, respectively, 3.2 and 3.0 eV **[30–32]**. For brookite, controversy persists in relation to its optical response, whether direct or indirect transitions. The reported band gap value is around 3.1–3.4 eV **[30, 32]**. Some band gap values are presented in **Table 1** **[32–35]**.

For an n-type semiconductor such as TiO_2, the flat band potential (E_{FB}) is the position of its Fermi level. It is always slightly below the conduction band edge. Consequently, the flat band potential is commonly used to state the lower edge of the conduction band (CB) **[29]**. Not only the crystallography, but the form of the electrode material (thin film, single crystal, and polycrystalline ceramics) and measurement methods influence the values of flat band potentials **[36–39]**. Although the flat band position of brookite remains uncertain, the lower edge of conduction band of brookite is apparently shifted from that of anatase around 0.1 V. Using the average value presented in previous reports **[35–40]**, a visual conclusion on the electronic band structure of TiO_2 is depicted in **Figure 1-2**. However, the electronic band of TiO_2 remains controversial. For example, against the general consensus, Scanlon et al. **[41]** recently reported the conduction band of anatase as 0.4 eV below (more positive) that of rutile based on some evidence from XPS and hybrid quantum-mechanical/molecular-mechanical (QM/MM) analyses.

1.2.3. Photocatalytic decomposition activity

When TiO_2 receives photon energy that is greater than its band gap (E_G), electron and hole pairs are generated. Most organic compounds are decomposed by this hole and active oxygens (such as O_2^-, $^{\bullet}OH$, $HO_2^{\bullet}$ and $O^{\bullet}$). Some of them recombine at the surface or in the bulk. Some electrons and holes are trapped on surface irregularities whose band energy differs from that of bulk: so-called trapped electron (e_{tr}^-) and hole (h_{tr}^+). **Figure 1-3** depicts photocatalytic mechanism on TiO_2. The trapping process increases the lifetime of the separated electron and hole to more than a scale of nanoseconds **[42]**.

From **Figure 1-2**, flat band potential of TiO_2 is around -0.15 to 0.15 V vs. NHE. Considering one electron reduction, the reduction potential for O_2/O_2^- is -0.563 V vs. NHE and for O_2, H^+/HO_2^- is -0.13 V vs. NHE **[43]**. Therefore the conduction band for TiO_2 is not anodic sufficient for the reduction of O_2/O_2^- and the reduction of O_2, H^+/HO_2^- is also quite difficult. Consequently, despite strong oxidation power, reduction power of TiO_2 is not so strong.

The oxidation on hole (or trapped hole) occurs from 2 μs to 80 μs. The reduction on electron (or trapped electron) by oxygen occurs from 100 ns to 100 μs **[1]**. Charge recombination occurs during 1–25 μs, which is competitive with surface redox reaction. Consequently, the photocatalytic activity of TiO_2 is improved with suppression of the charge recombination. When adding a small amount of noble metal such as platinum (Pt) onto TiO_2, photogenerated electrons from TiO_2 quickly transfer to the loaded metal particle. Holes remain on TiO_2 (**Figure 1-4**). In other words, charge separation is enhanced **[44, 45]**. From ESR signal, the Ti^{3+} intensity on TiO_2 increased under UV illumination although the Ti^{3+} intensity on Pt–TiO_2 did not increase significantly. In other words, only a few Ti^{3+} were observed on Pt–TiO_2, which is evidence that the photogenerated electron transfer occurred from TiO_2 to Pt **[3]**.

1.2.4. Photoinduced hydrophilicity (PIH)

When TiO_2 is illuminated under UV for a certain period, its surface becomes highly hydrophilic **[11]**. This phenomenon, commonly designated as photoinduced hydrophilicity (PIH), is a metastable state from the viewpoint of thermodynamics. Once UV illumination is stopped, the water contact angle (WCA) of the TiO_2 surface increases gradually.

First, this phenomenon was tentatively explained using the same mechanism of photocatalytic decomposition. Nevertheless, many experimentally obtained results demonstrated that the photoinduced hydrophilicizing process includes something more. For example, Miyauchi et al. **[17, 46]** reported that, dissimilar from TiO_2, strontium titanate ($SrTiO_3$) and tungsten trioxide (WO_3) showed no corresponding effect between photocatalytic decomposition and photoinduced hydrophilicity. At least two steps are expected for PIH: (i) decomposition of hydrophobic organic contaminants, which decreases WCA to around 20–30°, and (ii) an additional effect for decreasing WCA to almost 0°, such as surface structural change and resultant adsorption of water molecules **[13, 47–49]**. From FTIR and XPS analyses, the OH groups on TiO_2 surface were more numerous after UV illumination **[50–52]**. The mechanisms might include the bridging OH group on Ti from direct reduction by generated electron, the oxidative hole that adsorbs OH radical and the redox mechanism of water and oxygen **[1]**. Superhydrophilic surfaces might also be enhanced by introducing tensile residual stress in a TiO_2 film because PIH involves a structural change in the outer surface of TiO_2 **[53]**. Compressive stress near the surface is increased during UV illumination because hydrogen insertion on the trapped hole or increase in the number of hydroxyl groups at the surface results in volume expansion **[48, 54, 55]**. Some researchers have commented that the clean TiO_2 surface is naturally hydrophilic and that it does not need surface defects for PIH **[56]**.

1.3. Heteropolyacids (HPAs)

1.3.1. POM structure

Polyoxometalates (POMs) are metal oxide clusters in a well-defined structure. Their chemical formula is based on $(MO_x)_n$, where M is usually Mo, W, or V. The POMs structure is divisible into three subsets **[18]**.

(i) Heteropolyacids (HPAs) are a metal oxide framework called polyanions that include heteroanions such as tetrahedra of PO_4^{3-} inside. Generally, it is represented by the formula of $[X_xM_mO_p]^{n-}$, (M = W, Mo, V, Nb, Cr, and Ta and X= Si, P, etc.) consisting of an M–O octahedral basic structure unit. Keggin ($XM_{12}O_{40}^{n-}$) and Dawson structures ($X_2M_{18}O_{62}^{n-}$) are examples in this class. **Figure 1-5** **[57]** portrays these two structures.

(ii) Isopolyanions are a metal oxide framework without a heteroanion such as a Lindqvist structure ($M_6O_{19}^{n-}$) **[58]**.

(iii) Molybdenum blue and molybdenum brown are reduced POM clusters. They contain molybdenum with high nuclearity in a pentagon building block unit such as the wheel-like $(Mo_{154}O_{462}H_{14}(H_2O)_{70})^{14-}$ and the ball-like Keplerate $(Mo_{132}O_{372}(CH_3COO)_{30}(H_2O)_{72})^{42-}$.

Actually, HPAs are soluble in a polar solvent such as water and their structures are maintained in the solution as well as in the solid state **[59]**. They also have a small specific surface area (1–5 m^2/g) **[60]**. Consequently, preparation of water-insoluble salts with large specific surface area, such as $Cs_{2.5}H_{0.5}PW_{12}O_{40}$ **[61]**, is designed for liquid–solid heterogeneous catalysis. An alternative is the combination with a support that has a large specific surface area. A support should be neutral or acid, generally SiO_2 and activated-carbon are used because basic supports such as MgO decompose HPAs.

For better understanding of heterogeneous HPA catalysts, HPAs are divided into three substructures: primary, secondary, and tertiary structures **[62]**. The primary structure is the HPA structure itself such as Keggin-type HPAs. The secondary structure is the three-dimensional arrangement including polyanions, counter cations and additional molecules. The secondary structure relates to the activity of bulk-type HPA catalysts. The tertiary structure is the assembly of secondary structure to form primary particles, which are related to physical properties such as particle size, surface area, and pore structure.

1.3.2. Acid catalysts of HPAs

Heteropolyacids are known as acid catalysts, which have several economic and environmental benefits attributable to either (i) their potential oxidation power and redox properties in mild condition, deriving from their Brønsted acid site, or (ii) their thermal stability (decomposition temperature ca. 350–450 °C). The most common HPAs are Keggin-type HPAs, comprised of a XO_4 tetrahedron surrounded by 12 MO_6 octahedra, where X is a so-called central heteroatom. The M is also a so-called polyatom (see **Figure 1-5 (a)**). Normally, Keggin type HPA formulas are described as XM_{12}, e.g., PW_{12} is 12 tungsto (VI) phosphoric acid, $[PW_{12}O_{40}]^{3-}$. Typically, even though $[H_2W_{12}O_{40}]^{6+}$ isopolytungstate is not categorized in a class of heteropolyacids, many studies, including this paper, merge $H_2W_{12}O_{40}$ into the comparative series of $XM_{12}O_{40}$ because its structure (shown in **Figure 1-6 [63]**) and its reduction property closely resemble Keggin-type HPAs. In solution, acidities of HPAs are stronger than those of the common acids such as HCl, HNO_3, and H_2SO_4 **[60]**. Tungsten acid possesses stronger acidity than molybdenum acid, and PW_{12} is the strongest acid in the

Keggin series **[60]**. The acidic series of HPA solid phase is PW_{12}> SiW_{12}> PMo_{12} > $SiMo_{12}$ **[60, 64]**. Acidity of HPAs is related to proton conductivity of the solid phase. Polar molecules such as alcohols, ethers, and amines are readily absorbed in the HPA bulk and are adsorbed onto the HPAs. Consequently, not only on the surface but also in the bulk, the pseudo-homogeneous catalytic reactions advance. These solid HPA behaviors seem like those of a highly concentrated solution, causing a bulk-type reaction. This phenomenon is commonly designated as "pseudo-liquid phase in HPAs". **Figures 1-7** and **1-8** (referred from **[62]**) depict catalyses of three types for solid HPAs and various reaction fields of catalysis. Additionally, depending on their support for immobilized HPAs, the acid strength and catalytic activity differ.

1.3.3. Photoreaction of HPAs

HPAs also present photochromism and electrochromism **[65, 66]**. The reaction is known as the photoexcitation of the oxygen-to-metal, ligand-to-metal charge transfer (O→ M, LMCT). An electron from the low energy stage (mainly composed of the O2p orbital) is excited to the higher energy state (mainly composed of the metal d orbital) when UV light is illuminated. In other words, O and M orbitals are recognized respectively as the highest occupied molecular orbital (HOMO) and the lowest unoccupied molecular orbital (LUMO) levels. The holes in the HOMO level decompose organic molecules. The electrons in the LUMO level are delocalized to the excited state via the intervalence charge transfer among metal centers by receiving visible light energy **[67]**. Their reoxidation to the ground state is obtained with the common reducing agents: O_2 and H_2O_2 **[68]**. A schematic explanation of photocatalysis of Keggin-type HPAs is presented in **Figure 1-9**.

The following shows theoretical redox reactions of oxygen in acid aqueous HPA solutions and their redox potential (V vs. NHE, pH 0) **[60]**.

$O_2 + e^- + H^+ \rightarrow HO_2$	E = -0.05 V
$O_2 + 2e^- + 2H^+ \rightarrow H_2O_2$	E = 0.68 V
$O_2 + 4e^- + 4H^+ \rightarrow 2H_2O$	E = 1.23 V
$HO_2 + e^- + H^+ \rightarrow H_2O_2$	E = 1.44 V
$H_2O_2 + e^- + H^+ \rightarrow HO + H_2O$	E = 0.71 V
$H_2O_2 + 2e^- + 2H^+ \rightarrow 2\ H_2O$	E = 1.76 V
$OH + e^- + H^+ \rightarrow H_2O$	E = 2.81 V

The reduction potential of HPAs depends on the central heteroatoms. The more negative charge of the heteroatom is the more positive reduction potential, as shown in the following order: $PW_{12}^{3-} > GeW_{12}^{4-} > SiW_{12}^{4-} > FeW_{12}^{5-} > BW_{12}^{5-} > CoW_{12}^{6-} > CuW_{12}^{6-}$ **[18, 56, 69]**. The reduction potential of HPAs decreases concomitantly with increasing electronegativity of the polyatom or decreasing electronegativity of the heteroatom **[70]**. Reduction potentials for some HPAs have also been reported **[71–73]**. Some examples are the reduction potentials of $PW_{12}O_{40}^{3-}$, $SiW_{12}O_{40}^{4-}$, and $H_2W_{12}O_{40}^{6-}$, which are +0.218 V, +0.054 V and -0.162 V vs. NHE (1 M H_2SO_4) **[71]**. Considering the oxygen reduction and the reduction potential of HPAs, one-electron reduction of O_2 on HPAs (O_2, H^+/ HO_2) is quite unfavorable for some HPAs.

Broadly speaking, two photocatalyst types exist for HPAs: homogeneous reactions **[74-76]** and heterogeneous reactions **[77-80]**. These categories are similar to the reaction fields of HPA acid catalysis presented in **Figure 1-8**. First, because of their

good solubility in water and polar solvents, HPAs are applied as a photocatalyst in a homogeneous reaction. They can mineralize several organic molecules such as alcohols and proteins. Despite good photocatalytic activity in homogeneous systems, as described previously, the separation of HPAs from the reaction vessel is difficult. Therefore, insoluble HPAs were developed as supported HPAs or their insoluble salts. Not only hybridization with the high surface area substrate **[81–83]**, HPAs are combined to some organic component as HPA-based inorganic/organic composite. This composite is usually fabricated in lamellar composites via layer-by-layer (LBL) self-assembly, Langmuir–Blodgett (LB), or sol–gel method **[84, 85]**. Moreover, HPAs are attractive materials for a hybrid photosystem because they act as electron pools in photoelectrochemical processes **[86]**.

1.4. HPA/TiO_2 systems

HPAs and TiO_2 possess the close excitation energies for promoting electron from VB to CB or from HOMO to LUMO under near-UV light (300–375 nm). Therefore, reduced HPAs and electron–hole pairs are generated simultaneously under UV illumination.

1.4.1. HPA solution/TiO_2 particles

Yoon et al. **[19]** incorporated TiO_2 colloid with 12-tungstophosphoric acid ($(PW_{12}O_{40})^{3-}$) in an acid aqueous solution. They proposed a Z-scheme mechanism, which is similar to photosynthesis in green plants. When HPA was illuminated in 0.1% polyvinyl alcohol (PVA) aqueous solution, electrons from the CB of TiO_2 directly transfer to interfacial HPA and form heteropolyblue (HPB) confirmed by ns-transient

absorption spectroscopy. Next, HPB receives energy from visible light. It then becomes excited HPB (HPB*) via d–d transition or intervalence transition. The HPB* promotes the reduction methyl orange and it revert to HPA in a process designated as reoxidation. Ozer and Ferry **[87]** published concurrent works related to the oxidation ability of 1,2-dichlorobenzene (DCB) in the system of $PW_{12}O_{40}^{3-}/TiO_2$, $SiW_{12}O_{40}^{4-}/TiO_2$, and $W_{10}O_{32}^{4-}/TiO_2$ in aqueous solution. Considering concentration-independent-degradation rate constant of DCB derived from Langmuir–Hinshelwood plots, the reduction of the HPAs is more kinetically favored than the reduction of O_2. They revealed that $PW_{12}O_{40}^{3-}$ was the best electron scavenger of the three. Moreover, competition between those two reductions occurs when O_2 and HPAs coexist in the TiO_2 suspension. The electron transfer for HPA/TiO_2 might occur as depicted in **Figure 9**.

Park and Choi **[88]** investigated the electron shuttle behavior of $PW_{12}O_{40}^{3-}/PW_{12}O_{40}^{4-}$ and Fe^{3+}/Fe^{2+} in the suspension of TiO_2 or Pt/TiO_2. HPAs receive electrons from the CB of TiO_2 and carry them to the inert electrode for producing photocurrent under UV illumination. Generated photocurrent from HPA/TiO_2 was larger than that from HPA alone. In fact, TiO_2 enhances $PW_{12}O_{40}^{4-}$ formation. Additionally, the photocurrent from HPA/TiO_2 system decreased when oxygen was dissolved in the system. This effect was not found when using Fe^{3+}/Fe^{2+} as the electron shuttle. Their research supports that HPAs carry electrons efficiently from TiO_2 to O_2. Furthermore, the combination of both Pt and HPA to TiO_2 is decrease charge transfer efficiency. When TiO_2 is changed to Pt–TiO_2, Pt becomes a surface catalyst for the reoxidation of HPA^-/HPA via reduction of H^+ ($PW_{12}O_{40}^{4-} + H^+ \rightarrow PW_{12}O_{40}^{3-} + 1/2H_2$), and results in poor electron transfer to the inert electrode.

Zhao and his group **[89]** investigated the mechanism of the photocatalytic activity for HPA/TiO_2 systems using TiO_2 sol and $PW_{12}O_{40}^{3-}$ solution containing 2-propanol (IPA). Under anaerobic conditions, the solution turned blue during UV illumination because of the reduced HPAs, although the solution with oxygen remained transparent. Charge separation was improved when TiO_2 powder was dispersed in the solution of $PW_{12}O_{40}^{3-}$ and 2,4-dichlorophenol (DCP). However, when HPAs adsorb completely onto the TiO_2 site, the reaction rate begins to decrease. Moreover, complete mineralization of DCP was suppressed by increasing the HPA concentration because various aromatic intermediates were produced. They proposed that the formation of $O_2^{\bullet-}$ as a necessary step for mineralization. However, from Electron Study Resonance (ESR) study in this current experiment, $PW_{12}O_{40}^{3-}$ suppress the generation of $O_2^{\bullet-}$ because the intramolecular electron transfer between reduced HPA and dioxygen involve M-O covalent bound result in the peroxide compound such as $M(O_2)^{2-}$ rather than free $O_2^{\bullet-}$ **[90]**.

Tachikawa et al. **[91]** investigated electron transfer from CB of TiO_2 to a series of HPAs: $PW_{12}O_{40}^{3-}$, $SiW_{12}O_{40}^{4-}$, and $H_2W_{12}O_{40}^{6-}$ using two-color, two-laser flash photolysis. The equilibrium constants of adsorption of HPAs on the TiO_2 powder in water (pH 1) were reported respectively as 5.7, 6.0, and 20×10^4 M^{-1}. In fact, $H_2W_{12}O_{40}$ has the highest adsorption on TiO_2 because of its highest anion valence. Considering the generation yield of HPA^- and their adsorption capability of HPAs on TiO_2, the electron transfer efficiency order should correspond with their reduction potential as $PW_{12}O_{40}^{3-}$> $SiW_{12}O_{40}^{4-}$ > $H_2W_{12}O_{40}^{6-}$. In lacking an electron acceptor system, they found that electron transfer from HPA^{-}* to CB of TiO_2 and rapidly (within 5 ns) recombine with h_{tr}^+. Therefore, the $TiO_2/PW_{12}O_{40}^{3-}/MV^{2+}$ ternary system was proposed. Methyl

viologen dichloride hydrate (MV^{2+}) has more negative reduction potential (-0.45 V vs. NHE) than either HPA^{-}* or TiO_2. It cannot adsorb on the surface of TiO_2, but it has good attraction for HPAs because of its positive surface charge in acid solution. Therefore, it is an electron acceptor for HPA^{-}*. Finally, it re-transfers the electron to HPA and provides HPA^{-}.

1.4.2. Immobilized HPA/TiO_2: solid/liquid reaction

Yang et al. **[92]** used two transition-metal-monosubstituted polyoxometalates to conjoin with mesoporous TiO_2 to decrease both the charge recombination in TiO_2 and the solubility of HPAs. 3-aminopropyl triethoxysilane (APS) was used to modify the TiO_2 surface for conjunction with HPAs. This photocatalyst was able to degrade hexachlorobenzene and various dyes. Later, Yang et al. studied a composite of $PW_{12}O_{40}/TiO_2$ under visible light irradiation **[93]**. They reported acid–base interaction between TiO_2 and PW_{12}; $(\equiv TiOH_2^{+})(H_2PW_{12}O_{40})$ was confirmed by the shift from the peak characterized by ^{31}P magic angle spinning (MAS) NMR. The composite possessed a bimodal pore system (4 nm and 0.6 nm). Its poor solubility was confirmed by determining the dissolved amount of W atom after the reaction. They also found the red shift of oxygen–metal charge transfer (OMCT), which was enabled by the hybridization of Ti3d and W5d orbitals and resultant narrowing band gap of TiO_2. Depending on the adsorption ability between dye and composite surface, dye is decomposed by oxidation of photogenerated hole directly. Directed oxidation by the hole was also proposed for the decomposition of cyanide by a composite of $PW_{12}O_{40}/TiO_2$, although $OH^{\bullet}$ played an important role in the decomposition for the pure TiO_2 **[94]**. Li et al. also compared photocatalytic performances between $H_3PW_{12}O_{40}/TiO_2$ and $H_6P_2W_{18}O_{62}/TiO_2$ which

have the different heteroatom-polyatom ratio; Keggin-type HPA (1:12) and dawson-type HPA (2:18) **[95]**. The order of degradation rates of parathion-methyl is $H_3PW_{12}O_{40}/TiO_2$ > $H_6P_2W_{18}O_{62}/TiO_2$ > TiO_2. When the photocatalytic reaction occurred in an inert atmosphere (absent of O_2), the composite catalyst surface became blue, indicating the reduction product of HPAs produced via intervalence electron transfer. This situation is similar to the HPA(aq)/TiO_2(s) system, but the heterogeneous HPAs give much higher superoxide ($O_2^{\bullet-}$) concentration.

Lv and Xu **[96]** reported hindrance on the photocatalytic decomposition of organic dye (X3B) on HPAs/TiO_2. The positive surface charge of TiO_2 in acid solution is decreased by hybridization with HPAs, resulting in the lower adsorption of X3B on TiO_2. Simultaneously, the combination site between HPA/TiO_2, ($\equiv TiOH_2^+$)($H_2PW_{12}O_{40}$), accelerates surface-bound $OH^\bullet$ radicals (not free $OH^\bullet$). Therefore, the photocatalytic decomposition of X3B was inhibited by HPA/TiO_2, which suggests that the substance characteristics such as polarity and the surface migration are also important.

Li et al. **[97, 98]** varied the loading amounts of $H_3PW_{12}O_{40}$ on TiO_2, and studied their respective degrees of photoreactivity for the decomposition of methyl orange under simulated sunlight. They prepared the composites using an evaporation-induced self-assembly (EISA) method on the triblock copolymer surfactant P123. Thereby, ordered mesoporous $H_3PW_{12}O_{40}/TiO_2$ was obtained. Because of the well-matched electronegativity and ionic radius between Ti^{4+} and W^{6+}, $H_3PW_{12}O_{40}$ connects to TiO_2 via a W–O–Ti bond. Actually, $H_3PW_{12}O_{40}$ leakage during the photocatalytic reaction was suppressed by this bonding. The loading amount of HPA was controlled by the initial concentration of $H_3PW_{12}O_{40}$ solution. Photodecomposition of methyl orange increased concomitantly with increasing HPA loading amount during 8.8–32.3%. They

also prepared a series of various mesoporous $H_3PW_{12}O_{40}/TiO_2$. The order of photocatalytic activity was 3D-disordered > 3D-ordered > 2D-ordered because of the different pore size, porosity, crystallinity, and accessibility to the active site of the catalyst.

Nakajima et al. prepared a hybrid film of $Cs_{2.5}H_{0.5}PW_{12}O_{40}$ (Cs2.5)/TiO_2 on Pyrex glass **[99]**. The Cs2.5 film was prepared on Pyrex via continuous spin coating using Si-alkoxide. The Cs2.5 coating possessed an acid site on the film surface. Translucent TiO_2-Cs2.5 hybrid films were prepared by laminating TiO_2 films with holes on the Cs2.5 coating using phase-separation of Ti-alkoxide. The decomposition amounts of 1,4- dioxane per unit film area of the no-hole film and the hybrid film were almost equal, although the TiO_2 ratio on the no-hole film is larger than that of the hybrid film. The result suggests that the hybrid film gives better photocatalytic activity than TiO_2. It is particularly interesting that ethylene glycol diformate (EGDF, an intermediate with poor affinity to TiO_2) generation on the hybrid film is less than on the no-hole film. The holes in the film served as the adsorption field for EGDF because the high electron density in C=O bound of EGDF presents Lewis basicity and interacts with the acid site in Cs2.5. In addition to charge separation, HPAs can also increase affinity to basic substances and enhance photocatalytic efficiency on TiO_2. Recently, they also prepared porous spherical TiO_2 particles comprising $H_3PW_{12}O_{40}$ in hydrophobic nanopores using octadecylphosphinic acid (ODP), and demonstrated that hydrophobic acidic nanopores enhance adsorption of EGDF in water and play an important role in the overall photocatalytic performance of this system **[9]**. Zhang et al. **[100]** prepared $PW_{12}O_{40}^{3-}$ /Cr-TiO_2 nanotube photocatalysts for visible light. Charge recombination is suppressed by HPA and visible light response is improved by Cr^{3+} doping.

1.4.3. Immobilized HPA/TiO_2: The solid/gas reaction

Yanagida et al. prepared $XW_{12}O_{40}/TiO_2$, anatase hybrid films via LBL processing: XW_{12}/TiO_2 **[101]**. Additionally, the effect of HPAs on photocatalytic properties of the hybrid films was studied using various Keggin-type HPAs **[102]**. TiO_2 and HPAs have different surface charges in acid solution. Therefore, by Coulombic attraction, TiO_2 particles and HPAs are self-assembled on the silica substrate during alternate immersion the substrate into the sol of TiO_2 or the solution of HPAs. With increasing the polyanion charge, the TiO_2 deposition amount decreases because of anion–anion repulsion **[103]** and XW_{12}/TiO_2 charge balance. The photocatalytic activity of the hybrid films (XW_{12}/TiO_2) was studied via gaseous 2-propanol (IPA) decomposition. HPAs enhanced the activity of the hybrid films because of their charge separation efficiency. When both UV and visible light from Hg-Xe lamp are applied, the photocatalytic activity order was H_2W_{12}/TiO_2 > PW_{12}/TiO_2 > SiW_{12}/TiO_2 > TiO_2. The IPA decomposition of the six-bilayer sample was 2.5 times higher than that of the two-bilayer sample, indicating that the bulk part also participates in the decomposition. When visible light was cut, the activity of PW_{12}/TiO_2 was decreased greatly, although those of the other HPAs were unaffected. When the UV light was cut, the SiW_{12}/TiO_2 and H_2W_{12}/TiO_2 activities were decreased remarkably. Moreover, different surface-coverage films were prepared: $(PW_{12}/TiO_2)_6$ and $(PW_{12}/TiO_2)_6 + PW_{12}$. When UV light for exciting PW_{12} (< 350 nm) was cut, the activity of $(PW_{12}/TiO_2)_6$ was minor compared to $(PW_{12}/TiO_2)_6 + PW_{12}$. When visible light for exciting PW_{12}^- to PW_{12}^{-*} (> 400 nm) was cut, the activity of $(PW_{12}/TiO_2)_6$ was greater than $(PW_{12}/TiO_2)_6 + PW_{12}$. Based on these experiments, the redox system is shown in **Figure 10**. When UV is sufficient, oxidation occurs effectively. Therefore, there are many holes at HOMO. For that reason, electron

transfers to HOMO instead of LUMO. Because of the H_2W_{12} and SiW_{12} band structure, O_2 reduction occurs on their LUMO and the ground-state H_2W_{12} and SiW_{12} are recovered. Consequently, UV excitation alone is important for H_2W_{12}/TiO_2 and SiW_{12}/TiO_2 systems. Visible light is unimportant for their activity. In contrast, UV excitation alone is inadequate for PW_{12} reoxidation. Visible light is needed for second excitation to form PW_{12}^{-*}, which has higher reduction potential than O_2 does.

Nakajima et al. also studied the effects of substituted W in PMo_{12} as $[PW_xMo_{12-x}O_{40}]^{3-}$ (X= 0, 6 and 12), on the photocatalytic activity of the films **[104]**. Results showed that PMo_{12} exhibited the highest IPA adsorption capacity. However, under a Hg-Xe lamp, the photocatalytic activity of $(PMo_{12}/TiO_2)_5$ was the worst among these three films; $(PW_{12}/TiO_2)_5$ was the best. The visible light for the secondary excitation of reduced PMo_{12}^- to PMo_{12}^{-*} is around 600–750 nm. Therefore, not only a Hg-Xe lamp but also a Xe-lamp was applied in extended experiments investigating $(PMo_{12}/TiO_2)_5$. These lamps were combined with glass filters to control the wavelength range. When light for secondary excitation of PMo_{12}^- to PMo_{12}^{-*} was illuminated, IPA decomposition decreased remarkably. Surprisingly, the secondary excitation diminishes the photocatalytic activity in PMo_{12}/TiO_2 system. The secondary excitation exists (thermodynamical viewpoint), but its electron transfer rate is small (kinetics viewpoint). Consequently, the excited electron in LUMO prefers to transfer to VB of TiO_2. Then the electron recombines with the hole there. Accordingly, the PMo_{12}/TiO_2 system gives better photocatalytic activity when it is under a rich-UV and little-visible light condition. The electron transfer for PMo_{12}/TiO_2 system is shown in **Figure 11**.

Marci and co-workers investigated photocatalytic degradation of IPA on a $PW_{12}O_{40}/TiO_2$ solid **[105–107]**. Powders of PW_{12}/TiO_2 were prepared by impregnation,

evaporation, and then annealing. The PW_{12}/TiO_2 ratio was varied in 5–30% PW_{12}. The sample with 20% PW_{12} provided the best performance in photocatalytic activity. Moreover, intermediates differed during mineralization between bare TiO_2 and PW_{12}/TiO_2. This selectivity was attributed to the physicochemical characteristics of the solid catalyst surface.

1.5. Objective of this study

As explained earlier, three TiO_2 polymorphs exist: rutile, anatase, and brookite. Anatase has been commonly used as a photocatalytic material. Brookite is a metastable phase. Therefore, it is difficult to prepare brookite in pure phase. Recently however, several methods have been devised for the preparation of pure brookite such as hydrothermal method, which is able to control reaction-chemistry parameters (pH, temperature, etc.) **[108–112]**. Moreover, many calculations and experiments provide reasons for the better photocatalytic activity of brookite. Wei-Kun Li et al., using density functional theory (DFT) calculations, shows that brookite (210), which has the same structural building blocks but different orientation and shorter interatomic distance than those of anatase (110), has a better active site at the junction between its unit structures than anatase has (110) **[113]**. Several reports describe the high photocatalytic activity of brookite on the decomposition of IPA and acetaldehyde **[109–112]** and photoinduced hydrophilicity **[114–116]**. Addamo et al. **[117]** prepared nanostructured anatase, rutile, and brookite thin films via dip coating in TiO_2 dispersions from a $TiCl_4$ precursor. Shibata et al. **[114]** reported that although anatase and brookite-rich films exhibited almost identical methylene blue and cis-9-octadecanoic acid degradation rates,

the rate constant for the photoinduced hydrophilicity for the brookite-rich film is better than that of the anatase film under weak UV illumination.

Based on the assumption that an HPA/brookite system might give better photocatalytic activity than a HPA/anatase system, hybridized PW_{12} with brookite-type TiO_2 nanoparticles shall be prepared using the same method as that used in previous work. Some processing parameters will be varied to obtain optimum conditions for HPA/brookite systems such as TiO_2 concentration. Then, their photocatalytic activities and photoinduced hydrophilic will be evaluated. Based on results of these evaluations, together with film characterizations, the photocatalysis model for HPA/brookite systems will be clarified.

References

[1] A. Fujishima, X. Zhang, D. A. Tryk, *Surf. Sci. Rep.*, 63, 515-582 (2008).

[2] S. Sato, J. M. White, *Chem. Lett.*, 72, 83-86 (1980).

[3] M. Anpo, M. Takeuchi, *J. Catal.*, 216, 505-516 (2003).

[4] M. Miyauchi, A. Nakajima, K. Hashimoto, T. Watanabe, *Adv. Mater.*, 12, 1923-1927 (2000).

[5] K. Sayama, K. Mukasa, R. Abe, H. Arakawa, *Chem. Commun*., 2416-2417 (2001).

[6] Z. Jiang, W. Haiyan, Y. Hongwei, *Chemosphere*, 56, 503-508 (2004).

[7] Y Kado, M Atobe, T Nonaka, *Ultrasonic Sonochem.*, 8, 69-74, (2001).

[8] H.G Yangi, X. Quan, X.Y. Li, N. Fangi, N. Zhangi, H.M. Zhao, *J. Environ. Sci.*, 17, 2, 290-293 (2005).

[9] K. Yasui, T. Isobe, S. Matsushita, A. Nakajima *J. Mater. Sci.*, 48, 2290-2298 (2013)

[10] L. Liu, T. Isobe, H. Lin, K. Okada, A. Nakajima *Mater. Res. Bull*., 46, 175-184 (2011).

[11] R. Wang, K. Hashimoto, A. Fujishima, M. Chikuni, E. Kojima, A. Kitamura, T. Shimohigoshi, T. Watanabe, *Nature*, 388, 431-432 (1997).

[12] A. Fujishima, K. Hashimoto, T. Watanabe, TiO_2 Photocatalysis: Fundamentals and Applications, BKC Inc., Tokyo, 1999, pp. 66.

[13] T. Zubkov, D. Stahl, T.L. Thompson, D. Panayotov, O. Diwald, J.T. Yates, *J. Phys. Chem. B*, 109, 15454-15462 (2005).

[14] C.Y. Wang, H. Groenzin, M.J. Shultz, *Langmuir*, 19, 7330-7334 (2003).

[15] J.M.White, J. Szanyi, M.A. Henderson, *J. Phys. Chem. B.*, 107, 9023-9033 (2003).

[16] N. Sakai, A. Fujishima, T. Watanabe, K. Hashimoto, *J. Phys. Chem. B*, 107, 1028-1035 (2003).

[17] M. Miyauchi, A. Nakajima, A. Fujishima, K. Hashimoto, T. Watanabe, *Chem. Mater.*, 12, 3-5 (2000).

[18] D.L. Long, Y Tsunashima, L Cronin, *Angew. Chem. Int. Ed.*, 49, 1736-1758 (2010).

[19] M. Yoon, J. A. Chang, Y. Kim, J. R. Choi, K. Kim, S. J. Lee, *J. Phys. Chem. B*, 105, 2539-2545 (2001).

[20] K. Pruethiarenun, T. Isobe, S. Matsushita, A. Nakajima, *Appl. Catal. A: Gen.*, 445-446, 274–279 (2012).

[21] Winkler, Jochen, Titanium dioxide, Hannover Vincentz 2003, European coatings literature, ISBN 3-87870-148-9.

[22] A. F. Wells, 'Structural Inorganic Chemistry, Fifth ed., Oxford University Press, Oxford, UK, 1984.

[23] National Science Foundation grants EAR9614919 and EAR9725627 to Joseph R. Smyth, "TiO_2 Group", University of Colorado Mineral Structure and Properties Data. http://ruby.colorado.edu/~smyth/min/tio2.html (July 12, 2011)

[24] M. Ramamoorth, D. Vanderbit, *Phys. Rev. B*, 49, 23, 16 721-16 727 (1994).

[25] [24] S.D. Burnside, V. Shklover, C. Barbe, P. Comte, F. Arendse, K. Brooks, M. Grätzel, *Chem. Mater.*, 10, 2419-2425 (1998).

[26] R. Hengerer, B. Bolliger, M. Erbudak, M. Grätzel, *Surf. Sci.*, 460, 162-169 (2000).

[27] A. Beltrán, L. Gracia, J. Andrés, *Phys. Chem. B*, 110, 23417-23423 (2006).

[28] A. Fujishima, K. Honda, *Nature*, 238, 37-38 (1972).

[29] R. van de Krol, M. Grätzel, Electronic Materials: Science & Technology, Vol. 102, Photoelectrochemical Hydrogen Production, VIII, 324 p. (2012).

[30] A Di Paola, M Bellardita, L Palmisano, *Catalysts*, 3, 36-73 (2013).

[31] K. Kalyanasundaram, M. Grätzel, *Coordination Chemistry Reviews*,77, 347-414 (1998)

[32] D. Reyes-Coronado, G. Rodriguez-Gattorno, M. E. Espinosa-Pesqueira, C. Cab, R. de Coss, G. Oskam, *Nanotechnology*, 19, 145605 (10pp), (2008).

[33] M. Grätzel, F.P. Rotzinger, *Chemical Physics Letters*, 118, 5, 474–477 (1985).

[34] M. Landmann, E. Rauls, W-G Schmidt, *J. Phys.: Condens. Matter*, 24, 195503 (2012)

[35] J-G. Li, T. Ishigaki, X. Sun, *J. Phys. Chem. C*, 111, 4969-4976 (2007).

[36] A. Di Paola, M. Bellardita, R. Ceccato, L. Palmisano, F. Parrino, *J. Phys. Chem. C*, 113, 15166-15174 (2009).

[37] M. Radecka, M. Rekas, A. Trenczek-Zajac, K. Zakrzewska, *J. Power Sources*, 181, 46-55 (2008).

[38] Q. Tay, X. Liu, Y. Tang, Z. Jiang, T.C. Sum, A. Chen, *J. Phys. Chem. C*., 117, 14973-14982 (2013).

[39] T.A. Kandiel, A. Feldhoff, L. Robben, R. Dillert, D.W. Bahnemann, *Chem. Mater*., 22, 2050-2060 (2010).

[40] M. Grätzel, F.P. Rotzinger, *Chem. Phys. Lett.*, 118, 5, 474-477 (1985).

[41] D. O. Scanlon, C. W. Dunnill, J. Buckeridge, S. A. Shevlin, A. J. Logsdail, S. M. Woodley, C. R. A. Catlow, M. J. Powell, R. G. Palgrave, I. P. Parkin, G. W.

Watson, T. W. Keal, P. Sherwood, A. Walsh and A. A. Sokol, *Nat. Mater.,* 12, 798-801 (2013).

[42] A. L. Linsebigler, G. Lu, J. T. Yates, Jr., *Chem. Rev.,* 95, 3, 735-758 (1995).

[43] "NyuumonHikari Shokubai" Ed. Y. Nosaka and A. Nosaka, Tokyo, Tosho Press, 2004, Tokyo, Japan, pp 49.

[44] Y. Mizukoshi, Y. Makise, T. Shuto, J. Hu, A. Tominaga, S. Shironita, S. Tanabe, *Ultrasonics Sonochem.,* 14,3, 387-392 (2007).

[45] Y.Z. Yang, C.-H. Chang, H. Idriss, *Appl. Catal. B: Environ.,* 67, 3-4, 217-222 (2006)

[46] M Miyauchi, A Nakajima, T Watanabe, K Hashimoto, *Chem. Mater.,* 14, 6, 2812-2816 (2002).

[47] X. Yan, R. Abe, T. Ohno, M. Toyofuku, B. Ohtani, *Thin Solid Films*, 516, 5872-5876 (2008).

[48] D.C. Hennessy, M. Pierce, K.-C. Chang, S. Takakusagi, H. You, K. Uosaki, *Electrochim. Acta*, 53, 6173-6177(2008).

[49] K. Okudaira, T. Kato, T. Isobe, S. Matsushita, T. Kogure, A, Nakajima *J. Photochem. Photobiol. A. Chem.,* 222, 64-69 (2011).

[50] N. Sakai, A. Fujishima, T. Watanabe, K. Hashimoto, *J. Phys. Chem. B*, 105, 15, 3023-3026 (2001).

[51] R. Wang, K. Hashimoto A. Fujishima, M. Chikuni, E. Kojima, A. Kitamura, M. Shimohigoshi, T. Watanabe, *Adv. Mater.,* 10, 135-138 (1998).

[52] R.D. Song, A. Nakajima, A. Fujishima, T. Watanabe, K. Hashimoto, *J. Phys. Chem. B*, 105, 1984-1990 (2001)

[53] T. Shibata, H. Irie, K. Hashimoto, *J. Phys. Chem. B*, 107, 10696-10698 (2003).

[54] T. Shibata, H. Irie, K. Hashimoto, *Chem. Commun.*, 3735-3737 (2009).

[55] M.V. Koudriachova, S.W. de Leeuw, N.M. Harrison, *Phys. Rev. B*, 70, 165421-5 (2004).

[56] M.A. Henderson, *Surf. Sci. Rep.*, 66, 185-297 (2011).

[57] Wikipedia, "Heteropoly acid", http://en.wikipedia.org/wiki/Heteropoly_acid, (May 2014)

[58] R. Sivakumara, J. Thomasa, M. Yoon, *J. Photochem. Photobiol. C: Photochemistry Reviews*, 13, 4, 277-298 (2012).

[59] E. Coronado, C.J. Gomez-Garcia, *Chem. Rev*., 98, 273-296 (1998)

[60] I. V. Kozhevnikov, *Chem. Rev.*, 98, 171-198 (1998).

[61] T. Okuhara, H. Watanabe, T. Nishimura, K. Inumaru, M. Misono, *Chem. Mater.*, 12, 2230-2238 (2000).

[62] M. Misono, *Chem. Commun.*, 1141-1152 (2001).

[63] M.J.G. Fait, H.-J. Lunk, M. Feist, M. Schneider, J.N. Dann, T.A. Frisk, *Thermochimica Acta*, 469, 1–2, 12–22 (2008)

[64] M. Misono, *Catal. Rev. Sci. Eng*., 29 (2&3), 269- 321 (1987).

[65] T. Yamas, *Catalysis Surveys from Asia*, 7, 4, 203-217 (2003).

[66] T. Yamase, K. Ohtaka, *J. Chem. Soc. Dalton Trans*., 18, 2599-2680 (1994).

[67] T. Yamas, *Chem. Rev.*, 98, 307-325(1998).

[68] E. Papaconstantinou, *Chem. Soc. Rev.*, 18, 1-31 (1989).

[69] P. E. Katsolis, M. T. Pope, *J. Am. Chem. Soc.*, 106, 2737-2788 (1984).

[70] I. K. Song, M. A. Barteau, *J. Mol. Catal. A: Chemical*, 212, 229-236 (2004).

[71] I. A. Weinstick, *Chem. Rev.*, 98, 113-170 (1998).

[72] B. Keita, T. Liu, L. Nadjo, *J. Mater. Chem.*, 19, 19-33 (2009).

[73] K. P. Barteau, J. E. Lyons, I. K. Song, M. A. Barteau, *Topic in Catalysis*, 14, Nos.1-4, 55- 62 (2006).

[74] C.L. Hill, C.M. Prosser-McCartha, *Coordination Chemistry Reviews*, 143, 407-455 (1995)

[75] S. Kim, H. Park, W. Choi, *Phys. Chem. B*, 108, 6402-6411 (2004).

[76] A. Harriman, K. J. Elliott, M.A. H. Alamiry, L.L Pleux, M. Séverac, Y. Pellegrin, E. Blart, C. Fosse, C. Cannizzo, C.R. Mayer, F Odobel, *J. Phys. Chem. C*, 113 (14), 5834-5842 (2009).

[77] A. Lewera, G. Zukowaska, K. Miecznikowshi, M. Choajak, W. Wieczorek, P. J. Kulesza, *Anal. Chim. Acta*, 536, 275-281 (2005).

[78] R. N. Biboum, F. Doungmene, B. Keita, P. de Oliveira, L. Nadjo, B. Lepoittevin, P. Roger, F. Brisset, P. Mialane, A. Dolbecq, I. M. Mbomekalle, C. Pichon, P. Yin, T. Liu and R. Contant, *J. Mater. Chem.*, 22, 319-323 (2012).

[79] Y. Leng, J. Liu, P. Jiang, J. Wang, *RSC Adv.*, 2, 11653-11656 (2012).

[80] W. Feng, T. R. Zhang, Y. Liu, L. Wei, R. Lu, T. J. Li, Y. Y. Zhao, Y. N. Yao, *J. Mater. Res.*, 1, 133-136 (2002).

[81] Y. Guo, Y. Wang, C. Hu, Y. Wang, E. Wang, *Chem. Mater.*, 12, 11,3501-3508 (2000).

[82] S. Li, X. Yu, G. Zhang, Y. Ma, J. Yao, B. Keita, N. Louis, H. Zhao, *J. Mater. Chem.*, 21, 2282-2287 (2011).

[83] X. Au, Y. Guo, C. Hu, *J. Mol. Catal. A: Chem.*, 262,128-135 (2007).

[84] S.Y. Guo, R. Cao, C.P. Yang, *J. Colloid Interface Sci.*, 324, 156-166 (2008).

[85] T. Ito, H. Yashiro, T. Yamase, *Langmuir*, 22, 2805-2810 (2006).

[86] P. Ngaotrakanwiwat, S. Saitoh, Y.Ohko, T. Tatsuma, A. Fujishima, *J. Electrochem. Soc*., 150(11), A1405-A1407 (2003).

[87] R. R Ozer, J. L. Ferry, *Environ. Sci. Technol.*, 35, 3242-3246 (2001).

[88] H. Park, W. Choi, *J. Phys. Chem. B*, 107, 16, 3885-3890 (2003).

[89] C. Chen, P. Lei, H. Ji, W. Ma, J. Zhao, *Environ. Sci. Technol.,* 38, 1, 329-337 (2004).

[90] A. Hiskia, E. Papaconstantinou, *Inorg. Chem.*, 31, 163-167 (1992).

[91] T. Tachikawa, S. Tojo, M. Fujitsuka, T. Majima, *Chem. Eur. J.*, 12, 3124-3131 (2006).

[92] Y. Yang, Y. Guo, C. Hu, Y. Wang, E. Wang,, *Appl. Catal. A*, 273, 201-210 (2004).

[93] Y. Yang, Q. Wu, Y. Guo, C. Hu, E. Wang, *J. Mol. Catal. A: Chem.,* 225, 203-212 (2005).

[94] J. H. Kim, H. I. Lee, *Korean J. Chem. Eng*., 21(1), 116-122 (2004).

[95] L. Li, Q. Wu, Y. Guo, C. Hu, *Microporous Mesoporous Mater.*, 87, 1-9 (2005).

[96] K. L. Lv, Y. M. Xu, *J. Phy. Chem. B*, 110, 6204-6212 (2006).

[97] K. Li, Y. Guo, F. Ma, H. Li, L. Chen, Y. Guo, *Catal. Commun.*, 11, 839-843 (2010).

[98] K. Li, X. Yang, Y. Guo, F. Ma, H. Li, L. Chen, Y. Guo, *Appl. Catal. B: Environ.*, 99, 364-375 (2010).

[99] A. Nakajima, S. Matsui, S. Yanagida, Y. Kameshima, K. Okada, *Surf. Coat. Technol.*, 203, 1133-1137 (2009).

[100] X. Zhang, L. Li, J. Zhang, Q. Chen, J. Bao, B. Fang, *Separation and Purification Technol.*, 67, 50-57 (2009).

[101] S. Yanagida, A. Nakajima, T. Sasaki, Y. Kameshima, K. Okada, *Chem. Mater.,* 20, 3757-3764 (2008).

[102] S. Yanagida, A. Nakajima, T. Sasaki, T. Isobe, Y. Kameshima, K. Okada., *Appl. Catal. A: Gen.,* 366, 148-153 (2009).

[103] M. Fournier, R. Thouvend, C. Rocchiccioli, *J Chem. Soc. Faraday Trans*., 87(2), 349-356 (1991).

[104] A. Nakajima, T. Koike, S. Yanagida, T. Isobe, Y. Kameshima, K. Okada, *Appl. Catal. A: Gen.,* 385, 130-135 (2010).

[105] G. Marci, E.Garcia-Lopez, L. Palmisano, *Catal. Today,* 144, 42-47 (2009).

[106] D. Carriazo, M. Addamo, G. Marci, C. Martin, L. Palmisano, V. Rives, *Appl. Catal. A: Gen.,* 356, 172-179 (2009).

[107] G. Marci, E.Garcia-Lopez, L. Palmisano, D. Carriazo, C. Martin, V. Rives, *Appl. Catal. B: Envir.,* 90, 497-506 (2009).

[108] M Fournier et al., *J Chem. Soc. Faraday Trans*., 87(2), 349-356 (1991)

[109] H. Kominami, Y. Ishii, M. Kohno, S. Konishi, Y. Kera, B. Ohtani, *Catal. Lett*. 91, 41-47, (2003)

[110] S. Cassaignon, M. Koelsch and J. Jolivet, *J. Mater. Sci*., 42:6689–6695(2007)

[111] Naoya Murakami Murakami, T. Kamai, T. Tsubota and T. Ohno, *Catalysis Communications,* 10, 963–966 (2009)

[112] J. Guang, C. Tang, D. Li, H. Haneda, T. Ishigaki, *J. Am. Ceram. Soc*., 87 1358-1361, (2004)

[113] W. K. Li, X. Q. Gong, G. Lu, A. Selloni, *Phys. Chem. C,* 112 6594-6596 (2008)

[114] T. Shibata, H. Irie, M. Ohmori, A. Nakajima, T. Watanabe, K. Hashimoto, *Phys. Chem. Chem. Phys*., 6, 1359 -1362 (2004)

[115] P. Novotna, J. Krysa, J. Maixner, P. Kluson, P. Novak, *Surf. Coat. Technol*., 204, 3570-3575 (2010).

[116] M. Bellardita, A. Di Paola, L. Palmisano, F. Parrino, G. Buscarino, R. Amadelli, *Appl. Catal. B: Environ.*, 104, 291-299 (2011).

Table 1. Reported band gap energy for each polymorph of TiO_2

Year	Method	Band gap energies (E_g)/ eV			Ref.
		rutile	anatase	brookite	
Calculation					
1985	Extended Huckel MO calculations and Double-zeta functions for the 3d orbit & of Ti.	3.02	3.23	3.14	[33]
2012	A combined density functional theory (DFT) and perturbation theory •Heyd, Scuseria and Ernzerhof (HSE06)	3.39 (d)	3.60 (id)	3.30 (d)	[34]
Experiment					
2007	UV--vis spectra	3.00	3.19	3.11	[35]
2008	Reflectance spectra analysis using the Kubelka--Munk formalism	3.00 (id) 3.37 (d)	3.21(id) 3.53 (d)	3.13 (id) 3.56 (d)	[32]

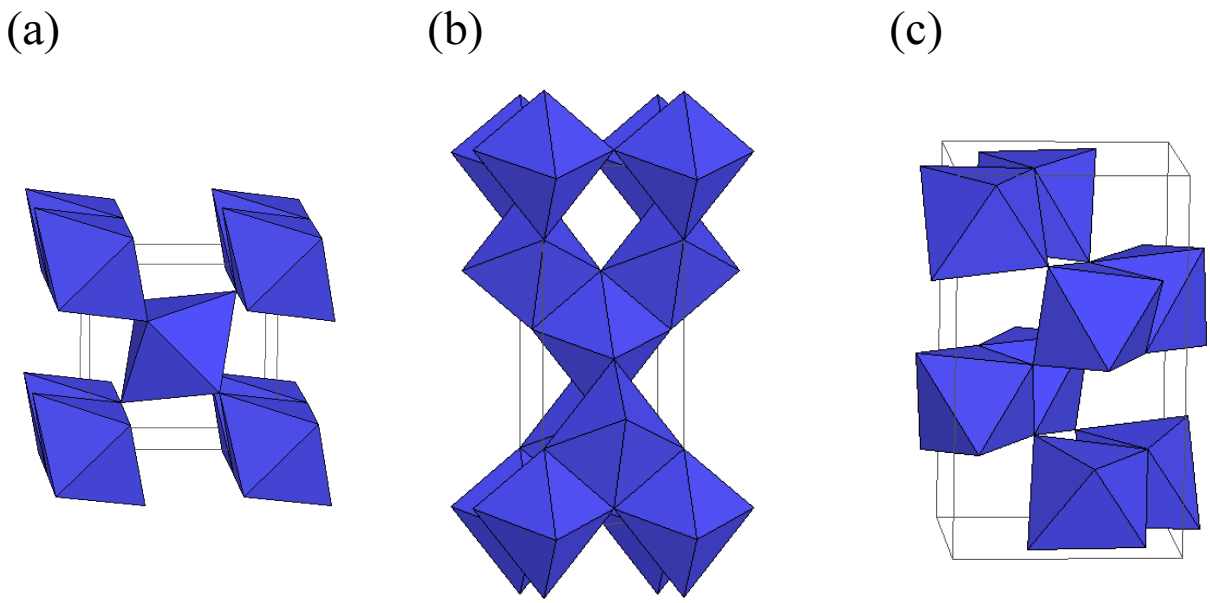

Figure 1-1. Band energy diagram for (a) rutile (b) anatase and (c) brookite

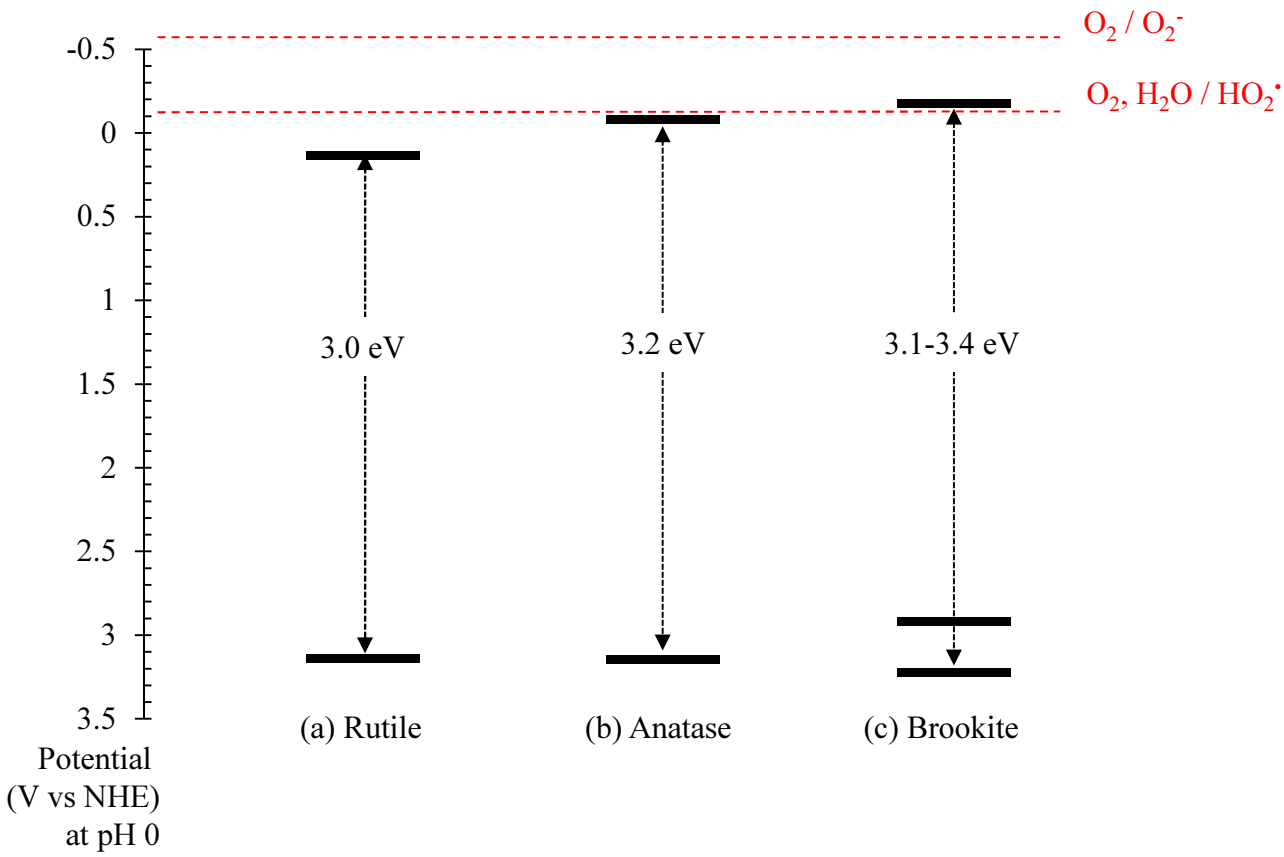

Figure 2. Band energy diagram for (a) rutile (b) anatase and (c) brookite

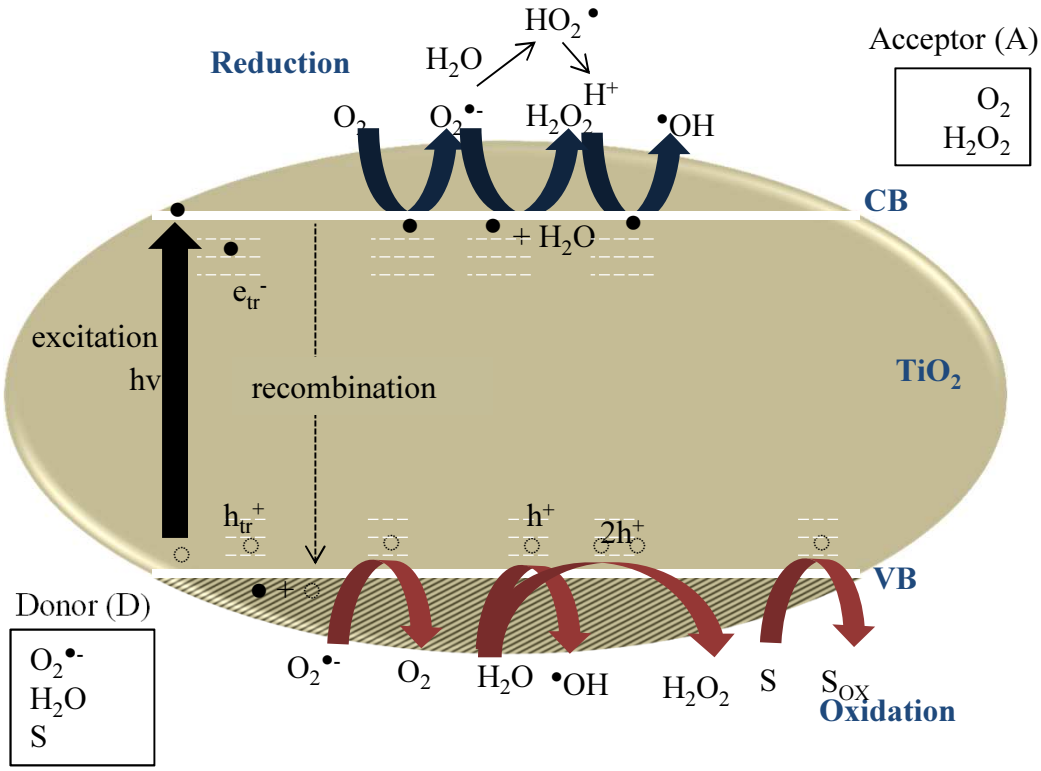

Figure 1-3. Photocatalytic mechanism and their related electrochemical reaction

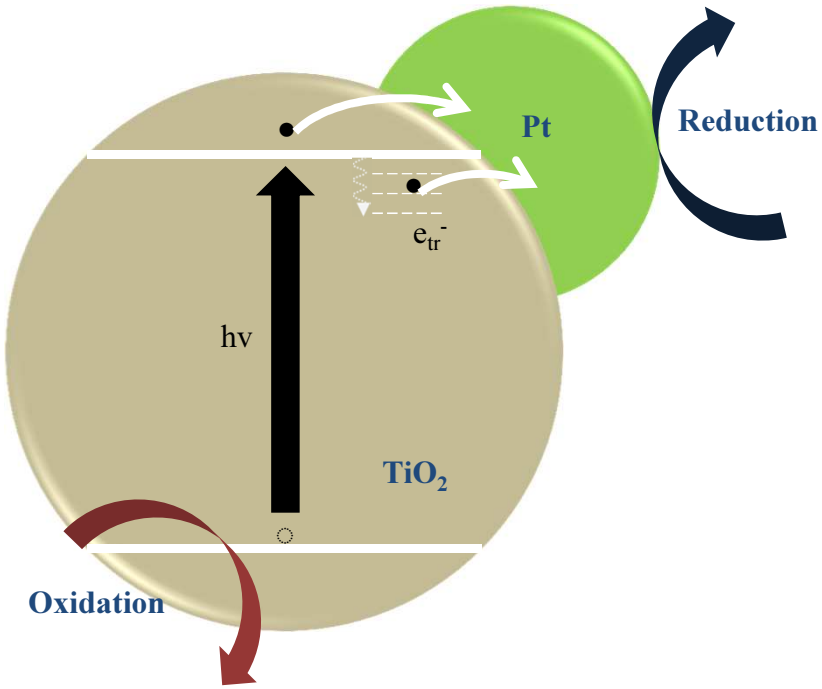

Figure 1-4. Schematic illustration of the electron transportation in Pt–TiO_2 cocatalyst.

(a) Keggin structure, $XM_{12}O_{40}^{n-}$

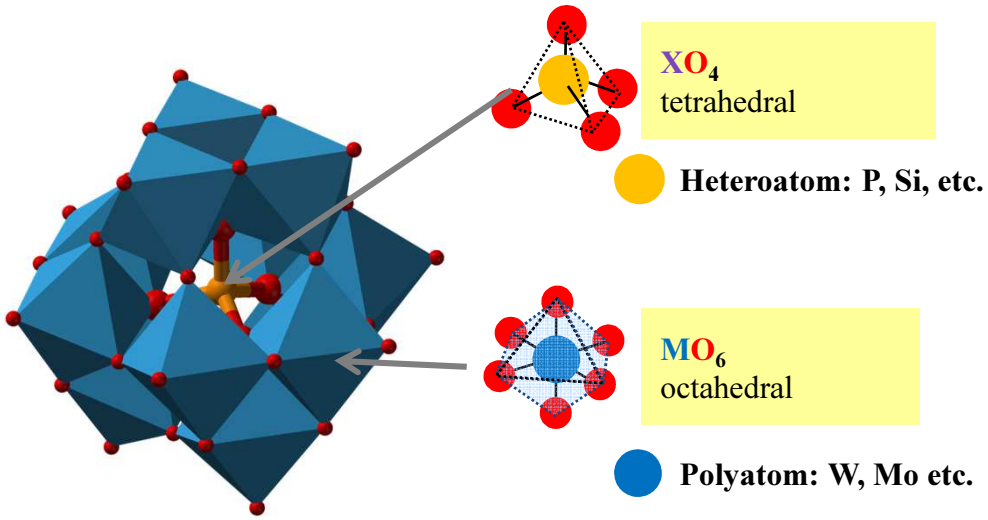

(b) Dawson structure, $X_2M_{18}O_{62}^{n-}$

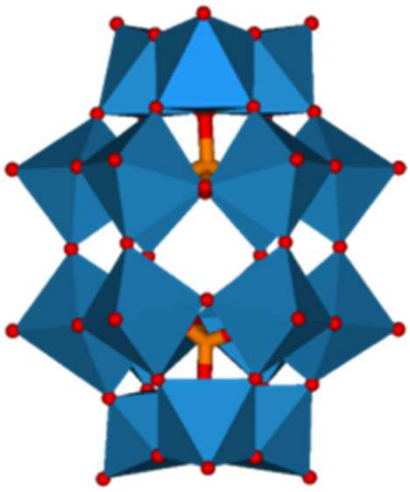

Figure 1-5. Schematic illustration of the structure of heteropolyacid structure: (a) Keggin structure, and (b) Dawson structure..

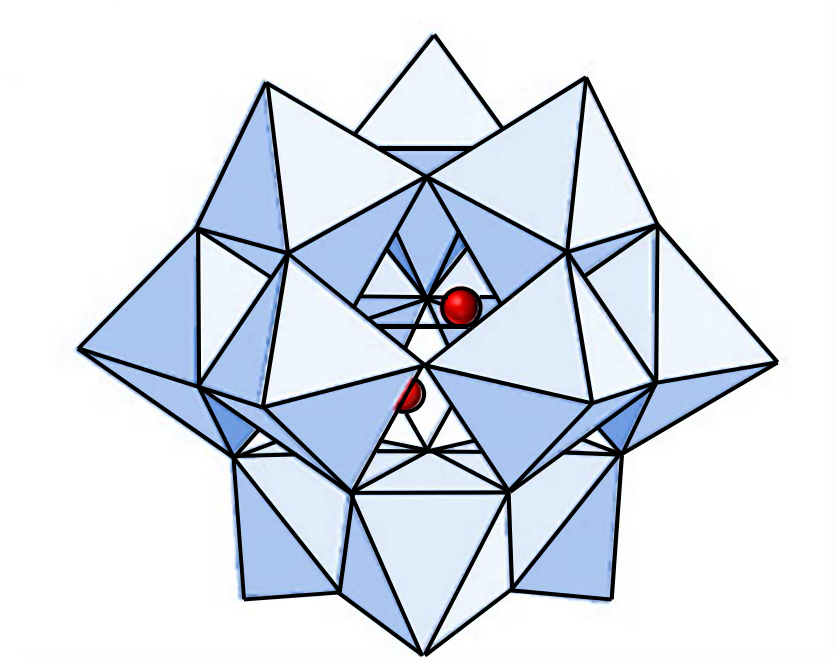

Figure 1-6. Polyhedral representation of the metatungstate anion $[\alpha\text{–}H_2W_{12}O_{40}]^{6-}$

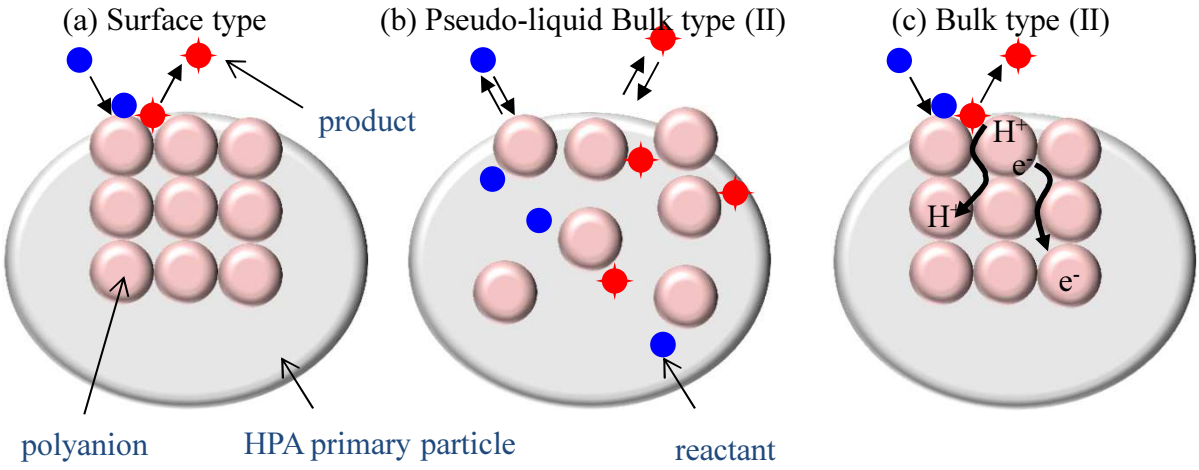

Figure 1-7. Three types of catalysis for solid heteropoly compounds: (a) surface type and (b) pseudoliquids of bulk type (i) and (c) bulk type (II).

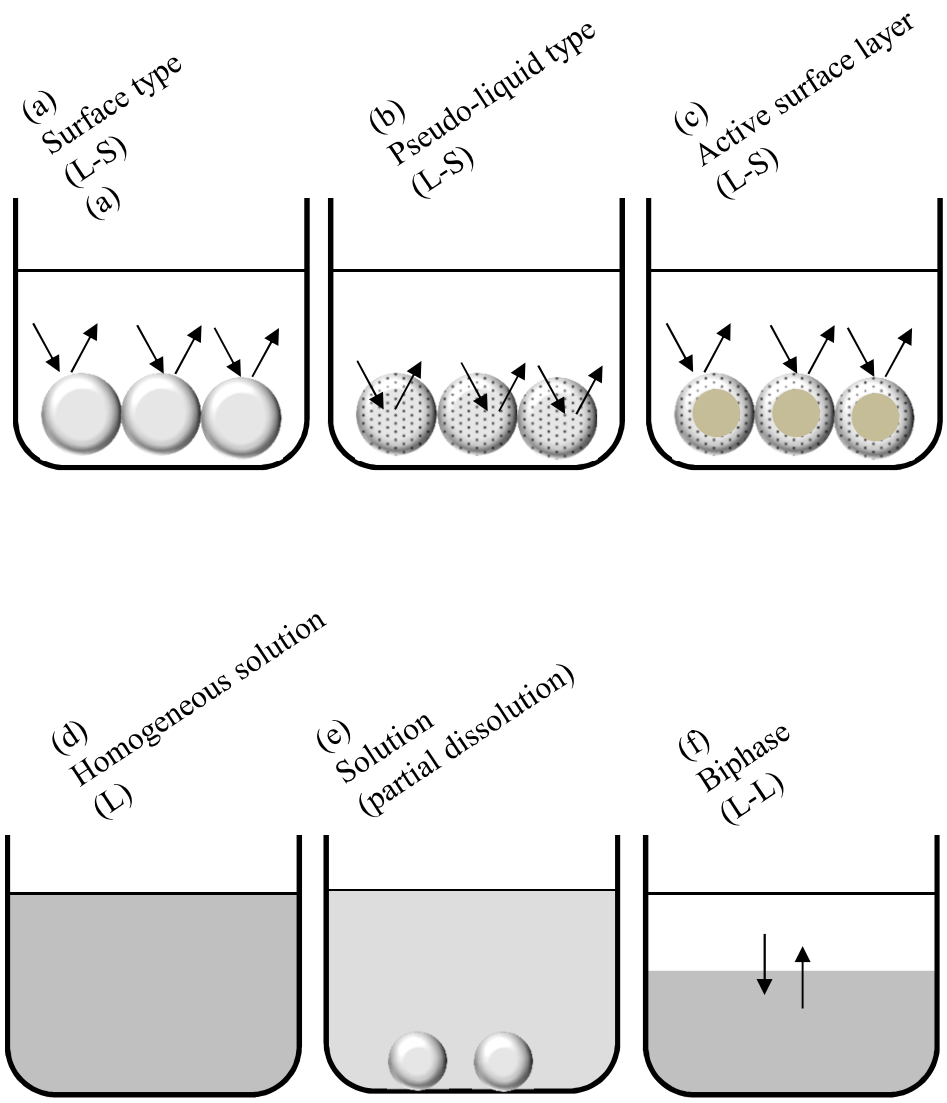

Figure 1-8. Various reaction fields of HPA catalysis in reaction systems containing a liquid phase.

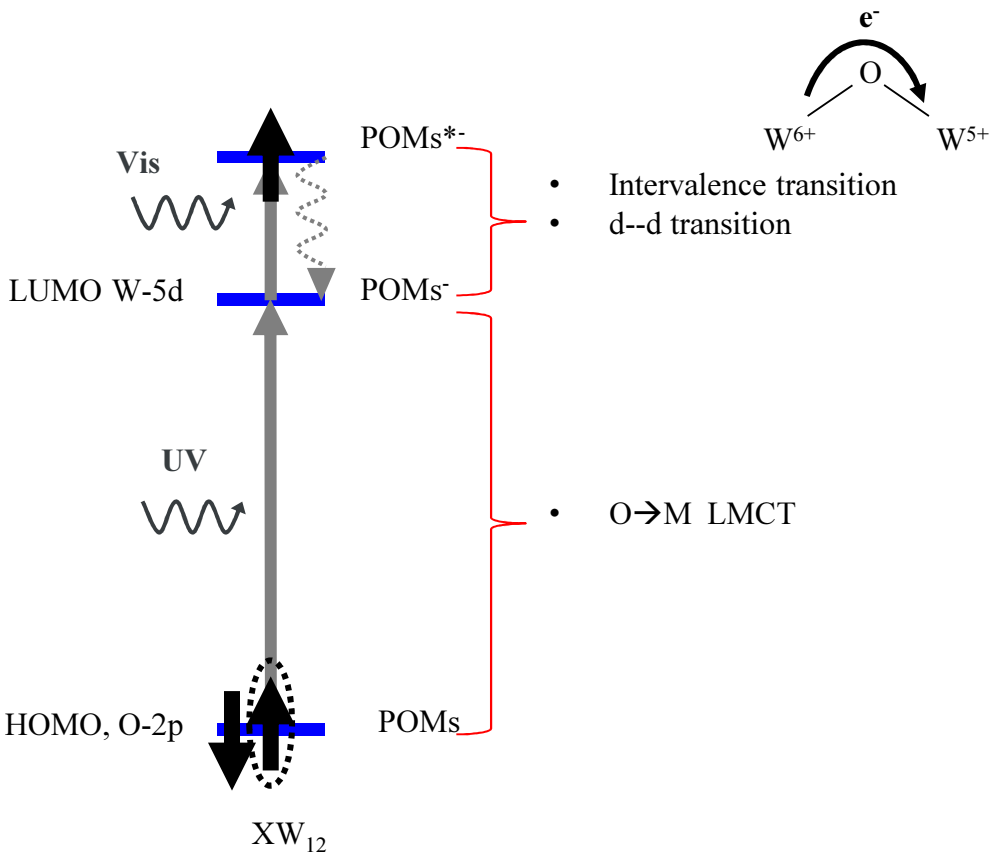

Figure 1-8. Band structure for heteropolyacids.

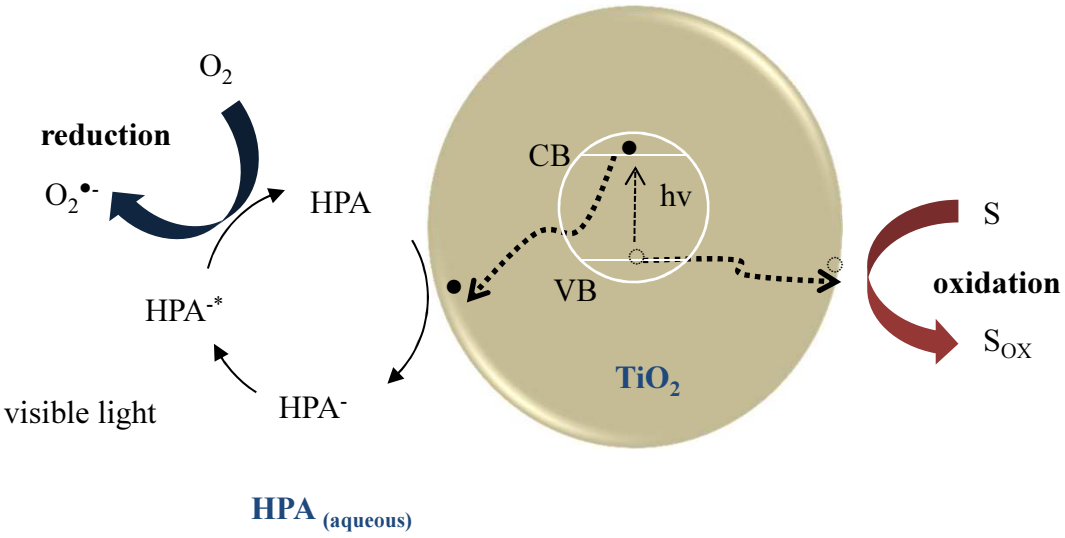

Figure 1-9. Z-scheme for TiO_2-HPAs..

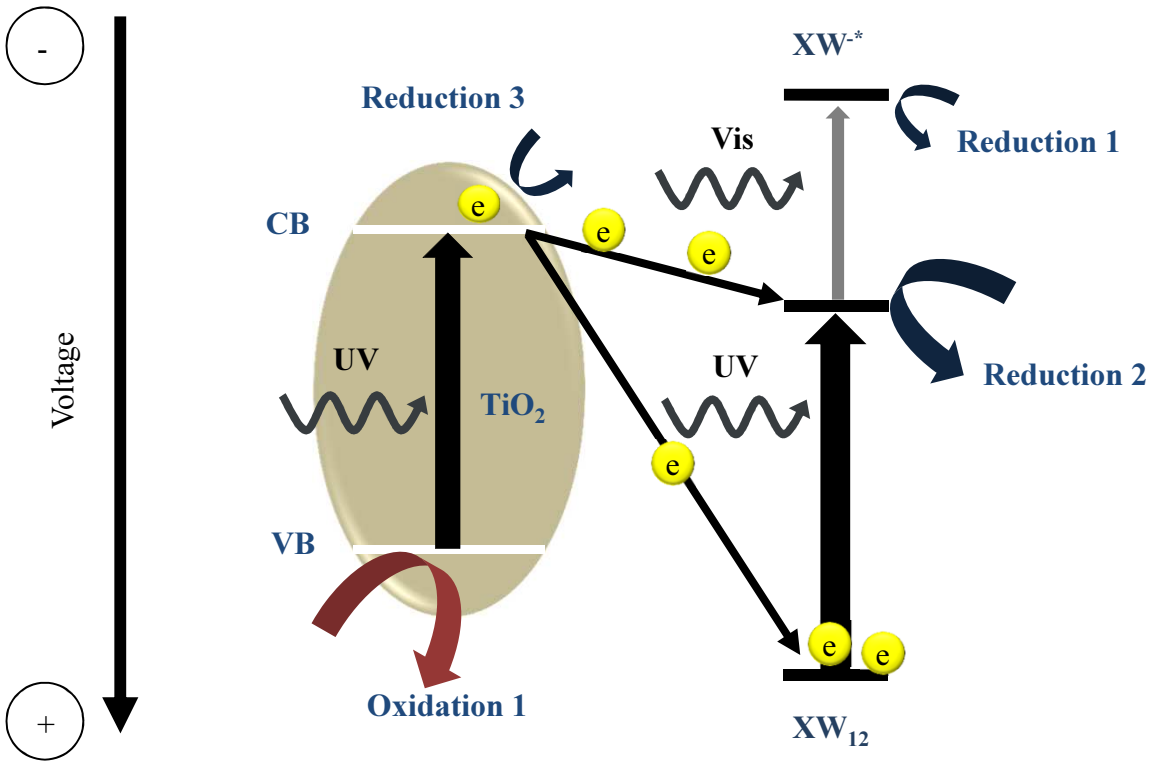

Figure 1-10. Redox system and the band energy for anatase-XW_{12}.

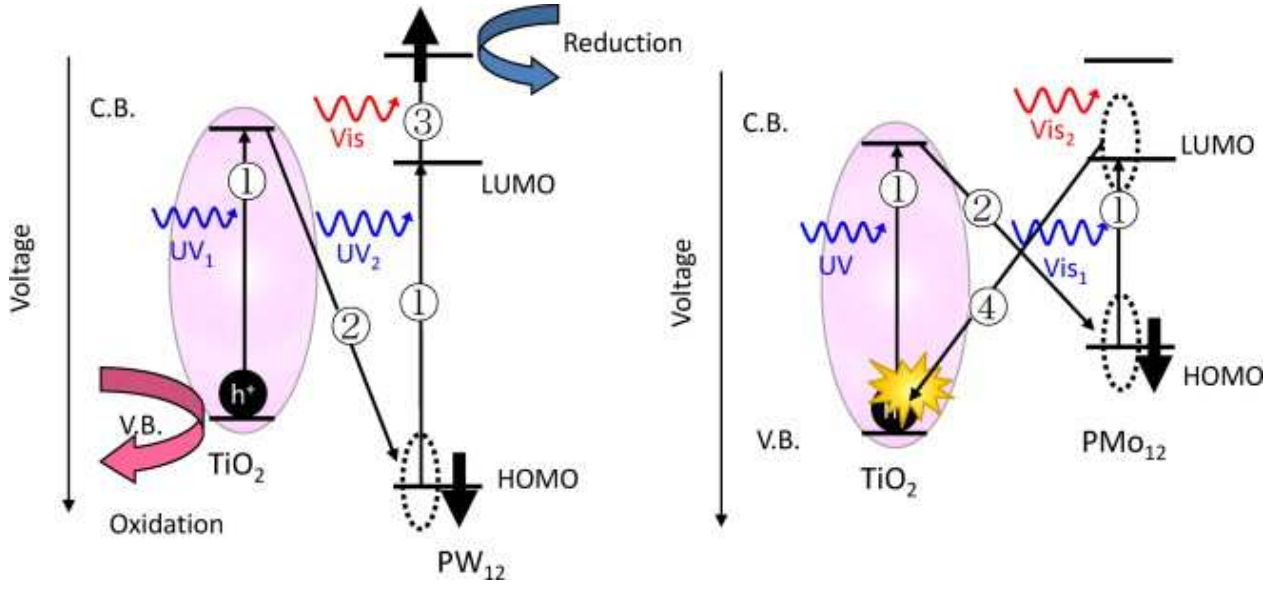

Figure 1-11. Electron transfer pathways of a PMo_{12}/TiO_2 system and a PW_{12}/TiO_2 system.

CHAPTER 2

Photocatalytic activity and its stacking order of transparent $[PW_{12}O_{40}]^{3-}$/brookite hybrid films

2.1. Introduction

2.1.1. Layer-by-layer method

Layer-by-layer (LBL) method is a self-assembly process in which different kinds of materials are alternatively deposited layer by layer. The LBL composite-thin-film-preparation method used for decades **[1,2]**. Spontaneous deposition results from strong electrostatic attraction on charged surface and oppositely charged molecule in the solution. **Figure 2-1** depicts the preparation of alternative polyanion–polycation film on planar substrate **[2]**. It is an easy and simple process. Naturally, the surface charge of colloid particles depends on pH so surface charge of many materials can be controlled. Various materials can be composited via LBL method including polyelectrolyte and other charged materials. Moreover, with LBL, layer thickness of the film is easily controlled by building block materials, layer number or deposition condition (e.g. deposit time, temperature and rinse solution). This technique also suits in-planar substrates such as sphere shape and quite independent of the initial surface roughness of the substrate. Not only electrostatic, as Quinn et al. reviewed, but also alternative driving forces such as hydrogen bonding and covalence interaction, drive self-assemble LBL process for uncharged material thin film **[3]**.

Sasaki et al. studied about TiO_2/polyion films by LBL assembly process **[4,5]**. TiO_2 colloidal particles are amphoteric: able to react with either acid or base. Therefore, pH

of their surrounding media can give positively or negatively charged on their surface. TiO_2 colloid surface is positive in acid suspension. Polydiallyldimethylammonium chloride (PDDA), which is polycation, and poly(sodium 4-styrene sulfonate) (PSS), which is polyanion, were used as the counter polyions for the growth of TiO_2 film. The structure of PSS and PDDA is shown in **Figure 2-2**. Key factors affecting the adsorption of TiO_2 are deposition time and concentration of TiO_2 suspension.

2.1.2. HPAs-TiO_2 via LBL process

Recently, Yanagida et al. prepared transparent $(XW_{12}/TiO_2)_n$ (n = times of bilayer deposition) hybrid thin films using layer-by-layer (LBL) method. We then investigated their photocatalytic decomposition activity using gaseous 2-propanol (IPA) **[6]**. The photocatalytic activity order of hybrid film under UV illumination is shown here: $(H_2W_{12}/TiO_2)_6 > (SiW_{12}/TiO_2)_6 > (PW_{12}/TiO_2)_6$. However, $(PW_{12}/TiO_2)_6$ was increased by the illumination of UV with visible light. Results suggest that second-step photoexcitation using visible light increased the reduction rate of PW_{12} and increased the charge separation efficiency. Moreover, we investigated effects of heteroatoms and polyatoms on these hybrid thin films using various tungstate, molybdate, and tungsto molybdate materials. However, the stacking-order dependence of photocatalytic activity on the hybrid films was not well investigated. Moreover, all of those earlier studies were conducted using anatase-type nanoparticles as a TiO_2 source.

Using the same method for this study, we hybridized PW_{12} with brookite-type TiO_2 nanoparticles. Then, their photocatalytic activities were evaluated using gaseous IPA decomposition. Moreover, the effect of stacking order on the entire photocatalytic activity was examined using counter polymers.

2.2. Experimental procedure

2.2.1. Preparation and Characterization of Brookite powder

The starting TiO_2 suspension (NTB 01, 15 wt% TiO_2, pH 4; Showa Denko K.K., Japan) was dried at 60 °C in air for one day, which produced the dry powder. The crystalline phase was evaluated using X-ray diffraction (XRD; XRD-6100, Shimadzu Corp., Japan) and Raman spectrophotometry (Ramanor T64000; Jobin Yvon Co., France). The chemical composition of the materials was evaluated using X-ray fluorescence analysis (XRF, RIX2000; Rigaku Corp. Tokyo Japan). The specific surface area of the powder was evaluated using BET method with N_2 (Autosorb-1; Quantachrome Instruments, Boynton Beach, FL, USA). The morphology and powder size in the starting TiO_2 suspension were observed using a transmission electron microscope (H-9000UHR; Hitachi Ltd., Japan). The band gap of the dry powder was evaluated from the diffuse reflectance spectra **[6]** using a UV–VIS–NIR scanning spectrophotometer (UV-2450; Shimadzu Corp., Tokyo Japan). Moreover, the flatband potential for brookite was also evaluated using Mott–Schottky plot. The commercial brookite sol used for this study was coated onto a transparent oxide coated glass substrate (15Ω/sq resistivity, High-durability Transparent Conductive Oxide film, TCO; Geomatec Co. Ltd., Yokohama, Japan) using dip-coating. Then the film was heated at 400 °C for 1 h in air. The coating procedures were repeated seven times. The electrolysis solution for Mott–Schottky plot was prepared by dissolving Na_2SO_4 (0.5 M) into commercial buffer solutions. Practical pH value of the solutions was 3.68. The brookite-coated electrode was soaked into the solution with Pt (counter electrode) and Ag/AgCl electrodes; then Mott–Schottky plots were measured using a potentiostat (HZ-500; HD Hokuto Denko Co. Ltd., Kanagawa, Japan). The voltage was changed from -1 V to +0.4 V. Frequencies used in the

measurements were 215.4 Hz and 2154 Hz. The procedures for measurement flatband potential are depicted in **Figure 2-3**.

2.2.2. Preparation and characterization of $(XW_{12}/TiO_2)_n$ films

For $(XW_{12}/TiO_2)_3$ film preparation (**Figure 2-4**), a commercial brookite aqueous suspension (NTB 01, 15 wt% TiO_2, pH 4; Showa Denko K.K., Japan) was used as the starting material. This suspension was diluted to concentrations of 0.05–0.5 g/l (0.05, 0.1, 0.3, 0.5 g/l), and the pH value was adjusted to 1.5 using a HNO_3 aqueous solution because PW_{12} requires pH lower than 2 to avoid a hydrolysis reaction and TiO_2 needs low pH to maintain its well dispersion state in the suspension. For these experiments, 12 tungsto(VI) phosphoric acid n-hydrate ($H_3(PW_{12}O_{40})nH_2O$; Wako Pure Chemical Industries, Ltd., Japan) or ammonium metatungstate hydrate ($(NH_4)_6[H_2W_{12}O_{40}]$, Stream Chemical, USA) was used with no purification. These chemicals were also dissolved into diluted HNO_3 aqueous solution to reach a concentration of 0.5–2 mM (0.5, 1, and 2 mM).

A quartz glass plate (30 mm × 60 mm × 1 mm; Tosoh Corp. Japan) was washed and soaked in HCl and methanol mixture (1:1) for 30 min and then soaked into conc. (95%) H_2SO_4 for another 30 min. The substrate was washed using distilled water. Then it was immersed into prepared PW_{12} solution for 20 min. The substrate surface is positively charged in acid solution. Therefore, the first layer of PW_{12} molecules was adsorbed onto the surface of substrates by Coulombic potential. Subsequently, the sample was rinsed twice in pH 1.5 HNO_3 aqueous solutions and dried at 60 °C in the oven under air atmosphere until dry. To grow the next TiO_2 layer on PW_{12}, the $(PW_{12})_1$ film was immersed again into brookite suspension. The brookite particles have a

sufficient positive charge for maintaining a well-dispersed state and for LBL coating using Coulombic attraction with a polyacid ion. Rinsing twice in HNO_3 and drying at 60 °C in an oven were also conducted, which produced $(PW_{12}/TiO_2)_1$ film. These procedures were repeated twice to obtain three bilayers $(PW_{12}/TiO_2)_3$. Identical procedures were also performed for preparation of other films.

The control $(PW_{12})_3$ films and $(TiO_2)_3$ films were prepared using either poly diallyldimethylammonium chloride (PDDA, typical Mw 100,000–200,000, 20 wt% aqueous solution; Aldrich Chemical Co., Inc.) or poly sodium 4-styrene sulfonate (PSS, average Mw ca. 70,000, 30 wt% aqueous solution; Aldrich Chemical Co., Inc.) as counter polymers. After coating, UV illumination (66 mW/cm^2 at λ = 365 nm) was conducted for the photocatalytic decomposition of counter polymers using a Hg–Xe lamp for 6 h.

Using these polymers, films with different stacking order such as (PW_{12}→TiO_2→TiO_2 (PTT), TiO_2→PW_{12}→TiO_2 (TPT), and TiO_2→TiO_2→PW_{12} (TTP)) were also prepared. **Table 2-1** shows prepared films with their abbreviation and schematic of their stacking structure. Detailed procedures for the control films were described in an earlier report **[6]**. In the present study, we controlled UV absorbance of TiO_2 in all films prepared to almost identical values.

The UV–VIS spectra were also measured at each coating step using a different UV–VIS-NIR scanning spectrophotometer (V-630; Jasco Corp., Tokyo, Japan). X-ray photoelectron spectroscopy (XPS, PHI Quantera SXM; PHI Co., U.S.A.) with an Al Kα X-ray source (1468 eV) was used to evaluate the Ti and W concentration ratio on the film surface at different LBL step. The $(PW_{12}/TiO_2)_3$ films morphology and thickness were evaluated through direct observation of the top surface and crosscut section using

a field emission scanning electron microscope (FE–SEM, S4500; Hitachi, Ltd., Tokyo, Japan). Surface roughness of the film was evaluated in 500-nm-square area by atomic force microscopy (AFM, JSPM-5200; JEOL, Tokyo, Japan) with a Si cantilever (NSC36-b; Mikromasch, Narva Mtn., Estonia).

2.2.3. Evaluation of photocatalytic activity

To preparation of 2-propanol standard gas, reagent grade 2-propanol (2 mL, 99.5% purity; Wako Pure Chemical Industries Ltd., Japan) was injected into a 1 L glass bottle which was filled with ambient air. The bottom was sealed tightly with injection rubber; then it was kept in the dark under constant temperature (20 °C) for 24 h. The liquid–vapor equilibrium condition was obtained under this condition. The concentration of gaseous 2-propanol (IPA) inside of the glass bottle was estimated using the following equation.

$$C = \frac{P_{IPA}(T)}{P_{atm} + P_{IPA}(T)}$$

In that equation, C is the gaseous IPA concentration

$P_{IPA}(T)$ is the saturated vapor pressure of IPA (cal. 4.4 kPa)

P_{atm} is the atmospheric pressure (cal. 101.3 kPa)

Consequently, the gaseous IPA concentration in the bottle is the following.

$$C = \frac{4.4}{101.3 + 4.4} \times 10^{-6} \quad ; \text{ppm}$$

With this concentration, gas-injection amount, which determines the initial IPA concentration in the 500 ml sample set, is calculated. Photocatalytic activity was evaluated using the decomposition of gaseous IPA.

Before measurement, prepared films were exposed to UV light (1 mW/cm^2, 365 nm) for 30 min to remove organic compounds adsorbed onto the surface. A Pyrex glass vessel (500 mL volume) with a quartz glass lid was used as a batch reactor shown in **Figure 2-5**. A sample film was set at the center of the vessel; then the atmosphere in the reactor was replaced using a gas flow (1.0 L/min, 5 min) of air at 20 °C and 80% relative humidity. Subsequently, the vessel was sealed. Then 2-propanol standard gas was injected into it. The injected gas amount was equivalent to that for 500 ppm concentration. The vessel was then stored in the dark for 5 h.

After the adsorption equilibrium was confirmed, UV illumination was conducted using a UV illuminator (LA-410UV-1; Hayashi Watch Works Co., Ltd., Japan) equipped with a Hg–Xe lamp. This light source includes several peaks in the 280–450 nm range, with the strongest peak at 365 nm **[6]** (See **Figure 2-7 (a)**). The illumination intensity at the sample surface was adjusted to 1 mW/cm^2 at 365 nm (even when filters were used). The photocatalytic decomposition pathway of IPA has been studied extensively **[7–10]**. The molecule of gaseous IPA is initially decomposed into acetone, and finally decomposed to H_2O and CO_2. The photocatalytic decomposition rate of acetone by TiO_2 photocatalyst is much slower than that of IPA because of displacement by water vapor from the TiO_2 surface **[26]** and because of the reaction rate difference from ·OH radical **[10]**. In the present study, the IPA, acetone, and CO_2 concentrations were evaluated every 30 min or 1 h for 5 h using a gas chromatograph (GC-14A; Shimadzu Corp., Tokyo, Japan) equipped with a flame ionization detector (FID), a methanizer, and a Sunpak-A column (Shimadzu Corp.). The carrier gas was nitrogen. The respective temperatures for the detector and injection port were 230 °C and 200 °C. The initial column temperature was 50 °C, which was maintained for 2.5 min. The

temperature was increased 20 °C/min to 130 °C to achieve peak separation. This experiment procedure is shown in **Figure 2-6**.

Two colored glass filters were used to limit the wavelength range of light illumination: UV-33 (absorbed UV < 330 nm; Asahi Glass Co., Ltd., Japan) and UV-D33S (absorbed visible light > 400 nm; Asahi Glass Co., Ltd.); see **Figures 2-7b and 2-7c** respectively. In both the UV-limited and Vis-limited case, the illumination intensity was 1 mW/cm^2 at 365 nm. Other experimental conditions were identical to those of the all-light illumination cases.

2.3. Results and discussion

2.3.1. Characterization of brookite

The specific surface area of dried brookite powder was 174 m^2/g. **Figure 2-8** shows the XRD pattern and Raman spectra of the powder. Although the peaks of brookite by XRD pattern resemble those of anatase, the obtained Raman spectra coincided well with those described in previous reports on brookite **[11]** (such as 128, 153, 247, 322 and 636 cm^{-1}, whereas the spectra of commercial anatase powder (ST-21; Ishihara Sangyo Kaisha, Ltd., Japan) provided peaks at 144, 397, 515, and 639 cm^{-1} under the same measurement conditions.). This result confirmed that crystalline phase of the TiO_2 in the suspension used for this study was brookite. Subsequent XRF analysis revealed that the powder had greater than 99% purity of TiO_2. **Figure 2-9** presents TEM image of the TiO_2 powder. The particle sizes are 5–20 nm. Their morphology was a square plate-like shape, as reported by Shibata et al. **[12]**.

For diffuse reflectance spectra, the Kubelka–Munk (KM) function is used extensively to obtain information (diffuse reflectance) related to the absorption and scattering term **[13–14]**.

$$\mathrm{F(E)} = \frac{\mathrm{a(E)}}{\mathrm{S(E,r)}} = \frac{(1 - \mathrm{Rd(E,r)})^2}{2(RdE,r)}$$

In that equation, F is the KM function.

a is the absorption coefficient.

S is the scattering coefficient

Rd is the relative diffuse reflectance (this experiment used $BaSO_4$ as a reference)

E is the photon energy

r is the particle radius

A UV–Vis spectrophotometer was used in reflectance mode. The data were reported as % diffuse reflectance against each wavelength. The dependence of scattering on photon energy is not constant. In general, the KM-function is assumed as an apparent a(E). Therefore, we can calculate apparent absorbance using the diffuse reflectance.

$$\mathrm{a(E)} = \frac{(1 - \mathrm{Rd(E,r)})^2}{2Rd(E,r)}$$

Photon energy is calculated from the following.

$$\mathrm{E} = \frac{hc}{\lambda} = \frac{(6.62 \times 10^{-34})(3 \times 10^{8})}{\lambda_{(\mathrm{m})}} \quad ; unit = \ Joule$$

An electron volt is the energy necessary to raise an electron through 1 volt. Thereby 1 eV = 1.602×10^{-19} J.

$$\mathrm{E} = \frac{hc}{\lambda} = \frac{(6.62 \times 10^{-34})(3 \times 10^{8})}{\lambda_{(\mathrm{m})}(1.602 \times 10^{-19})} = \frac{1.24}{\lambda_{(\mu\mathrm{m})}} \quad ; unit = \ eV$$

The band gap is estimated by the X-axis interception of the $a(E)^{1/n}$ and the photon energy. In addition, n is ½ for direct transition; n is 2 for indirect transition. For brookite, its optical response remains controversial: whether for direct or indirect transition, the reported values are around 3.1–3.4 eV **[15–16]**. The band-gap of the powder was calculated as 3.18 eV from diffuse reflectance spectra by assuming direct transition (see **Figure 2-10**). This value is nearly equal to the previously reported value **[17]**.

For TiO_2 (n-type semiconductor), the flatband potential (E_{FB}) is the position of its Fermi level; it is always slightly below the conduction band edge. Consequently, the flatband potential is used to state the lower edge of conduction band (CB) **[18]**. The conduction band edge of TiO_2 can be measured as the flatband potential from the Mott–Schottky relation **[19]**.

$$\frac{1}{C_{sc}^2} = \frac{2}{\varepsilon\varepsilon_0 q N_D}\left(E_{appl} - E_{FB} - \frac{kT}{q}\right)$$

In that equation, the following variables are used.

C_{sc} = capacitance of the space charge region

q = electron charge (1.602×10^{-19} C)

ε = dielectric constant of the semiconductor

ε_0 = permittivity of the free space (8.85×10^{-14} F cm^{-1})

N_D = donor density (electron donor concentration for n-type semiconductor or hole acceptor concentration for a p-type semiconductor)

E_{appl} = applied potential

E_{FB} = flatband potential

k = Boltzmann's constant (1.38×10^{-23} J K^{-1})

T = absolute temperature.

From the Mott–Schottky plot ($1/C^2$ vs. E), the donor density can be calculated from the slope. The flatband potential can be determined from the X intercept ($1/C^2 \rightarrow 0$) **[20]**. This model is based on the following two assumptions.

(i) The capacitance of the space charge region and that of the double layers must be considered. However, the double layer capacitance is 2–3 times greater than the space charge. Therefore, the reciprocal value of the double charge to the total capacitance is negligible.

(ii) The capacitance is calculated from the imaginary component of the impedances (Z'') given by $Z'' = 1/2\ \pi fC$.

The X intercept obtained from **Figure 2-11** was about -0.51 V. vs. Ag/AgCl (std), pH 3.68

In principle, the lattice Ti atoms are regarded as Lewis acid sites (adsorb hydroxyl ion). The bridging lattice oxygen is a Lewis base site (adsorb proton). Therefore, depending on the pH, the TiO_2 surface becomes charged either positively or negatively **[19]** as shown in the following relation.

$$TiO(O) + H^+ + e^- = TiO(OH)$$ **[21]**

Considering the acid–base equilibrium for TiO_2, the flat band potential of TiO_2 is pH dependent. Fujishima et al. proposed this relation for rutile (001), where the linear line with slope -59 mV/pH (at 25 °C) was obtained corresponding to the Nernst equation **[22]**. This relation is also works for most oxides in water.

Therefore, the flat band potential for brookite used for this study was calculated from the results as about -0.10 V vs. NHE, pH 0; (-0.51 V vs. Ag/AgCl, pH 3.68) + (0.059 × 3.68 V per pH) + (0.197 V vs. NHE) = - 0.096 V as NHE, pH 0.

2.3.2. Characterization of $(XW_{12}/TiO_2)_3$ thin films

Figure 2-12 portrays UV–Vis spectra of $(PW_{12}/TiO_2)_3$. Both PW_{12} and TiO_2 deposition increase the absorbance in the UV range. The spectra for $(PW_{12}/TiO_2)_3$ hybrid films imply that transmittance in the visible area (λ = 400–780 nm) was higher than 80%. **Figure 2-13** shows absorbance from UV–Vis spectra at 249 nm of $(PW_{12}/TiO_2)_3$ prepared using different concentrations of TiO_2 suspensions (0.05, 0.1, 0.3, and 0.5 g/l). No significant absorbance variance was found for films prepared using this difference concentration. The concentration should not be extremely high. It might cause undesired agglomeration on the film. Therefore the $(PW_{12}/TiO_2)_n$ preparation parameters are fixed for future experiments in this research: 1 mM of PW_{12} solution, 0.1g/l of TiO_2 suspensions, and 20 min immersion time. **Figure 2-14** also shows absorbance from UV–Vis spectra at 249 nm of $(H_2W_{12}/TiO_2)_3$ prepared using different immersing times (5, 10, or 20 min) in different concentrations of TiO_2 suspension (0.1 and 0.5 g/l). Nevertheless, for $(H_2W_{12}/TiO_2)_3$ prepared from 1 mM of H_2W_{12} solution, 0.1g/l of TiO_2 suspensions, and 20 min immersing time, the absorbance of TiO_2 second layer drastically increased compared with the first layer. One possibility is that H_2W_{12} anion is more negatively charged than PW_{12} causing difference of charge-balancing of H_2W_{12}/TiO_2 and PW_{12}/TiO_2 system as a result of higher deposition and coagulation of TiO_2 for H_2W_{12}/TiO_2 systems. In contrast, considering H_2W_{12} deposited on TiO_2, despite H_2W_{12} has a high anion charge (-6) raising capability of anion–anion repulsion, which obstructs the deposition onto the substrate surface itself. Coexisting NH_4 ion remedies this effect **[23]**. It is expected that, if the absorbance changes during preparation of $(H_2W_{12}/TiO_2)_3$ and $(PW_{12}/TiO_2)_3$ are equivalent, then the comparable TiO_2 amount is predictable. To prepare the matching absorbance of $(H_2W_{12}/TiO_2)_3$ and

$(PW_{12}/TiO_2)_3$,the $(H_2W_{12}/TiO_2)_n$ the preparation parameters of 1 mM of H_2W_{12} solution, 0.1 g/l of TiO_2 suspensions, 20 min H_2W_{12} immersion time and 10 min TiO_2 immersion time were fixed. The steady bilayer-step increment indicates that the thicknesses of PW_{12}/TiO_2, H_2W_{12}/TiO_2 and PSS/TiO_2 are almost equal (see **Figure 2-15**).

Figures 2-16 and 2-17 respectively show UV–Vis spectra of $(PW_{12}/PDDA)_3$, $(PSS/TiO_2)_3$ film. Both PW_{12} and TiO_2 deposition increase the absorbance in UV range. After illumination, the decreasing absorbance spectra marks the decomposition of the counter polymer by TiO_2 or PW_{12}. For $(PW_{12}/PDDA)_3$ film, the absorbance of PDDA (wavelength 400 -200 nm, mainly lower than 250 nm) disappeared after illumination for 16 h because of photocatalytic decomposition of PDDA by PW_{12}. The peak at 250 nm comes from the difference form of the supporter **[6]**. For $(PSS/TiO_2)_3$ film, PSS absorbance at wavelengths of 300–200 nm decreased after 6 h UV illumination because of the photocatalytic decomposition by TiO_2. **Figure 2-18** shows the UV–Vis spectra of $(PSS/TiO_2)_3$ film after different illumination time. The absorbance no longer decreases even if the illumination time is greater than 6 h.

Figure 2-19 presents the surface atomic ratio of W/Ti for $(PW_{12}/TiO_2)_1+PW_{12}$ (top surface is PW_{12}) and $(PW_{12}/TiO_2)_1$ films (top surface is TiO_2). **Figure 2-20** shows the surface atomic ratio of W/Ti for $(H_2W_{12}/TiO_2)_1+H_2W_{12}$ (top surface is H_2W_{12}) and $(H_2W_{12}/TiO_2)_1$ films (top surface is TiO_2) by XPS measurement. The ratio dependence on the coating cycle suggests alternative coating using this method. Additionally, the W/Ti ratios for $(PW_{12}/TiO_2)_1+PW_{12}$ and $H_2W_{12}/TiO_2)_1+H_2W_{12}$ were almost equal, representing the same concentration of PW_{12} and H_2W_{12} on TiO_2.

Figure 2-21 shows top and crosscut section views of $(PW_{12}/TiO_2)_3$, $(H_2W_{12}/TiO_2)_3$ and $(TiO_2)_3$ by SEM. The thicknesses of these films were 60–80 nm. From TEM image,

brookite primary particles were 5–20 nm. Therefore, one might infer that the TiO_2 is frequently single-particle adsorption onto the films.

The R_a values of the coatings obtained by AFM at five points on the top surface of $(PW_{12}/TiO_2)_3$, $(H_2W_{12}/TiO_2)_3$ and $(TiO_2)_3$ films were, 5–10 nm for $(PW_{12}/TiO_2)_3$ $(H_2W_{12}/TiO_2)_3$ and 4–7 nm for $(TiO_2)_3$. The AFM images of these films are shown in **Figure 2-22**.

From IR spectra in the previous work **[24, 25]**, the Keggin structure of PW_{12} was maintained after film processing. With the identical processing to those works, the existence of Keggin structure in reference $(PW_{12})_3$ films and $(PW_{12}/TiO_2)_3$ films might be inferred.

The XRD pattern of $(PW_{12}/TiO_2)_3$ is shown in **Figure 2-23**. Incident angle is 0.25 degree which corresponds to penetration depth of 10 nm. The peak is merely TiO_2 top layer. The main peak resembles to that of brookite, suggesting that the phase is retained even after film processing.

2.3.3. Photocatalytic properties

Both acetone and CO_2 were also produced during the IPA decomposition as shown in **Figure 2-24** and **Figure 2-25**. However, for the future figure, the plots are shown only the change of IPA to avoid complexity. The C represents IPA concentration and C_0 represents the initial concentration after the storage in the dark for 5 h. The practical C_0 values are shown in **Table 2-2**.

Figure 2-26 shows the IPA concentration change for the $(PW_{12}/TiO_2)_3$, $(TiO_2)_3$ and $(H_2W_{12}/TiO_2)_3$ films under all-light (no filters) UV illumination. Both $(PW_{12}/TiO_2)_3$ and

$(H_2W_{12}/TiO_2)_3$ films give better decomposition rate than that of $(TiO_2)_3$. The activity of $(PW_{12}/TiO_2)_3$ and $(H_2W_{12}/TiO_2)_3$ are quite similar; $(H_2W_{12}/TiO_2)_3$ showed only a low higher decomposition rate, irrespective of the lower reoxidation potential of PW_{12}^-.

As described in the *Introduction*, visible light is expected to be involved in XW_{12} photocatalysis mechanism as the secondary excitation especially for PW_{12}. For better understanding of the mechanism of PW_{12}/TiO_2 hybrid, primary or secondary excitation for XW_{12} was alternately cut. **Figures 2-7(b-c)** portray wavelength spectra of the light source (Hg–Xe lamp) with filters (gray region is light filtered region). The UV-33 filter cuts the wavelength of the light for the HOMO–LUMO excitation of XW_{12}, and the UVD-33S filter cuts the wavelength higher than 400 nm which the light for the excitation of reduced XW_{12} (XW_{12}^-) to XW_{12}^-* in general **[6]**.

When most UV light was cut by UV33 (see **Figure 2-27**), the IPA decomposition rate of all $(PW_{12}/TiO_2)_3$, $(TiO_2)_3$ and $(H_2W_{12}/TiO_2)_3$ decreased greatly compared with the decomposition rate under all-light UV illumination. The UV33 filter not only cut HOMO–LUMO excitation of XW_{12} but also the VB-CB excitation of TiO_2. Therefore, it is difficult to conclude that the decomposition rate decreases by the lack of HOMO–LUMO excitation of XW_{12} or the VB-CB excitation of TiO_2. However, $(PW_{12}/TiO_2)_3$ and $(H_2W_{12}/TiO_2)_3$ still showed better photocatalytic activity than $(TiO_2)_3$. This result indicates that H_2W_{12} and PW_{12} receive electrons from TiO_2.

Figure 2-28 presents the concentration change for $(PW_{12}/TiO_2)_3$, $(TiO_2)_3$ and $(H_2W_{12}/TiO_2)_3$ under light illumination through UVD33S. The IPA decomposition rate was slightly lower than the case under all-light UV illumination in $(PW_{12}/TiO_2)_3$ and $(TiO_2)_3$ films. For $(H_2W_{12}/TiO_2)_3$, the IPA decomposition rate was slightly higher than the case under all-light UV illumination. The higher and the lower decomposition rate

differences were extremely small. Accordingly, they were ignored. The activities of $(PW_{12}/TiO_2)_3$ and $(H_2W_{12}/TiO_2)_3$ are higher than that of $(TiO_2)_3$. It is clear that the activity of $(H_2W_{12}/TiO_2)_3$ is irrespective to visible light as a result of band position of $H_2W_{12}^-$, as described previously. However, PW_{12}^- presents the secondary band level on the visible light region **[26]**. Tachikawa et al. and Yanagida et al. also report reduced PW_{12} (PW_{12}^-) absorbs visible light to form an excited state PW_{12}^- (PW_{12}^{-*}), which can reduce organic compounds such as methyl viologen or methyl orange in water and 2-propanol in gas **[6, 27]**. In addition, the photocatalysis enhancement by visible light is expected in $(PW_{12}/TiO_2)_3$ because of the generation of PW_{12}^{-*}. Even so, this result suggests that the effect of visible light on $(PW_{12}/TiO_2)_3$ hybrid film on the overall photocatalytic activity is small.

Additionally, **Figure 2-29(a)** shows the IPA concentration change for the $(PW_{12}/TiO_2)_3$, $(TiO_2)_3$ and $(PW_{12})_3$ films under all-light (no filters) UV illumination. The changes of acetone and CO_2 are shown in **Figure 2-29(b)**. Results show that $(PW_{12}/TiO_2)_3$ decomposed IPA faster than $(TiO_2)_3$, although $(PW_{12})_3$ showed no IPA decomposition activity. The combination of PW_{12} to brookite increased photocatalytic activity. These results not only show that PW_{12} enhances electron–hole separation, as discussed. They also suggest that PW_{12} presents much slower reduction or oxidation rate than TiO_2.

In conclusion, TiO_2 shows largely higher activity than PW_{12} and photocatalytic activity of PW_{12}/TiO_2 binary system is almost independent from visible light used for this study. These suggest an alternative explanation for electron mass transfer in z-schematic model of PW_{12}/TiO_2 system.

When UV light is illuminated on the surface of this hybrid film, electrons are excited and holes are generated simultaneously at the valence band (VB) of TiO_2 and HOMO level of PW_{12}. Generated holes in TiO_2 oxidize IPA directly or through radical species, whereas the holes in HOMO level of PW_{12} trap electrons from TiO_2 effectively. Consequently, it is reduced to PW_{12}^-, which absorbs visible light and produces a stronger reduction power than ground-state PW_{12}^-. Ground-state PW_{12} was regenerated by O_2 reduction **[6]**. In the case presented herein, the absorbance of TiO_2 is 4–5 times greater than that described in reports of previous studies **[6, 24, 28]**. Therefore, it is expected that the amount of electrons excited in TiO_2 is larger than that in PW_{12} in the present case. $(PW_{12}/TiO_2)_3$ thin film was also prepared using an anatase suspension (STS-100, 20 wt% concentration; Ishihara Sangyo Kaisha, Ltd., Mie, Japan) used in an earlier study **[6]**. Then we examined its photocatalytic activity under the same conditions. The result is depicted in **Figure 2-30**. The photocatalytic decomposition activity against gaseous IPA for the case of brookite is higher than that for anatase. However, this result cannot be attributed simply to the crystalline phase difference. As described earlier, the absorbance of UV per layer for anatase is less than that for brookite (see **Figure 2-31**). Moreover, the specific surface area (anatase, 236 m^2/g; brookite, 174 m^2/g) and crystallinity differ. Unless the TiO_2 particles have the same physical and chemical properties, the crystalline phase dependence cannot be discussed.

For this study, **Figure 2-32** depicts the expected electron transfer scheme of the hybrid film of PW_{12} and TiO_2 (brookite). When TiO_2 received excited energy, many electron delocalize from VB to CB. Although some electrons in TiO_2 are consumed for healing holes in PW_{12}, because of numerous electrons in TiO_2 conduction band and

lower reduction rate of PW_{12}, excess electrons would transfer directly to LUMO level of PW_{12} (Some disappear by recombination with holes in TiO_2.). This study uses a Hg-Xe lamp as the light source. Even if visible light is generated, the intensity is extremely low compared with its UV intensity (see **Figure 2-7**). When the excitation efficiency by visible light to form PW_{12}^{-*} from PW_{12}^{-} is not high, Reduction 1 in **Figure 2-32** might become more important than Reduction 2 as the practical reduction path. Experimental results show that PW_{12} acts effectively as an electron scavenger and that it inhibits the charge recombination of TiO_2, consequently increasing the overall photocatalytic activity.

Base on this scheme, TiO_2 surface is expected to be main oxidation site and PW_{12} surface is also expected to be main reduction site. Because PW_{12} exists both above and below the TiO_2 layer, electrons from TiO_2 move in two directions. Hole in TiO_2 also travels randomly to TiO_2 surface and reduction and oxidation site are quite mixed inside the film. These would cause more chance of electron–hole recombination. For the optimization of electron transfer and reduction–oxidation site on TiO_2/PW_{12} hybrid film, different stacking pattern films are prepared and their photocatalytic properties are evaluated.

In **Figure 2-33**, $TiO_2/TiO_2/TiO_2/PW_{12}$ (TTTP) and $(PW_{12}/TiO_2)_3$ presented the same IPA decomposition rate under all-light UV illumination despite TTTP has lower amount of PW_{12}. Additionally, however, the PW_{12} layer exists on the bottom-most of $PW_{12}/TiO_2/TiO_2/TiO_2$ (PTTT) films, the equivalent IPA decomposition rate was obtained from $(TiO_2)_3$ and PTTT. Both PTTT and TTTP have the same amount of TiO_2 and PW_{12} but showed the different decomposition rate; TTTP significantly faster

decomposed IPA than PTTT. These results suggest that positioning of PW_{12} layer is crucial to the entire photocalytic activity of the film; topmost PW_{12} might be beneficial.

To study the effect of PW_{12} position on entire photocatalytic activity, a series of TiO_2 two layers films were prepared: TiO_2/TiO_2 (TT), $PW_{12}/TiO_2/TiO_2$ (PTT), $TiO_2/PW_{12}/TiO_2$ (TPT), and $TiO_2/TiO_2/PW_{12}$ (TTP). The results of photocatalytic activity measurements are shown in **Figure 2-34**. The activity order was TT < PTT < TPT < TTP. Therefore, the hypothesis was confirmed, as shown in **Figure 2-35**.

For the PTT film, PW_{12} exists on the bottom layer. Despite oxidation site in TiO_2 is on the top which is easy for hole oxidation. Actually, O_2 and water must penetrate through two layers of TiO_2. Insufficient O_2 and water on the PW_{12} surface decrease the reduction rate and so the entire photocatalytic activity of the PTT film. Results show that the electron–hole recombination in the top TiO_2 coating was not inhibited by PW_{12} effectively. This film exhibited the lowest photocatalytic ability among the three films. Consequently, PTT show similar photocatalytic activity of TT.

For TPT, more O_2 is able to reach the PW_{12} surface. However, O_2 and water must penetrate through the first layer of TiO_2. Electrons move in two directions against each other because of the PW_{12} position in the film (sandwiched by two TiO_2 layers). In this alignment, the bottom TiO_2 does not contribute well to the overall photocatalytic activity because holes generated in the bottom TiO_2 do not transfer to the main reaction field: the hybrid film top surface. Therefore, TPT showed moderate photocatalytic activity.

The best stacking order among these three films was TTP. Its activity was almost equivalent to that of $(PW_{12}/TiO_2)_3$ despite its smaller amounts of TiO_2 and PW_{12}. Its high photocatalytic activity is attributable to the effective electron transport in one

direction and the abundance of oxygen and water. Although PW_{12} is located on the top surface, the UV absorbance of PW_{12} is extremely small compared with that of TiO_2, as shown in UV-Vis spectra. Therefore, the existence of PW_{12} does not affect the excitation of TiO_2 remarkably. Rather, charge separation was attained on the top surface by virtue of this film alignment. The overall photocatalytic activity was increased. **Figure 2-36** shows that IPA degradation rate on TTTP was slightly faster than the rate on TTP. However, TTP and TTPT presented very similar IPA decomposition rates in the initial stage and finally IPA was decomposed completely by TTP earlier than by TTPT despite TTPT has more TiO_2 layer number. These reconfirm the importance of PW_{12} scavenger for the HPA/TiO_2 system.

2.4. Conclusion

The design of stacking order of PW_{12} and TiO_2 is necessary to obtain high photocatalytic activity from these hybrid film composites. It was deduced that electron scavenger effect of PW_{12} plays an important role in this mechanism. Among the prepared films, their photocatalytic activity was highest when PW_{12} was arranged on the film's topmost surface. The IPA decomposition rate of the (TiO_2/TiO_2/TiO_2/PW_{12}) was equivalent and (TiO_2/TiO_2/PW_{12}) film was also almost equivalent to that of (PW_{12}/TiO_2)$_3$ in spite of its smaller material amount.

References

[1] R.K. Iler, *Journal of Colloid and Interface Science*, 21, 569–594 (1966)

[2] Gero Decher, *Science*, 277,1232–1237 (1997)

[3] J. F. Quinn, A. P. R. Johnston, G. K. Such, A. N. Zelikin, F. Caruso, *Chem. Soc. Rev*., 36, 707–718 (2007)

[4] T. Sasaki, Y. Ebina, T. Tanaka, M. Harada, M. Watanabe, *Chem. Mater*., 13, 4661–4667 (2001)

[5] Z.-S. Wang, T. Sasaki, M. Muramatsu, Y. Ebina, T. Tanaka, L. Wang, M. Watanabe, *Chem. Mater*., 15, 807–812 (2003)

[6] S. Yanagida, A. Nakajima, T. Sasaki, Y. Kameshima, K. Okada, *Chem. Mater*. 20 3757–3764 (2008)

[7] P. R. Harvey, R. Rudham, S. Ward, *J. Chem. Soc. Faraday Trans*., 79, 1381–1390 (1983).

[8] Y. Ohko, K. Hashimoto, A. Fujishima, *J. Phys. Chem. A*, 101, 8057–8062 (1997).

[9] A. Mylonas, A. Hiskia, E. Androulaki, D. Dimotikali, E. Papaconstantinou, *Phys. Chem. Chem. Phys*., 1, 437–440 (1999).

[10] S. A. Lanson, J. A. Widegren, J. L. Falconer, *J. Catal*., 157, 611–625 (1995).

[11] J. Guang, C. Tang, D. Li, H. Haneda, T. Ishigaki, *J. Am. Ceram. Soc*., 87, 1358–1361 (2004).

[12] T. Shibata, H. Irie, M. Ohmori, A. Nakajima, T. Watanabe, K. Hashimoto, *Phys. Chem. Chem. Phys*., 6, 1359 –1362 (2004)

[13] P. Kubelka, F. Munk, *Zeit. Für Tekn. Physik*. 12, 593 (1931)

[14] S.K. Loyalka, C.A. Riggs, *Applied Spectroscopy*, 49, 1107–1110,(1995)

[15] A Di Paola, M Bellardita, L Palmisano, *Catalysts*, 3, 36–73 (2013)

[16] D. Reyes-Coronado, G. Rodriguez-Gattorno, M. E. Espinosa-Pesqueira, C. Cab, R. de Coss, G. Oskam, *Nanotechnology*, 19, 145605 (2008).

[17] M. Gratzel, F. P. Rotzinger, *Chem. Phys. Lett*., 118, 474–477(1985)

[18] R. van de Krol, M. Grätzel (eds) 2012, VIII, 13–67, "Principles of Photoelectrochemical Cells," Photoelectrochemical Hydrogen Production, Electronic Materials: Science & Technology, Vol. 102, Springer Science+Business Media, LLC

[19] R. Beranek, *Adv. Chem. Phys*., 786759 (2011).

[20] A.W. Bott, *Current Separation*., 17:3, 87–91 (1998)

[21] A. Fujishima, X. Zhang, D. A. Tryk, *Surface Science Reports*, 63, 515–582 (2008).

[22] A. Fujishima, A. Sakamoto, K. Honda: *Seisan Kenkyu*, 21, 450 (1969).

[23] J.J. Borrás-Almenar, E. Cororado, A. Müller, M. Pope, Polyoxometalate Molecular Science; Kluwer Academic Publishers: Dordrecht/ Boston/ London, 441–446 (2003)

[24] S. Yanagida, A. Nakajima, T. Sasaki, T. Isobe, Y. Kameshima, K. Okada, *Appl. Catal. A: Gen*., 366, 148–153 (2009)

[25] J. Edward, C.Y Thiel, B. Benac, J.F Knifton, *Catal. Lett*., 51, 77−83 (1998)

[26] T. Yamase, *Chem. Rev*., 98, 307–325 (1998)

[27] T. Tachikawa, S. Tojo, M. Fujitsuka, T. Majima, *Chem. Eur. J*., 12, 3124–3131 (2006)

[28] A. Nakajima, Y. Akiyama, S. Yanagida, T. Koike, T. Isobe, Y. Kameshima, K. Okada, *Materials Letters*, 63 1699–170,(2009)

Table 2-1. Abbreviation and structure of prepared films sample

Immersion step	Abbreviation Name	Schematic Structure
PW_{12}→TiO_2→PW_{12}→TiO_2→PW_{12}→TiO_2	$(PW_{12}/TiO_2)_3$ or PTPTPT	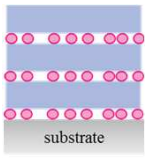
PSS→TiO_2→PSS→TiO_2→PSS→TiO_2	$(TiO_2)_3$ or TTT	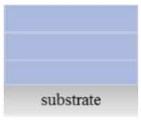
PSS→TiO_2→PSS→TiO_2→PSS→TiO_2→PW_{12}	TTTP	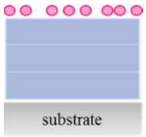
PW_{12}→TiO_2→PSS→TiO_2→PSS→TiO_2	PTTT	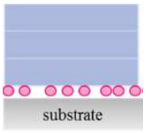
PSS→TiO_2→PSS→TiO_2	TT	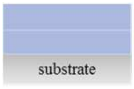
PSS→TiO_2→PSS→TiO_2→PW_{12}	TTP	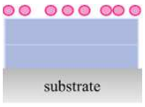
PSS→TiO_2→PW_{12}→TiO_2	TPT	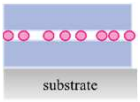
PW_{12}→TiO_2→PSS→TiO_2	PTT	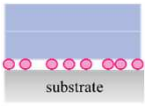

Table 2-2. Practical C_0 value

Film type	average C_0 (ppm)
$(PW_{12}/TiO_2)_3$	449
$(TiO_2)_3$	465
$(PW_{12})_3$	514
$(H_2W_{12}/TiO_2)_3$	475

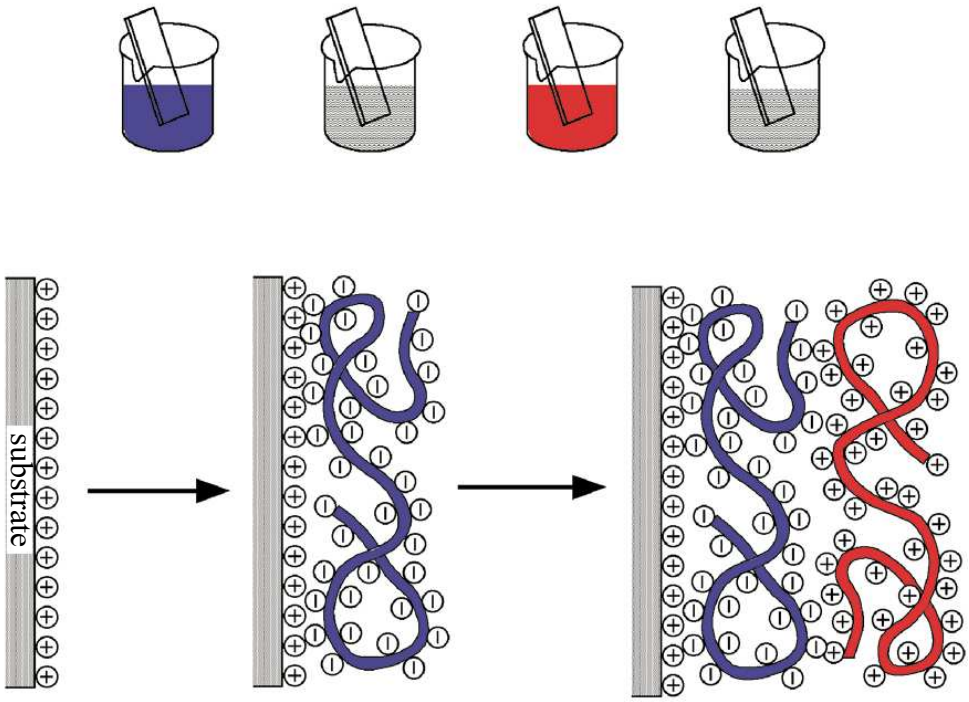

Figure 2-1. Schematic illustration of LBL method [2]

PDDA

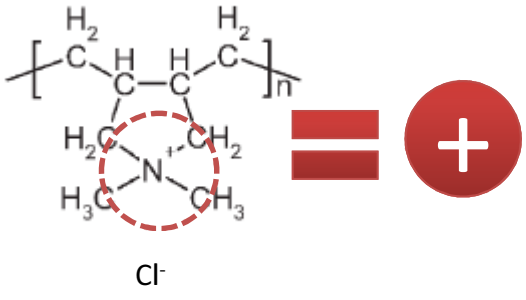

PSS

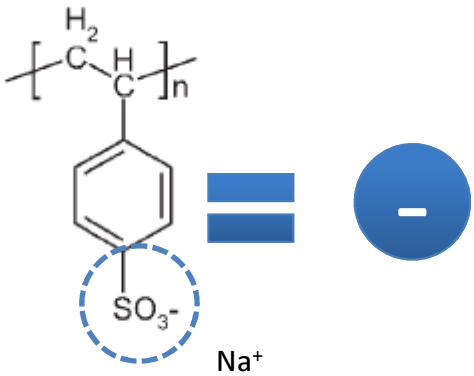

Figure 2-2. The structure of Poly(diallyldimethylammonium chloride (PDDA), and Poly(sodium 4-styrene sulfonate)

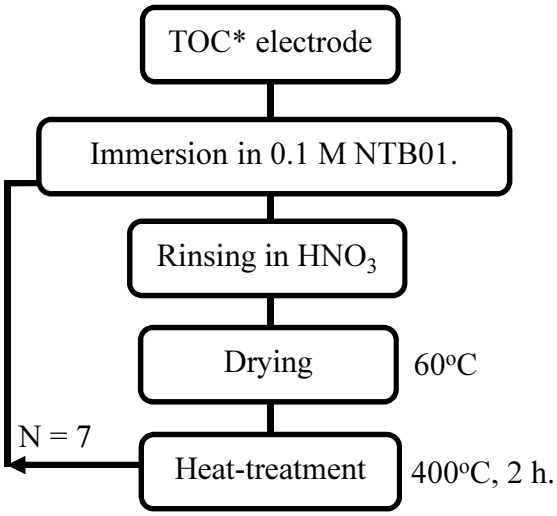

*** Transparent oxide coated**

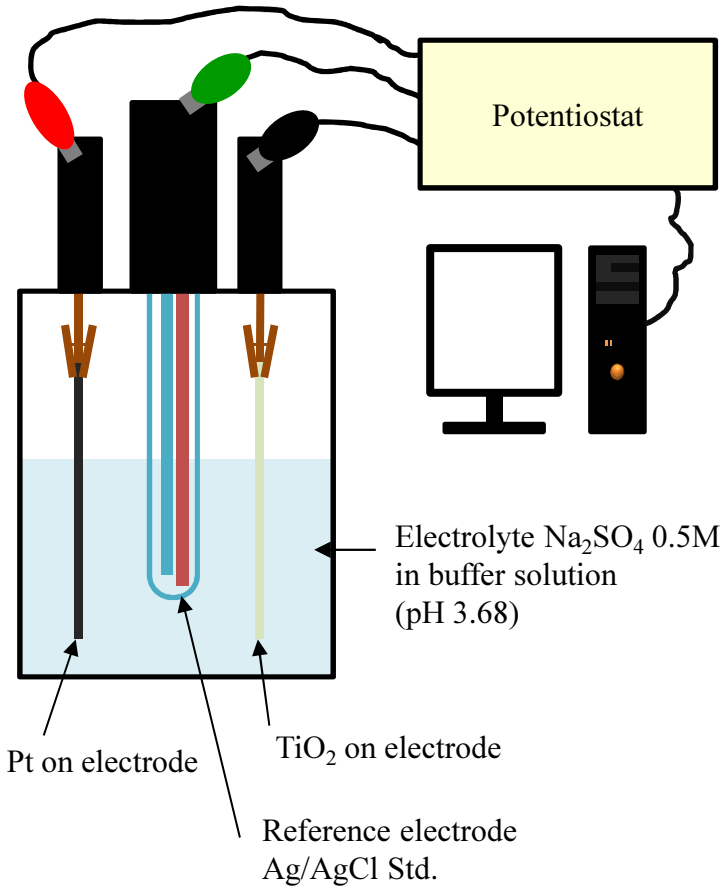

Figure 2-3. Experimental procedure of 2-propanol decomposition

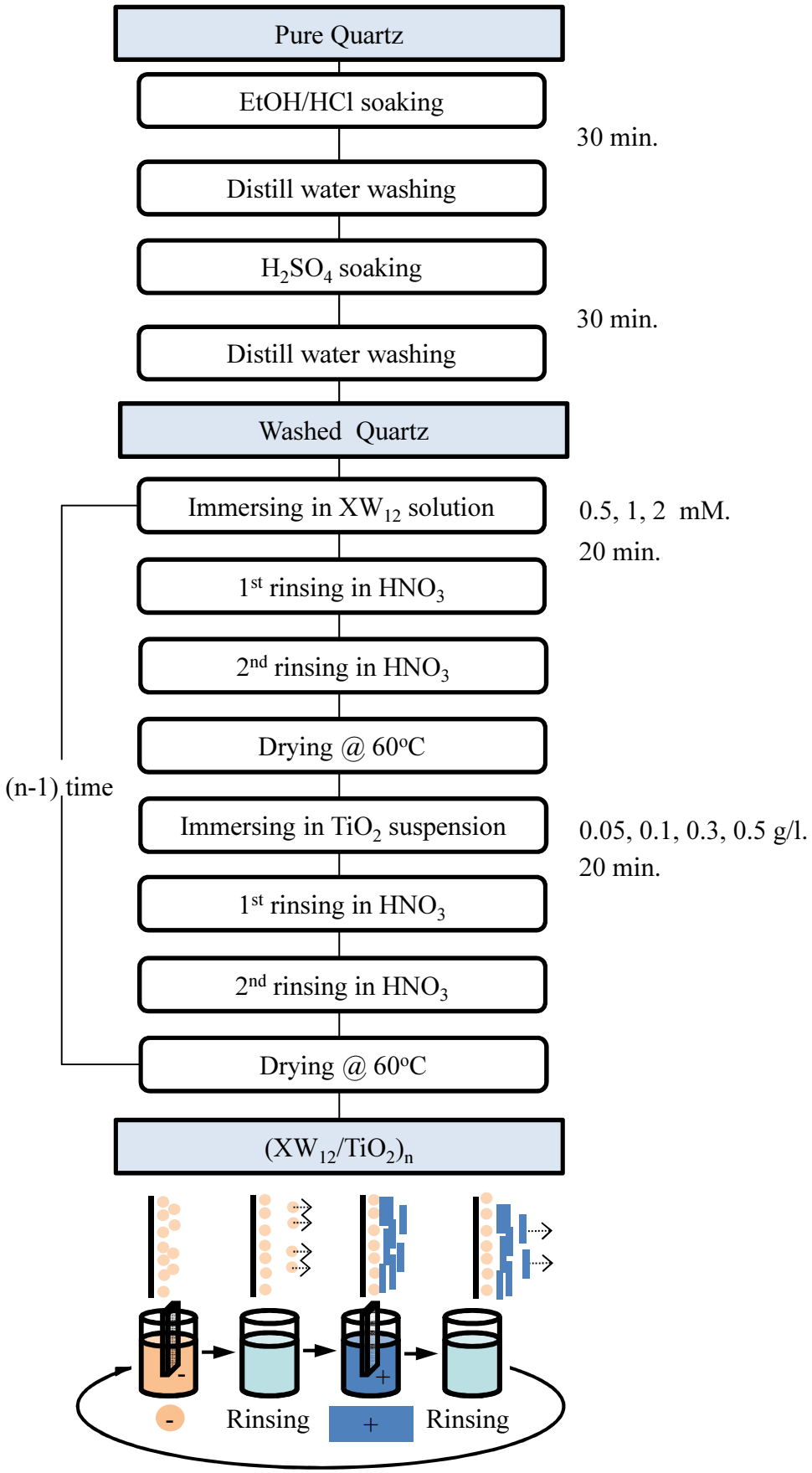

Figure 2-4. $(XW_{12}/TiO_2)_n$ preparation procedure

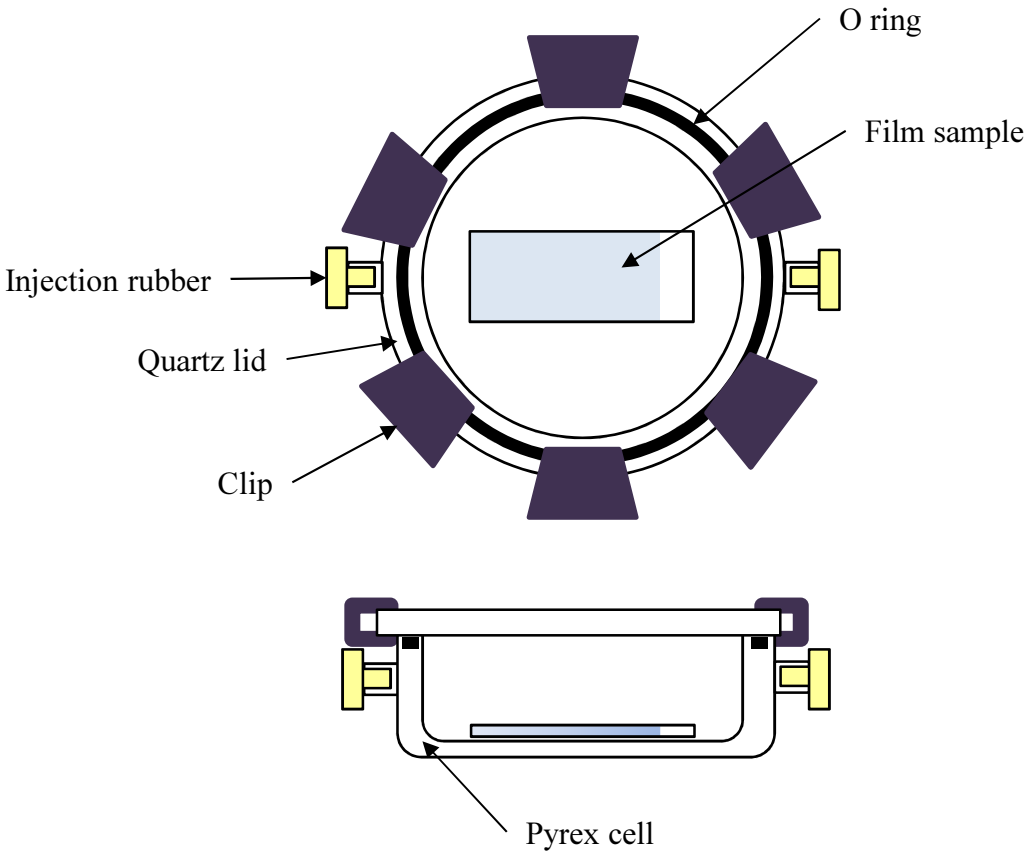

Figure 2-5.Iillustration of sample setting

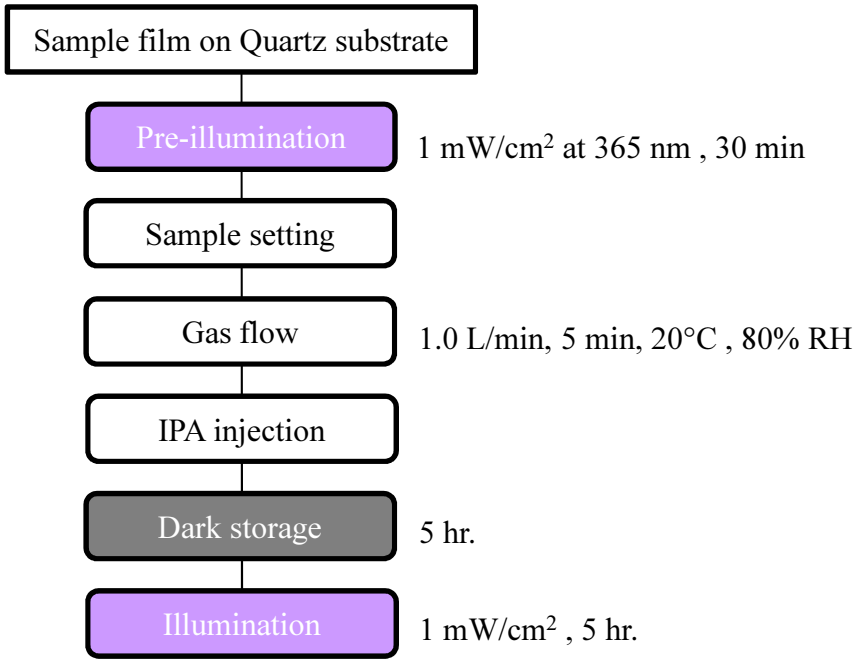

Figure 2-6. Experimental procedure of 2-propanol decomposition

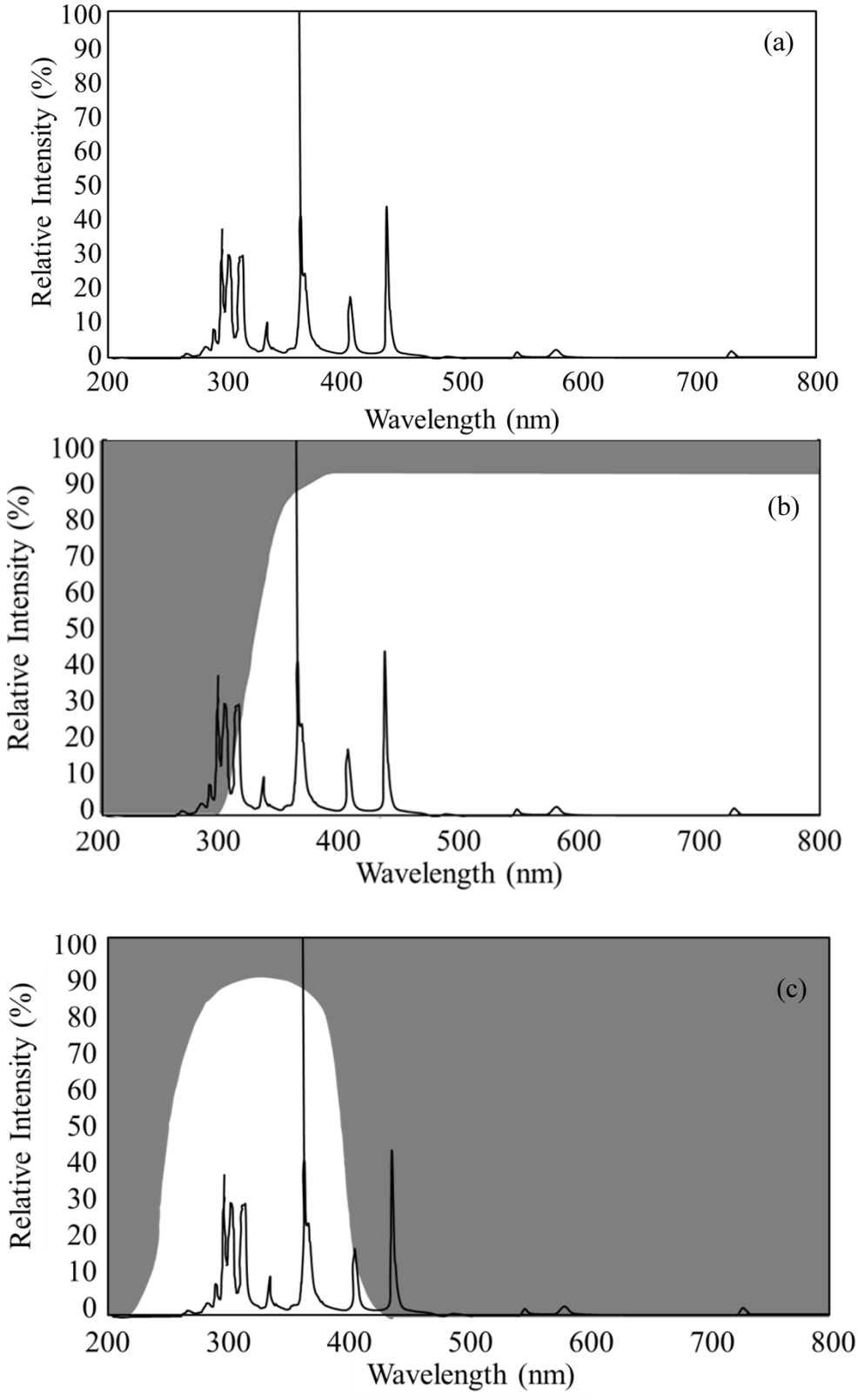

Figure 2-7 .Wavelength spectra of the light source (a), light illumination with UV-33 which absorbing UV < 330 nm) (b), and light illumination with UV-D33S adsorbing visible light > 400 nm (c)

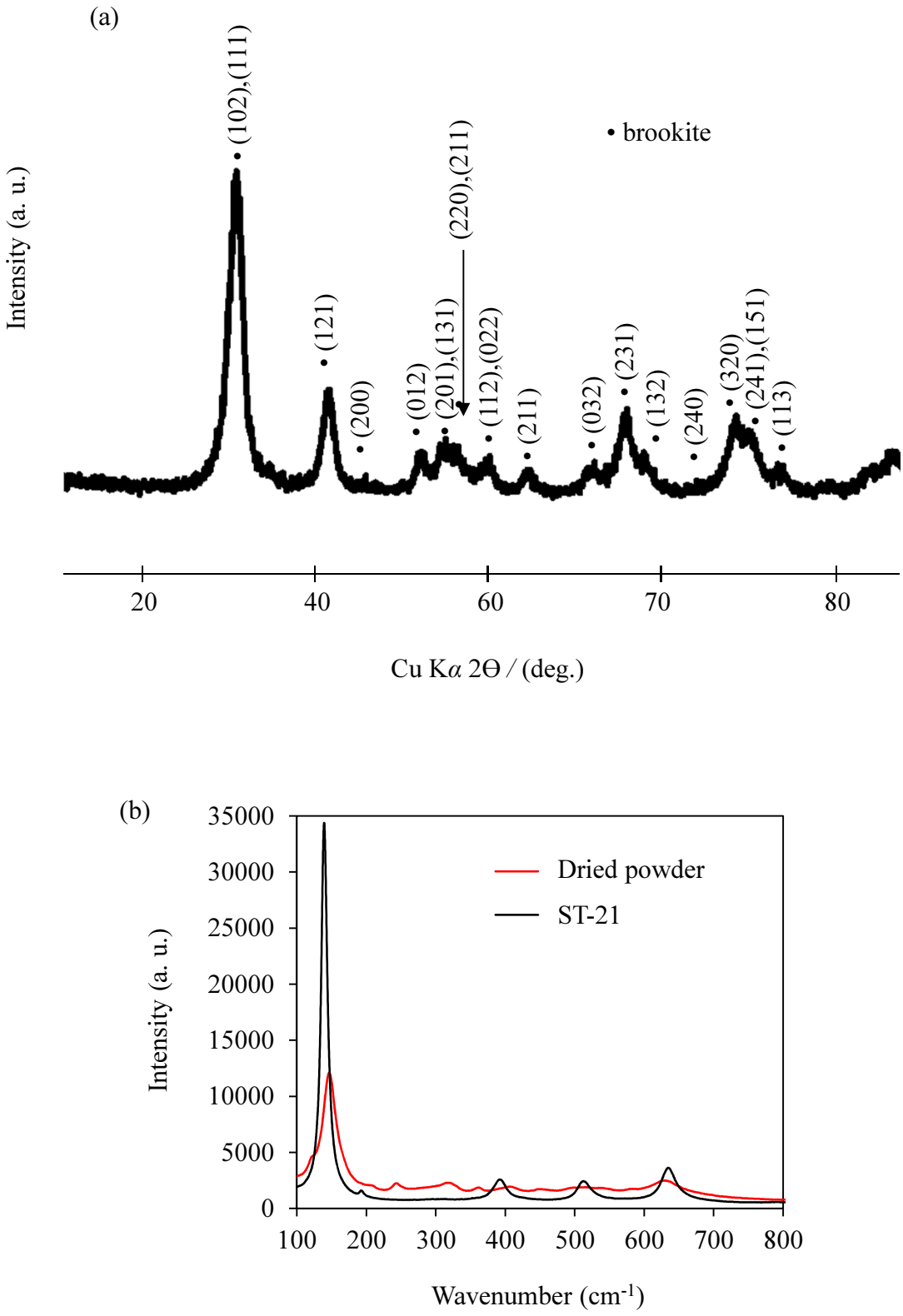

Figure 2-8. (a) XRD pattern, and (b) Raman spectra of dried brookite powder.

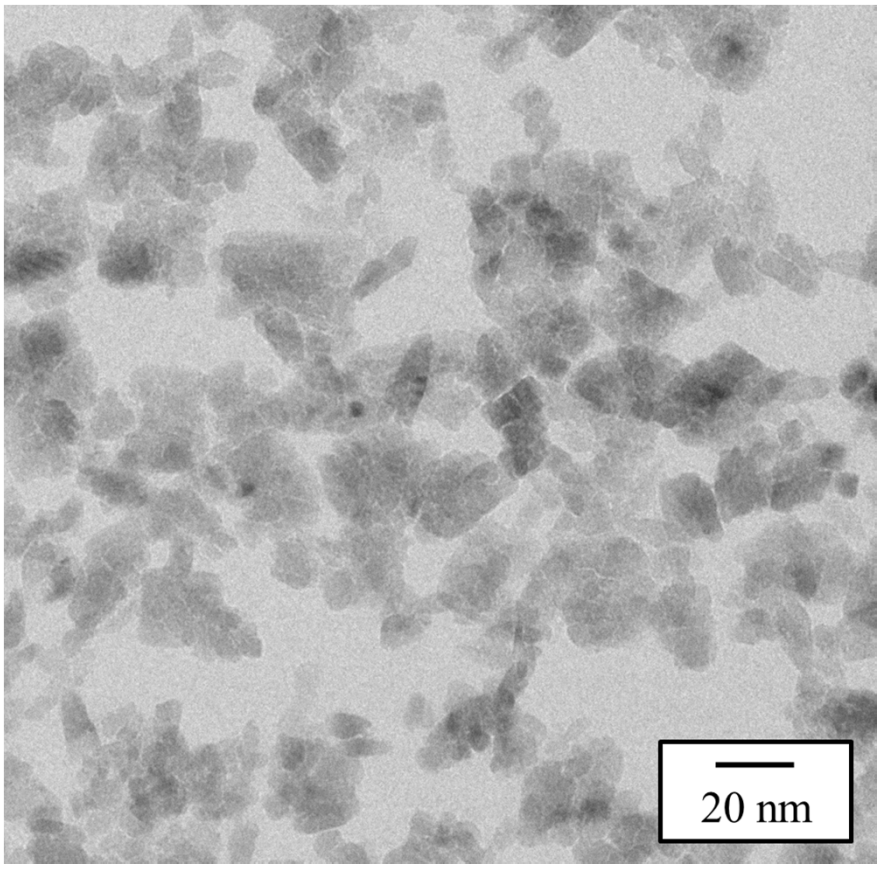

Figure 2-9. TEM micrograph of dried brookite powder

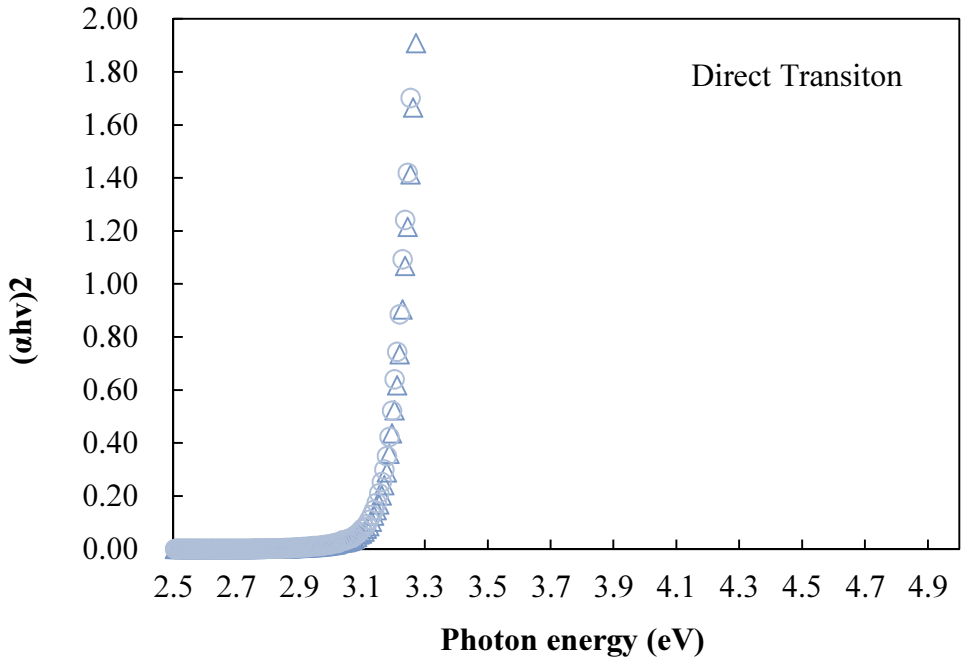

Figure2-10. Band gap estimation from diffuse reflection spectra

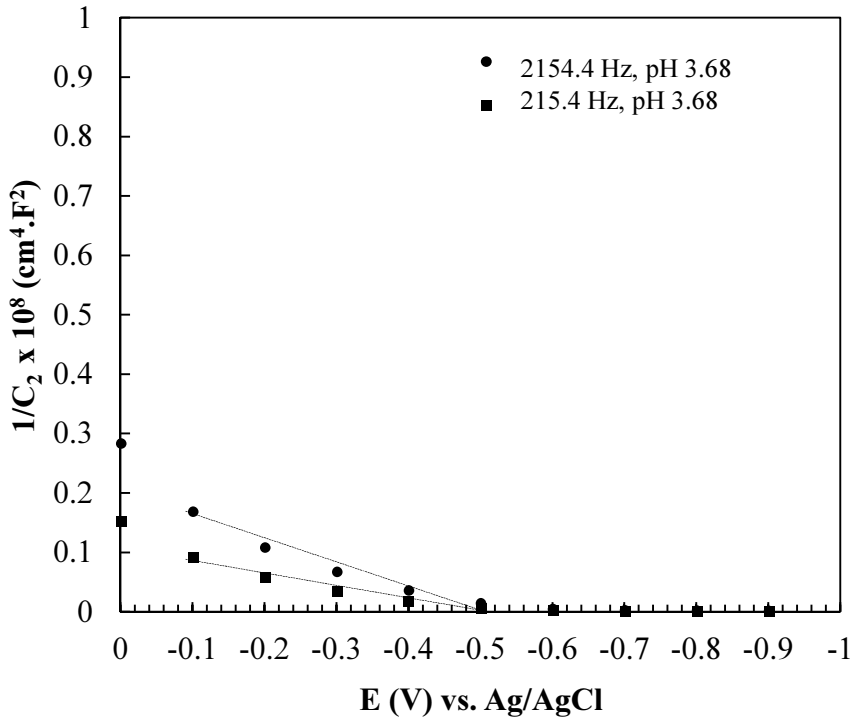

Figure 2-11. Mott–Schottky plots for the brookite used in this study.

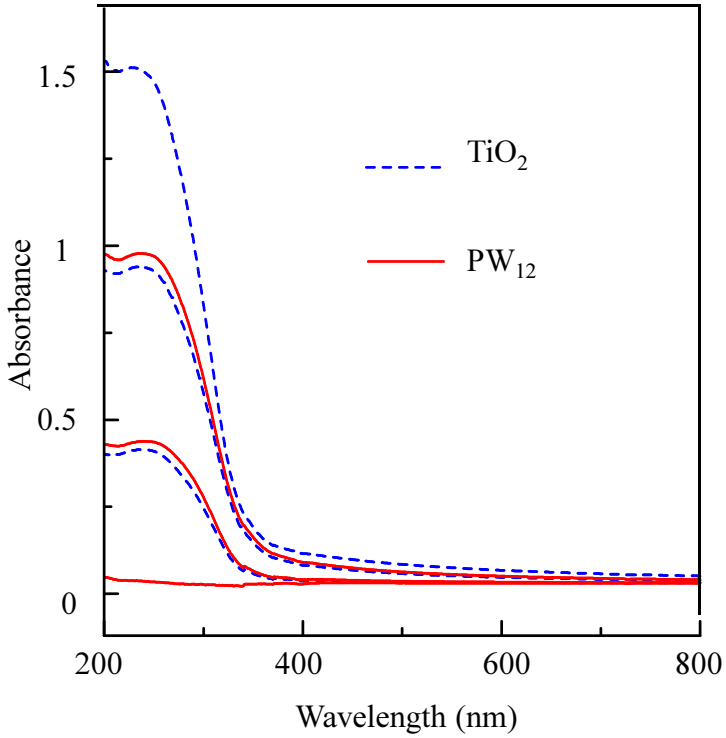

Figure 2-11. UV-vis absorbance spectra increment per layer of PW_{12} and TiO_2 of $(PW_{12}/TiO_2)_3$,

69

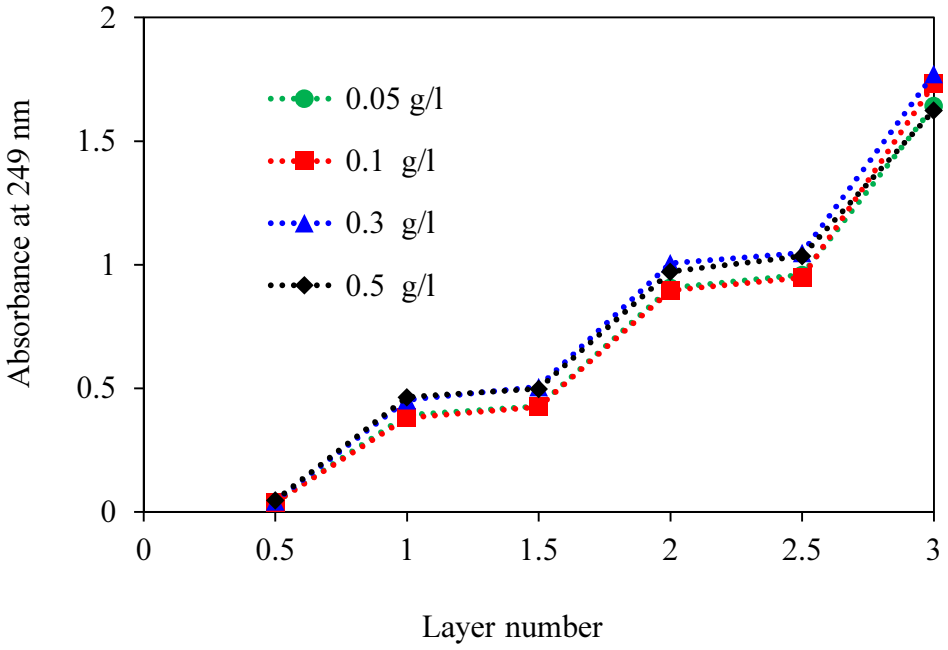

Figure 2-13. UV absorbance spectra increment at 249 nm per layer of PW_{12} and TiO_2 of $(PW_{12}/TiO_2)_3$ from TiO_2 suspensions with different concentrations

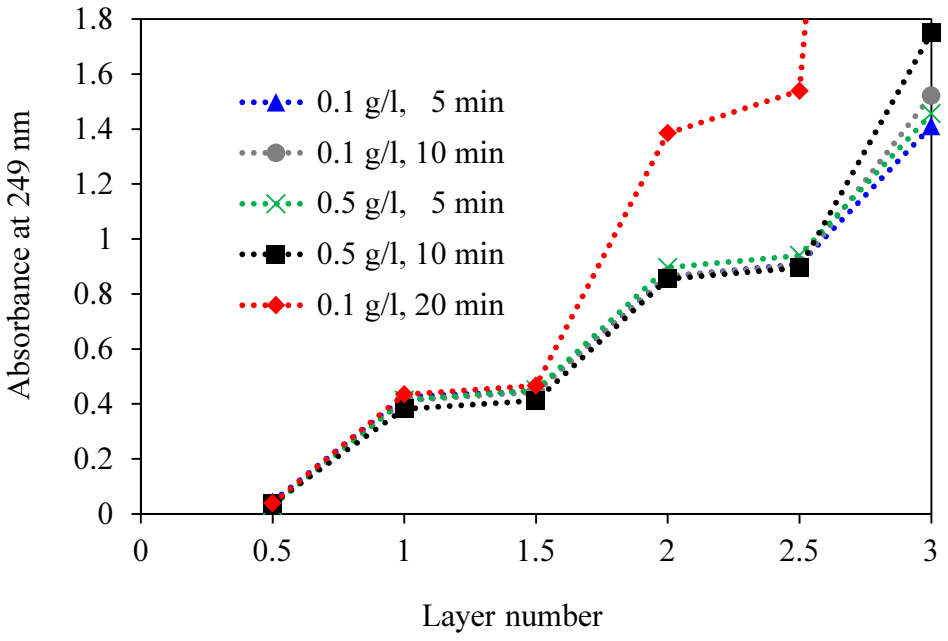

Figure 2-14. UV absorbance spectra increment at 249 nm per layer of H_2W_{12} and TiO_2 of (H_2W_{12}/TiO_2) from different concentration and immersing time of TiO_2 suspension

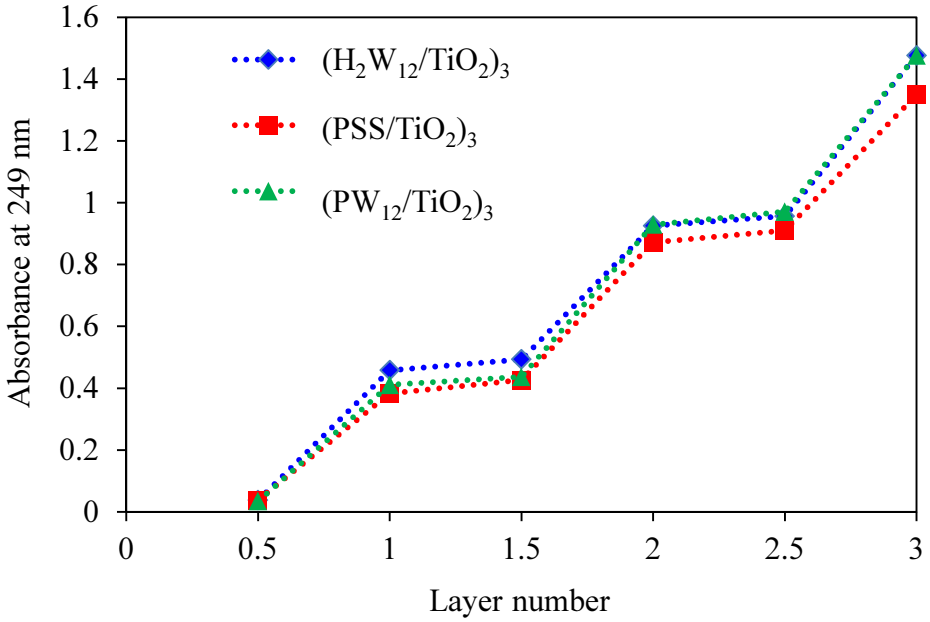

Figure 2-15. UV absorbance spectra increment at 249 nm per layer of $(PW_{12}/TiO_2)_3$, $(H_2W_{12}/TiO_2)_3$ and $(PSS/TiO_2)_3$.

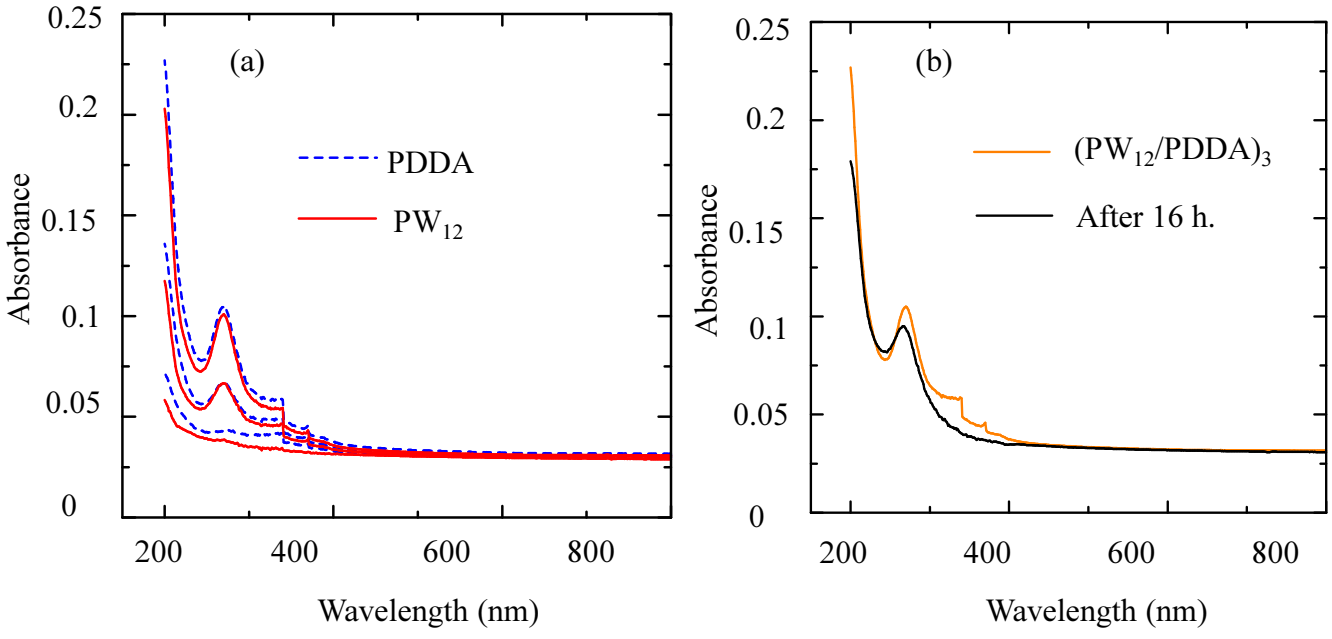

Figure 2-16. UV-vis absorbance spectra (a) increment per layer of PW_{12} and PDDA of $(PW_{12}/PDDA)_3$, (b) change before and after UV illumination for 16 hours

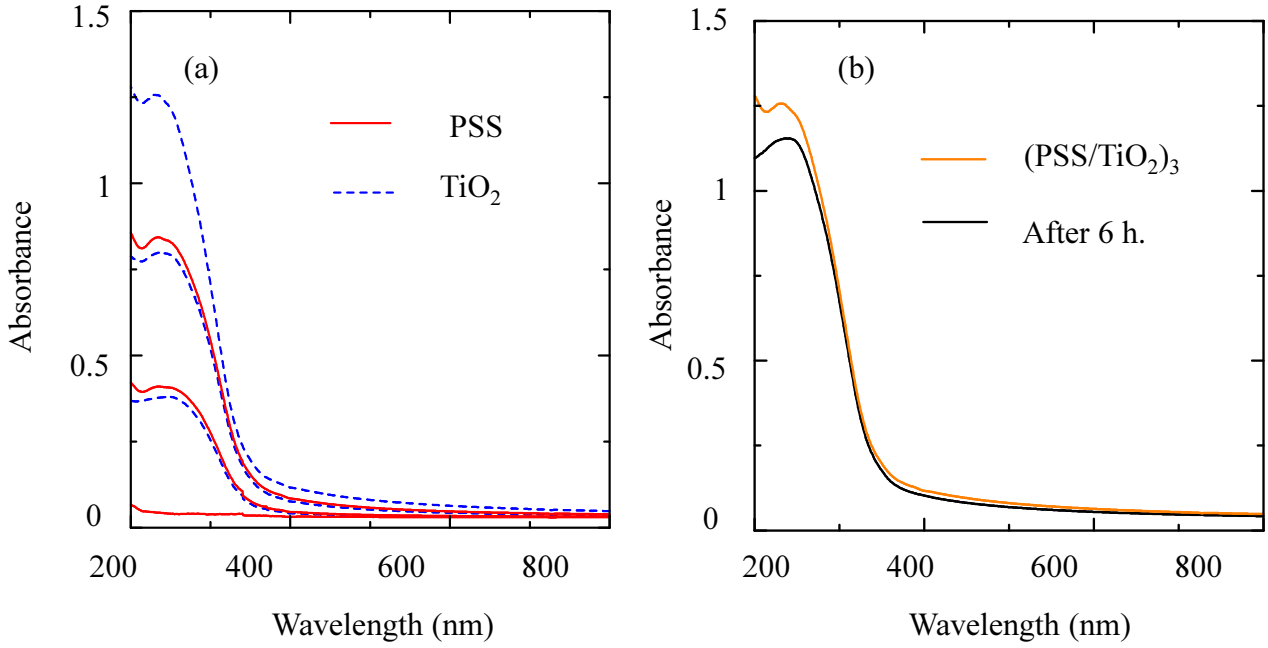

Figure 2-17. UV-vis absorbance spectra (a) increment per layer of PSS and TiO_2 of $(PDDA/TiO_2)_3$, (b) change before and after UV illumination for 6 hours.

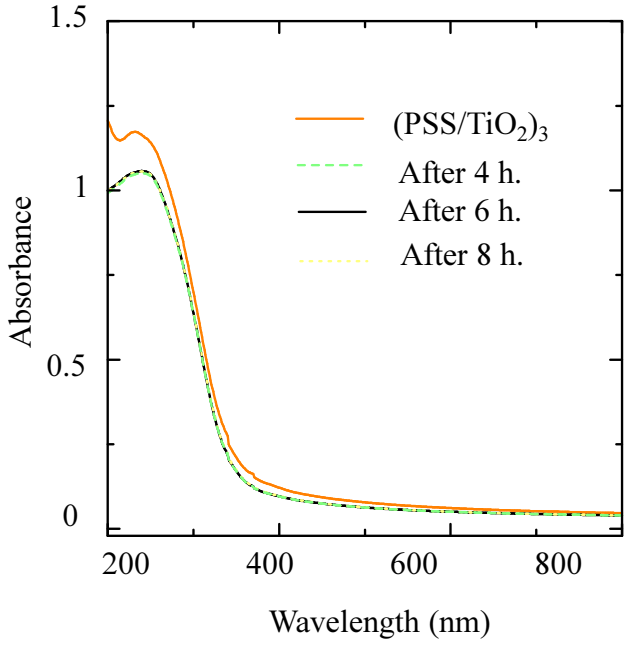

Figure 2-18. UV-vis absorbance spectra change before and after UV illumination

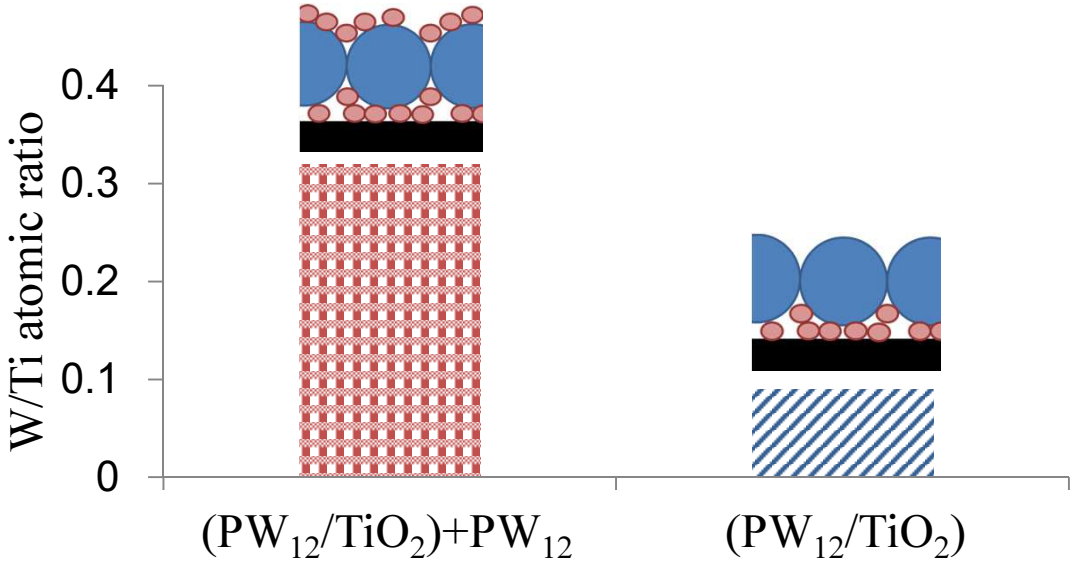

Figure 2-19 Surface atomic ratio of W/Ti for (PW_{12}/TiO_2) + PW_{12} (top surface is PW_{12}), and (PW_{12}/TiO_2) films (top surface is TiO_2) according to XPS measurements.

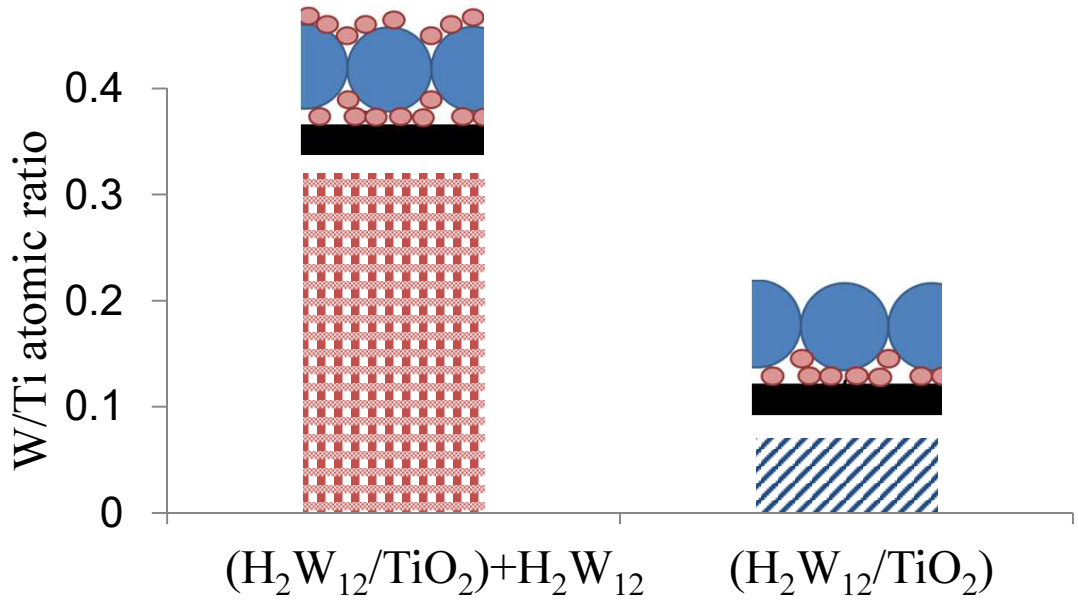

Figure 2-20. Surface atomic ratio of W/Ti for (H_2W_{12}/TiO_2) + PW_{12} (top surface is H_2W_{12}), and (H_2W_{12}/TiO_2) films (top surface is TiO_2) according to XPS measurements.

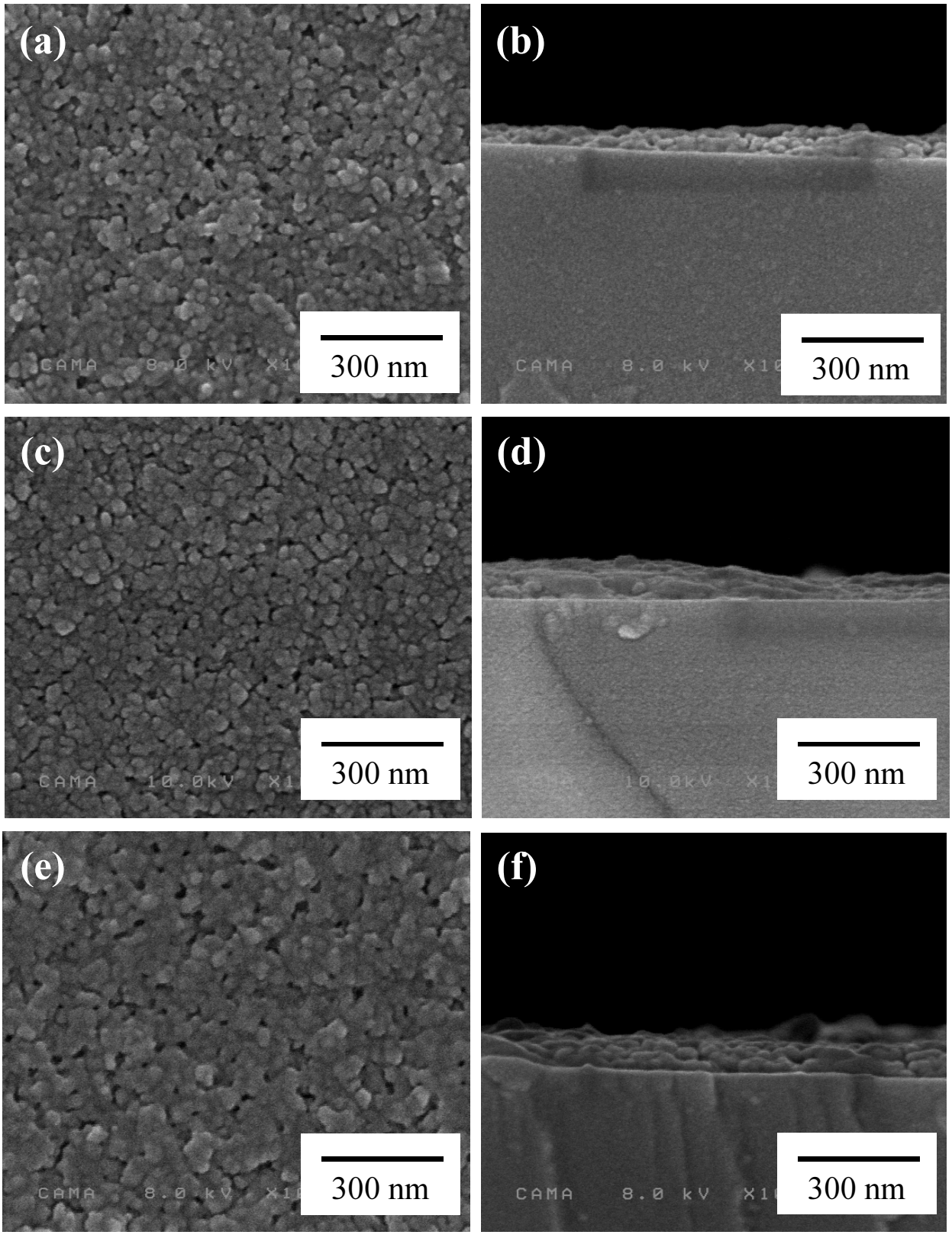

Figure 2-21 SEM images of $(PW_{12}/TiO_2)_3$ ((a) and (b)), $(H_2W_{12}/TiO_2)_3$ ((c) and (d)) and $(TiO_2)_3$ ((e) and (f)) films: (a), (c) and (e) shows top views; (b), (d) and (f) are crosscut sections..

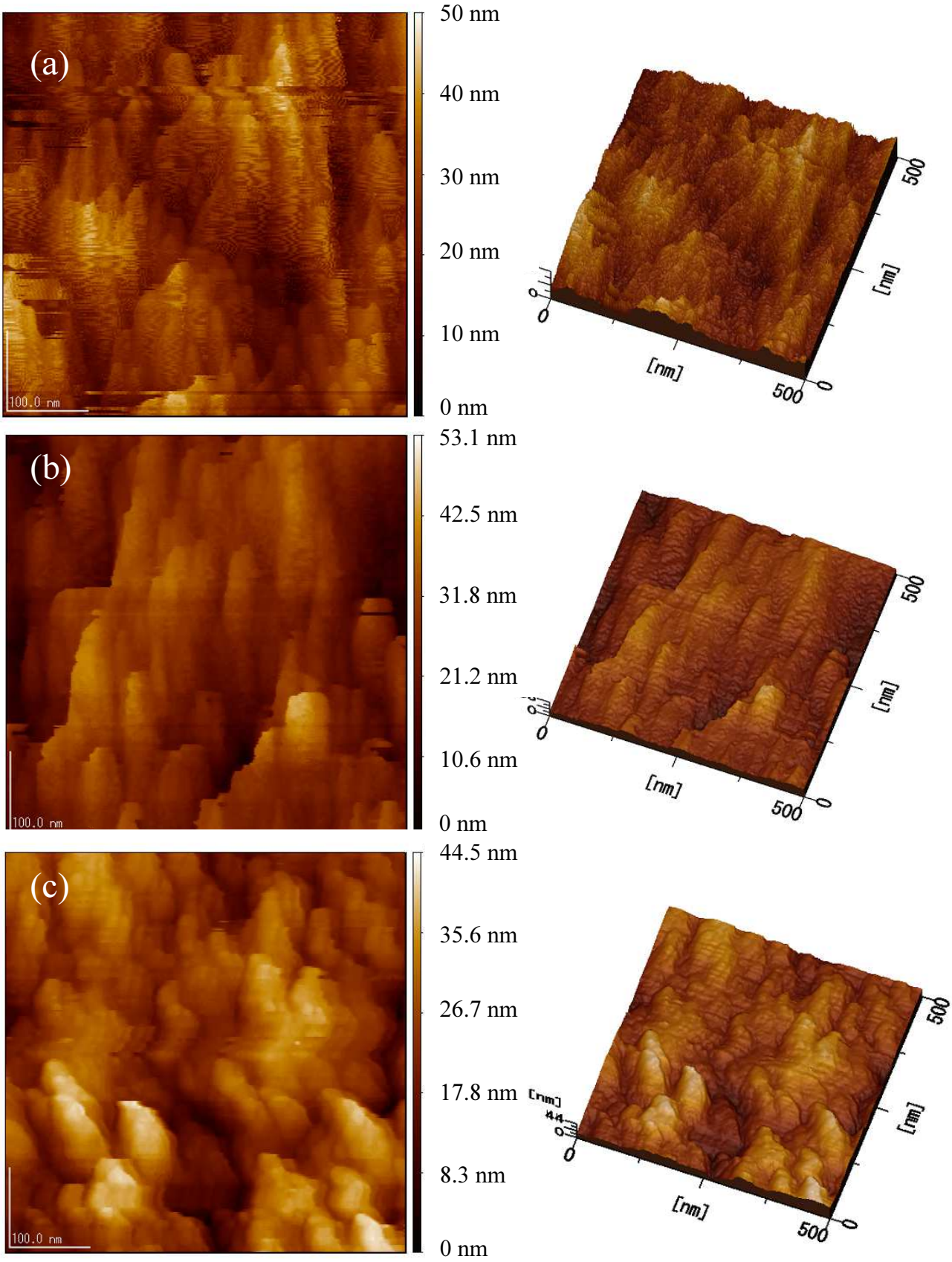

Figure 2-22. Surface atomic ratio of W/Ti for (H_2W_{12}/TiO_2) + PW_{12} (top surface is H_2W_{12}), and (H_2W_{12}/TiO_2) films (top surface is TiO_2) according to XPS measurements.

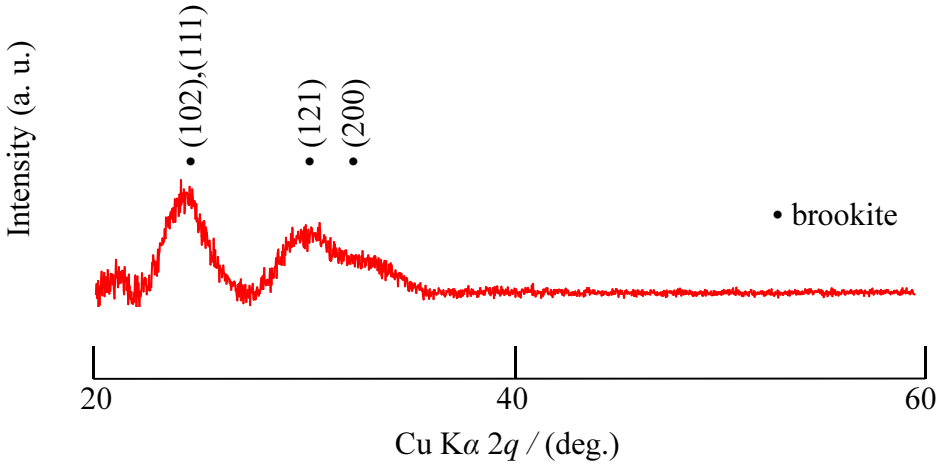

Figure 2-23. XRD pattern of $(PW_{12}/TiO_2)_3$ from using 0.25 degree incident angle

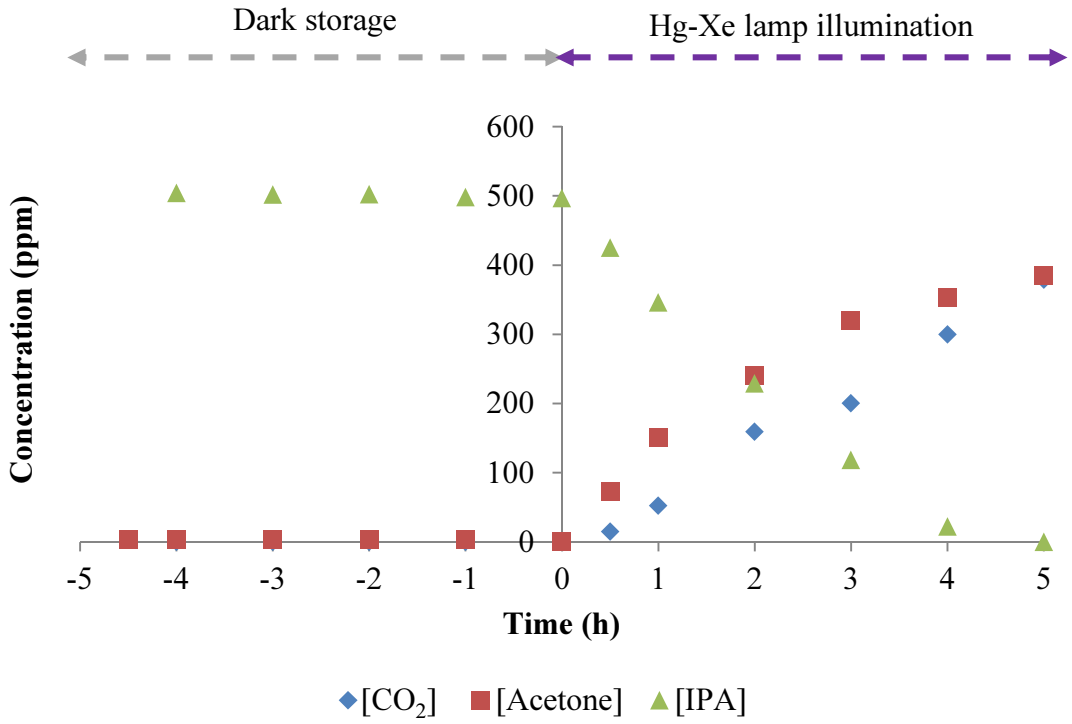

Figure 2-24. Concentration change during dark storage and Hg-Xe lamp illumination for $(TiO_2)_3$ film.

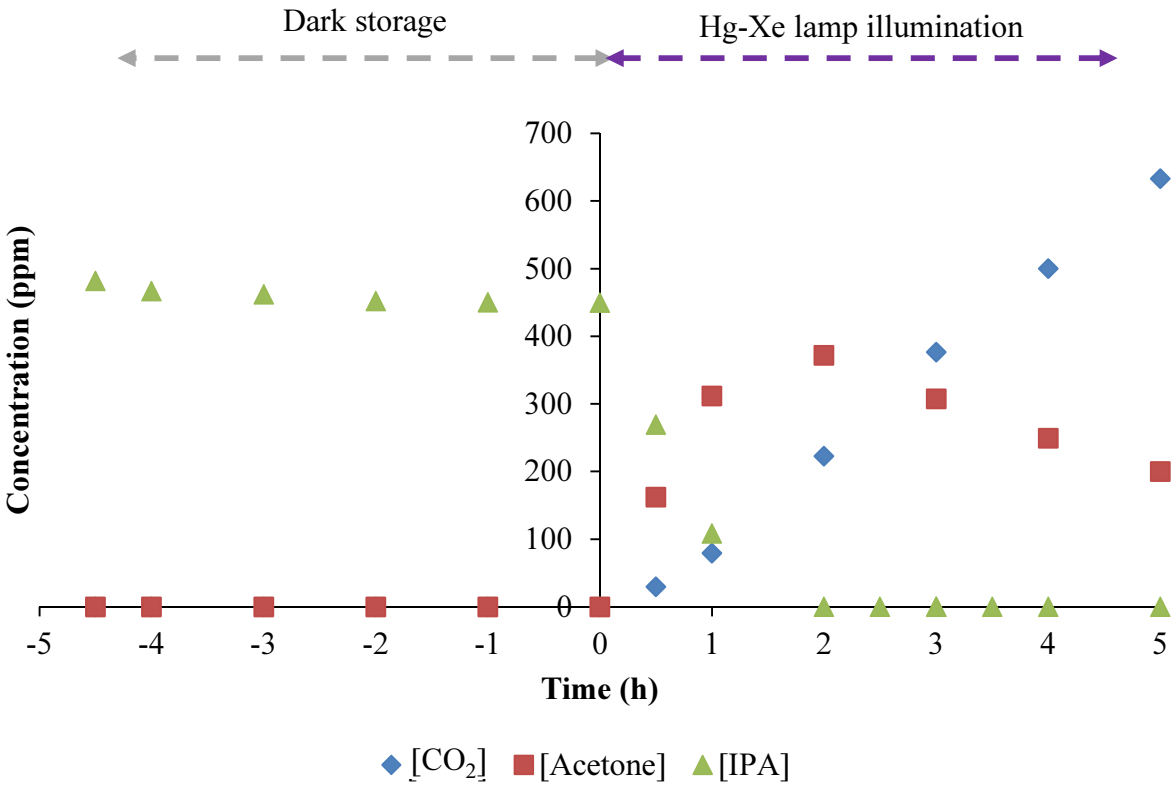

Figure 2-25. Concentration change during dark storage and Hg-Xe lamp illumination for $(PW_{12}/TiO_2)_3$ film

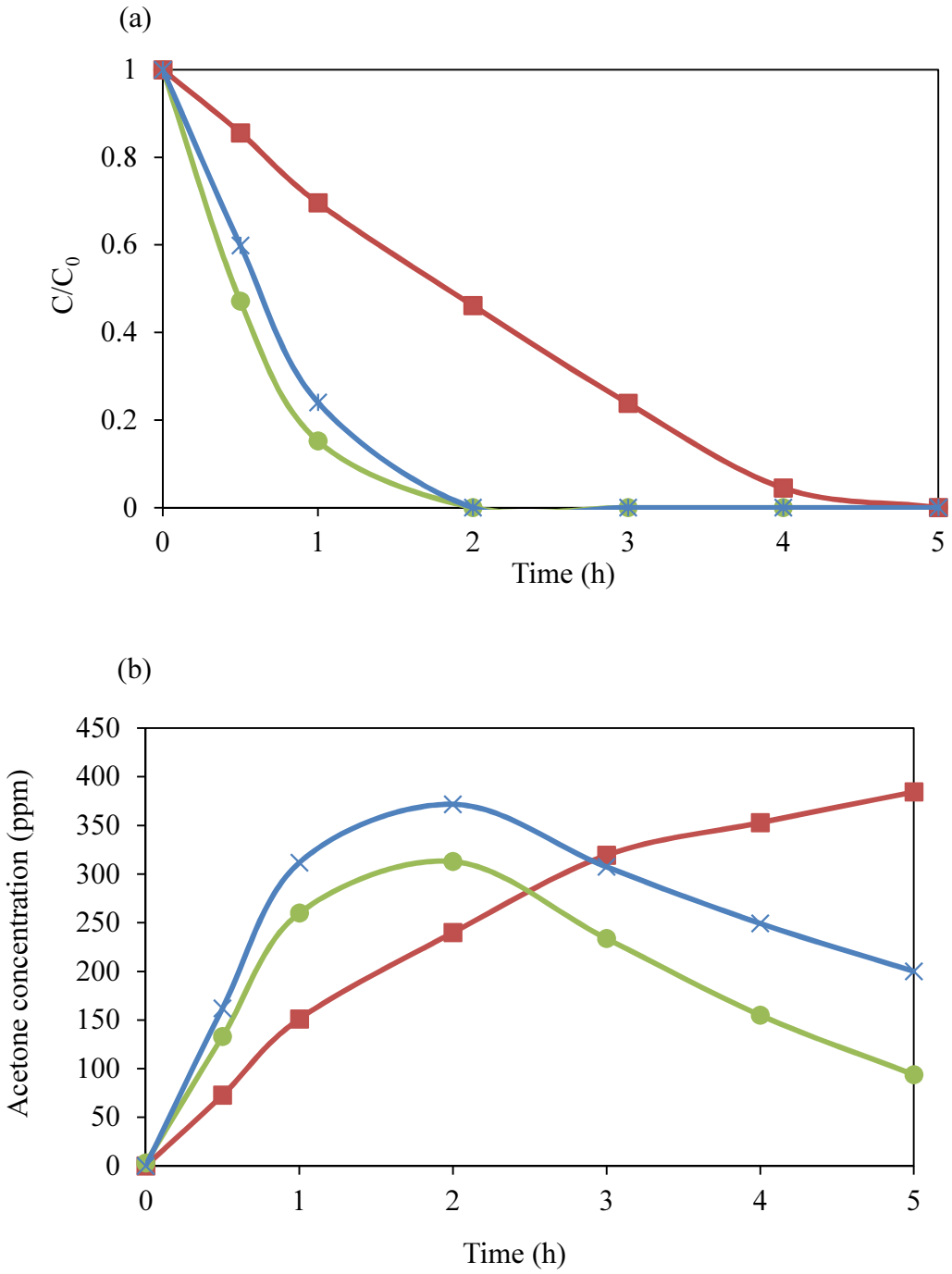

Figure 2-26. (a) Decomposition rate of IPA for $(PW_{12}/TiO_2)_3$ (×), $(TiO_2)_3$ (■) and $(H_2W_{12}/TiO_2)_3$ (●) films under UV illumination without filter.; (b) Concentration changes of CO_2 (dotted line) and acetone (solid line) for (a)

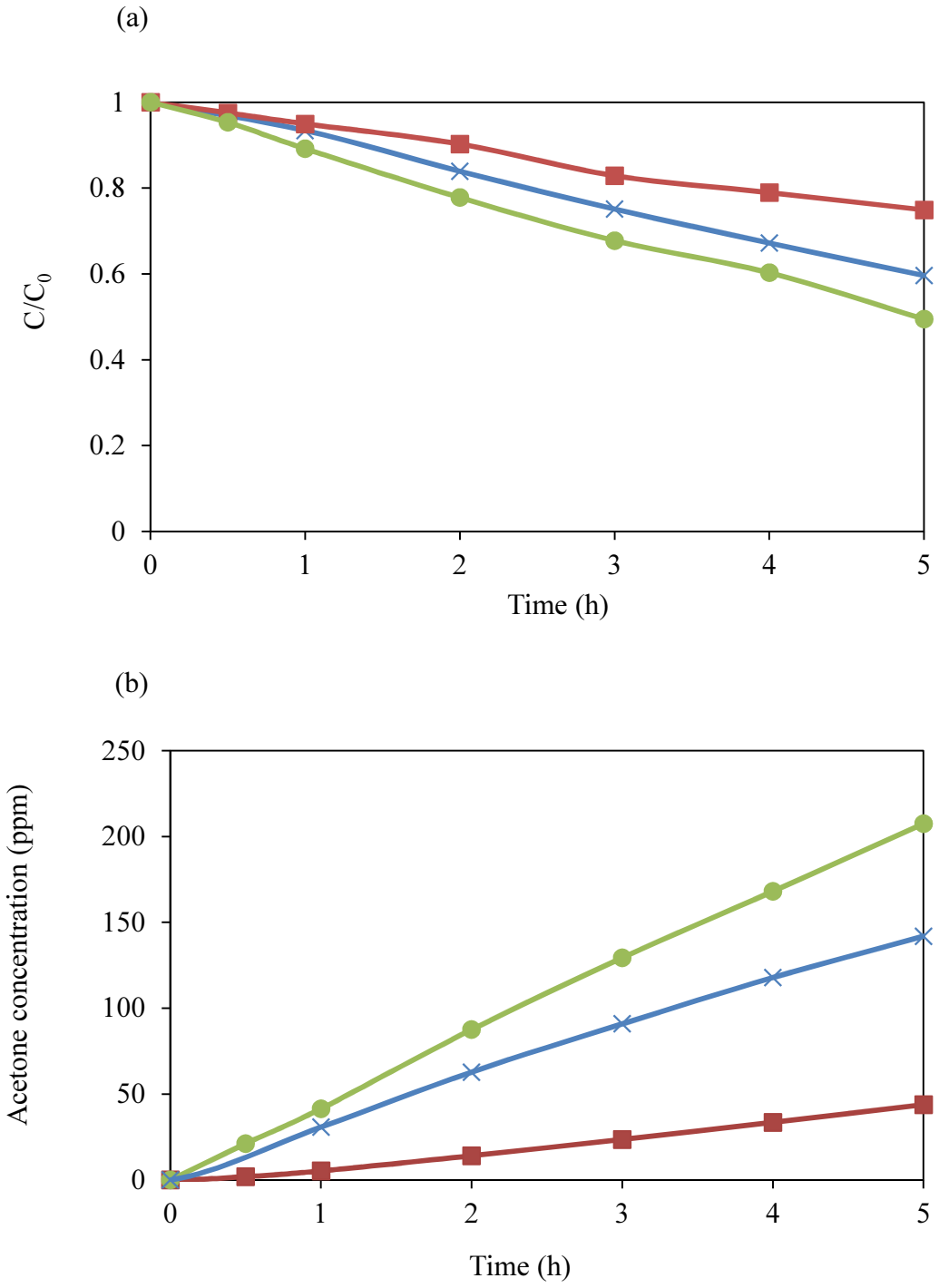

Figure 2-27.(a) Decomposition rate of IPA for $(PW_{12}/TiO_2)_3$ (×), $(TiO_2)_3$ (■) and $(H_2W_{12}/TiO_2)_3$ (●) films under UV illumination with UV33 filter; (b) Concentration changes of CO_2 (dotted line) and acetone (solid line) for (a)

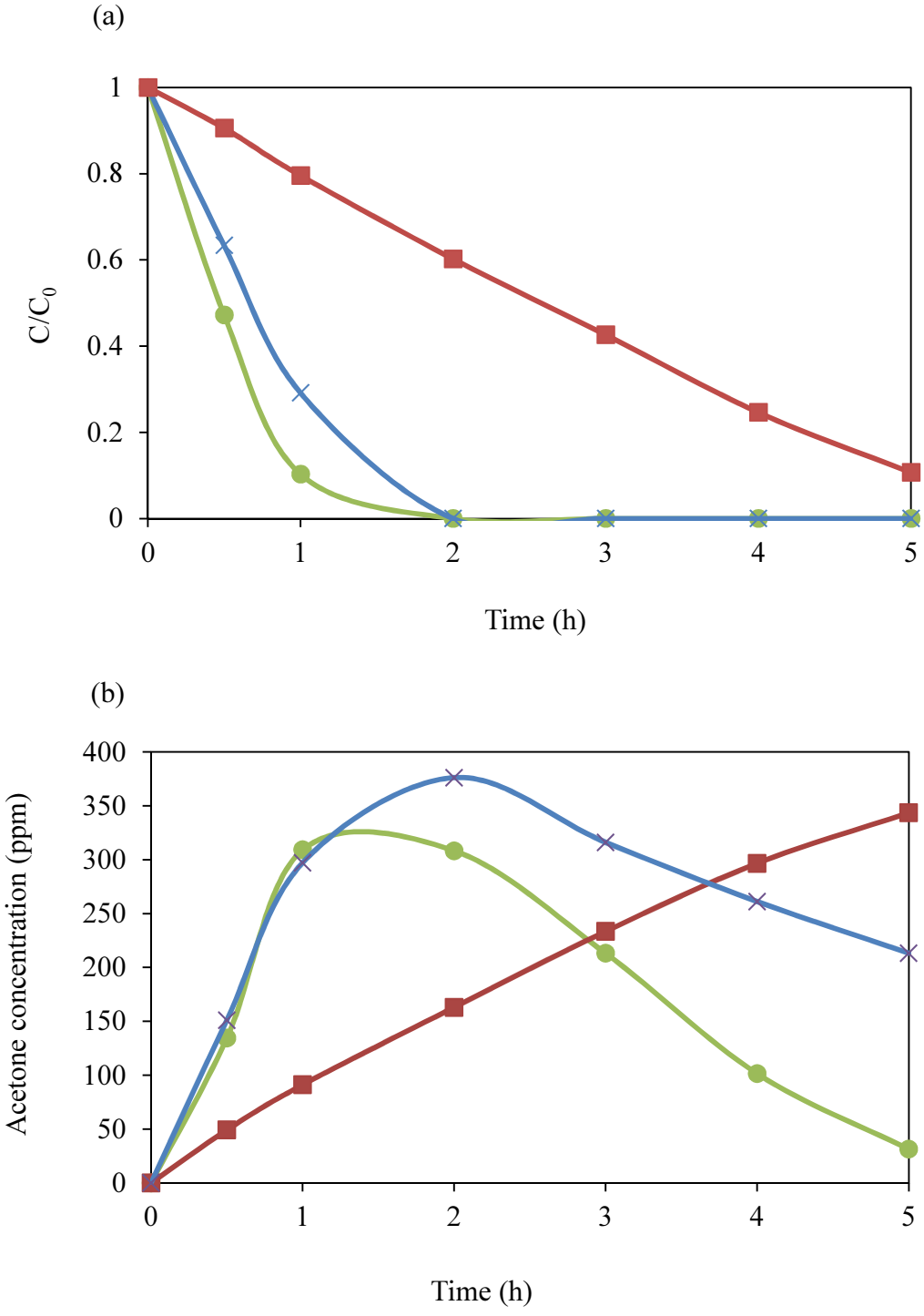

Figure 2-28.(a) Decomposition rate of IPA for $(PW_{12}/TiO_2)_3$ (×), $(TiO_2)_3$ (■) and $(H_2W_{12}/TiO_2)_3$ (●) films under UV illumination with UVD33S filter; (b) Concentration changes of CO_2 (dotted line) and acetone (solid line) for (a)

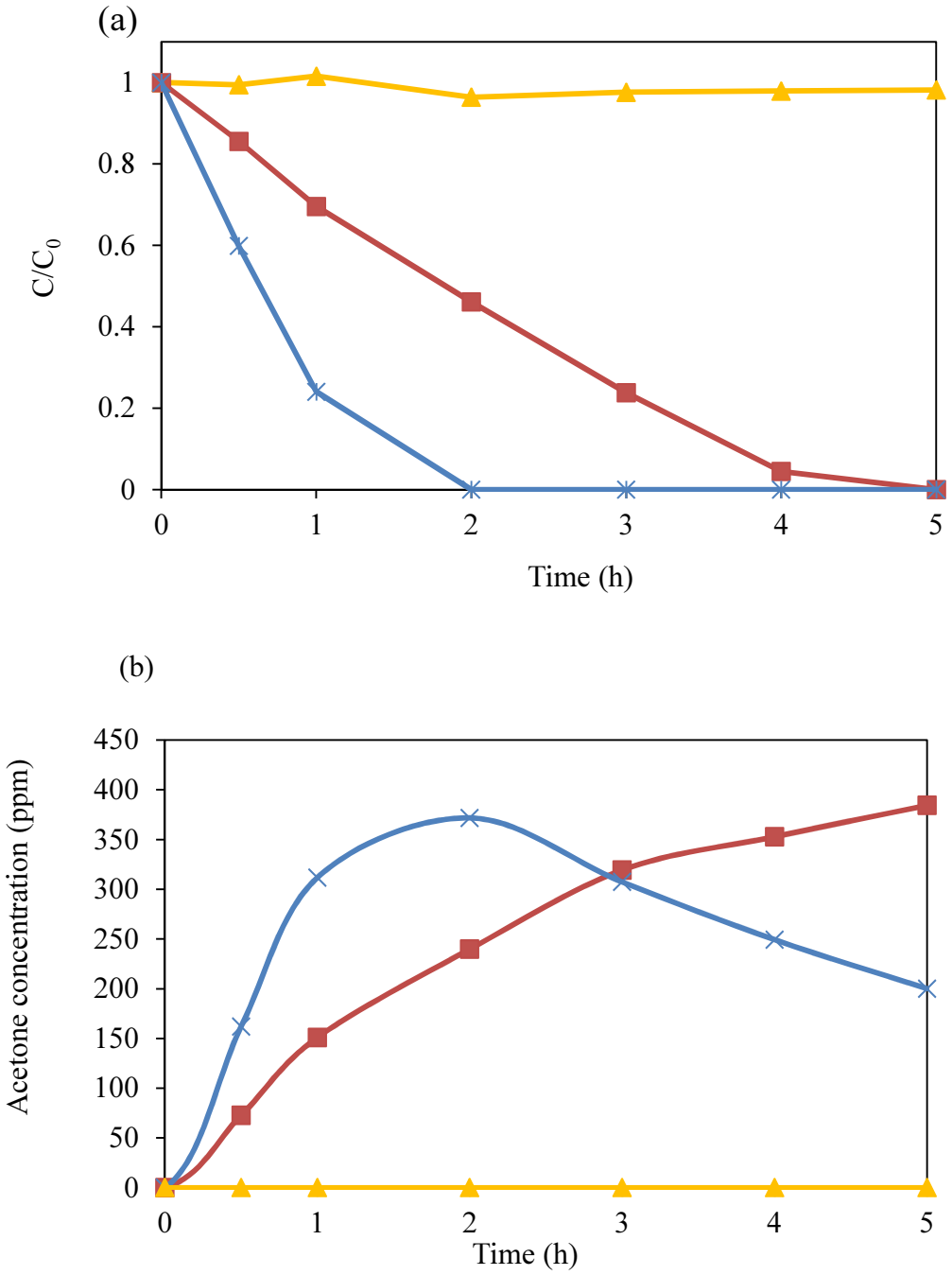

Figure 2-29. (a) Decomposition rate of IPA for $(PW_{12}/TiO_2)_3$ (×), $(TiO_2)_3$ (■) and $(PW_{12})_3$ (▲) films under all-light UV illumination, (b) Concentration changes of CO_2 (dotted line) and acetone (solid line) for (a)

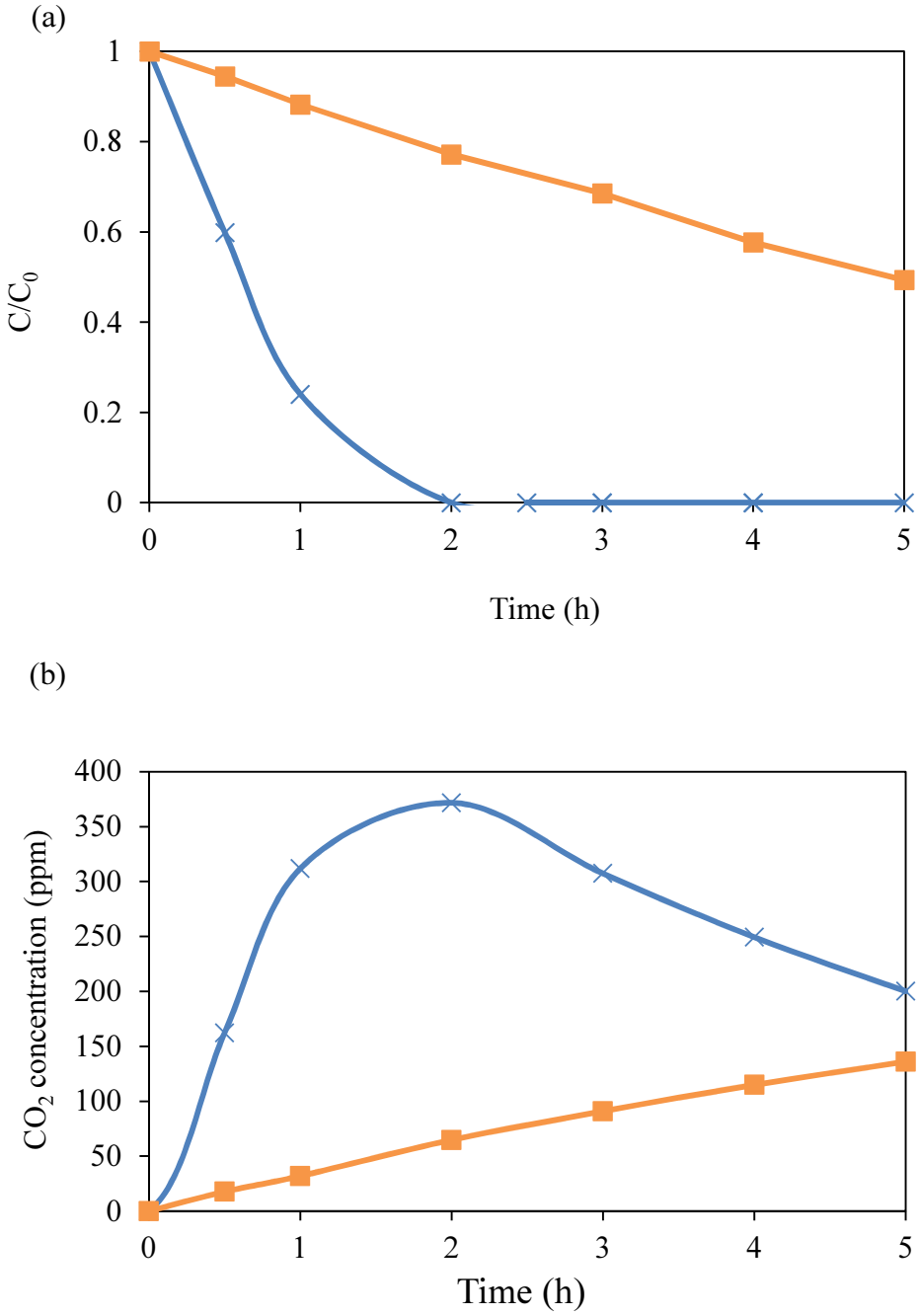

Figure 2-30.(a) Decomposition rate of IPA for $(PW_{12}/TiO_2)_3$ from NTB01 (×) suspension and $(PW_{12}/TiO_2)_3$ from STS100 (-) films under UV illumination without filter; (b) Concentration changes of CO_2 (dotted line) and acetone (solid line) for (a)

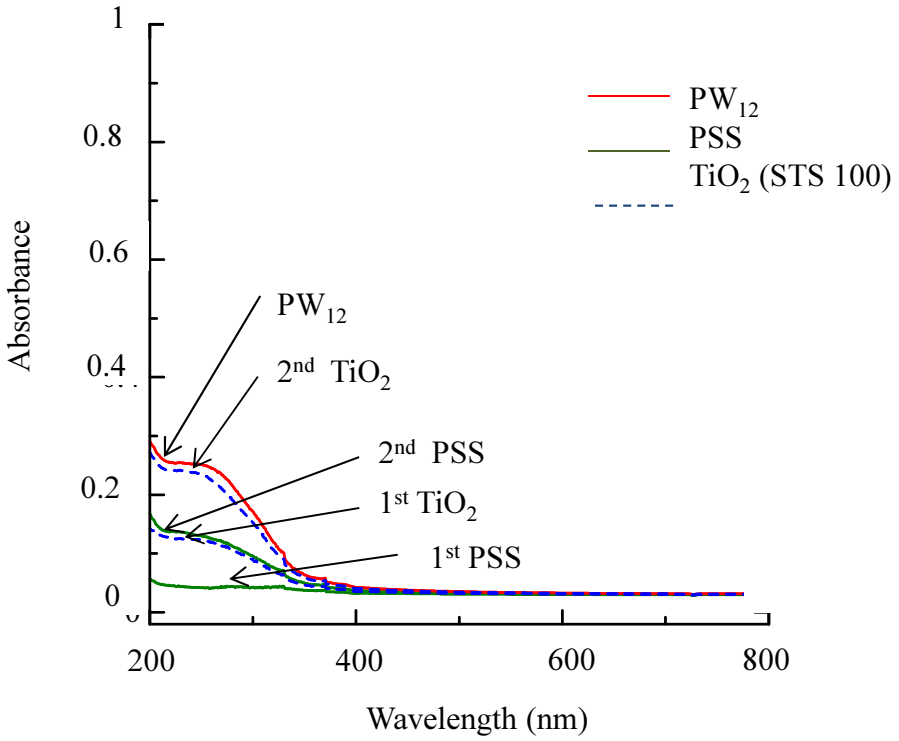

Figure 2-31 UV-vis absorbance spectra increment per layer of PW_{12} and TiO_2 of $(PW_{12}/TiO_2)_3$

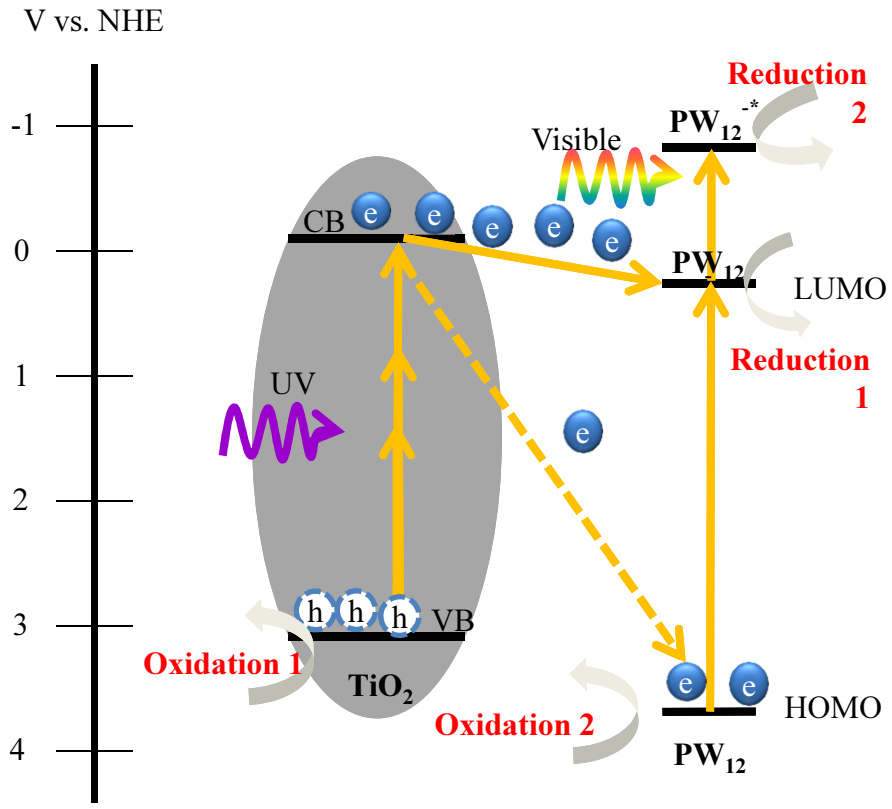

Figure 2-32. Energy diagram of TiO_2 (brookite)-PW_{12} system.

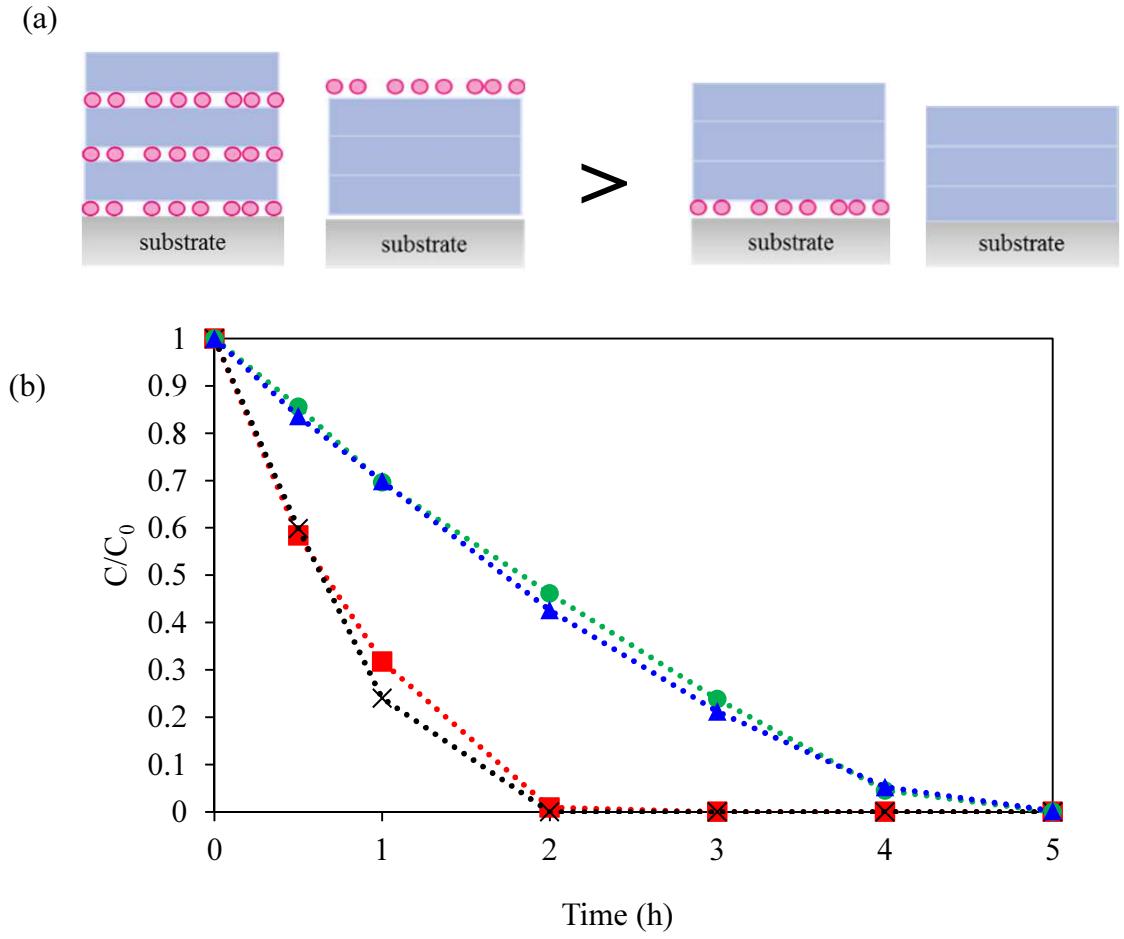

Figure 2-33. (a) schematic structure of $(PW_{12}/TiO_2)_3$ (×), TTTP (■) , PTTT (▲), and $(TiO_2)_3$ (●), from left to right, (b) Decomposition rate of IPA for those films under all-light UV illumination.

(a)

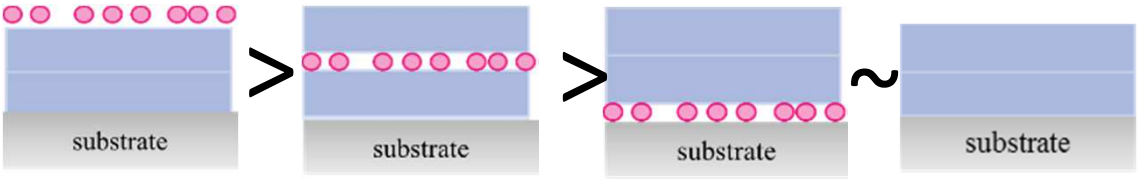

(b)

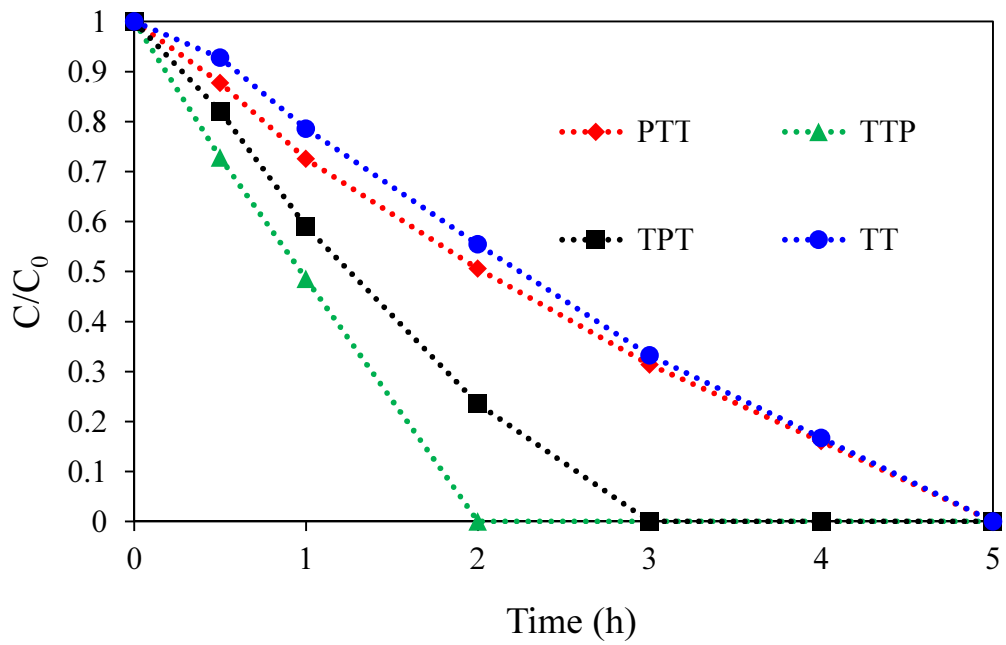

Figure 2-34. (a) Schematic structure of TTP (▲), TPT (■) , PTT (×) and TTT (●), from left to right, (b) Decomposition rate of IPA for those films under all-light UV illumination.

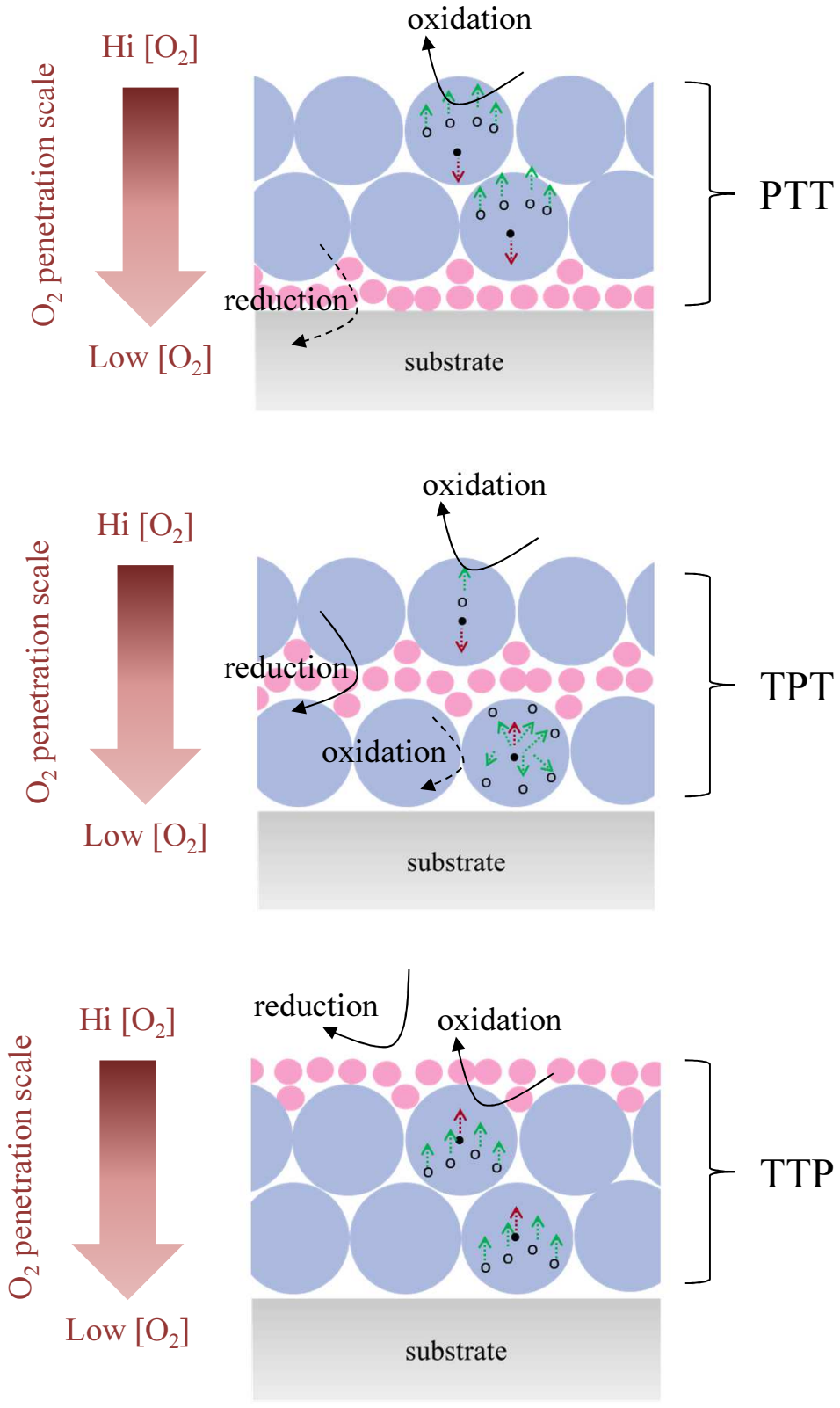

Figure 2-35. Electron-hole transportation, O_2 penetration under illumination by Hg-Xe lamp effect on oxidation and reduction on the film.

(a)

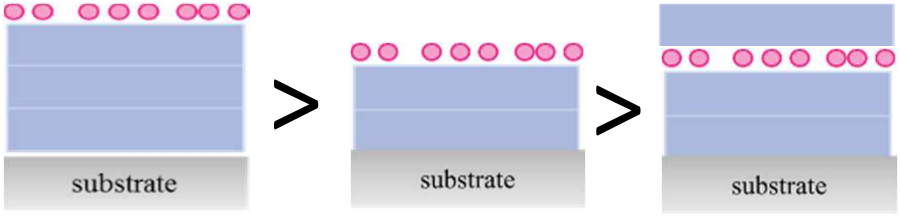

(b)

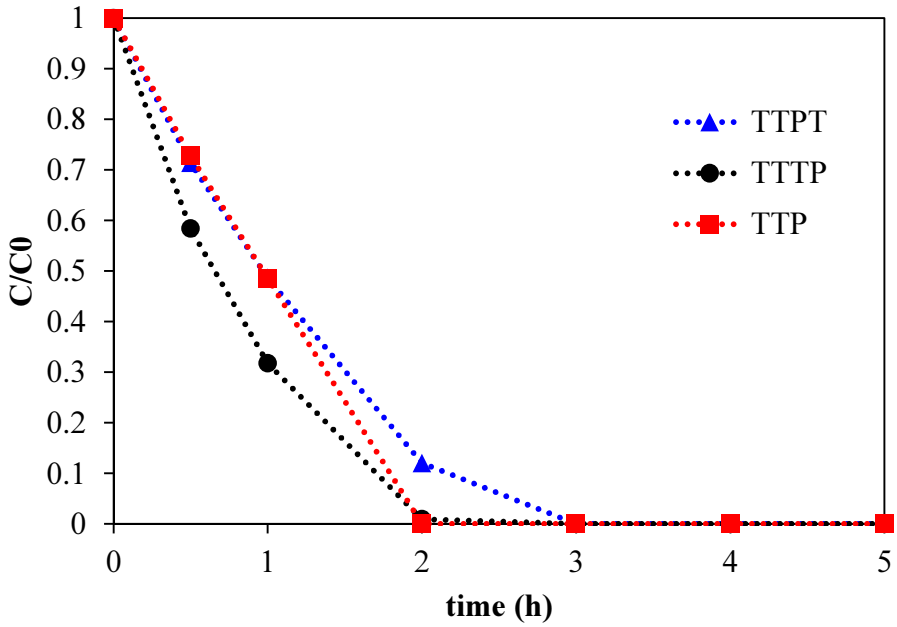

Figure 2-36. (a) Schematic structure of TTTP (●), TTP (■) , and TTPT (▲) from left to right, (b) Decomposition rate of IPA for those films under all-light UV illumination.

CHAPTER 3

Photoinduced hydrophilicity of $[PW_{12}O_{40}]^{3-}$/brookite hybrid films

3.1. Introduction

3.1.1. Photoinduced hydrophilicity

Together with the photocatalytic decomposition activity, a highly hydrophilic state can be obtained on a TiO_2 surface under UV illumination (photoinduced hydrophilicity) **[1–3]**. As described in chapter 1, Shibata et al. reported that brookite exhibited the best photoinduced hydrophilicity among the three polymorphs of TiO_2 (rutile, anatase and brookite) because of the exposure of bridging-site oxygen on the surface **[4]**. In addition, a relation exists between the photocatalytic activity and photoinduced hydrophilicity on the anatase thin film. The transformation behavior of film (from hydrophobic to hydrophilic after light illumination) corresponds to the photocatalytic performance of the anatase film **[5]**. However, no comparative study of photocatalytic decomposition activity and photoinduced hydrophilicity for PW_{12}/TiO_2 hybrid films has been reported to date. For this study, we prepared PPP ($PW_{12}/PW_{12}/PW_{12}$), TT (TiO_2/TiO_2), TTP ($TiO_2/TiO_2/PW_{12}$), and PTT ($PW_{12}/TiO_2/TiO_2$) films using brookite with the same method as that used in our previous study. Then their wettability conversion during and after UV illumination was investigated with comparison of photocatalytic activity on the decomposition of gaseous 2-propanol (IPA).

3.1.2. Water solubility and thermostability of Keggin-type HPAs

Normally, a Keggin type HPA formula is abbreviated to XM_{12}. For example, PW_{12} is 12 tungsto (VI) phosphoric acid, $[PW_{12}O_{40}]^{3-}$. Keggin anions have outer oxygen atoms of three types **[6]**: (i) terminal oxygen M=O, (ii) edge-shared, and (iii) corner-shared bridging oxygen M–O–M, as a proton donor, or so-called Brønsted acid sites, as shown in **Figure 3-1** (replicate from **[7]**). In solution, bridging oxygen is protonated. In the solid phase and gas phase, the respective proton donors are the terminal oxygen and edge-shared bridging oxygen **[6].** Therefore, HPAs have extremely high solubility in polar solvents such as water and alcohol, but they are insoluble in nonpolar solvents such as hydrocarbons. Their stability order for hydrolysis in water is SiW_{12} > PW_{12} > $SiMo_{12}$ > PMo_{12} **[6]**. The thermal stability of solid HPAs was reportedly fairly high. Decomposition temperatures of some Keggin-type HPAs were reported: PW_{12} (465 °C) > SiW_{12} (445 °C) > PMo_{12} (375 °C) > $SiMo_{12}$ (350 °C). Consequently, to stabilize HPAs for hydrolysis on the films, the films should be heat-treated at 300 °C.

3.2 Experimental

3.2.1 Sample preparation and characterization

All pH values of solutions and suspensions used for film preparation were adjusted to 1.5 using a HNO_3 aqueous solution to avoid hydrolysis of PW_{12} and to maintain a well-dispersed state of brookite. For film preparation, 12 tungsto(VI) phosphoric acid n-hydrate ($H_3(PW_{12}O_{40})nH_2O$; Wako Pure Chemical Industries Ltd., Japan) was used with no purification. This chemical was dissolved into diluted HNO_3 aqueous solution (1 mM). A commercial brookite aqueous suspension (NTB 01, 15 wt% TiO_2, pH 4; Showa Denko K.K., Japan) was used as the TiO_2 source. This suspension was diluted to

concentrations of 0.1 g/l; the pH value was adjusted to 1.5. Either poly diallyldimethylammonium chloride (PDDA, typical Mw 100,000–200,000, 20 wt% aqueous solution; Aldrich Chemical Co. Inc.) or poly sodium 4-styrene sulfonate (PSS, average Mw ca. 70,000, 30 wt% aqueous solution; Aldrich Chemical Co. Inc.) was used as a counter polymer.

The hybrid films and control films were prepared via a self-assembly LBL process, as conducted in a previous study. A quartz glass plate (30 mm × 60 mm × 1 mm; Tosoh Corp. Japan) was washed and soaked in a HCl and methanol mixture (1:1) for 30 min and then soaked in conc. (95%) H_2SO_4 for another 30 min. The substrate was washed using distilled water. Then it was immersed in a prepared solution or suspension for 20 min for each deposition. The substrate surface is positively charged in the acid solution. Therefore, the first deposition of the negative molecule, PW_{12} or PSS, was adsorbed onto the surface of substrates by Coulombic interaction. Subsequently, the sample was rinsed twice in pH 1.5 HNO_3 aqueous solutions and dried at 60 °C in the oven under air atmosphere until dry. The film was immersed again into TiO_2 suspension or PDDA solution to grow the next positive deposition, thereby preparing PSS/TiO_2/PSS/TiO_2/PW_{12}, PW_{12}/TiO_2/PSS/TiO_2, PW_{12}/PDDA/PW_{12}/PDDA/PW_{12}, and PSS/TiO_2/PSS/TiO_2 films. Subsequently, both PSS and PDDA were decomposed using UV illumination (66 mW/cm^2 at λ = 365 nm) with a Hg–Xe lamp for 6 h (PSS) or 16 h (PDDA) to prepare TTP, PTT, PPP, and TT films. Detailed procedures used for film preparation were described in our earlier reports. For this study, we heated the obtained films at 300 °C for 1 h in air because preliminary experiments revealed that this treatment suppresses the water-solubility of PW_{12}.

The UV–Vis spectra were measured at each coating step using a UV–Vis–NIR scanning spectrophotometer (V-630; Jasco Corp., Tokyo, Japan). X-ray photoelectron spectroscopy (XPS, PHI Quantera SXM; PHI Co., U.S.A.) with an Al Kα X-ray source (1468 eV) was used to evaluate the film surface composition. The binding energy scales were referenced to 284.5 eV, as determined from the locations of peaks on the C1s spectra of hydrocarbon (CH_x) for correcting the deviation. The Ti and W concentrations on the surface were evaluated using Ti2p and W4f spectra. The infrared spectra of the thin films on Si substrate were recorded using a Fourier transform infrared spectrophotometer (FT–IR 6100; Jasco Corp., Tokyo, Japan). The transmission mode was used with an incidence angle of 75 ° (Brewster's angle). Using inductively coupled plasma optical emission spectrometry (ICP–OES; Prodigy ICP, Leeman Labs, INC U.S.A.) to confirm the dissolubility of PW_{12} from the heat-treated films to water. Surface roughness of the film was evaluated in a 5-μm-square area using atomic force microscopy (AFM, JSPM-5200; JEOL, Tokyo, Japan) with a Si cantilever (NSC36-b; μ-mash Ltd., Narva mnt., Estonia). Using Si cantilever/Ti-Pt probes (NSC35/Ti-Pt-a; μ-mash Ltd., Narva mnt., Estonia), the contact surface potential distribution (CPD) of samples was also evaluated using Kelvin force microscopy (KFM) mode with the same system (JSPM-5200). The films' thickness was evaluated through direct observation of the crosscut section using a field emission scanning electron microscope (FE–SEM, S4500; Hitachi Ltd., Tokyo, Japan).

3.2.2. Evaluation of photocatalytic decomposition activity

Before measurements, these films were exposed to UV light (1 mW/cm^2, 365 nm) to remove organic compounds that had adsorbed onto the surface. A Pyrex glass vessel

(500 mL volume) with a quartz glass lid was used as a batch reactor. A sample film was set at the center of the vessel. Then the atmosphere in the reactor was replaced by gas flow (1.0 L/min, 5 min) with air at 20 °C and 80% relative humidity. Subsequently, the vessel was sealed. Then IPA gas was injected into it. The injected gas amount was equivalent to that for 500 ppm concentration. The vessel was subsequently stored in the dark for 5 h.

After the adsorption equilibrium was confirmed, UV illumination was conducted using a UV illuminator (LA-410UV-1; Hayashi Watch Works, Japan) equipped with a Hg–Xe lamp (MX4010). The illumination intensity at the sample surface was 1 mW/cm^2 at 365 nm. The IPA and acetone concentrations were evaluated every 30 min or every 1 h for 5 h using a gas chromatograph (GC-14A; Shimadzu Corp., Tokyo, Japan) equipped with a flame ionization detector (FID), a methanizer, and a Sunpak-A column (Shimadzu Corp.). The carrier gas was nitrogen. The respective temperatures for the detector and injection port were 230 °C and 200 °C. The initial column temperature was 50 °C, which was maintained for 2.5 min. The temperature was increased 20 °C /min to 130 °C to gain peak separation.

3.2.3. Evaluation of photoinduced hydrophilicity

The films were cleaned using vacuuming and pre-UV illumination (1 mW/cm^2). Then the films were stored in the dark for 5–9 days to allow hydrophobicizing. Subsequently the static water contact angle (WCA) change on the films in every 5, 10, 30, or 60 min during UV illumination (30 $\mu W/cm^2$) was observed using sessile drop method with a 2 µl distilled water (**Figure 3-2**) and contact angle meter (CA-X; Kyowa Interface Science Co. Ltd., Saitama, Japan). The UV light source was that used for

photocatalytic activity evaluation. The water droplet should be put at the dot marked on the opposite side of the testing surface. The procedure is presented in **Figure 3-3**. In some cases, to control the surface contamination, the films should be coated with 0.3 wt% stearic acid before evaluation of their photoinduced hydrophilicity. Stearic acid aqueous solutions were prepared by dissolving 0.015 g of stearic acid ($CH_3(CH_2)_{16}COOH$ = 284.48, Wako Pure Chemical Industries Ltd., Japan) in 5 g of distilled water. The TTP, PTT, and TT films were coated by stearic acid using spin coating conducted at 2,000 rpm for 30 s. Then these films were dried in a 70 °C oven for 10 min. This procedure is presented in **Figure 3-4**.

To evaluate the sustainability of hydrophilicity, we also evaluated the WCA increase during hydrophobicizing in the dark. We also investigated the effect of atmosphere on the hydrophobicizing using pure synthesized air and nitrogen (N_2) with 10% relative humidity. The pre-cleaned films were put into a Pyrex glass vessel (500 mL) sealed with a quartz glass lid in which 90 ml/min of dry air or nitrogen with 10 ml/min of water saturated air or nitrogen, 10% relative humidity, flowed continuously during dark storage. This system was broken down temporarily every 1 or 2 days to measure WCA. Then dark storage was continued under identical conditions.

3.3. Results and discussion

3.3.1. Characterization of films

Figure 3-5 presents UV–Vis spectra for TT, TTP and PTT during film preparation. The films were transparent with more than 80% transmission in the visible range (400–700 nm). Moreover, the UV–Vis absorbance increment corresponded with respective levels of deposition. This increment was steady for all film preparation. Nearly equal

absorbance between TT, TTP, and PTT films showed that the TiO_2 layer thicknesses were almost equal.

Figure 3-6 portrays the IR spectra of a PW_{12} film on a Si substrate. Because the peaks from the PPP film were quite weak, we have prepared a film by laminating PW_{12} 8 layers (namely PPPPPPPP) and have used it for this measurement. The absorbance of pure PW_{12} is reported as 1080, 983, and 889 cm^{-1} **[8]**. The film shows characteristic bands of PW_{12} around 1076, 973, 892, and 801 cm^{-1} that are ascribed to stretching vibration of P–O, W=O, and W–O–W bonds in the Keggin structure **[8–11]**. A nearly single P–O stretching peak (1080 cm^{-1}) reflects that the Keggin structure is retained in the film even after 300 °C heat treatment. The slight shift in the P–O band might be attributable to the interaction between the Keggin structure and substrate. Sustainability of $H_3(PW_{12}O_{40})$ crystal was also confirmed using X-ray diffraction analysis of the directly heated sample of the starting material (**Figure 3-7**). This result corresponds to reports of previous studies describing the thermal stability of PW_{12} **[12]**. The respective surface topographies of the PPP, TT, and TTP films obtained by AFM are depicted in **Figure 3-8**. The average surface roughness (R_a) values of the PPP, TT, and TTP films by AFM at five points were, respectively, 1.4, 7.4, and 9.3 nm. The film thicknesses ascertained from observations of the crosscut section of these films using SEM images were around 30 nm (PPP), 60 nm (TT), and 70 nm (TTP) shown in **Figure 3-9**. However, it is noteworthy that the section planes of these films were not perpendicular. They shifted from the perpendicular plane Θ degree, as shown in **Figure3-10**.

The concentration of W against Ti on the surface of TTP film by XPS analysis was around 5 atom%. Five pieces of the dried 60 °C TTP films or five pieces of the heat-treated 300 °C TTP were immersed into 100 ml of distilled water for 3 min. Then PW_{12}

dissolution was observed by ICP–OES. The tungsten (W) concentrations in the solution were shown in the **Figure 3-8**.

3.3.2. Photocatalytic activity and photoinduced hydrophilicity

Both TiO_2 and PW_{12} can decompose IPA through a photocatalytic reaction. The decomposition pathway of this reaction has been studied extensively **[13–15]**. Molecules of gaseous IPA are decomposed initially into acetone, and ultimately to H_2O and CO_2. However, the photocatalytic activity of solid state Keggin-type heteropolyacid was very low under 1 mW/cm^2 UV illumination **[8]**. In addition, the decomposition rate of acetone by TiO_2 photocatalyst is much lower than that of IPA because of displacement of water vapor from the TiO_2 surface [**16**] and the reaction rate difference against radical species [**17**].

Figure 3-11 portrays the concentration change of IPA by UV illumination. In the figure, C_0 represents the initial concentration after 5 h dark storage. The average C_0 values for TTP, PTT, and TT films were, respectively, 487 ppm, 470 ppm, and 487 ppm (for heat-treated 300 ℃ films) and 451 ppm, 457 ppm and 500 ppm (for dried 60 ℃ films). To avoid complexity, **Figure 3-11** shows only the change of IPA. The changes of acetone and CO_2 are presented in **Figure 3-12**. The order of IPA decomposition rate was TTP > PTT ~ TT corresponding with the experimentally obtained result in chapter 2. Heat-treatment did not change IPA decomposition ability of PTT and TT but, for only TTP, IPA decomposition rate decreased after heat-treatment. This might because the lower crystallinity of PW_{12} as shown before in **Figure 3-7**. However, TTP film decomposed IPA faster than TT and PTT. Consequently, PW_{12} enhances electron–hole

separation even after heat treatment at 300 °C. Here after, the mentions about TTP, PTT, TT or PPP refer to the heat-treated 300 °C films.

First, either dark storage or stearic-acid-coating was performed for hydrophobicizing processing (see **Figure 3-3** and **Figure 3-4**). To control surface contamination, stearic acid (0.3 mass%) was coated equally onto each cleaned film surface. For TTP, the initial water contact angle (WCA) was lower than those for TT or PTT shown in **Figure 3-13**. This might be explained by the difference in wettability between the TiO_2 top-most films and the PW_{12} top-most films, which causes deposition of different stearic acid amounts on each film, even when using the same spin coating conditions. Consequently, other spin conditions were tried to gain the initial WCA of around 120°. Mainly, angular velocity was decreased while the spin time and coating number were increased. However, the highest WCA was only 100°; the physical appearance of coated film was poor (sticky and smudged). The WCA conversion rates for the normal film occurred in the following order: TTP = PTT > TT (**Figure 3-13-(a)**). In contrast, the order for the stearic-acid-coated films was TTP > PTT = TT (**Figure 3-13-(b)**). Irrespective of the existence of PW_{12} on PTT, WCA conversion on stearic acid coated TT and stearic acid coated PTT was similar. Numerous reports support that the hydrophilicity relates to the organic decomposition especially in the early stage **[18, 19]**. Moreover, photogenerated holes play an important role for the hydrophiliciziing mechanism **[20]**. Charge separation by PW_{12} should therefore also affect the photoinduced hydrophilicity. In general, PW_{12} of PTT cannot consume electrons from TiO_2 effectively because of lacking of oxygen and water playing as an electron acceptor for reproducing ground-state-PW_{12}. However, when the film was moistened with water, the water dissolved the PW_{12} and brought it to the top surface so that charge separation

occurred. Consequently, the WCA conversion rates of TTP and PTT were the same. The result from the stearic coated film also corresponds with this assumption. Because stearic acid is water repellent, water cannot pass through the PTT film to bring PW_{12} to the surface. Consequently, the WCA conversion rate of TTP was higher than that of PTT. These explanations are presented in **Figure 3-14**. Additionally, the reusability for TTP and PTT was tested. After three test repetitions, the WCA conversion rates for both TTP and PTT remained unchanged, as shown in **Figure 13-15**.

Figure 3-16 portrays the IPA concentration change of IPA by UV illumination. In the figure, C_0 represents the initial concentration after dark storage. The practical value for PPP was 522 ppm. Results show that TTP film decomposed IPA faster than TT, although PPP showed almost no IPA decomposition activity. These results, which correspond with that of a previous study performed using samples without heat treatment, suggests that PW_{12} enhances electron–hole separation even after heat treatment at 300 °C. **Figure 3-17** presents the contact angle change on the sample surface under UV illumination in ambient air. The rate of hydrophilicization of the film was increased by coating PW_{12}, especially in the early stage of UV illumination. Its entire order was PPP << TT < TTP. This order is identical to that of photocatalytic decomposition activity for gaseous IPA, suggesting that the contribution of the decomposition of organic contaminant on the surface to the initial contact angle decreases the photoinduced hydrophilicity of brookite, as in anatase **[18, 21, 22]** and rutile [**23**]. The PPP film is more hydrophobic than the TT film under UV illumination. Therefore, another expected mechanism related to this phenomenon is the wettability difference between PW_{12} and brookite. Previous studies demonstrated that surfaces with different wettability sometimes provide a highly hydrophilic state by providing

hydrophilic channels and a resultant two-dimensional capillary effect **[24, 25]**. However, it is inferred that the contribution of this mechanism is not so important because of the following result.

Figure 3-18 portrays the sustainability of the hydrophilicity during dark storage. In this experiment, UV light was illuminated on samples for 8 h. Then they were stored in the dark. The TTP films exhibited not only a better hydrophilicizing process, but also better sustainability of hydrophilicity than the TT film showed. The surface wettability of a composite of two materials is well known to be estimable using Cassie's theory **[26]**. When the unit area of the surface comprises a solid surface area fraction f with a water contact angle θ_1, the resultant contact angle on the composite surface can be expressed as the following equation.

$$\cos\theta' = f\cos\theta_1 + (1-f)\cos\theta_2$$

Therein, θ_2 is the contact angle of the second phase. Based on this theory, PW_{12} is expected to be more hydrophilic in the TTP surface than TiO_2 to provide better sustainability of hydrophilicity. However, as presented in **Figuure 3-17**, the PPP film surface was more hydrophobic than that of the TT film.

Figure 3-19 depicts the expected electron transfer scheme of the hybrid film of PW_{12} and TiO_2. When UV light is illuminated on the surface of the TTP film, electrons are excited and holes are generated simultaneously at the valence band (VB) of TiO_2 and HOMO level of PW_{12}. Generated holes in TiO_2 oxidize IPA directly or through radical species, whereas the holes in HOMO level of PW_{12} trap electrons from TiO_2. Consequently, it is reduced to PW_{12}^-, which absorbs visible light and produces a stronger reduction power (PW_{12}^{-*}) than ground-state PW_{12}^- **[9]**.

As described in an earlier report [27], the electrons excited in TiO_2 are more numerous than those in PW_{12} in the (brookite) case examined here. Although some electrons in TiO_2 are consumed for healing holes in PW_{12}, excess electrons are expected to transfer directly to the LUMO level of PW_{12}, although some disappear by recombination with holes in TiO_2. The excitation efficiency by visible light to form PW_{12}^{-*} from PW_{12}^{-} is not high in this case. Therefore, the direct reduction by PW_{12}^{-} is more important than that by PW_{12}^{-*} as the practical reduction path. Experimental results show that PW_{12} functions effectively as an electron scavenger and that it inhibits the charge recombination of TiO_2, consequently increasing the overall photocatalytic activity. The difference of PW_{12} between on the TTP and on the PPP films is the electron scavenger history from TiO_2 by UV illumination. Reportedly, once PW_{12} is reduced into PW_{12}^{-} by electron injection from TiO_2, a certain period is necessary for complete reoxidation [28, 29]. Therefore, it is inferred that reduced PW_{12} (PW_{12}^{-}) adsorbs water molecules and thereby becomes more hydrophilic than brookite.

PW_{12}^{-} provides absorption in the visible wavelength range. Therefore, we measured UV–Vis spectra to identify PW_{12}^{-} for the TTP film after UV illumination. However, clear absorption was not well detected, probably because of a very thin PW_{12} deposition thickness. Therefore, we evaluated the state of W on the TTP film before and after UV illumination by XPS. The TTP film was illuminated by UV (1 mW) for 13 h, then the sample was set into the XPS. The W state was compared with the sample without UV illumination. The duration after stopping UV illumination until XPS measurement was around 1 h. The W(V) and W(VI) peaks are obtainable around 34–35 eV, and the peak separation of W4f revealed that the concentrations of W(V) in W(VI) were increased from 2%–7% by UV illumination.

A detailed explanation is presented here. The spectra of the TTP film before and after UV illumination after background subtraction and relative to C1s (248.5 eV) are shown in **Figure 3-20** (black line).

We conducted peak deconvolution again. The results are shown in **Figure 3-20**. The spectra of $W4f_{7/2}$, $W4f_{5/2}$, Ti3P, and $W5p_{3/2}$ exist in the 33–45 eV range. Their respective estimated binding energies are 35, 37, 37, and 40 eV. Precise separation of Ti3p and $W4f_{5/2}$ is not feasible. Therefore, in this study, only $W4f_{7/2}$ was considered. After deconvolution, main and minor peaks are apparent at 35.45 eV and 33.95 eV. Binding energy of $W4f_{7/2}$ was reported by Li *et al*. as 35.8 eV [30]. They revealed that the value shifts to the lower energy level when it is combined with TiO_2. Based on their result, the sample of 8.3% PW_{12} in TiO_2 showed $W4f_{7/2}$ at 35.3 eV. The XPS analysis (performed using $W4f_{7/2}$) revealed that TTP film in this study possesses 5% PW_{12}. Consequently, $W4f_{7/2}$ spectra should locate in the binding energy range of 35.3 and 35.8 eV. Rothschild *et al*. reported 1.1 eV shifting to lower energy side from the oxidation stage (+VI) to the reduction stage (+V) for W [31]. Therefore, the minor peak at 33.95 eV is attributable to the reduction state of $W4f_{7/2}$. In this study, TTP film was illuminated for 13 h. Then the sample was set into the XPS. The duration after stopping UV illumination until XPS measurement was around 1 h. After UV illumination, the ratio of the reduction stage increased from 1.7%–7.3%. However, after UV illumination, the deconvolution is more complex because the reduction stage of $W4f_{5/2}$ should also increase, but we were unable to include this peak.

Moreover, several additional results suggest the effect of PW_{12}^- in the TTP film on the sustainability of hydrophilicity. **Figure 3-21** shows contact angles and surface potentials measured using KFM for the samples stored in the dark for three days after

UV illumination for 8 h. In general, the surface potential exhibits a reverse trend against the contact angle **[32, 33]**. However that of the TTP film is more negative than expected. This result might derive from PW_{12}^- in the surface.

Furthermore, we examined the atmospheric dependence of the sustainability of hydrophilicity for the TTP film under synthesized air and N_2 with 10% relative humidity. As might be readily apparent from **Figure 3-22**, the sustainability is greater in N_2 than air. These results also suggest that the reoxidation process of PW_{12}^- by water and O_2 plays an important role in sustaining hydrophilicity.

We prepared a TTP thin film using an anatase suspension (STS-100, 20 wt% concentration, primary particle size = 6 nm; Ishihara Sangyo Kaisha, Ltd., Mie, Japan) employed in our previous study **[9, 34, 35]**, and examined the photoinduced hydrophilicity under the same conditions as those used in the present study. The result is presented in **Figure 3-23.** The photoinduced hydrophilicizing rate for the case of brookite is higher than that for anatase. However, these results cannot simply be attributable to the crystalline phase difference. As described in an earlier report **[27]**, absorbance of UV per deposition thickness for anatase is smaller than that for brookite. Moreover, the specific surface area and crystallinity differ. Unless the TiO_2 particle suspensions being examined have the same physical and chemical properties, except for crystalline phase, the crystalline phase dependence cannot be assessed.

Although Pt-loading is well known to improve the photocatalytic activity of TiO_2 by increasing electron–hole separation efficiency **[36]**, this treatment degrades photoinduced hydrophilicity because Pt is fundamentally hydrophobic **[37]**. From the viewpoint of photocatalytic decomposition, PW_{12} is a scavenger of electrons from TiO_2. Therefore, its role is the same as Pt. However, PW_{12} becomes hydrophilic by accepting

electrons. Therefore, even after stopping UV illumination, the TTP film can sustain a small contact angle of water for a certain period. Hybridization of SiO_2 with TiO_2 is well known to increase the rate of hydrophilicization under UV illumination and sustains hydrophilicity in the dark **[38–40]**. However, this combination decreases the surface area ratio (commonly 30–40%) of TiO_2 for photocatalytic decomposition. The TTP film in this study simultaneously attained high decomposition activity, a high hydrophilicization rate, and sustainability of hydrophilicity. The electron storage performance was also reported for the PW_{12}/ TiO_2 system **[28, 29]**. Hybrid films reported in this study, which are transparent in the visible wavelength range, are useful in various applications.

3.4 Conclusion

For this study, we prepared hybrid films of PW_{12} and TiO_2 (brookite) using LBL method. Then a comparative study was conducted of photocatalytic decomposition activity and photoinduced hydrophilicity of the films. The TTP (TiO_2/TiO_2/PW_{12}) film exhibited better photocatalytic activity on the decomposition of gaseous IPA than the TT (TiO_2/TiO_2) film. The TTP film also provided more rapid hydrophilicization under UV illumination, and better sustainability of the hydrophilicity than the TT film. Results show that the electron scavenger effect of PW_{12} and resultant generation of PW_{12}^- are key factors affecting the performance of wettability conversion before and after UV illumination of this hybrid film.

Acknowledgments

The authors are grateful to Mr. Katsuaki Hori and Mr. Jun Kouki of the Center of Advanced Materials Analysis at the Tokyo Institute of Technology for TEM and SEM observations.

Reference

[1] R. Wang, K. Hashimoto, A. Fujishima, M. Chikuni, E. Kojima, A. Kitamura, M. Shimohigoshi, and T. Watanabe, *Nature* 388, 431–432 (1997).

[2] R. Wang, K. Hashimoto, A. Fujishima, M. Chikuni, E. Kojima, A. Kitamura, M. Shimohigoshi, and T. Watanabe, *Adv. Mater*. 10, 135–138, (1998).

[3] T. Watanabe, A. Nakajima, R. Wang, M. Minabe, S. Koizumi, A. Fujishima, and K. Hashimoto, *Thin Solid Films*, 351, 260–263, (1999).

[4] T. Shibata, H. Irie, M. Ohmori, A. Nakajima, T. Watanabe, K. Hashimoto, *Phys. Chem. Chem. Phys*. 6, 1359 –1362, (2004).

[5] A. Kolouch, M. Horáková, P. Hájková1, E. Heyduková, P. Exnar1, P. Spatenka., Problems of Atomic Science and Technology., No. 6. Series: Plasma Physics (12), 198-200, (2006).

[6] I. V. Kozhevnikov, *Chemical Reviews*, 98, 171–198 (1998).

[7] J.C. Edwards, C.Y. Thiel, B. Benac, J. F. Knifton, *Catal. Lett*,51, 77–83 (1998).

[8] A. Bielańskia, A. Lubańska, *J. Mol. Catal. A: Chem.* 224, 1–2, 179–187 (2004)

[9] S. Yanagida, A. Nakajima, T. Sasaki, Y. Kameshima, K. Okada, *Chem. Mater*. 20, 3757–3764 (2008)

[10] B. Bachiller-Baeza, J. Alvarez-Rodrı´guez, A. Guerrero-Ruiz, I. Rodrı´guez-Ramos, *Appl. Catal. A: Gen.* 333, 281–289. (2007)

[11] Y. Xu, X. Zhang, H. Li, Y. Qi, G. Lu, S. Li, *Catal. Lett*. 125(3–4), 340–347 (2008).

[12] Qi Yunshi, Liu Jingfun, Wu Haixia, Su Xiaoli, *Studies in Surf. Sci. Catal*. 90, 77–84 (1994)

[13] P. R. Harvey, R. Rudham, S. Ward, J. *Chem. Soc. Faraday Trans*. 79, 1381–1390 (1983)

[14] Y. Ohko, K. Hashimoto, A. Fujishima, *J. Phys. Chem. A*, 101, 8057–8062 (1997)

[15] A. Mylonas, A. Hiskia, E. Androulaki, D. Dimotikali, E. Papaconstantinou, *Phys. Chem. Chem. Phys.* 1, 437–440 (1999)

[16] S. A. Lanson, J. A. Widegren, J. L. Falconer, *J. Catal.*, 157, 611–625. (1995)

[17] M. Anbar, P. Neta, *Int. J. Appl. Radiat. Isotopes*18, 493–523 (1967)

[18] T. Zubkov, D. Stahl, T. L. Thompson, D. Panayotov, O. Diwald, J. T. Yates, *J. Phys. Chem B* 109, 15454 –15462 (2005)

[19] X. Yan, R. Abe, T. Ohno, M. Toyofuku, B. Ohtani, *Thin solid film* ,5872-5876 (2008)

[20] N. Sagai, A. Fujishima, T. Watanabe, K. Hashimoto, *J. Phys. Chem B* 105, 3023-3026 (2001)

[21] C.Y. Wang, H. Groenzin, M.J. Shultz, *Langmuir* 19, 7330–7334 (2003)

[22] N. Arimitsu, A. Nakajima, T. Watanabe, Y. Kameshima, K. Okada, J. *Photochem. Photobiol. A: Chem.*, 203155–160 (2009)

[23] K. Okudaira, T. Kato, T. Isobe, S. Matsushita, T. Kogure, A, Nakajima, *J. Photochem. Photobiol. A: Chem.* 222, 64–69 (2011)

[24] A. Nakajima, S. Koizumi, T. Watanabe, K. Hashimoto, *Langmuir* 16, 7048–7050 (2000).

[25] Y. Ito, M. Heydari, A. Hashimoto, T. Konno, A. Hirasawa, S. Hori, K. Kurita, A. Nakajima, *Langmuir* 23, 1845–1850, (2007).

[26] A. B. D. Cassie, S. Baxter, *Trans. Faraday Soc.* 40, 546–551 (1944).

[27] K. Pruethiarenun, T. Isobe, S. Matsushita, A. Nakajima, *Appl. Catal. A: Gen.* 399, 22–27 (2011).

[28] P. Ngaotrakanwiwat, S. Saitoh, Y. Ohko, T. Tatsuma, A. Fujishima, *J. Electrochem. Soc.*, 150, A1405–A1407 (2003).

[29] P. Ngaotrakanwiwat, T. Tatsuma, *J. Electroanal. Chem.*, 573, 263–269, (2004).

[30] J. Li, W. Kang, X. Yang, X. Yu, L. Xu, Y. Guo, H. Fang, S. Zhang, *Desalination* 255, 107–116 (2010)

[31] R.M. Rassel, T. Kim, Z. Shen, S.A. Campbell, P.H. McMurry, *J. Vac. Sci. Tech. A* 18(5), 2441–2447 (2000).

[32] H. Sugimura, K. Hayashi, N. Saito, O. Takai, N. Nakagiri, *Jpn. J. Appl. Phys*. 40, 4373–4377 (2001).

[33] N. Saito, K. Hayashi, H. Sugimura, O. Takai, N. Nakagiri, *Chem. Phys. Lett.* 349, 172–176 (2001).

[34] S. Yanagida, A. Nakajima, T. Sasaki, T. Isobe, Y. Kameshima, K. Okada, *Appl. Catal. A: Gen.* 366, 148–153 (2009).

[35] A. Nakajima, T. Koike, S. Yanagida, T. Isobe, Y. Kameshima, K. Okada, *Appl. Catal. A: Gen.* 385, 130–135(2010).

[36] A. Fujishima, X. Zhang, D. A. Tryk, *Surf. Sci. Reports* 63, 515–582 (2008).

[37] M. Miyauchi, *Phys. Chem. Chem. Phys*. 10, 6258–6265 (2008).

[38] M. Machida, K. Norimoto, T. Watanabe K. Hashimoto, A. Fujishima, *J. Mater. Sci.* 34, 2569–2574 (1999).

[39] T. Watanabe, S. Fukayama, M. Miyauchi, A. Fujishima, K. Hashimoto, *J. Sol–gel Sci. Tech.* 19, 71–76 (2000).

[40] K. Guan, *Surf. Coatings Tech.*, 191, 155–160 (2005)

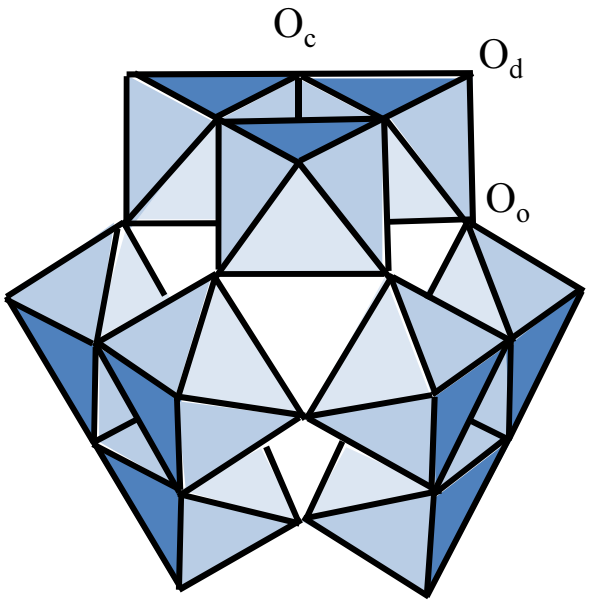

Figure 3-1 Keggin ion structure showing three type of outer oxygen atom; (O_d) terminal oxygen M=O, (O_b) corner-shared bridging oxygen M-O-M and (O_c) edge-shared [7]

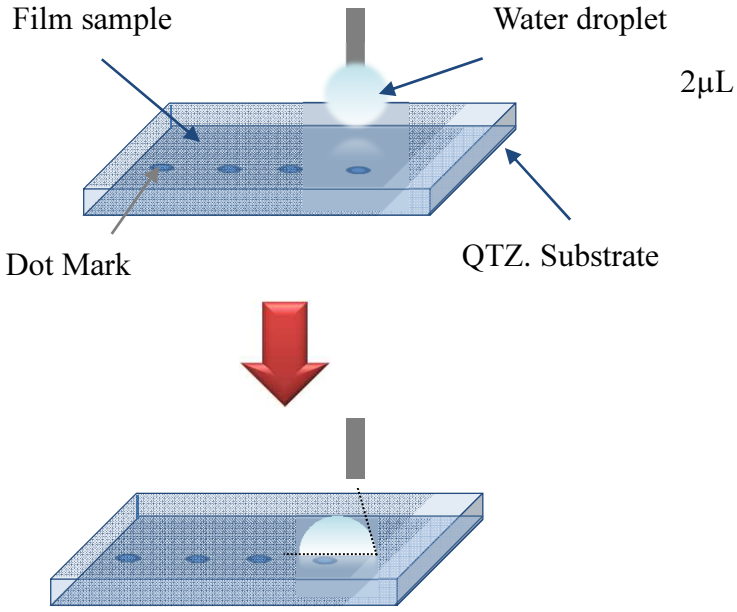

Figure 3-2 Scheme for sessile drop method

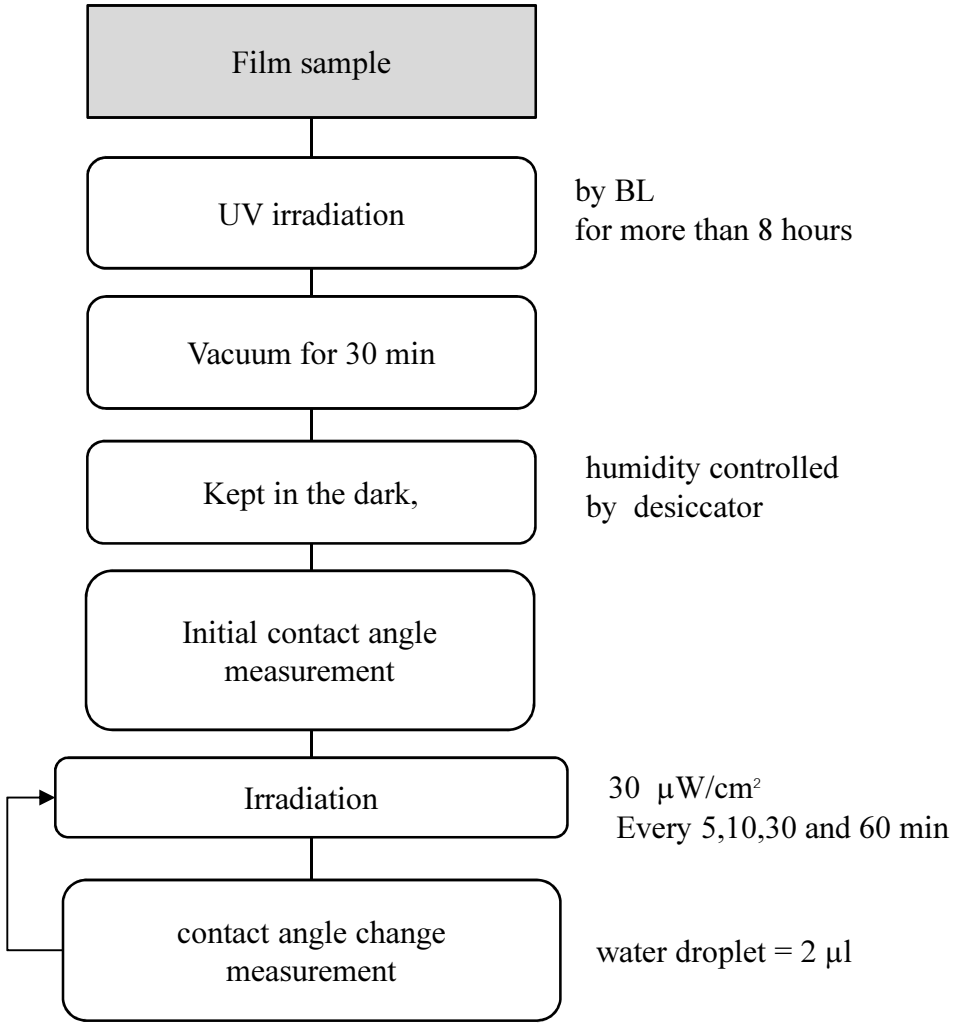

Figure 3-3 experiment procedure for investigating photoimduce hydrophilic property of the films

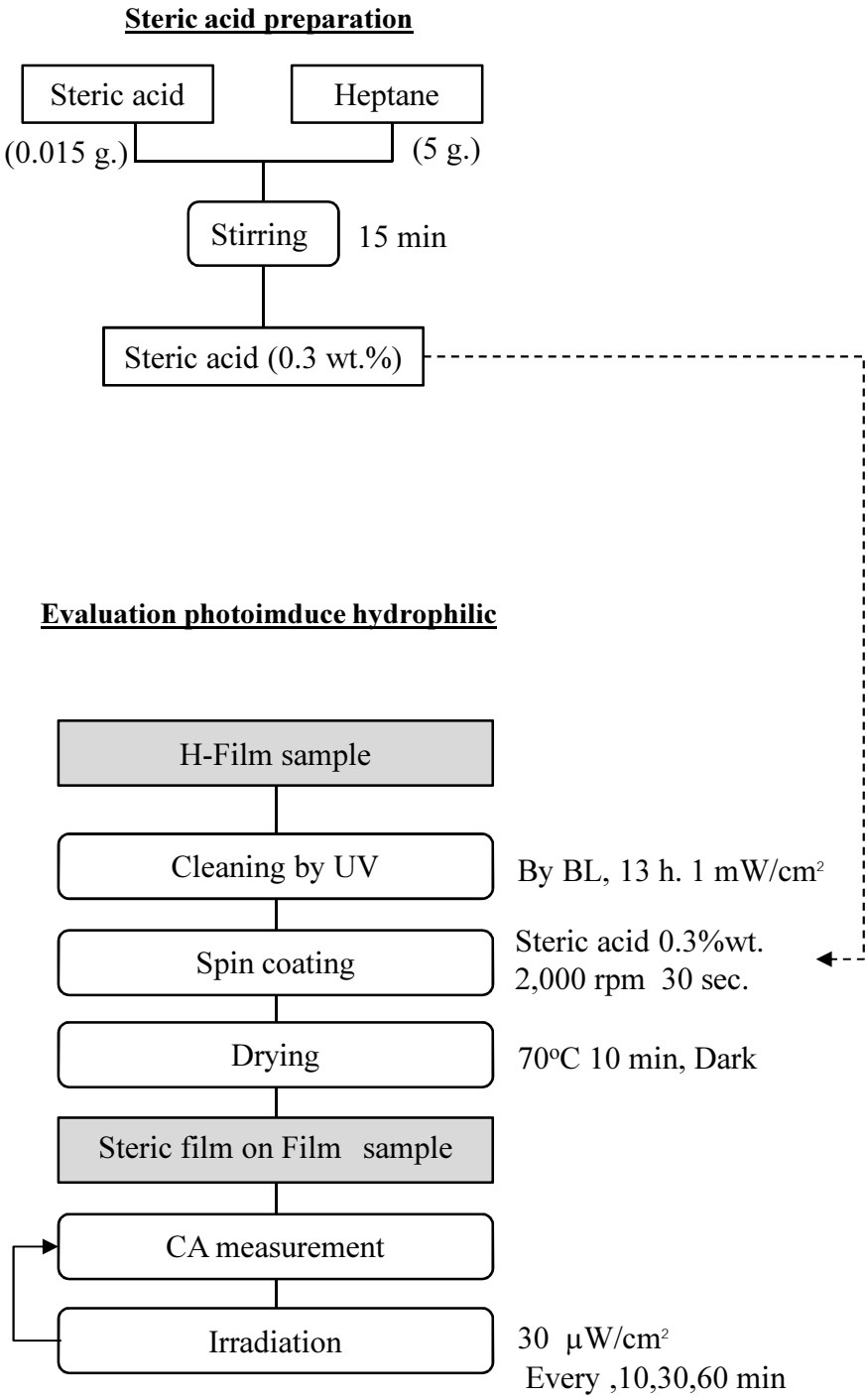

Figure 3-4 Steric coating procudure and evaluation photoimduce hydrophilic.

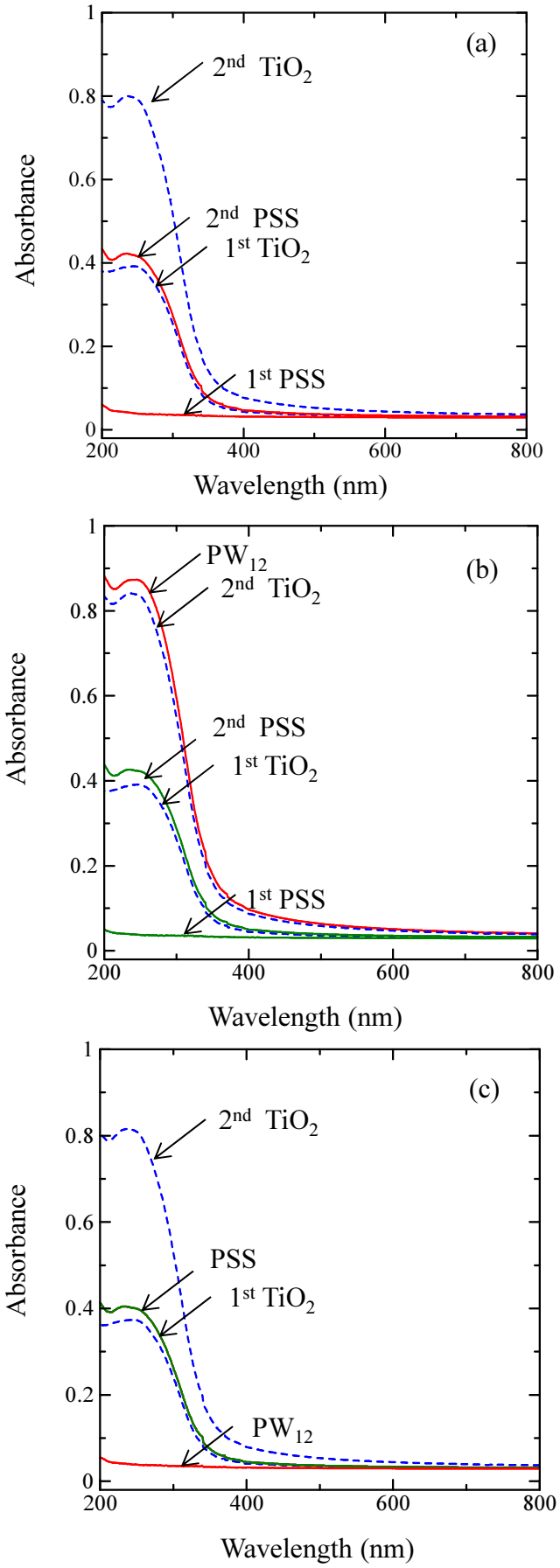

Figure 3-5 UV–Vis absorbance spectra increment per deposition of PSS, TiO_2 and PW_{12} of (a) TT (b) TTP and (c) PTT.

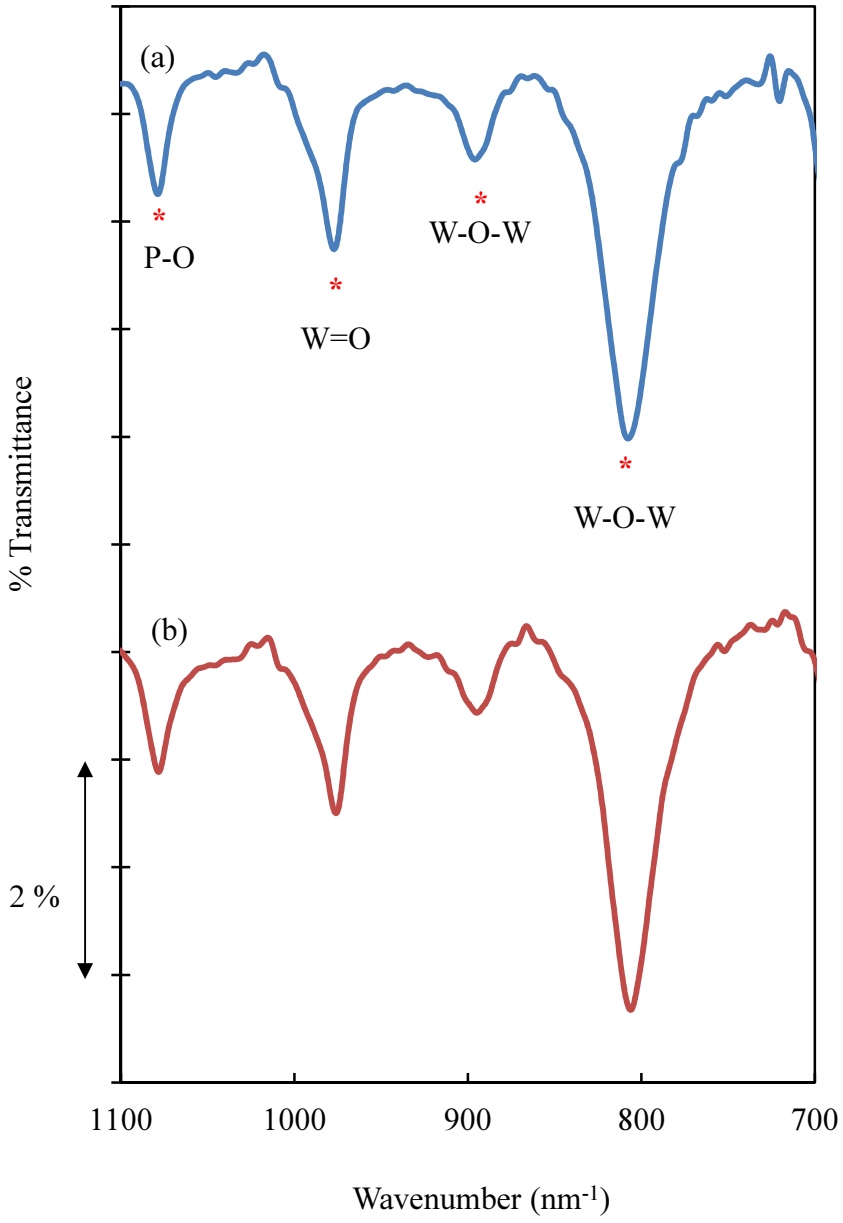

Figure 3-6 IR spectra of the $(PW_{12})_8$ film on Si substrate before (a) and after (b) heat treatment.

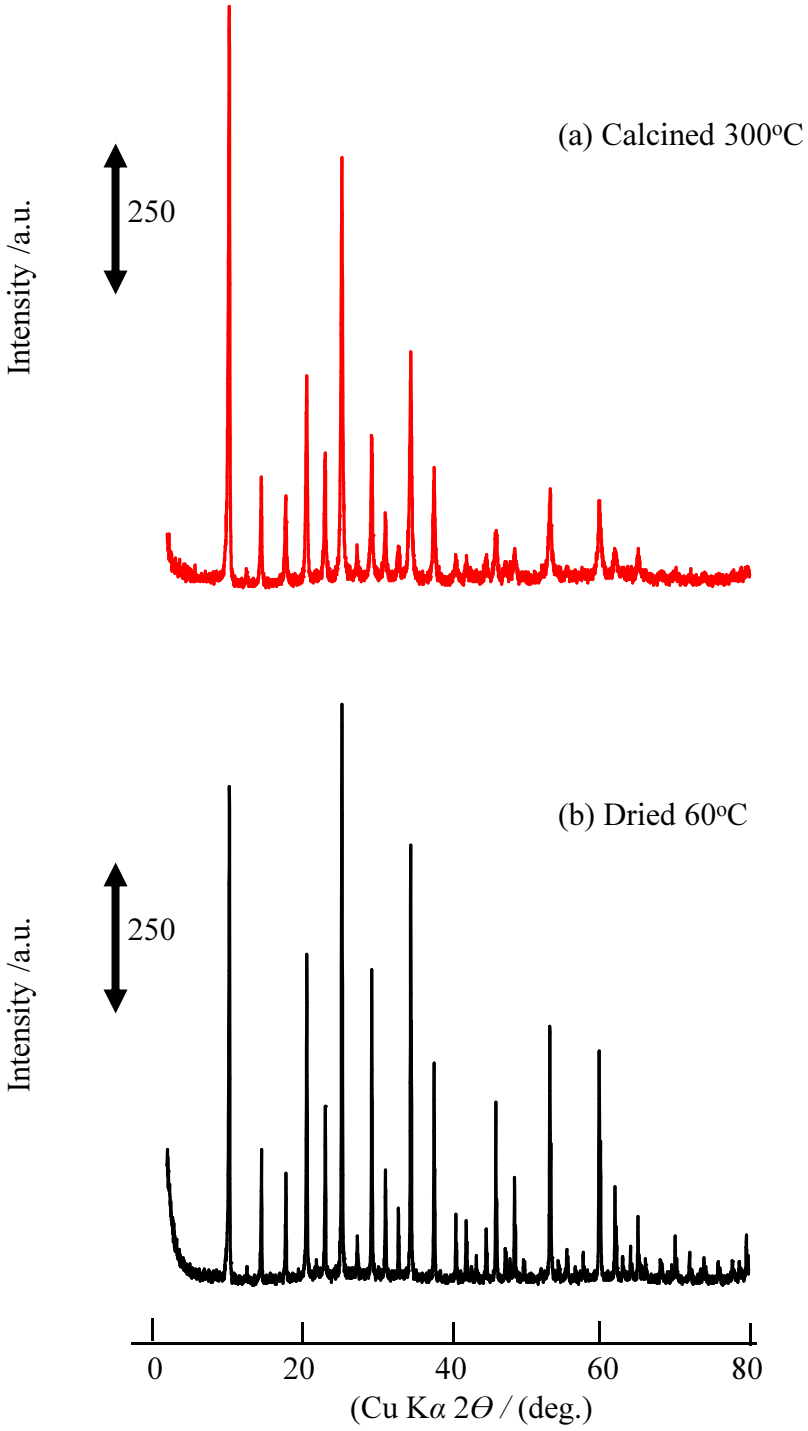

Figure 3-7 X-ray diffraction patterns of $H_3(PW_{12}O_{40})$ before (a) and after heat treatment at 300°C (b)

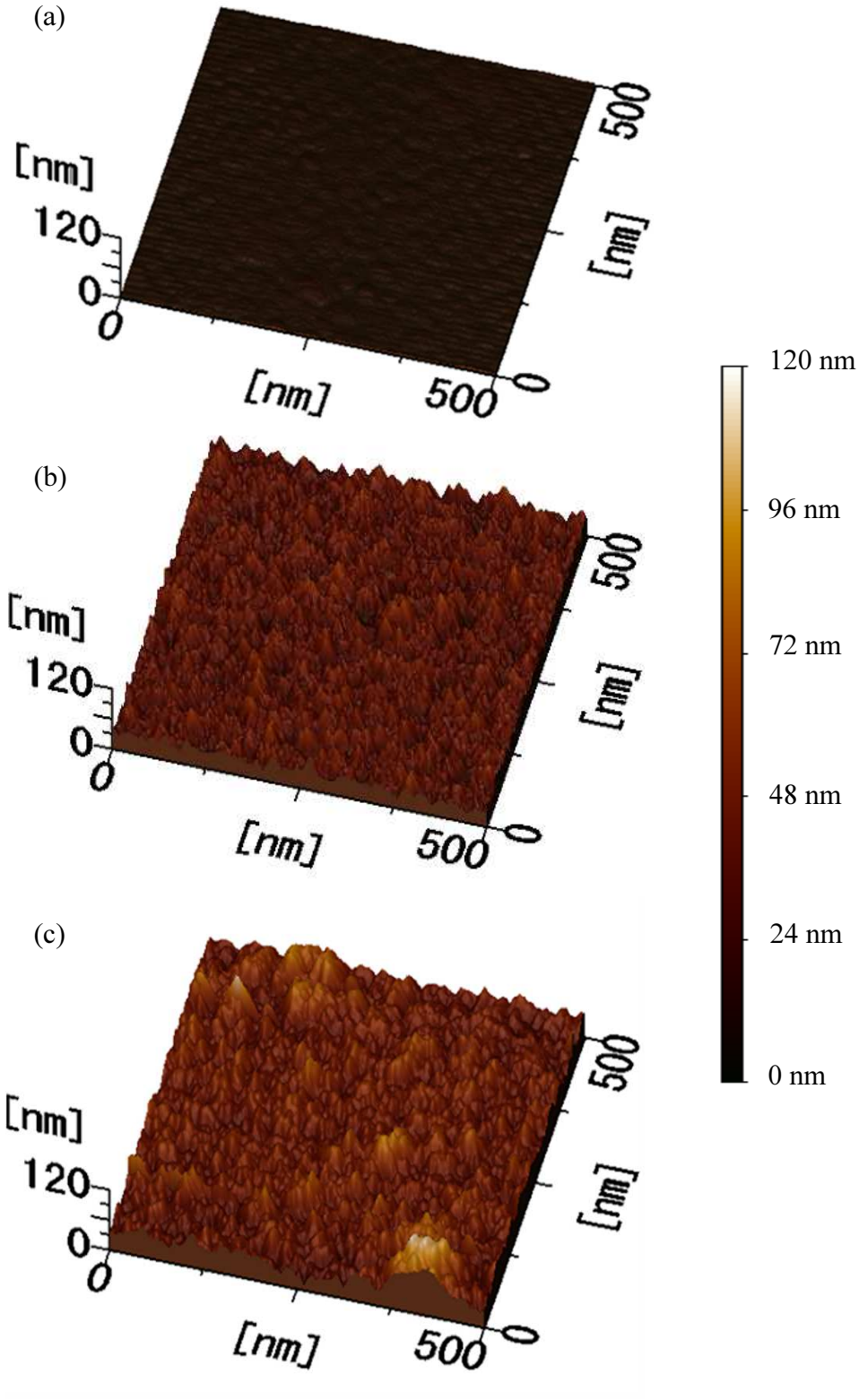

Figure 3-5 AFM images of (a) PPP, (b) TT, and (b) TTP films.

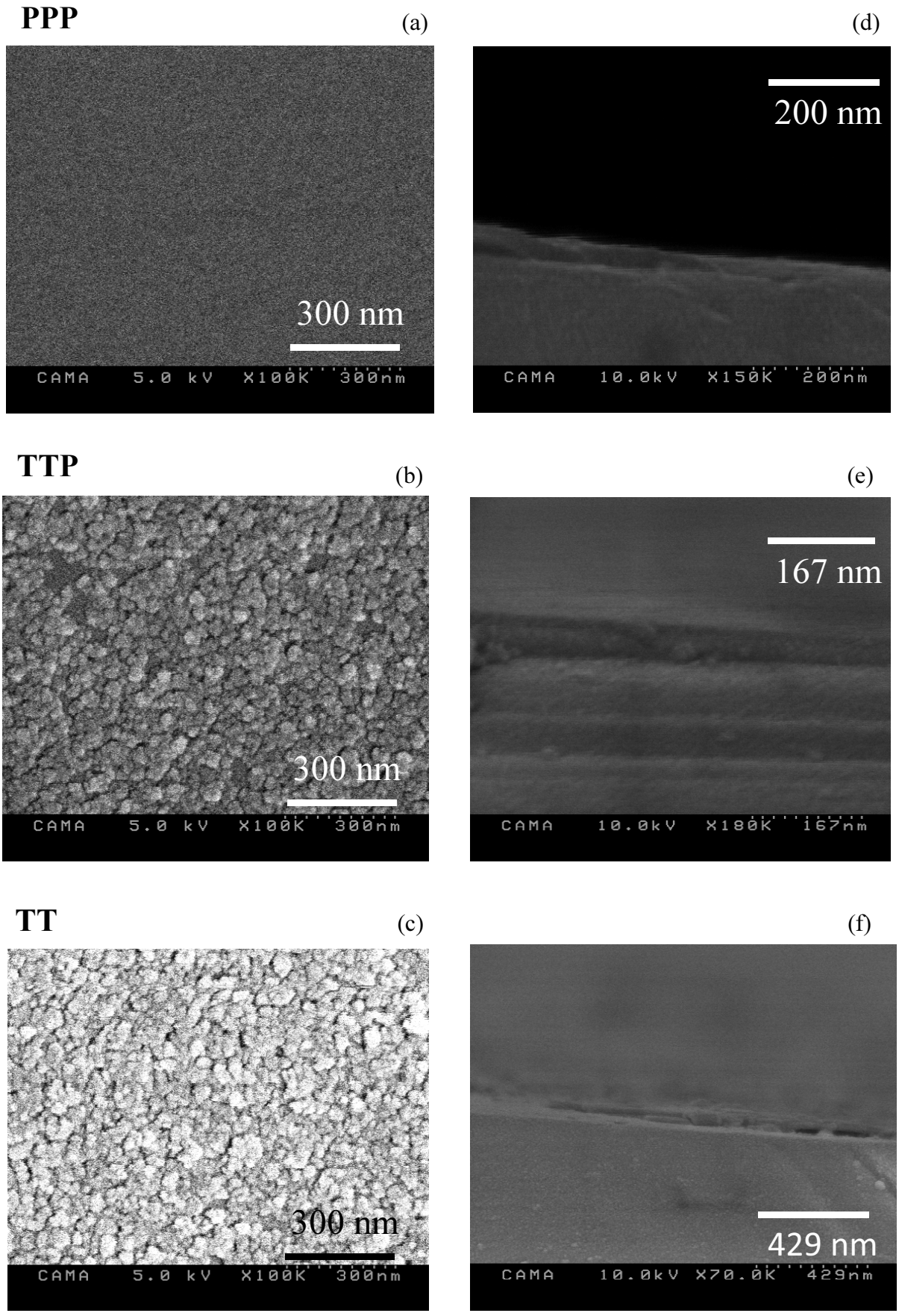

Figure 3-8 Top-view and cross-section SEM images of (a and d) PPP, (b and e) TTP, and (c and f) TT films.

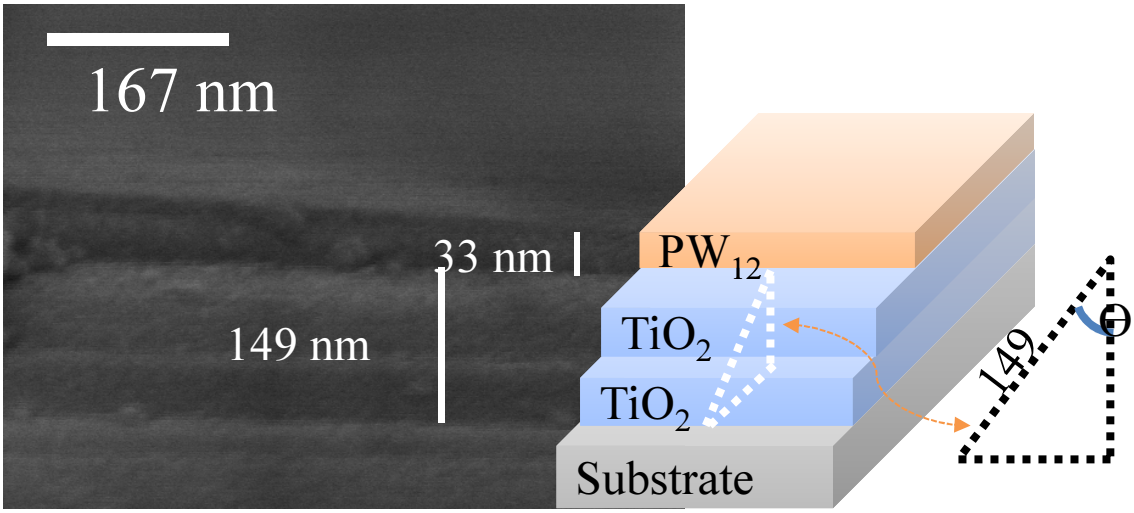

Figure 3-9 Section SEM images of TTP films.

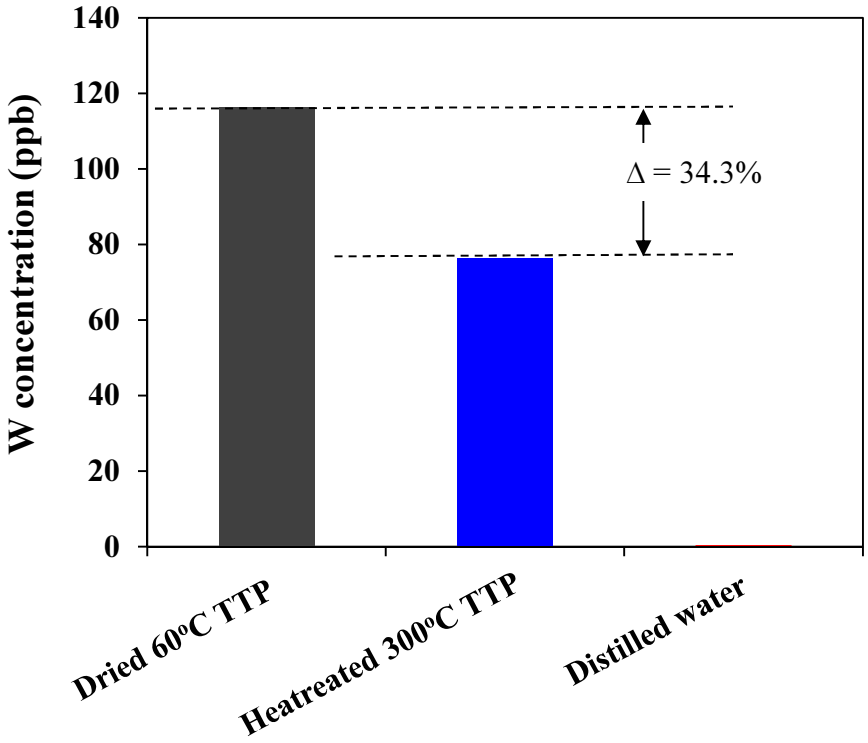

Figure 3-10 Dissolution of PW_{12} in distilled water

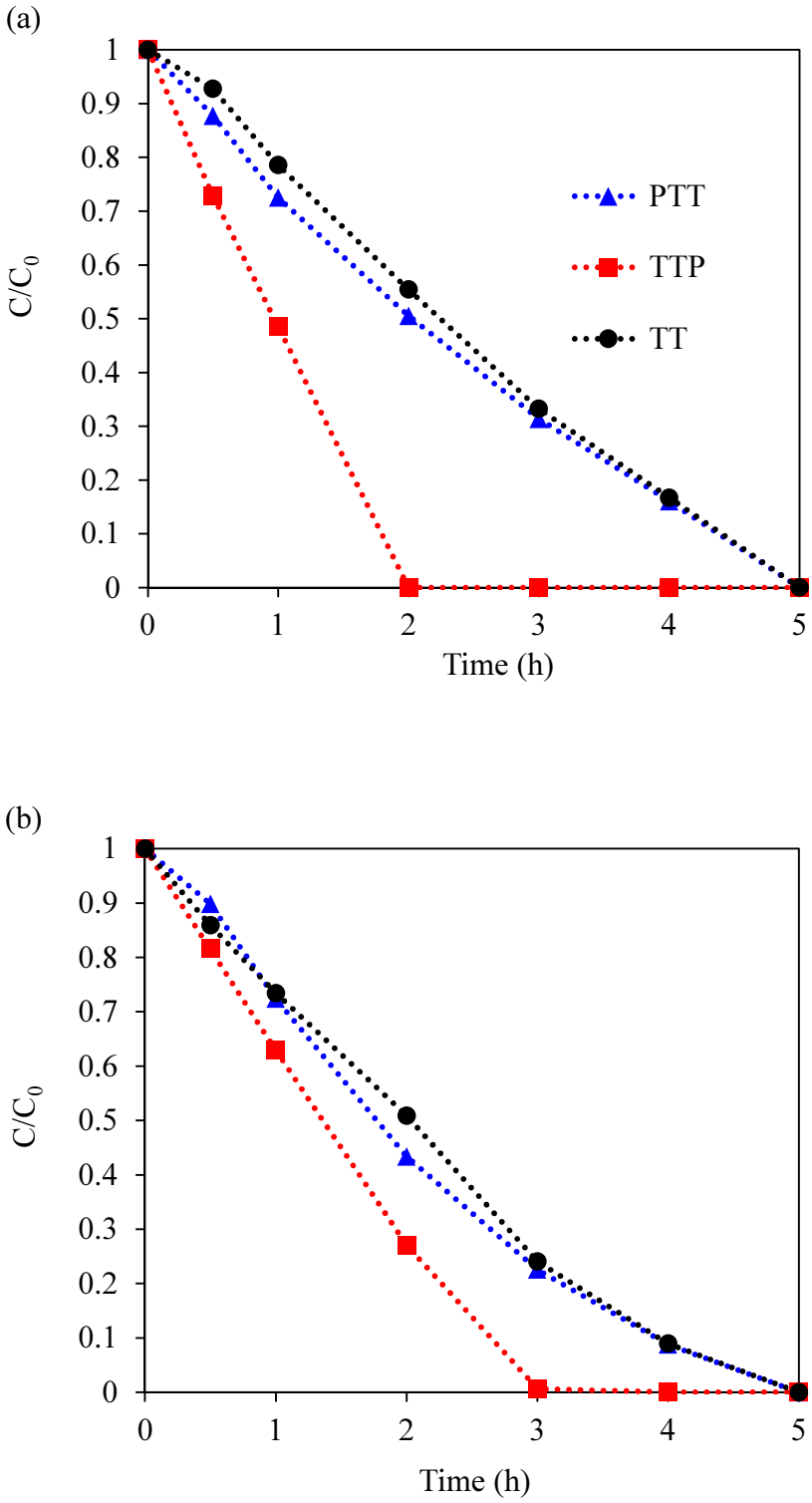

Figure 3-11 Concentration changes of IPA for TTP (■), PTT (▲), and TT (●) films under UV illumination (1 mW/cm^2); (a) dried 60^{o}C, (b) heat-treated 300^{o}C

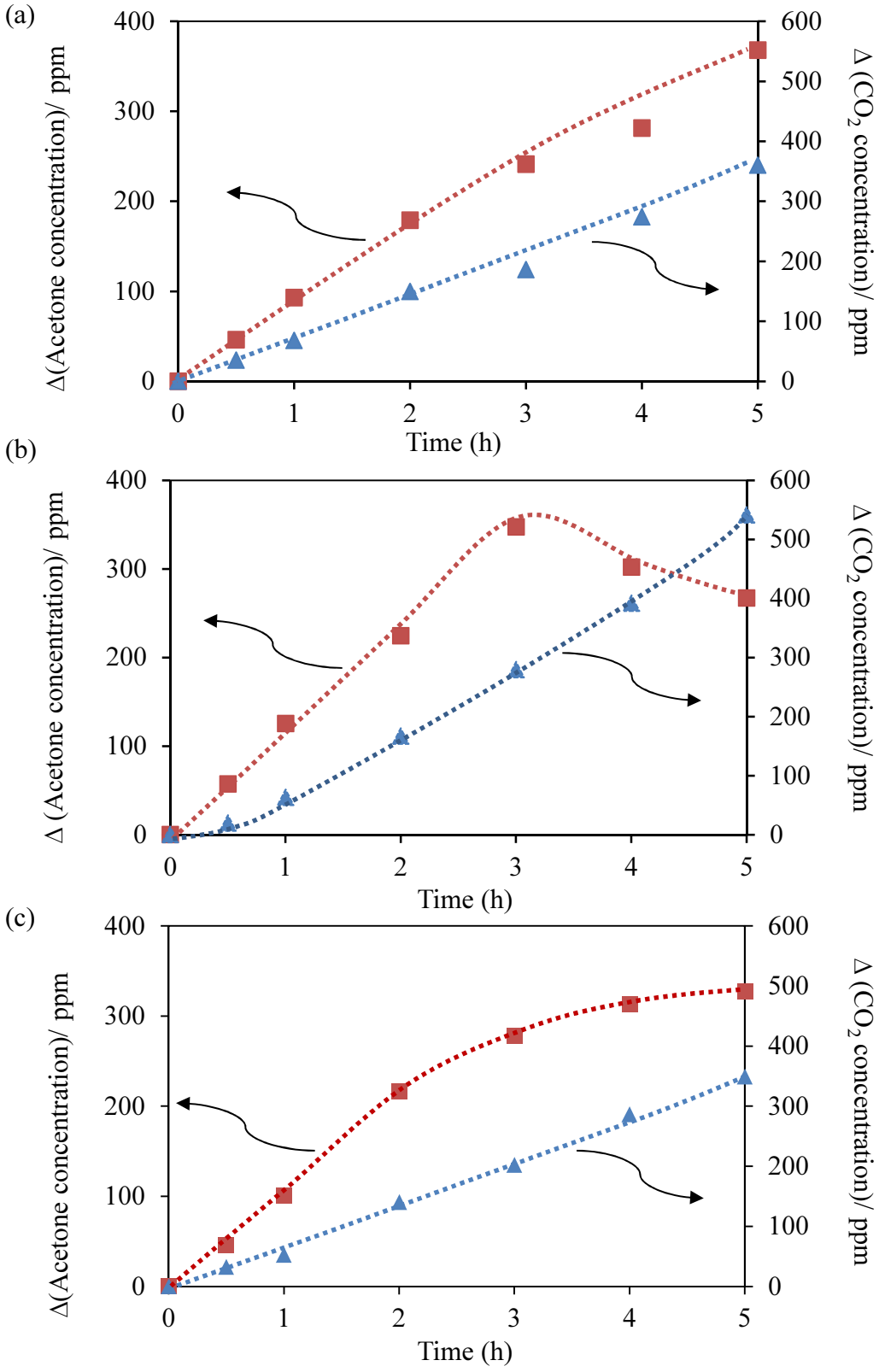

Figure 3-12 Concentration changes of acetone(■) and CO_2 (▲), for (a) TT, (b) TTP and (c) PTT under UV illumination (1 mW/cm^2)

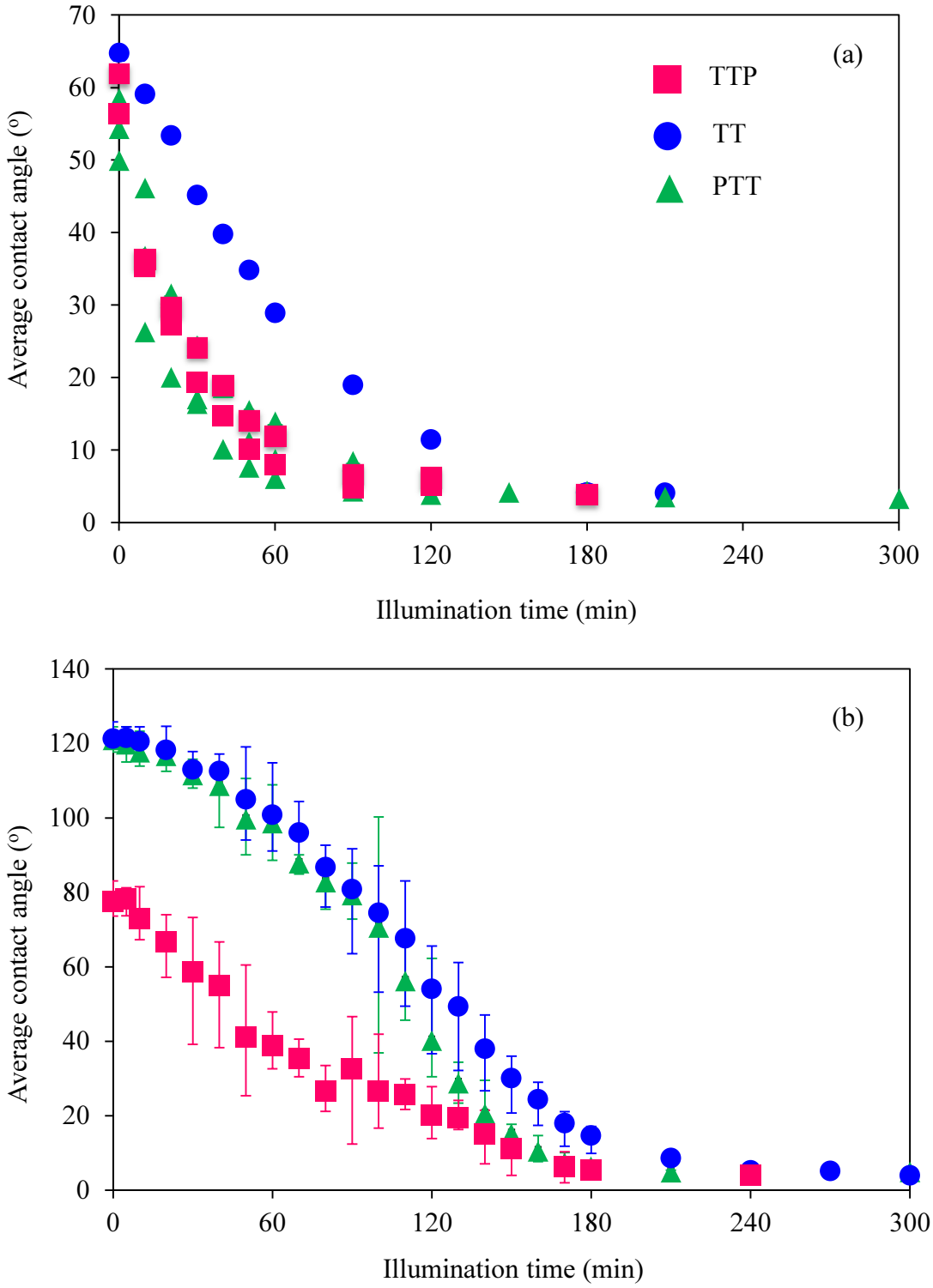

Figure 3-13 Water contact angle change on TTP (■), PTT (▲), and TT (●) films under UV illumination (30 μW/cm^2); (a) the normal films and (b) the steric acid coated films.

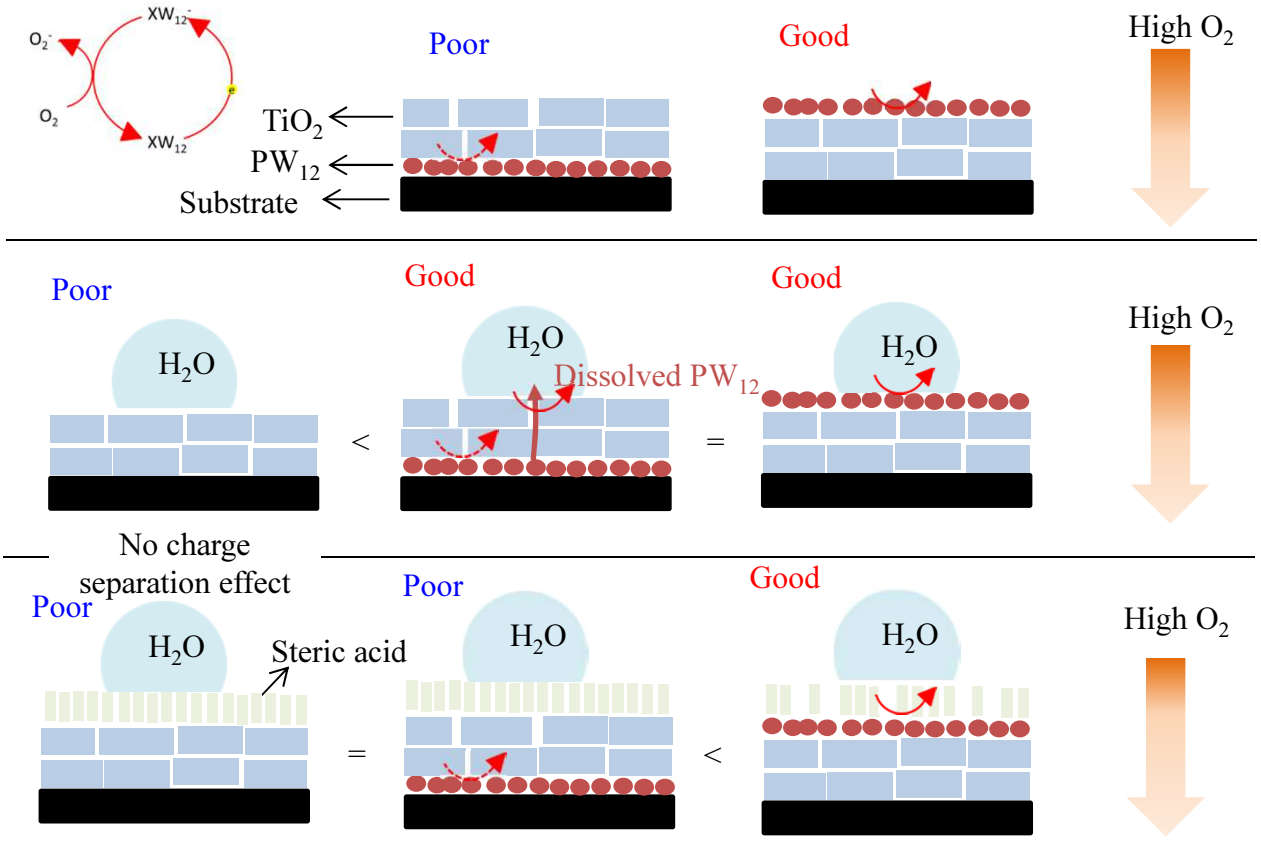

Figure 3-14 Water contact angle change on PTT (a) and PTT (b) under UV illumination (30 μW/cm^2) for the first (▲) second (♦), third (■), and fourth (●) test.

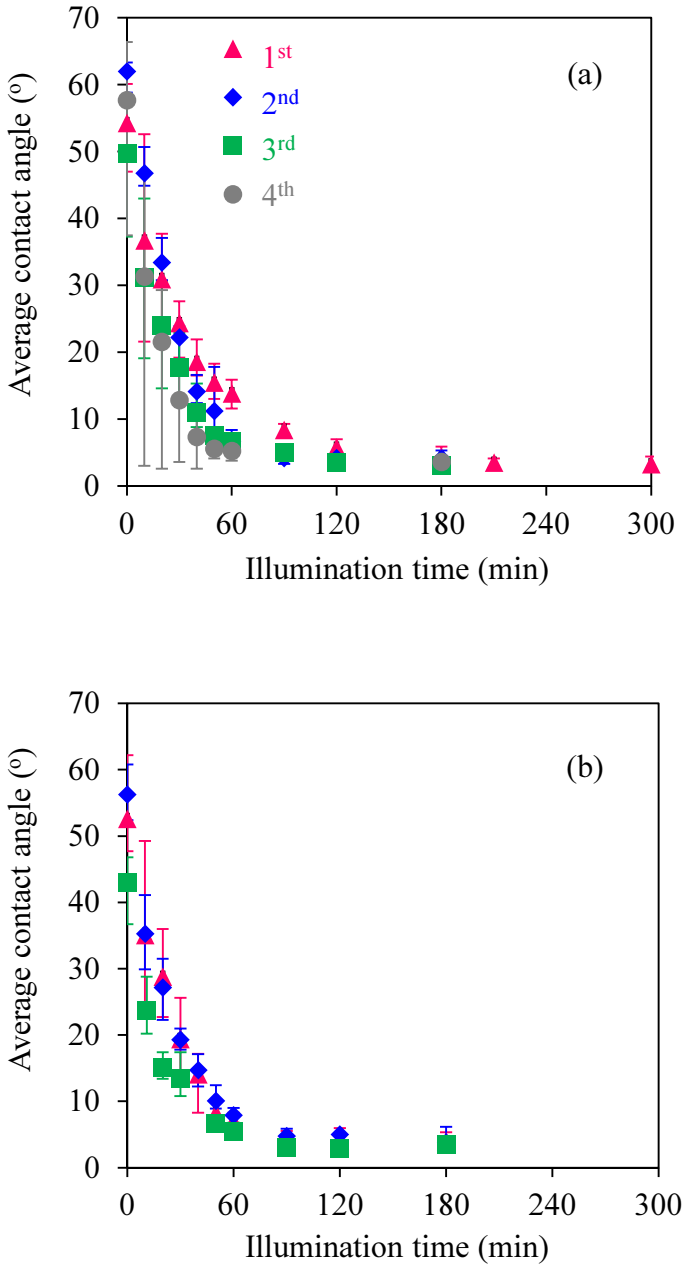

Figure 3-15 Water contact angle change on PTT (a) and PTT (b) under UV illumination (30 μW/cm^2) for the first (▲) second (♦), third (■), and fourth (●) test.

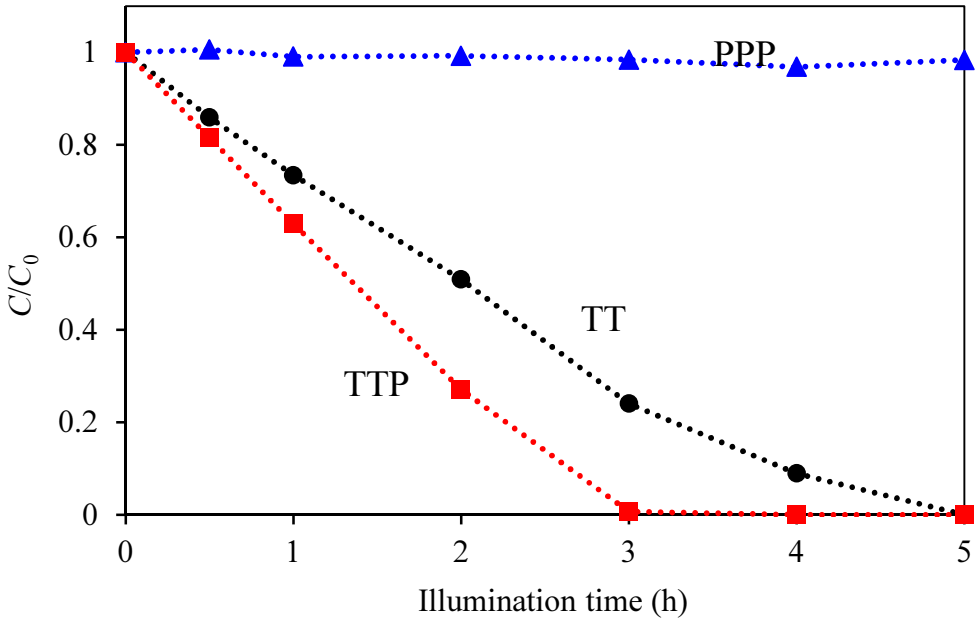

Figure 3-16 Concentration changes of IPA for PPP (▲), TT (●), and TTP (■) films under UV illumination (1 mW/cm^2).

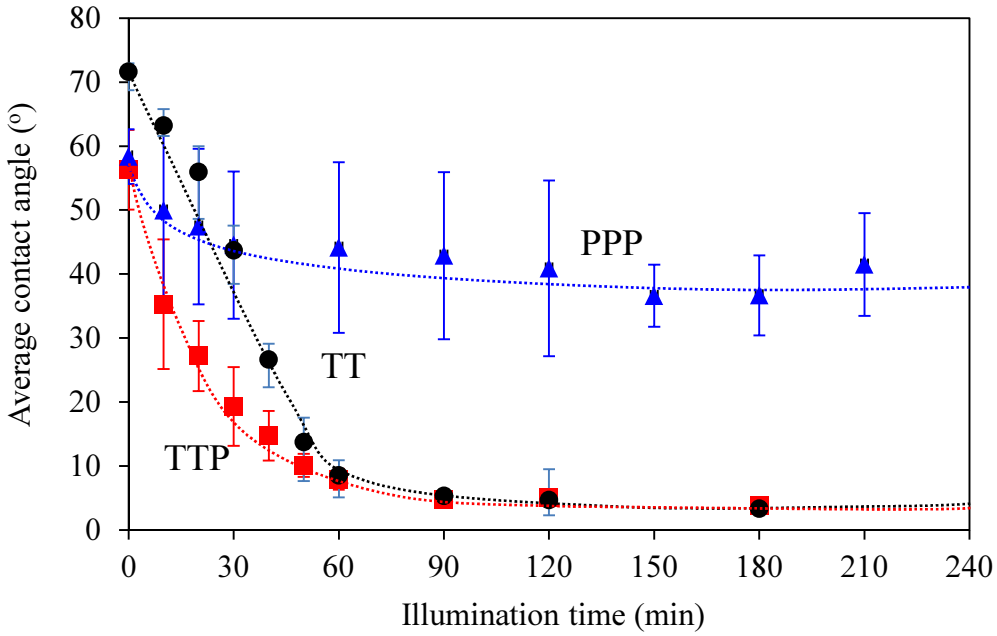

Figure 3-17 Water contact angle change on for PPP (▲), TT (●), and TTP (■) films under UV illumination (30 μW/cm^2)

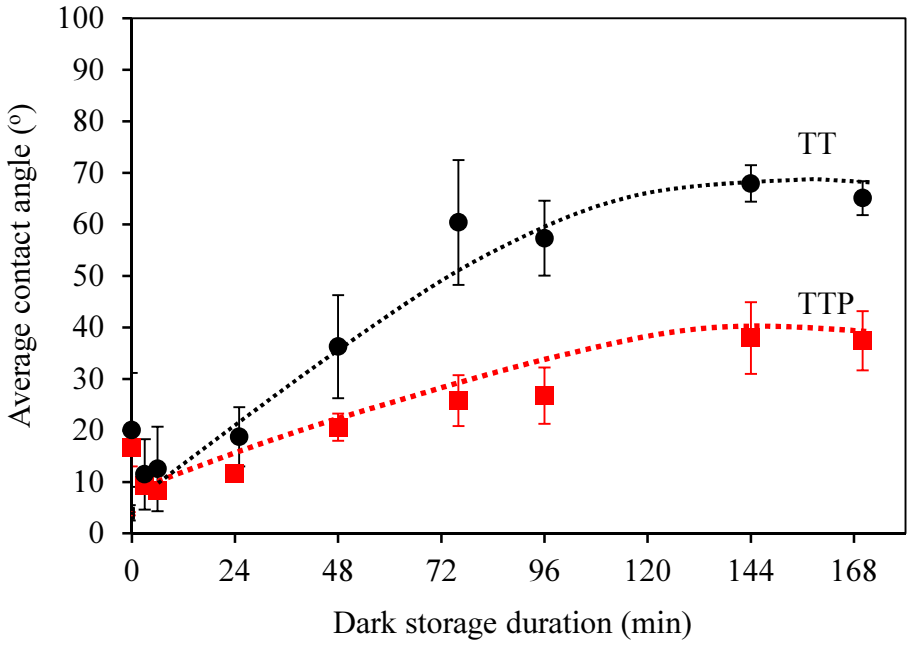

Figure 3-18 Water contact angle change on illumination TT (●) and TTP (■) films films during dark storage after UV

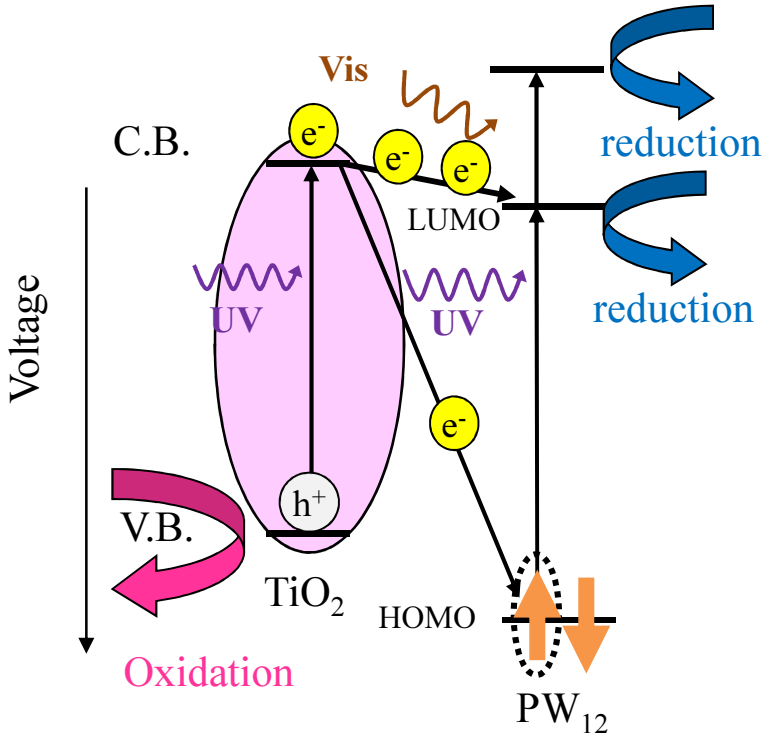

Figure 3-19 Expected electron transfer scheme of the hybrid film of PW_{12} and TiO_2 (brookite).

(a)

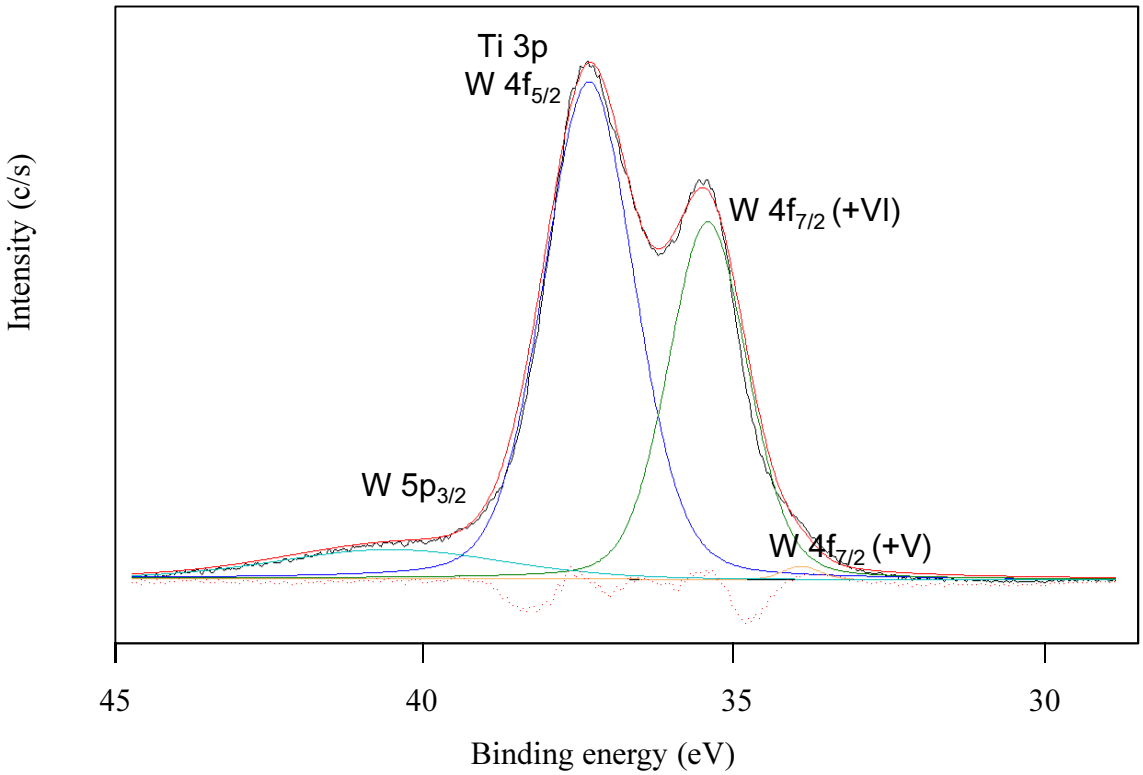

(b)

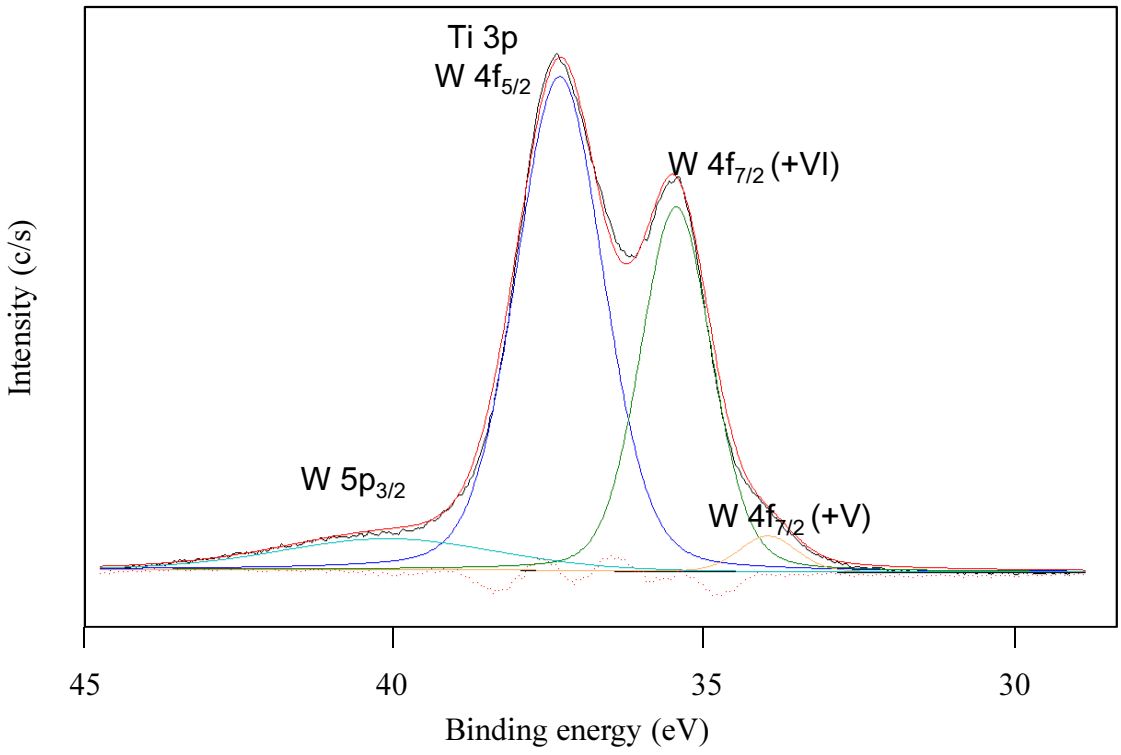

Figure 3-20 XPS spectra after deconvolution of TTP film before (a) and after (b) UV illumination.

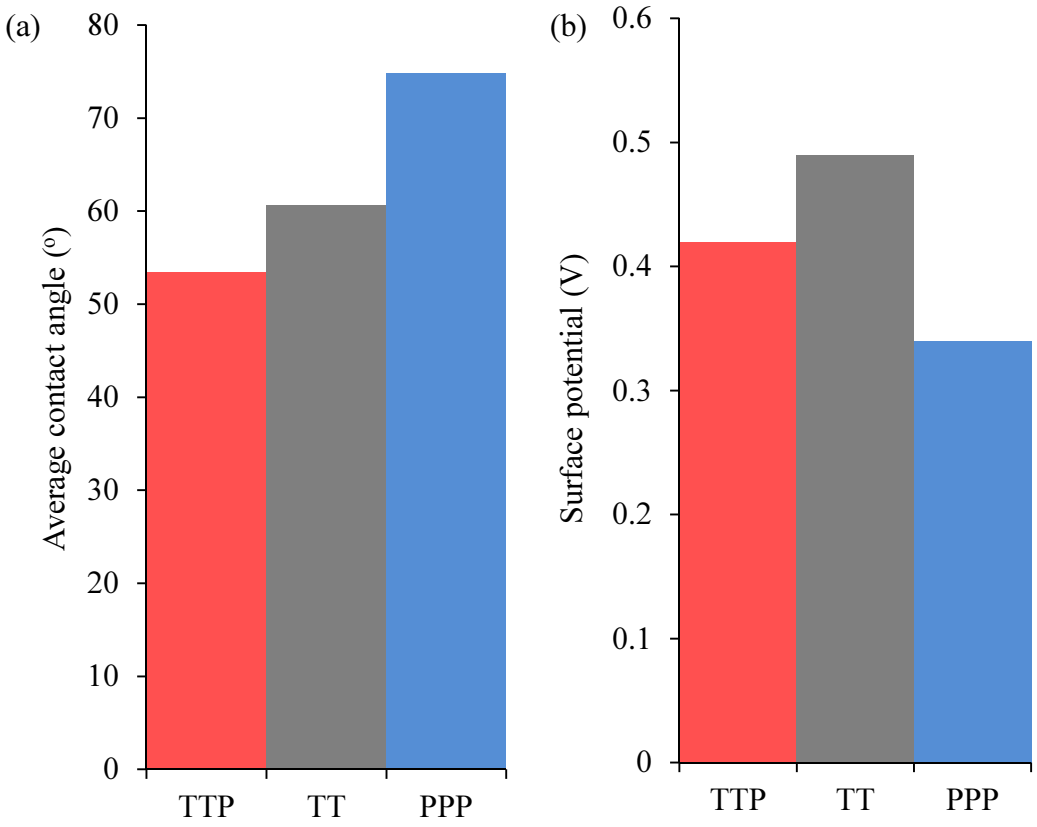

Figure 3-21 Comparative water contact angle and surface potential on PPP (■), TT (■), and TTP (■) films after 3 days' storage in the dark: (a) water contact angle and (b) surface potential.

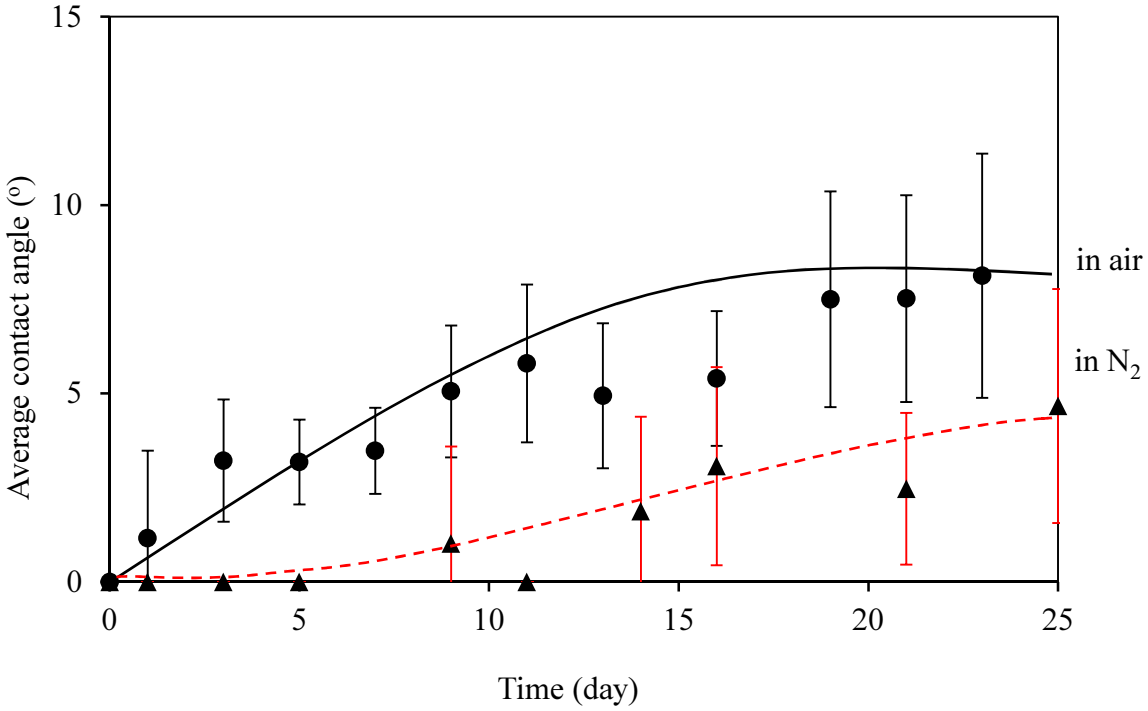

Figure 3-22 Water contact angle change on the TTP film during dark storage after UV illumination under synthesized air (●, solid line) and N_2 (▲, broken line).

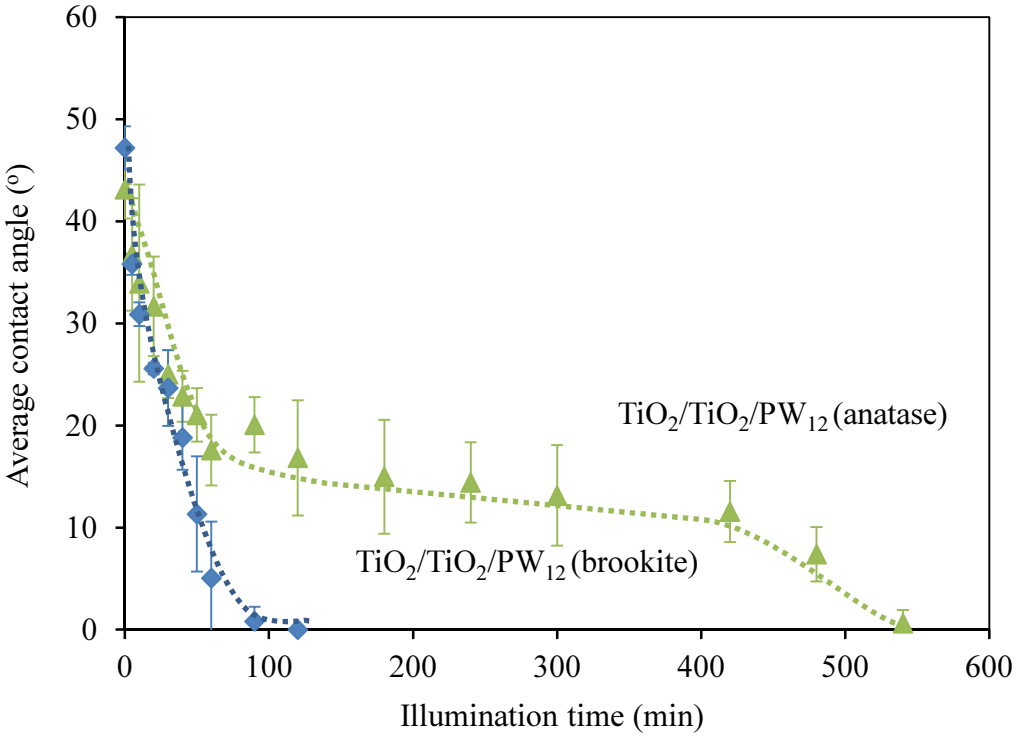

Figure 3-23 Average contact angle change during UV illumination (30 μW/cm^2) for TTP films prepared from different TiO_2 sources.

CHAPTER 4

Comparison of photoinduced hydrophilicity between $[PW_{12}O_{40}]^{3-}$ /brookite and $[SiW_{12}O_{40}]^{4-}$/brookite hybrid films

4.1. Introduction

Extensive comparative research using a different Keggin-type heteropolyacid tungstate is expected to yield additional information related to the wettability conversion performance. **Figure 1** portrays the band structures of TiO_2, $PW_{12}O_{40}^{3-}$ (PW_{12}), $SiW_{12}O_{40}^{4-}$ (SiW_{12}) and $H_2W_{12}O_{40}^{6-}$ (H_2W_{12}). For these HPAs, oxygen-to-metal charge transfer (OMCT) is present in the band of the UV region **[1, 2]**. The highest occupied molecular orbital (HOMO) is O2p; the LUMO level is W5d. After OMCT, the excited electron on the LUMO level delocalizes to an excited state via d–d transition when receiving visible light **[3, 4]**. The respective LUMO levels of PW_{12}, H_2W_{12} and of SiW_{12} are approximately +0.218, +0.054 and – 0.162 (V vs. NHE [pH=0]) **[5]**. The generated electrons on CB of TiO_2 under UV illumination transfer to the LUMO of HPAs. Alternatively, they are consumed by the generated hole on the HOMO of HPAs. Consequently, these HPAs are regarded as electron scavengers and are expected to enhance the photocatalytic performance with diminishing charge recombination. For use in this study, we prepared $TiO_2/TiO_2/[X_xW_{12}O_{40}]^{n-}$ films in the HPAs/TiO_2 (brookite) systems and pure brookite films using the same method as that used in an earlier study **[6]**. Then their photocatalytic decomposition activity, photoinduced hydrophilicity, and sustainability of the hydrophilicity were evaluated. Their relation was discussed from the viewpoint of charge transfer.

4.2. Experimental

4.2.1. Material characterization

12 tungsto(VI) phosphoric acid n-hydrate ($H_3(PW_{12}O_{40})nH_2O$; Wako Pure Chemical Industries Ltd., Japan), 12 tungsto(VI) silicic acid 26-hydrate ($H_3(SiW_{12}O_{40}).26H_2O$; Wako Pure Chemical Industries Ltd., Japan), and ammonium metatungstate hydrate ($(NH_4)_6[H_2W_{12}O_{40}]$, Stream Chemical, USA) were dried at 60 °C and then calcined at 300 °C. After drying or calcination, the powder of these three chemicals was characterized using a Fourier transform infrared spectrophotometer (FTIR; IRPrestige-21, Shimadzu Crop, Japan). For future characterizations of H_2W_{12}, X-ray diffraction analysis (XRD; X Pert Pro, PANalytical, Netherlands) and UV–Vis spectrophotometer (UV-2500PC; Shimadzu Crop, Tokyo, Japan) were used.

4.2.2. Sample preparation and characterization

All pH values of solutions and suspensions used for film preparation were adjusted to 1.5 using a HNO_3 aqueous solution to avoid hydrolysis of PW_{12} and to maintain a well-dispersed state of brookite. For film preparation, 12 tungsto(VI) phosphoric acid n-hydrate ($H_3PW_{12}O_{40}\cdot nH_2O$; Wako Pure Chemical Industries Ltd., Japan) or 12 tungsto(VI) silicic acid 26-hydrate ($H_4SiW_{12}O_{40}\cdot 26H_2O$; Wako Pure Chemical Industries Ltd., Japan) was used with no purification. These chemicals were dissolved into diluted HNO_3 aqueous solution (1 mM). A commercial brookite aqueous suspension (NTB-01, 15 wt% TiO_2, pH 4; Showa Denko K.K., Japan) was used as the TiO_2 source. This suspension was diluted to concentrations of 0.1 g/l. Then the pH value was adjusted to 1.5. Either poly diallyldimethylammonium chloride (PDDA, typical Mw 100,000–200,000, 20 wt% aqueous solution; Aldrich Chemical Co. Inc.) or

poly sodium 4-styrene sulfonate (PSS, average Mw ca. 70,000, 30 wt% aqueous solution; Aldrich Chemical Co. Inc.) was used as a counter polymer.

For this study, we prepared TiO_2/TiO_2 (TT; control TiO_2(brookite) film), $TiO_2/TiO_2/SiW_{12}$ (TTS), and $TiO_2/TiO_2/PW_{12}$ (TTP) films (left-hand-side is next to the substrate; a quartz glass plate (30 mm × 60 mm × 1 mm; Tosoh Corp. Japan), and the right-hand-side is the top deposition) for photocatalytic activity measurements, $SiW_{12}/SiW_{12}/SiW_{12}$ (SSS) and $PW_{12}/PW_{12}/PW_{12}$ (PPP) films for electrochemical experiments by preparation onto a transparent oxide coated glass substrate (High-durability Transparent Conductive Oxide film (TCO); Geomatec Co. Ltd., Yokohama, Japan, resistivity: 15 Ω/sq), and $SiW_{12}/SiW_{12}/SiW_{12}/SiW_{12}/SiW_{12}/SiW_{12}/SiW_{12}/SiW_{12}$ ($(SiW_{12})_8$) films on a Si (100) wafer (Aki Corp., Miyagi, Japan) for IR measurement. These hybrid films and the control film were prepared via a self-assembly LBL process, as described in reports of previous studies **[6–8]**. The UV–Vis spectra were measured at each coating step using a UV–Vis–NIR scanning spectrophotometer (V-630; Jasco Corp., Tokyo, Japan). After the LBL process, UV illumination (66 mW/cm^2 at λ = 365 nm) with a Hg–Xe lamp for 6 h (for the films used PSS) or 16 h (for the films used PDDA) was conducted to decompose PSS and PDDA. Moreover, we heated the obtained films at 300 °C for 1 h in air to decrease the water-solubility of PW_{12} and SiW_{12}.

Surface roughness of the film was evaluated in a 5-μm-square area using an atomic force microscope (AFM, JSPM-5200; JEOL, Tokyo, Japan) with a Si cantilever (NSC36-b; μ-mash Ltd., Narva mnt., Estonia). The films' thickness was evaluated through direct observation of the crosscut section using a field emission scanning electron microscope (FE–SEM, S4500; Hitachi Ltd., Tokyo, Japan). X-ray

photoelectron spectroscopy (XPS) analysis and infrared (IR) spectra measurement were conducted using the same conditions and apparatus as those used in an earlier study **[6]**.

4.2.3. Evaluation of photocatalytic decomposition activity

Before measurement, these films were exposed to UV (1 mW/cm^2, 365 nm) to remove organic compounds that had adsorbed onto the surface. A Pyrex glass vessel (500 mL volume) with a quartz glass lid was used as a batch reactor. A sample film was set at the center of the vessel. Then the atmosphere in the reactor was replaced by gas flow (1.0 l/min, 5 min) with air at 20 °C and 80% relative humidity. Subsequently, the vessel was sealed and IPA gas was injected into it. The injected gas amount was equivalent to that for 500 ppm concentration. The vessel was subsequently stored in the dark for 3 h.

After the adsorption equilibrium was confirmed, UV illumination was conducted using a UV illuminator (LA-410UV-1; Hayashi Watch Works, Japan) equipped with a Hg–Xe lamp (MX4010). Wavelength spectra of the light source were presented in a report of our previous study **[7]**. The illumination intensity at the sample surface was 1 mW/cm^2 at 365 nm. The concentrations of IPA, acetone, and CO_2 were evaluated every 30 min or every 1 h for 5 h using a gas chromatograph (GC-14A; Shimadzu Corp., Tokyo, Japan) equipped with a flame ionization detector (FID), a methanizer, and a Sunpak-A column (Shimadzu Corp.).

4.2.4. Evaluation of photoinduced hydrophilicity

The films were pre-cleaned using UV illumination (1 mW/cm^2, 365 nm) and were then stored in the dark for several days to allow hydrophobicizing. Subsequently, the static water contact angle (WCA) on the films was measured at every 5, 10, 30, or 60

min during UV illumination (30 μW/cm^2) using sessile drop method with 2 μl distilled water and a contact angle meter (CA-X; Kyowa Interface Science Co. Ltd., Saitama, Japan). The UV light source was that used for photocatalytic activity evaluation.

To evaluate the sustainability of hydrophilicity, we also evaluated WCA increase during hydrophobicizing in the dark storage using either pure synthesized air or nitrogen (N_2) with 10% relative humidity as the atmosphere. The pre-cleaned films (UV illumination under a black-light bulb, 0.5 mW/cm^2 365 nm for 72 h) were put into a Pyrex glass vessel (500 mL). Then the atmosphere was replaced to air or nitrogen (N_2) with 10% relative humidity at 20 °C. Subsequently, the vessel was sealed with a quartz glass lid and stored in the dark. This system was broken down temporarily every 1 or 2 days to measure WCA. Then dark storage was continued under the same conditions.

4.2.5 Electrochemical experiment

The initial WCA of SSS and PPP films was measured using the same contact angle meter. Then a small positive voltage (50 mV) was applied to the film using a potentiostat (HSV-100; HD Hokuto Denko Co. Ltd., Kanagawa, Japan). The WCA change under applying voltage was measured repeatedly every 5 or 10 min for 1 h. Then the film was stored in a dark desiccator for 2 h without applying voltage. The WCA change during this dark storage period was also evaluated. The flow diagram of electrochemical experiment is shown in **Figure 4-2**.

4.3. Results and discussion

4.3.1. Characterization of PW_{12}, SiW_{12} and H_2W_{12} powder

The infrared spectra of dried and calcined powders are shown in **Figure 4-3**. FTIR spectra during 700–1200 cm^{-1} are assigned to Keggin structure $[X_xM_mO_p]^{n-}$. the single peak of P–O and Si–O peak at 1080 and 925 cm^{-1} suggest that Keggin structure was reserved after heat treatment process. However, for H_2W_{12}, the W–O and W–O–W peaks during these wavenumber become broad, reflecting the destroyed Keggin structure. Because H_2W_{12} is isopolyanion, it could be more unstable than the heteropolyanion that has heteroatom. Young Il Pae **[9]** et al. reported that WO_3-TiO_2 prepared from an aqueous solution of ammonium metatungstate $[(NH_4)_6(H_2W_{12}O_{40})$-$nH_2O]$, which is the same material used for the current study, presented the high of Brønsted and Lewis acid sites on the surface of catalyst because of the W=O bond nature of complex formed by the interaction between WO_3 and TiO_2. From FTIR result, the calcined 300 °C H_2W_{12} powder present the characteristic band of ammonium ion formed on Brønsted acid site and ammonia coordinate bond to Lewis acid site at 1454 and 1610 cm^{-1}, respectively. From XRD analysis, the 300 °C calcined H_2W_{12} was amorphous and for higher calcination temperature; 400 °C and 500 °C, WO_3 phase were found (**Figure 4-4**). **Figure 4-5** shows diffuse reflectance spectra (DRS) of the calcined H_2W_{12} at 300 °C and dried H_2W_{12} at 60 °C. Estimated by KM (Kubelka–Munk) function, indirect transition band gap for H_2W_{12} was narrowed from 3.1 eV to 2.85 eV; the later one is correspond to the band gap of WO_3 (2.4–2.8 eV).

These results suggest that Keggin structure of H_2W_{12} could not be maintained after 300 °C film processing. Therefore, we prepared only films in the PW_{12}/TiO_2(brookite),

SiW_{12}/TiO_2(brookite) systems and pure brookite films using the same method as that used in an earlier study **[6]**. Then their photocatalytic decomposition activity, photoinduced hydrophilicity, and sustainability of the hydrophilicity were evaluated. Their relation was discussed from the viewpoint of charge transfer.

4.3.2. Characterization of films

The UV–Vis spectra measured at each coating step for TTP and TTS are portrayed in **Figures 4–6**. The UV–Vis absorbance increment corresponded with the respective levels of deposition. Moreover, the films were transparent, with more than 80% transmission in the visible range (400–700 nm). This increment was steady for all film preparation. Nearly equal absorbance between TTP and TTS films indicated that the TiO_2 layer thickness was almost identical. The concentration ratio values between W and Ti ([W]/[Ti]) shown in **Figure 4-7** on the surface of TTP and TTS films by XPS analysis were around 0.12 and 0.08, showing that the PW_{12} concentration on TiO_2 was around 1.5 times greater than that of SiW_{12}. In the LBL process, TiO_2 and HPAs were attracted by Coulombic interaction. Therefore, the adsorption amount of SiW_{12} on TiO_2 surface is expected to be smaller than that of PW_{12} because of the ionic charge difference ($[SiW_{12}O_{40}]^{4-}$ and $[PW_{12}O_{40}]^{3-}$). The XPS result is inferred to be close to the expected concentration ratio (1.3) according to their charge difference. The TTP and TTS films possessed spherical granule topography, and HPA deposition did not seem to provide remarkable morphological change to the pure brookite film by LBL process (**Figure 4-8**). Their corresponding surface roughness (R_a) values were 7.0 nm (TT), 6.3 nm (TTP) and 7.4 nm (TTS). The film thicknesses ascertained from observations of the crosscut section of these films using FE–SEM image were around 70 nm (**Figure 4-9**).

Figure 4-10 portrays the IR spectra of a SiW_{12} film on a Si substrate. The absorbance of pure SiW_{12} is reported as 980, 925, and 770 cm^{-1} **[10]**. The film shows characteristic bands of SiW_{12} around 967, 916, and 788 cm^{-1}, which are ascribed to stretching vibration of W=O, Si–O, and W–O–W bonds in the Keggin structure **[11]**. A single Si–O stretching peak (916 cm^{-1}) reflects that the Keggin structure is retained in the film even after 300 °C heat treatment. The slight shift in the bands might be attributable to interaction between the Keggin structure and substrate. The Keggin structure of PW_{12} is also retained, as described in a previous report **[6]**.

4.3.3. Photocatalytic activity and the surface wettability

The decomposition pathway of IPA by TiO_2 photocatalyst has been studied extensively **[12–14]**. Molecules of gaseous IPA are decomposed initially into acetone, and are ultimately decomposed to H_2O and CO_2. However, the photocatalytic activity of solid state Keggin-type heteropolyacid was extremely low under 1 mW/cm^2 UV illumination **[7, 15]**. Moreover, the decomposition rate of acetone by TiO_2 photocatalyst is reportedly much lower than that of IPA **[16, 17]**.

Figure 4-11 portrays the concentration changes of IPA, acetone, and CO_2 under UV illumination. The initial concentration values of IPA after 3 h dark storage before UV illumination for TTP, TTS, and TT films were, respectively, 487 ppm, 492 ppm, and 489 ppm. Based on these values, significant affinity difference against IPA does not exist for these films. Therefore, we can compare photocatalytic decomposition activity using IPA decomposition. Results show that both the TTP and TTS films decomposed IPA faster than the TT film. A similar trend was observed for acetone generation. The order of CO_2 generation differed from that for IPA decomposition and acetone

generation. Although the reason remains unclear, CO_2 is an ultimate product. Complex decomposition pathways exist from acetone to CO_2. The affinity difference of intermediate against PW_{12} and SiW_{12} might affect the entire CO_2 generation rate. The combination of SiW_{12} to brookite increased the photocatalytic activity to the same degree as PW_{12} did. This result, which corresponds with that of a previous study **[18]** performed using samples without heat treatment and anatase, suggests that SiW_{12} also enhances electron–hole separation even after heat treatment at 300 °C. **Figure 4-12** shows that IPA decomposition rate increase when the light intensity increase from 0-1 mW/cm^2. Therefore, at the testing condition (1 mW/cm^2), photocatalytic reaction was governed not by materials transport, but by a surface reaction. The average reaction constants in the early stage (0–2 h) for the TT, TTP and TTS films corresponding to the **Figure 4-11** were calculated respectively as 1.7, 3.1, and 2.9 ppm/min. Despite low surface concentration (66% of PW_{12}), the reaction constant value of the TTS film is close to that of the TTP film, suggesting efficient electron consumption of SiW_{12}. The concentration change of IPA for the TTP and TTS films under light illumination through a band-pass filter (absorbed visible light > 400 nm, UVD33S; Asahi Glass Co. Ltd.) revealed that the effect of visible light for the films on the overall photocatalytic activity is small (**Figure 4-14**, the wavelength range of UVD33S is shown in **Figure 2-7**). Therefore, it is deduced that the main reduction occurs on TiO_2 or LUMO of these HPAs.

Figure 4-15 presents the WCA change on the TTP, TTS, and TT films under UV illumination in ambient air. The hydrophilicizing rate was increased by combining PW_{12} and SiW_{12}, especially in the early stage of UV illumination. Its entire order was TT < TTS < TTP. This order is identical to that of photocatalytic decomposition activity for

gaseous IPA. It is noteworthy that WCA of pure PW_{12} and SiW_{12} films were approximately 75° and 45° and that the surface concentration of PW_{12} is greater than that of SiW_{12}. Compared to photocatalytic decomposition activity, the effect of PW_{12} for the increase of photoinduced hydrophilicizing rate is apparently greater than that of SiW_{12}. **Figure 4-16** shows the WCA change of the UV-illuminated films during dark storage under synthesized air with 10% relative humidity. The order of the hydrophobicizing rate was TTP < TTS < TT. **Figure 4-17** shows atmospheric dependence of the hydrophobicizing rate for UV-illuminated TTP and TTS films during dark storage. The WCA increment on the TTP film depends closely on the atmosphere; the increment rate was lower under an oxygen-absent condition. This dependence was not notable for the TTS film.

Based on these results, we present an expected electron transfer scheme for PW_{12}/TiO_2(brookite) and SiW_{12}/TiO_2(brookite) films in **Figure 4-18**. The band-gap of the brookite used for this study was measured optically. It is reported as 3.18 eV **[8]**. We obtained flat-band potential value of the brookite as -0.10 V using Mott–Schottky plots (Practical plots and their measurement conditions were described in **section 2.3.1.**). These are almost equal values to those reported from previous studies of brookite **[19, 20]**. **Figure 4-18** was depicted using these values. As described in the *Introduction*, HPA/TiO_2 systems have been investigated as Z-scheme photocatalytic systems. The direct electron transition from O2p orbitals of HPAs to unoccupied upper W5d level does not readily occur under the light source used for this study. According to an earlier study, a certain amount of generated electrons on CB of TiO_2 under UV illumination transfers to the LUMO level of HPAs **[8]**. The excitation efficiency by visible light to

form PW_{12}^{-*} from PW_{12}^{-} is not high in this case. Therefore, direct reduction by PW_{12}^{-} is more important than that by PW_{12}^{-*} as the practical reduction path.

Tatsuma et al. prepared TiO_2/WO_3 hybrid films and investigated their energy storage ability systematically. The CB for WO_3 is, like the LUMO levels of PW_{12} or SiW_{12}, more positive than the CB for TiO_2. They revealed that electron transfers from the CB of TiO_2 to that of WO_3 under UV illumination. The electrons are consumed by oxygen in the dark **[21]**. They proposed the following proton-related electron consumption pathways.

$O_2 + 2H^+ + 2e^- = H_2O_2$ (+0.682 V vs. NHE) **[22]**

$O_2 + 4H^+ + 4e^- = 2H_2O$ (+1.229 V vs. NHE) **[22]**

The potential levels of these reactions are feasible even for SiW_{12}^{-} and PW_{12}^{-} (**Figure 4-1**). Electrons accumulate on the WO_3 in this film under UV illumination. Therefore, these multi-electron reactions become feasible. The expected proton source is water. That earlier study also revealed that this reaction is feasible even in gas phase by consuming adsorbed water molecules on the surface **[23]**. Furthermore, Tatsuma et al. reported a similar trend for a PW_{12}/TiO_2 system **[24, 25]**. Based on that background, we can expect a similar reduction procedure in our study. The atmospheric dependence of the hydrophobicizing rate for UV-illuminated TTP and TTS films during dark storage (**Figure 4-17**) also suggests the reoxidation of reduced HPAs by water and O_2. The LUMO level of SiW_{12} is more negative than that of PW_{12}. Therefore, the electron transfer from CB of TiO_2 to PW_{12} is more thermodynamically favorable than to SiW_{12}. Similarly, the reoxidation by oxygen and water on SiW_{12}^{-} is expected to be more thermodynamically favorable than that on PW_{12}^{-} because of the potential difference between the two reactions above (+0.682 V, +1.229 V) and because of the reduced

HPAs (+0.218 V for PW_{12}^{-}, and +0.054 V for SiW_{12}^{-}). The reaction constant for oxygen reduction without visible light by SiW_{12}^{-} and PW_{12}^{-} in aqueous solution of pH = 1 and $[O_2] = 2\times10^{-4}$ M were reported as ca. 10^2 M^{-2} s^{-1} (for PW_{12}^{-}) and 10^4 $M^{-2}s^{-1}$ (for SiW_{12}^{-}) **[5]**. Therefore, the reoxidation rate of SiW_{12}^{-} is expected to be more efficient than that of $PW_{12}^{-}$from a kinetics viewpoint. Conversely, electrons are accumulated on the PW_{12} as PW_{12}^{-} under UV illumination. Then they are stored longer than on SiW_{12}. However, the possibility of reduction at the TiO_2 is also feasible in this system. The practical reduction ratio between TiO_2 and HPA remains unclear. That point is left to be addressed in future work.

The atmospheric dependence of WCA change during dark storage implies also that the reoxidation process of HPAs by water and O_2 plays an important role in sustaining hydrophilicity. Compared with PW_{12}^{-}, more efficient reoxidation is expected for SiW_{12}^{-} by water and O_2 at the break of the system every 1–2 days for 5–10 min for WCA measurement procedures. The main difference in sustainability of hydrophilicity between the TTP and TTS films, respectively, is attributable to their electron storage ability difference. Reportedly, once PW_{12} is reduced into PW_{12}^{-} by injected electron from TiO_2, a certain period is necessary for complete reoxidation **[24, 25]**. Correspondingly, from XPS analysis for oxidation state of W on the hybrid films before and after UV illumination, the W(V) and W(VI) peaks showing XW_{12} and reduced XW_{12} are obtained around 34–37 eV. Peak separation of W4f revealed that the concentrations of W(V) were increased from 8–20% by UV illumination for the TTP film, as shown in **Figure 4-19**, although no marked change of W(V) for the TTS film occurred after UV illumination.

Moreover, we evaluated WCA change for the PPP and SSS films on electrodes with and without applying voltage (**Figure 4-20**). The WCA of these films decreased during applying voltage, namely electron injection. Once the applied voltage was stopped, the WCA change became small or its value increased slightly. It is noteworthy that the surface roughness level of these films was almost identical (R_a = 2.6 nm (PPP) and 3.4 nm (SSS) in 5 μm square area). The initial contact angle of the PPP (around 75°) and SSS (around 45°) films differ. Therefore, we converted WCA change to the apparent change of the surface energy by wetting (the work of adhesion between solid and liquid) per unit time. The work of adhesion (W_a) is described by the following equation **[26]**

$$W_a = \gamma_{LV} (1+\cos \theta),$$

where γ_{LV} is a free surface energy of the liquid and θ is the contact angle of the liquid on the solid. Consequently, the apparent change of the surface energy by wetting per unit time is evaluated as

$$\{W_a(t_1) - W_a(t_2)\}/(t_1-t_2) = \gamma_{LV}(\cos\theta_1-\cos\theta_2)/(t_1-t_2),$$

where θ_1 and θ_2 respectively denote the contact angles at time t_1 and t_2. The obtained W_a values in the first 60 min biasing were 0.22 (PPP 77°–64°) and 0.05 (SSS 46°–43°) mJ/m^2 min. The W_a values during 2 h dark storage after stopping biasing were 0.04 (PPP 64°–58°) and –0.01 (SSS 43°–44°) mJ/m^2 min. These trends mean that both the enhancement of hydrophilicity by electron injection and its sustainability after stopping electron injection is more significant for PW_{12} than SiW_{12}, and that it corresponds to matters discussed in this report. Once PW_{12} is reduced into PW_{12}^- by electron injection from TiO_2, a certain period is necessary for complete reoxidation. Therefore, a plausible explanation of the sustainability of the hydrophilicity is that water molecules with a

dipole moment adsorb onto the reduced PW_{12} (PW_{12}^{-}) and thereby become more hydrophilic than pure brookite, providing hydrophilicity for a certain period. The possibility of the increase of polar interaction with water was also pointed out for the similar hydrophilic conversion behavior of hydroxyapatite ceramics by electrical polarization **[27]**. Detailed study of the state of water on the PW_{12} surface after electron injection will be addressed in future work.

4.4. Conclusion

For this study, we prepared a PW_{12}/TiO_2 and a SiW_{12}/TiO_2 hybrid films using brookite-type TiO_2 and LBL method. Then photocatalytic decomposition activity and photoinduced wettability conversion of the films were evaluated. Both hybrid films exhibited a higher gaseous IPA decomposition rate and a higher hydrophilicizing rate than those of the pure brookite film. However, the TTP ($TiO_2/TiO_2/PW_{12}$) film provided better photocatalytic performance than the TTS ($TiO_2/TiO_2/SiW_{12}$) film. The TTP film exhibited better sustainability of the hydrophilicity in the dark than the TTS film did. Based on the HOMO–LUMO levels of the heteropolyacids, it was deduced that the electron scavenger effect and reoxidation efficiency of HPAs are key factors affecting the performance of wettability conversion before and after UV illumination of this hybrid film system.

Acknowledgement

The author is grateful to Prof. M. Miyauchi of the Tokyo Institute of Technology for helpful discussion related to this research.

References

[1] Y. Guo, C. Hu, J. *Catal. A: Chem*., 262 ,136–148 (2007).

[2] A. Hiskia, A. Mylonas, E. Papaconstantinou, *Chem. Soc. Rev*., 30 ,62–69 (2001).

[3] T. Yamase, *Chem. Rev*., 98 ,307–325 (1998).

[4] E. Coronado, C.J. Gomez-Garcia, *Chem. Rev*., 98 273–296 (1998).

[5] I.A. Weinstock, *Chem. Rev*., 98, 113–170 (1998).

[6] K. Pruethiarenun, T. Isobe, S. Matsushita, A. Nakajima, *Appl. Catal. A: Gen.* 445–446, 274–279 (2012).

[7] S. Yanagida, A. Nakajima, T. Sasaki, Y. Kameshima, K. Okada, *Chem. Mater*., 20 , 3757–3764 (2008).

[8] K. Pruethiarenun, T. Isobe, S. Matsushita, A. Nakajima, *Appl. Catal. A: Gen*., 399, 22–27 (2011).

[9] Young Il Pae, Mu Hee Bae, Won Cheon Park, and Jong Rack Sohn, *Bull. Korean Chem. Soc*., 25, 12, 1881-1888 (2004).

[10] A. Micek-Ilnicka, *Journal of Molecular Catalysis A: Chemical*, 308, 1–2, 1–14 (2009).

[11] Y. Lua, H. Yina, H. Wub, H. Liua, T. Jianga, Y. Wadac, *Catal. Commun*., 7, 832–838 (2006).

[12] P.R. Harvey, R. Rudham, S. Ward, *J. Chem. Soc. Faraday Trans*., 79, 1381–1390 (1983).

[13] Y. Ohko, K. Hashimoto, A. Fujishima, *J. Phys. Chem. A*, 101, 8057–8062 (1997).

[14] A. Mylonas, A. Hiskia, E. Androulaki, D. Dimotikali, E. Papaconstantinou, Phys. Chem. Chem. Phys. 1, 437–440 (1999).

[15] A. Nakajima, T. Koike, S. Yanagida, T. Isobe, Y. Kameshima, K. Okada, *Appl. Catal. A: Gen*., 385, 130–135 (2010).

[16] S.A. Lanson, J.A. Widegren, J.L. Falconer, *J. Catal*., 157, 611–625 (1995).

[17] M. Anbar, P. Neta, *Int. J. Appl. Radiat. Isotopes*, 18, 493–523 (1967).

[18] S. Yanagida, A. Nakajima, T. Sasaki, T. Isobe, Y. Kameshima, K. Okada, *Appl. Catal. A: Gen*., 366, 148–153 (2009).

[19] T.A. Kandiel, A. Feldhoff, L. Robben, R. Dillert, D.W. Bahnemann, *Chem. Mater*., 22, 2050–2060 (2010).

[20] Q. Tay, X. Liu, Y. Tang, Z. Jiang, T.C. Sum, A. Chen, *J. Phys. Chem. C*., 117 14973–14982 (2013).

[21] T. Tatsuma, S. Saitoh, Y. Ohko, A. Fujishima, *Chem. Mater*., 13, 2838–2842 (2001).

[22] "Nyuumon Hikari Shokubai" Ed. Y. Nosaka and A. Nosaka, Tokyo Tosho Press, 2004, Tokyo, Japan, pp. 49.

[23] T. Tatsuma, S. Saitoh, P. Ngaotrakanwiwat, Y. Ohko, A. Fujishima, *Langmuir*, 18, 7777–7779 (2002).

[24] P. Ngaotrakanwiwat, S. Saitoh, Y. Ohko, T. Tatsuma, A. Fujishima, *J. Electrochem. Soc*., 150, A1405–A1407 (2003).

[25] P. Ngaotrakanwiwat, T. Tatsuma, *J. Electroanal. Chem*., 573, 263–269 (2004).

[26] A. Nakajima, K. Hashimoto, T. Watanabe, K. Takai, G. Yamauchi, A. Fujishima, *Langmuir*, 16, 7044–7047 (2000).

[27] M. Nakamura, A. Nagai, T. Okumura, Y. Sekijima, T. Hentunen, K. Yamashita, J. *Ceram. Soc. Jpn*., 118, 474–478 (2010).

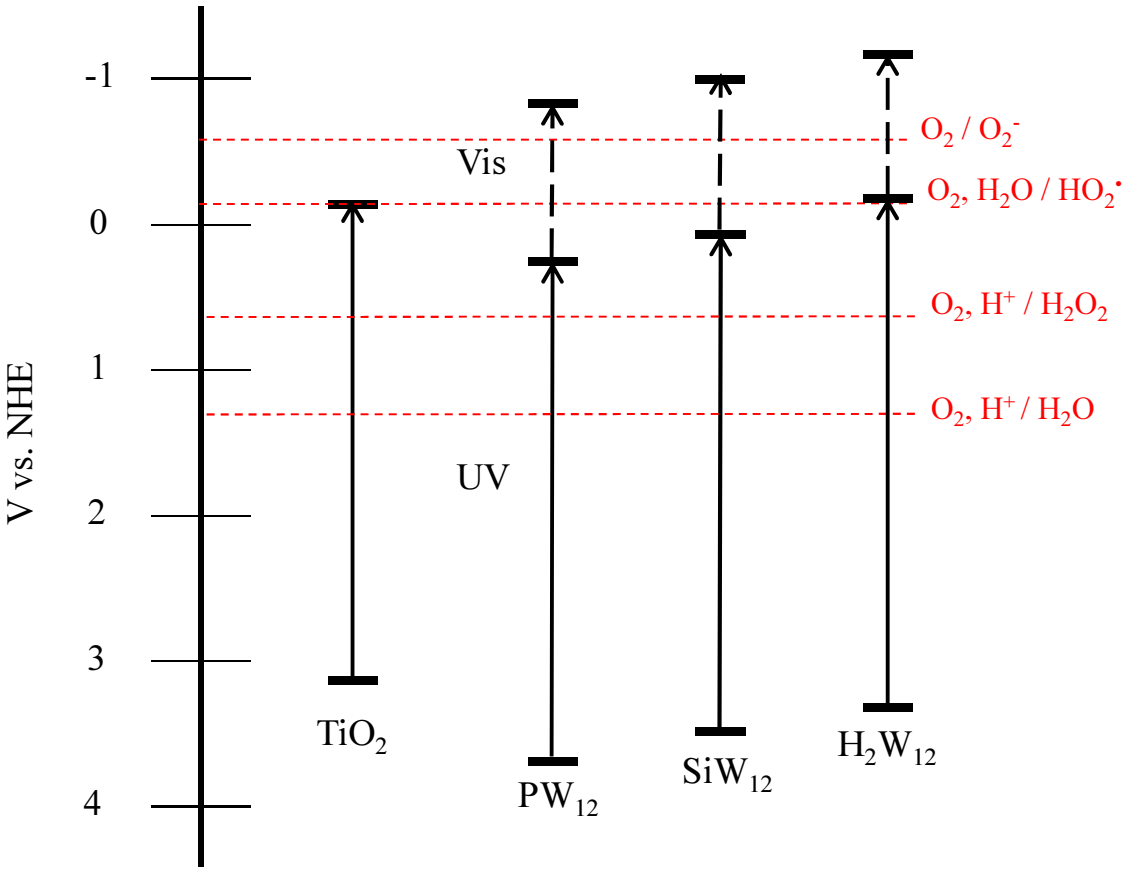

Figure 4-1 Energy diagram of TiO_2, PW_{12}, SiW_{12} and H_2W_{12}

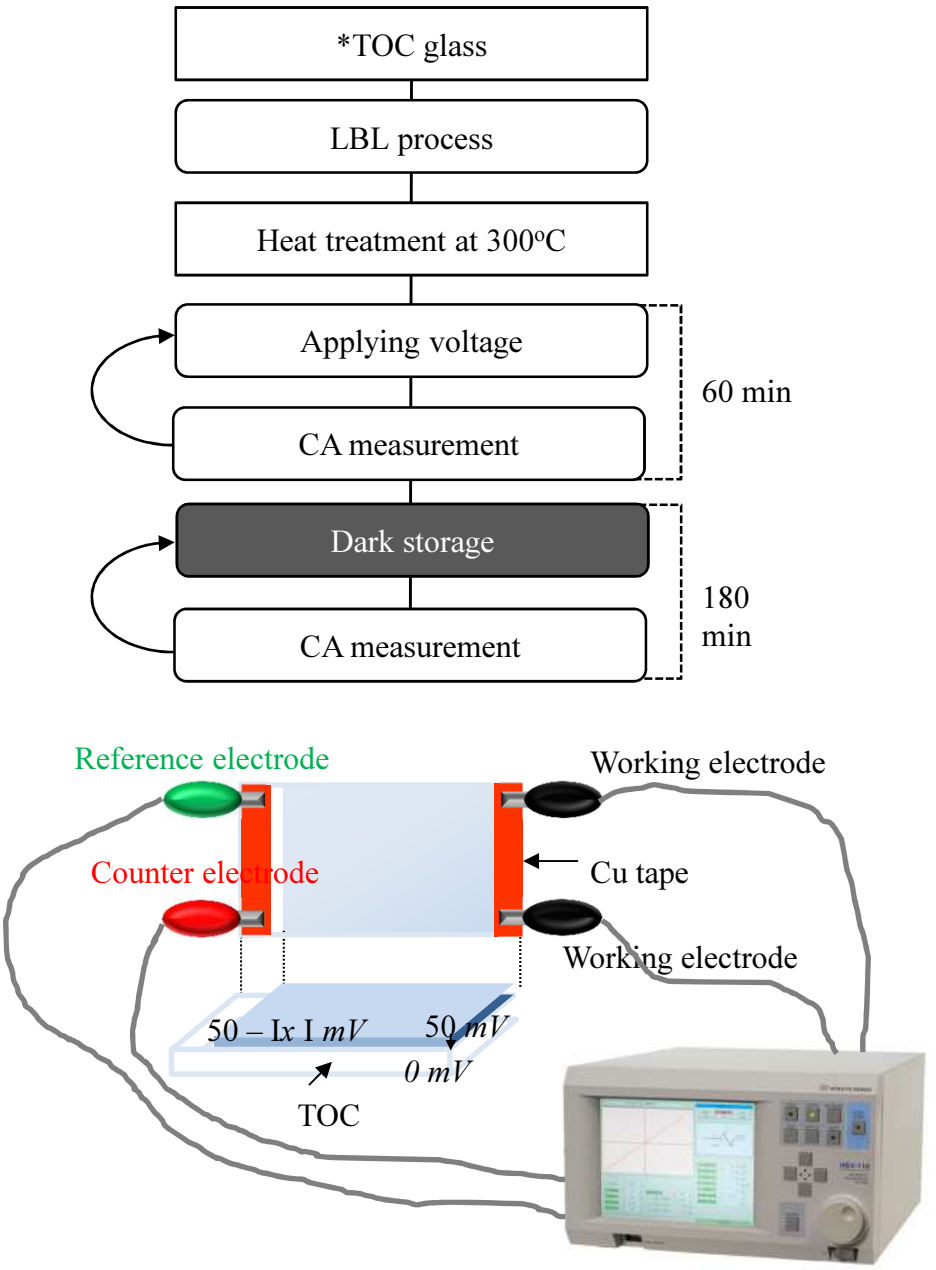

Figure 4-2 (a) Flow diagram of electrochemical experiment and the experimental setting

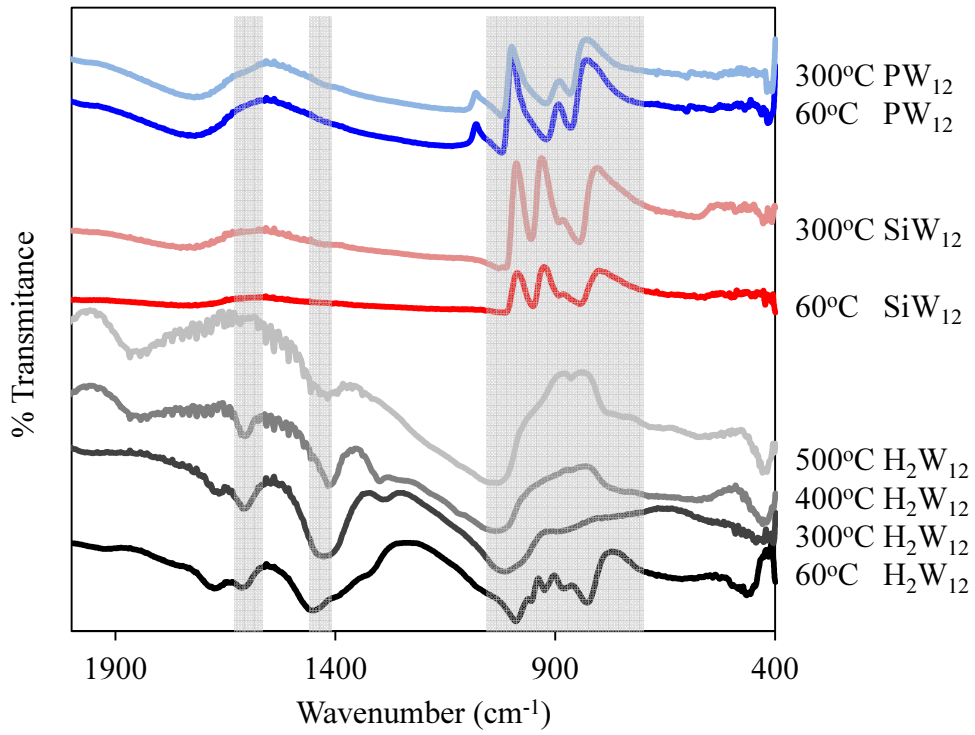

Figure 4-3 IR spectra of $H_3PW_{12}O_{40}$, H_4SiW_{12} and $(NH_4)_6(H_2W_{12}O_{40})$

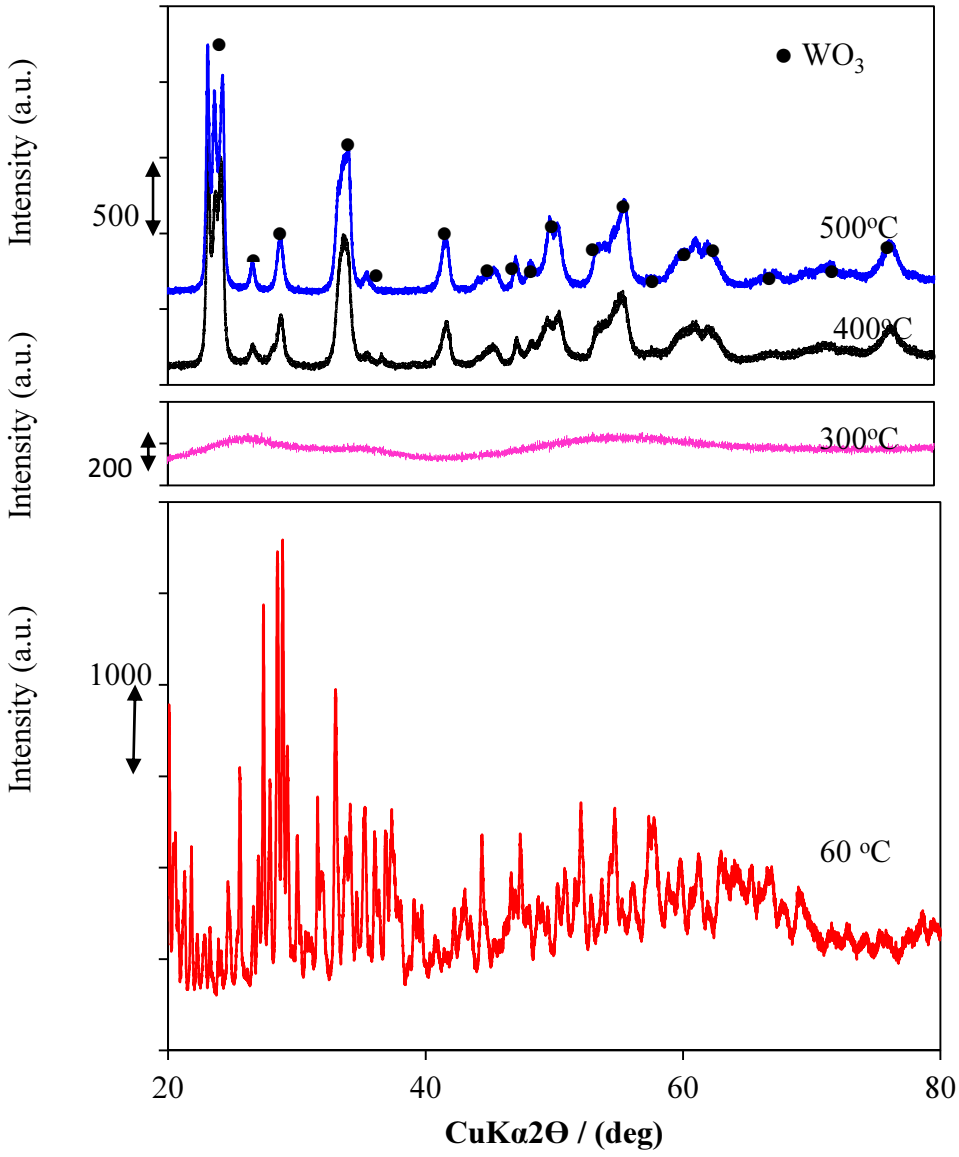

Figure 4-4 X-ray diffraction patterns of $H_3PW_{12}O_{40}$, H_4SiW_{12} and $(NH_4)_6(H_2W_{12}O_{40})$

(a)

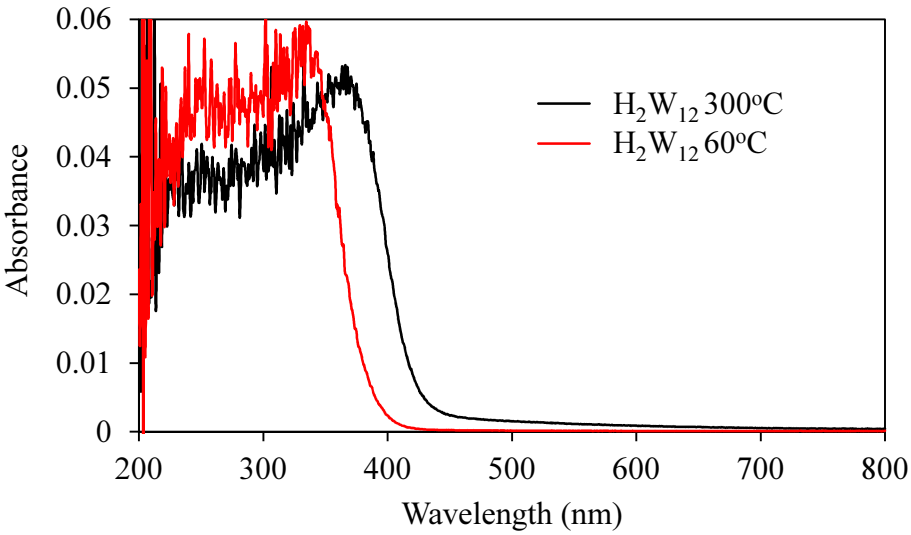

(b)

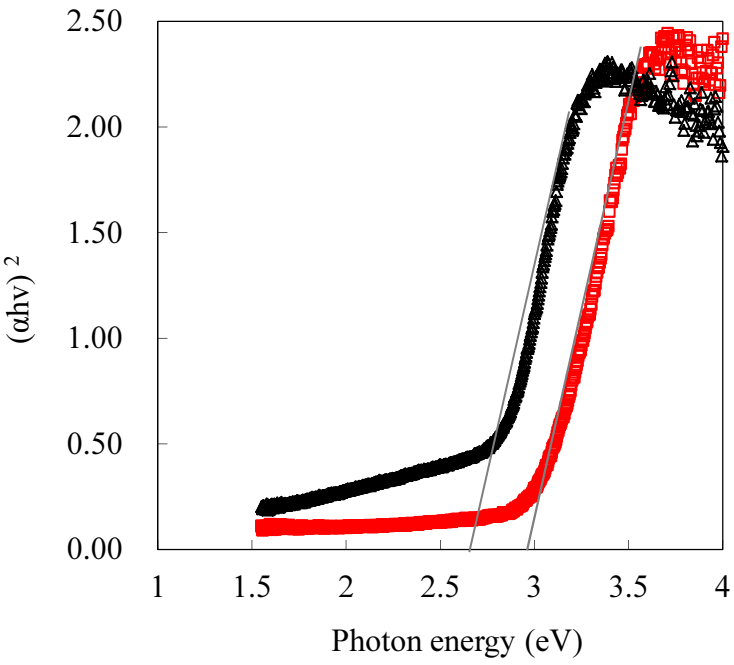

Figure 4-5 Diffuse reflectance spectra (DRS) obtained from heat treated $[(NH_4)_6(H_2W_{12}O_{40}\text{-}nH_2O)]$ at 300 °C and dried $[(NH_4)_6(H_2W_{12}O_{40}\text{-}nH_2O)]$ at 60 °C; (a) and band gap estimation from diffuse reflection spectra; (b)

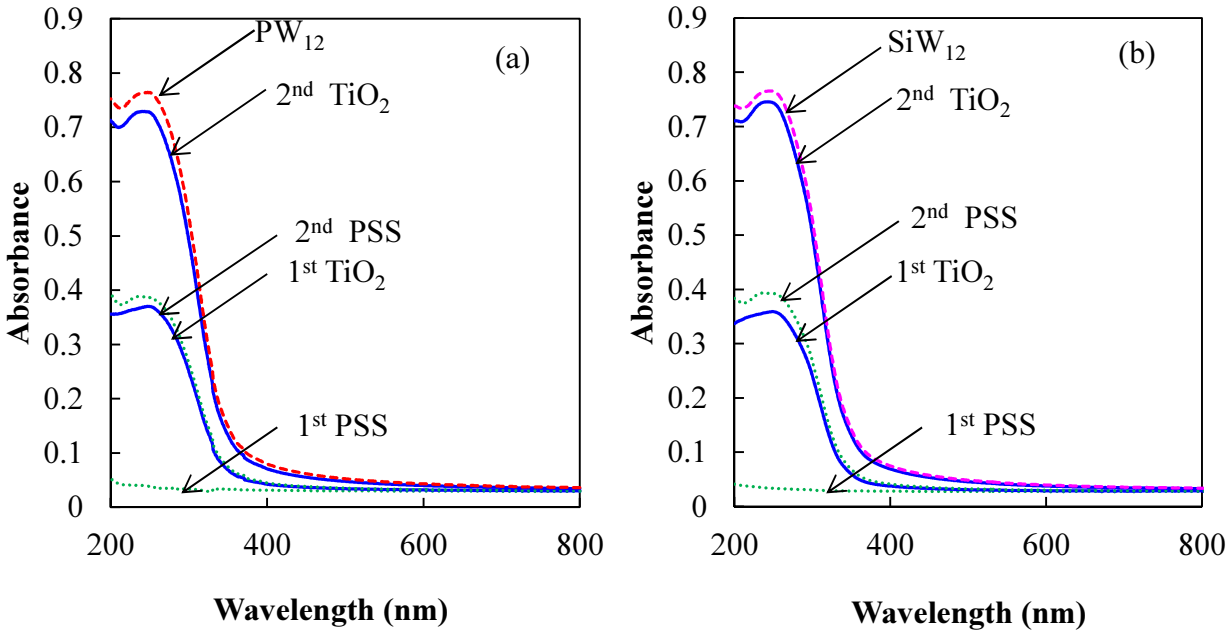

Figure 4-6 UV–Vis absorbance spectra increment for respective depositions of PSS, TiO_2, PW_{12} and SiW_{12} of (a) TTP and (b) TTS.

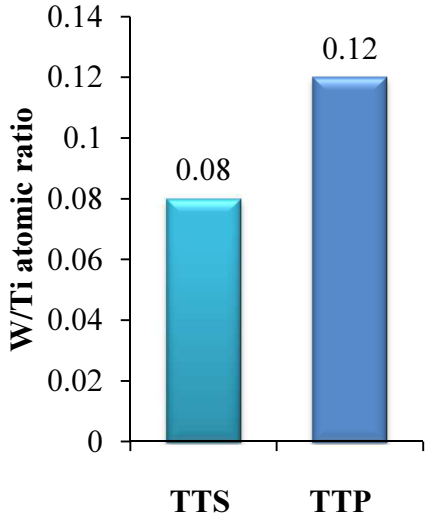

Figure 4-7 The concentration ratio values between W and Ti ([W]/[Ti]) on the surface of TTP and TTS films by XPS analysis

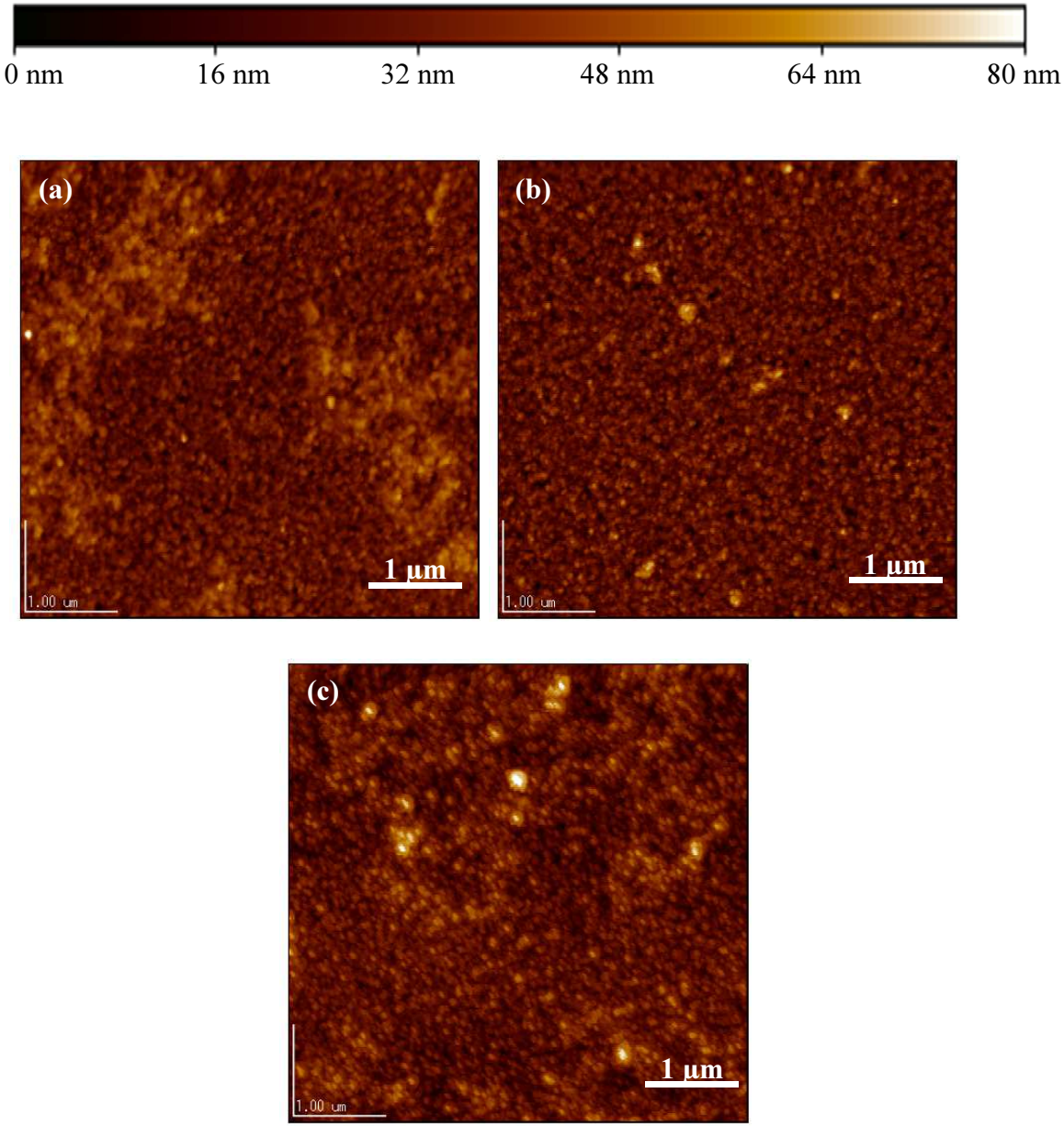

Figure 4-8 AFM images of (a) TT, (b) TTP, and (c) TTS films.

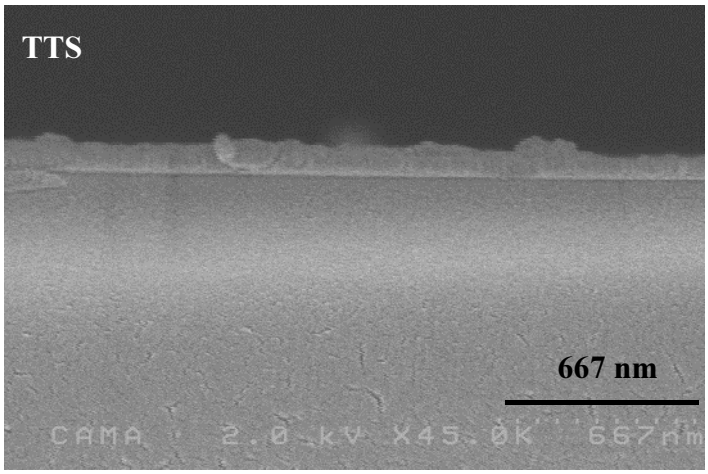

Figure 4-9 FE-SEM images of crosscut section TTS film.

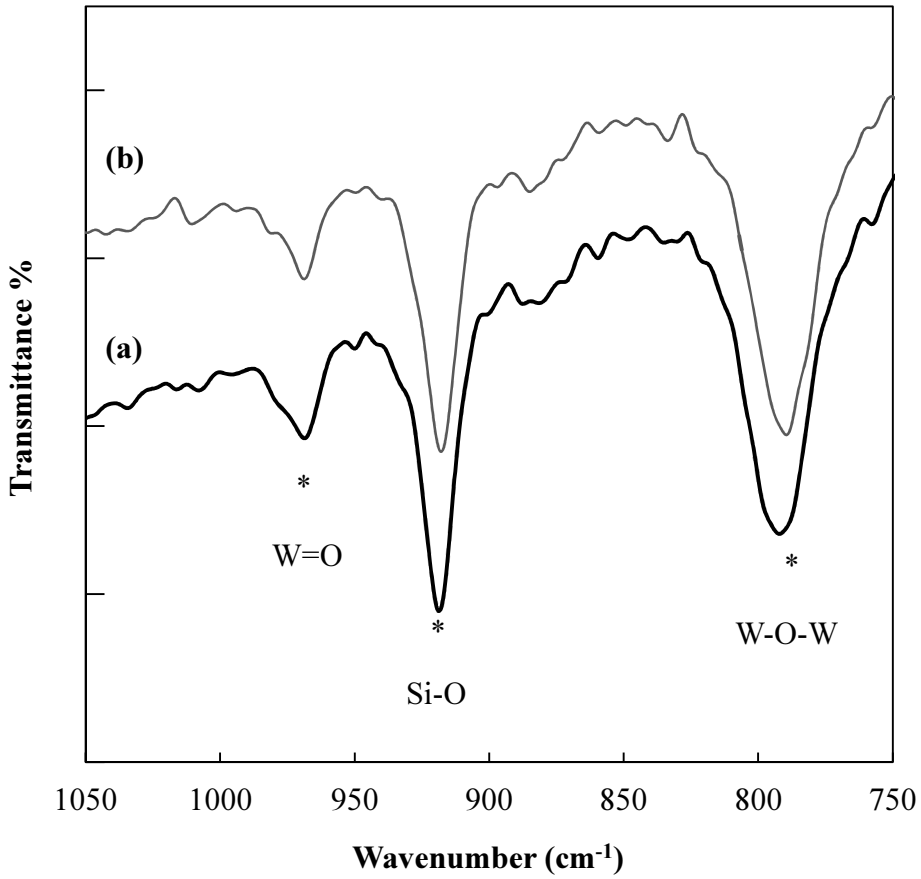

Figure 4-10 IR spectra of the $(SiW_{12})_8$ film on Si substrate before (a) and after (b) heat treatment.

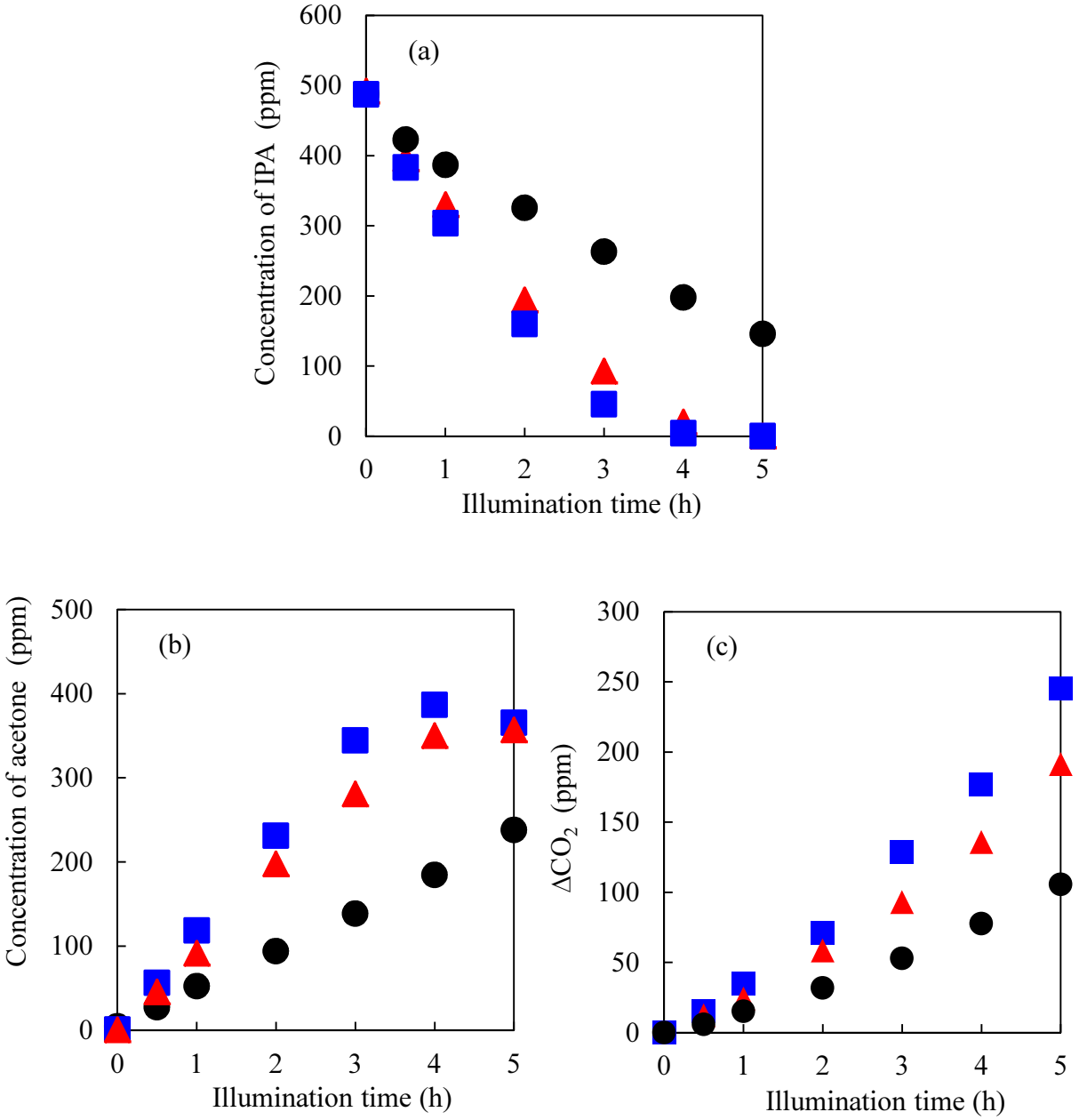

Figure 4-11 Concentration changes of (a) IPA, (b) acetone, and (c) CO_2 for the TTP (■), TTS (▲), and TT (●) films under UV illumination (1 mW/cm^2).

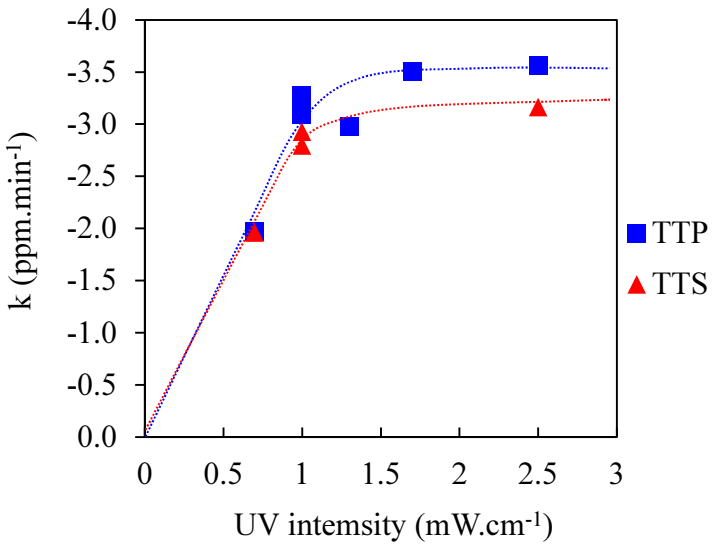

Figure 4-12 Average IPA decomposition rate under different UV intensity illumination in the early stage (0–2 h) for the TTP (■) and TTS (▲).

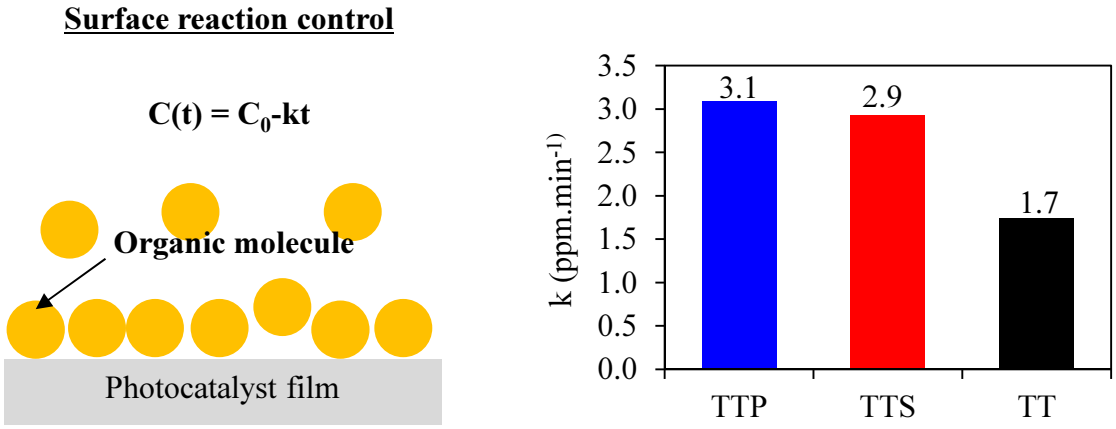

Figure 4-13 (a) Scheme for surface reaction control and (b) The average reaction constants in the early stage (0–2 h) for the TT, TTP and TTS films corresponding to the plots in **figure 4-11**

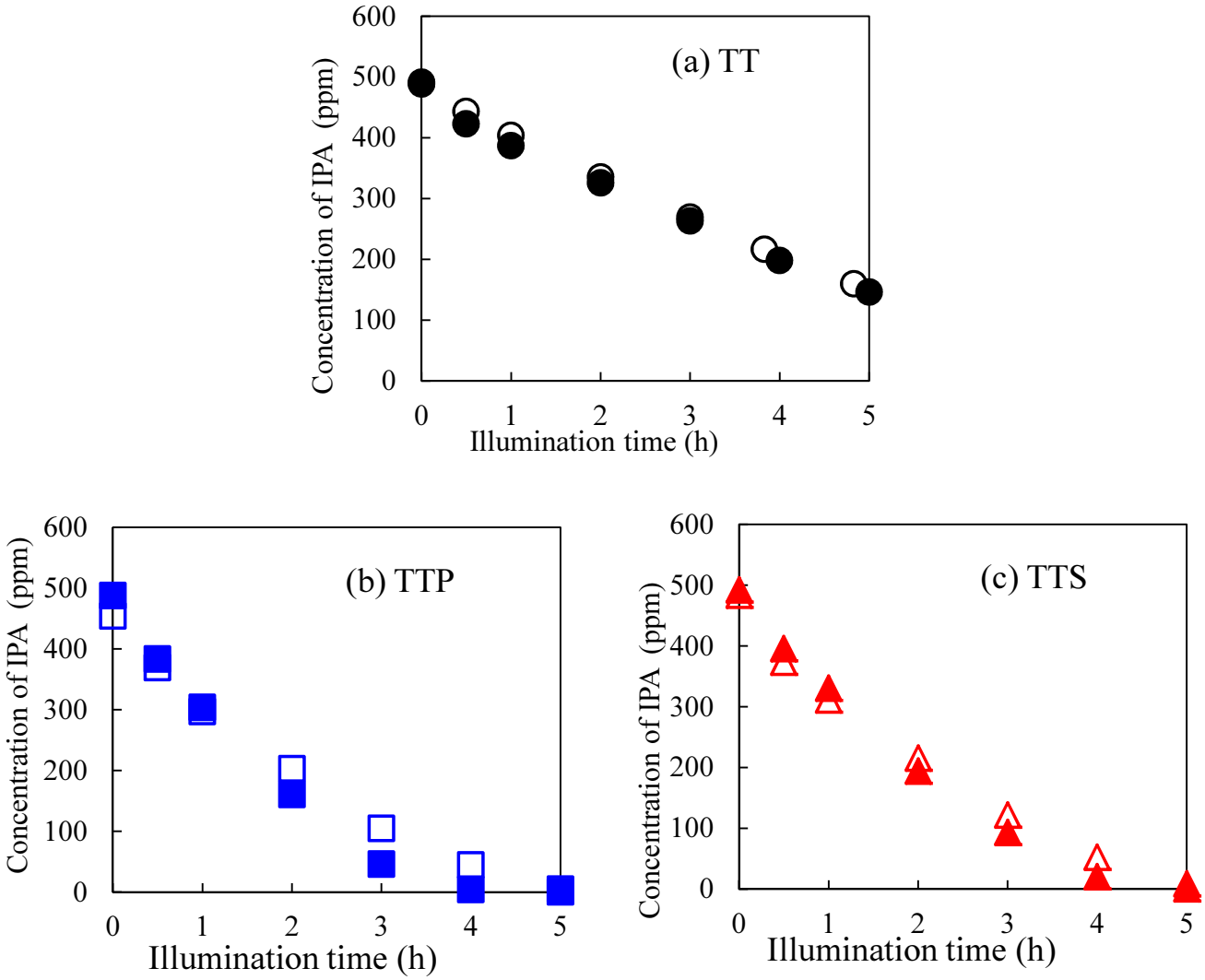

Figure 4-14 Concentration changes of IPA with (●, ▲, ■) and without visible light (○, △, □) using a UVD33S filter: (a) TT, (b) TTP, and (c) TTS films.

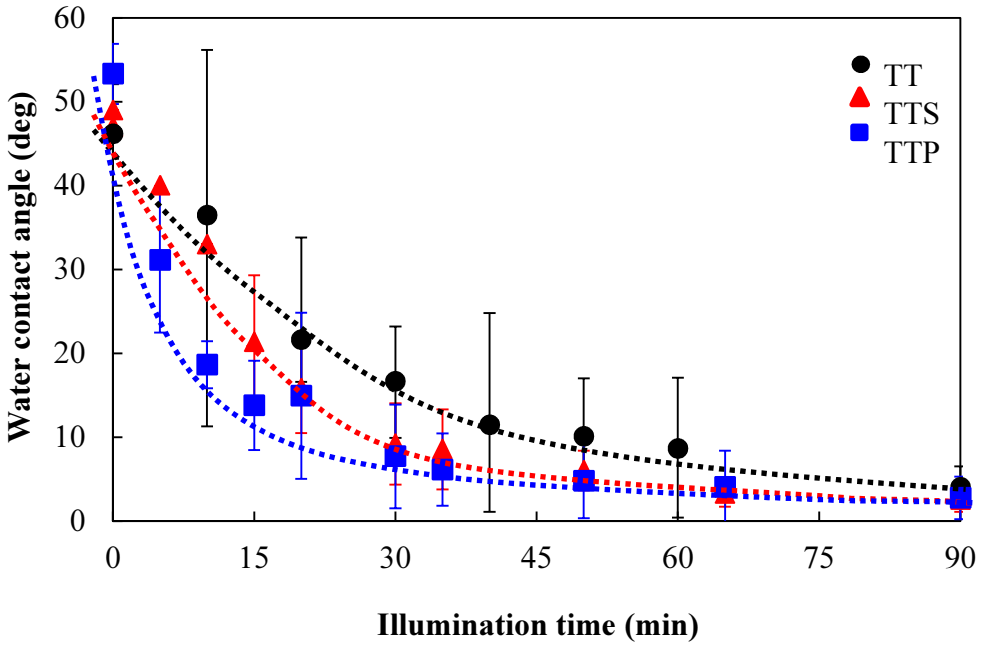

Figure 4-15 Water contact angle change on the TTP (■), TTS (▲), and TT (●) films under UV illumination (30 μW/cm^2)

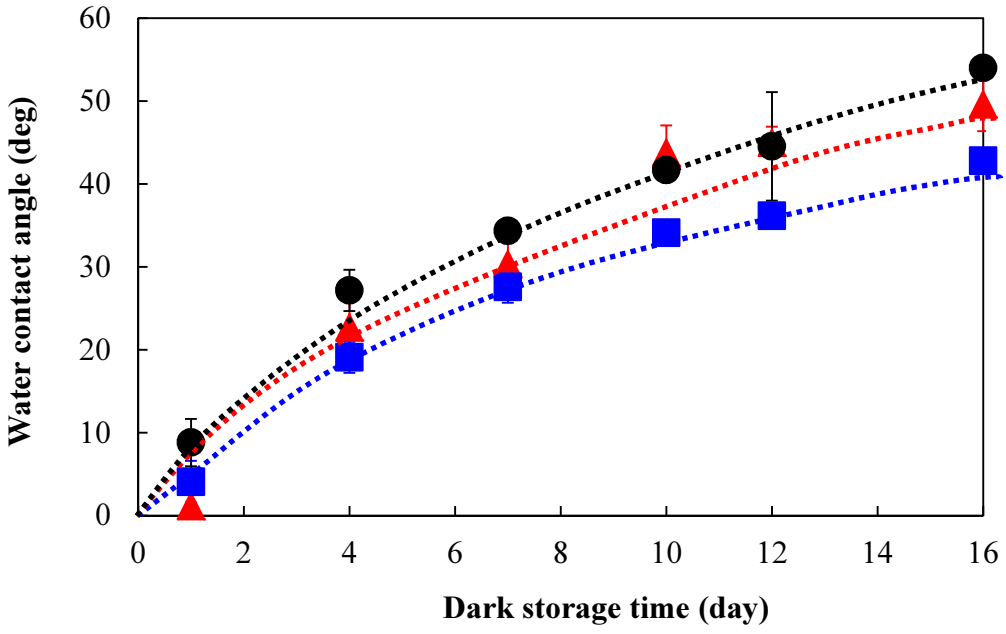

Figure 4-16 Water contact angle change on the TTP (■), TTS (▲) and TT (●) films films during dark storage after UV illumination.

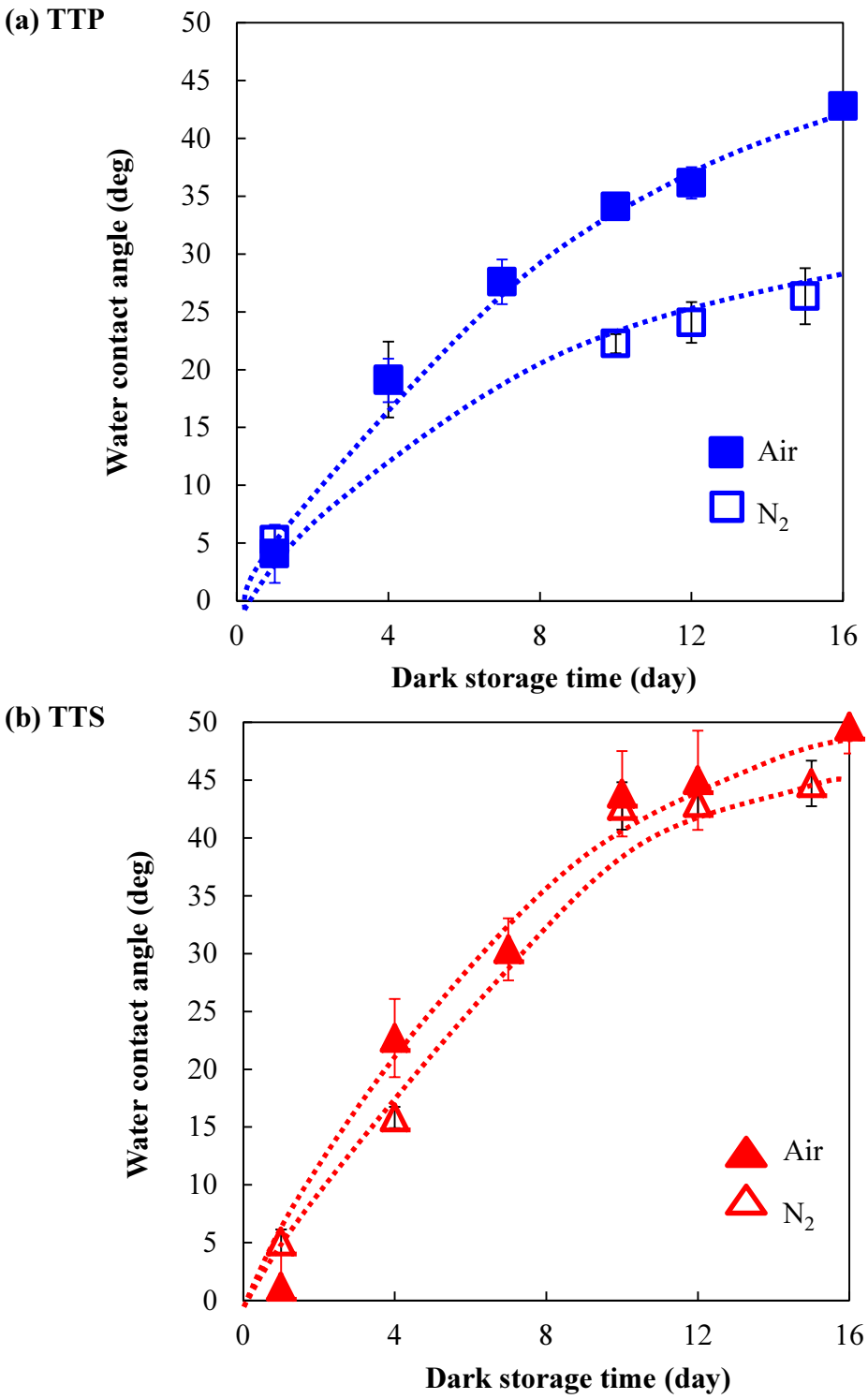

Figure 4-17 Water contact angle change on the TTP (■, □), and TTS (▲, △) films during dark storage after UV illumination in synthesized air (solid mark) and N_2 (non-filled mark).

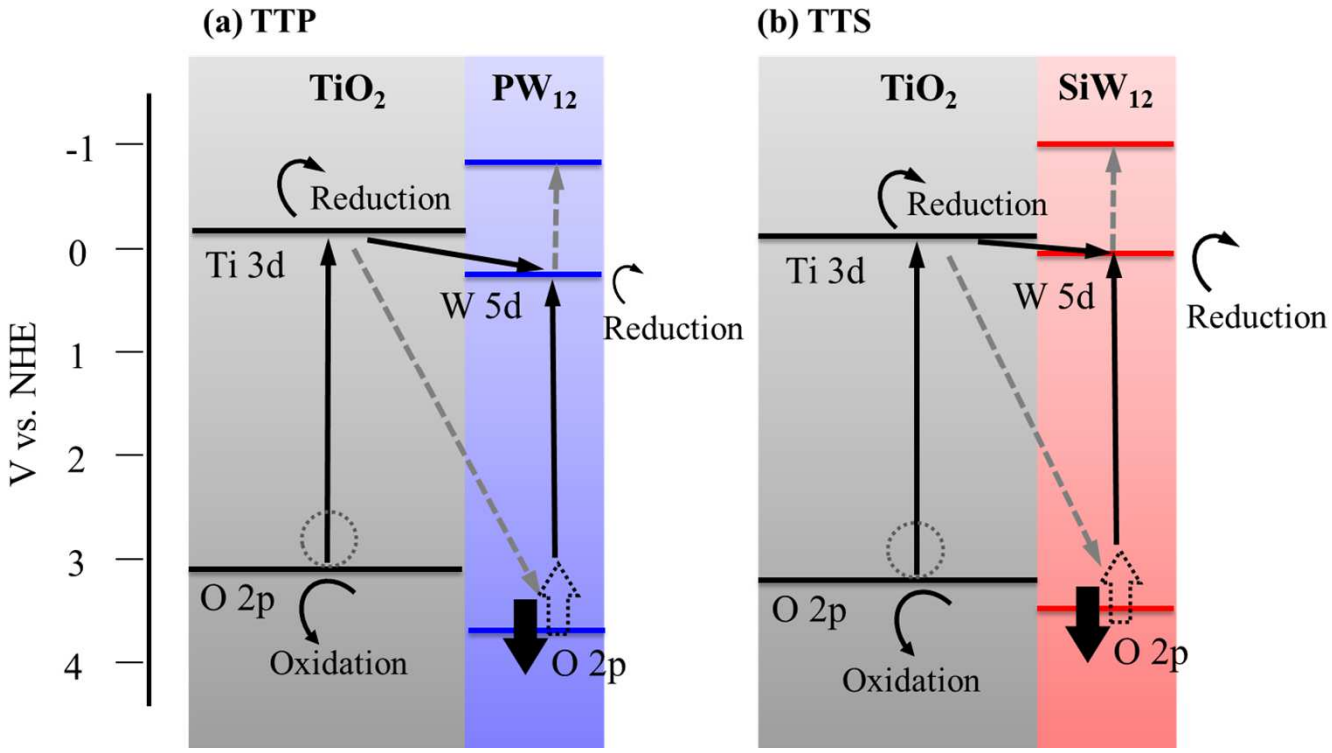

Figure 4-18 Expected electron transfer schemes of the hybrid film of the (a) PW_{12} /brookite and (b) SiW_{12}/brookite systems (pH=0).

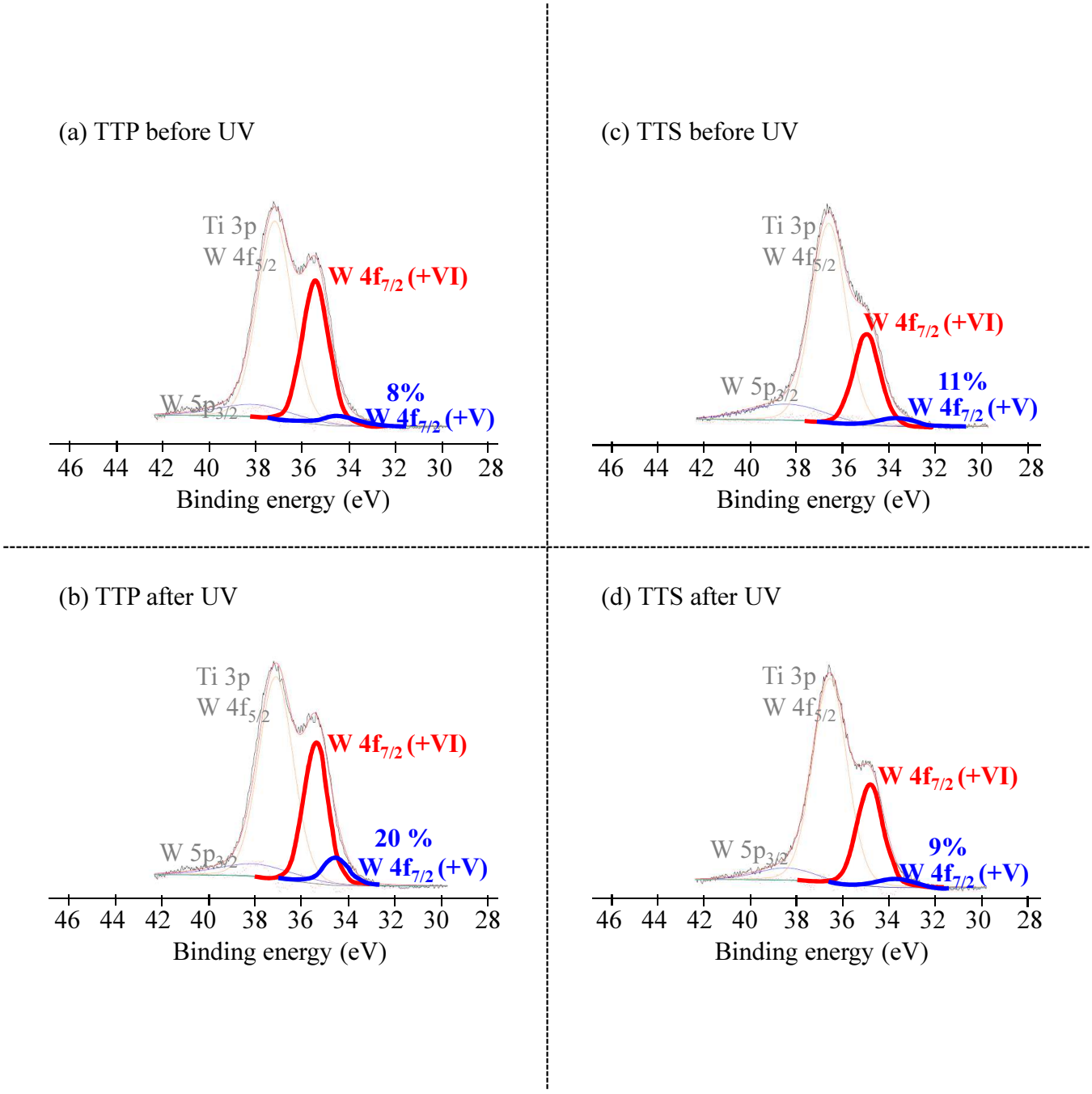

Figure 4-19 W4f spectra of TTP and TTS film by XPS before (a, b) and after (c, d) UV illumination.

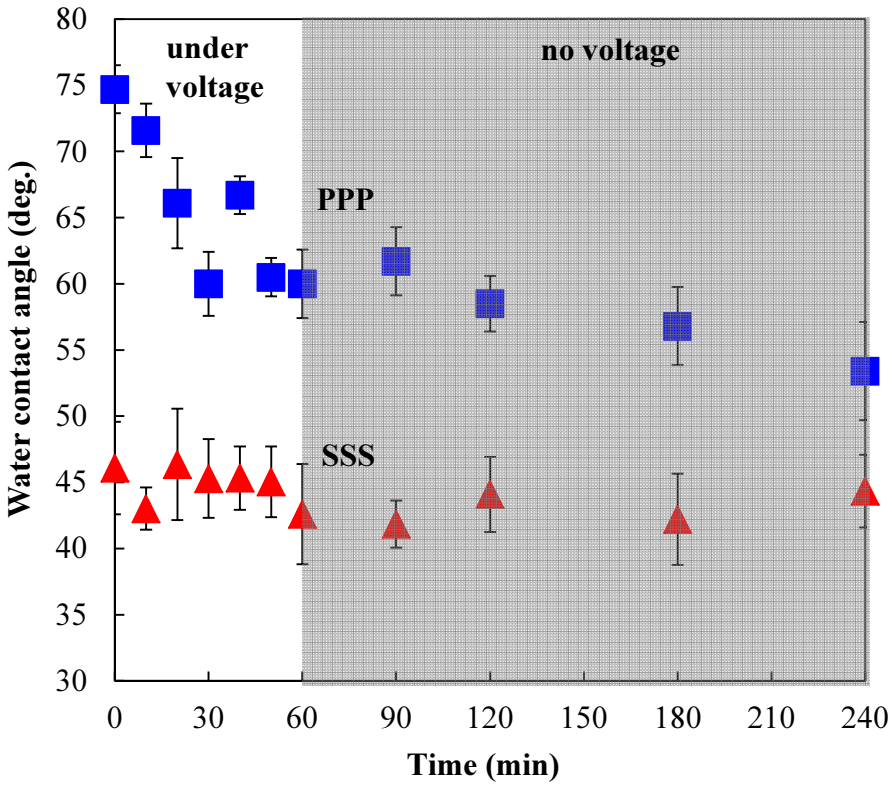

Figure 4-20 Water contact angle change on the PPP (■) and SSS (▲) films with and without applied voltage (50 mV).

CHAPTER 5

Summary

5.1. Result and conclusion

A hybrid system of PW_{12}-TiO_2 was extensively examined for applications of photocatalytic decomposition and wettability conversion. TiO_2 and PW_{12} were combined by Coulombic attraction via LBL process. Their solid–gas photoreactions were investigated. The results revealed that electron transfer from conduction band of TiO_2 to LUMO of PW_{12} is an important process for improving photocatalytic decomposition activity and this is also a key factor for the wettability of this hybrid material. The outline for these works is presented as the following.

Chapter 1

Fundamental knowledge for Titanium dioxide (TiO_2) and heteropolyacids (HPAs) are reported in this chapter. Moreover, the review of the TiO_2/HPAs hybrid material is also reported. Despite TiO_2 is the most effective photocatalytic material because of its high oxidation power which can decompose almost all organic compounds. Charge recombination and its low Fermi level for O_2 reduction remain as limitations for TiO_2. Among their three phases of anatase, rutile, and brookite, brookite recently showed better photocatalytic acityity and photoinduced hydrophilicity than anatase and rutile. Z-scheme electron transfer from TiO_2 to HPAs was designed to improve charge separation in TiO_2. There are primary and secondary excitations for HPAs which are UV excitation and visible light excitation, respectively. Because the HOMO–LUMO levels of HPAs

are slightly more positive than the CB of TiO_2, the generated electrons spontaneously move to HPAs result in suppressing electron–hole recombination in TiO_2. Initially, colloidal TiO_2 and HPAs solution were combined. The photocatalytic activity is improved but two limitations remain: (i) the separation of HPAs from the reaction vessel is difficult and (ii) the complete mineralization of aromatic compounds was suppressed because homogeneous HPAs enhance the formation of peroxide compound rather than that of free $O_2^{\bullet-}$. Therefore, the immobilized HPA on TiO_2 were finally designed. Recently, Yanagida prepared transparent hybrid HPA-TiO_2 thin film using layer by layer process. The photocatalytic activity of the hybrid films $((XW_{12}O_{40})^{n-}/TiO_2)$; where X is P, Si and H_2, n = 3, 4 and 6 respectively, was studied via gaseous 2-propanol (IPA) decomposition. As one might expect, $(PW_{12}O_{40})^{3-}$ requires visible light for improving the photocatalytic activity of $(PW_{12}O_{40})^{3-}/TiO_2$. Therefore, the objective of this work is to investigate photocatalytic property and wettability HPA/TiO_2 using TiO_2 (brookite). The study specifically examines $PW_{12}O_{40})^{3-}/TiO_2$.

Chapter 2

In this chapter, transparent hybrid films of brookite (TiO_2) and 12 tungsto(VI) phosphoric acid (PW_{12}: $([PW_{12}O_{40}]^{3-}$) were prepared via layer-by-layer (LBL) processes on a quartz substrate with various orders. The obtained films were transparent in the visible wavelength range. Their photocatalytic activities were evaluated using gaseous 2-propanol (IPA) decomposition. Pure brookite film showed higher photocatalytic activity than the pure PW_{12} one; the combination of PW_{12} to brookite increased the photocatalytic activity. The electron scavenger effect of PW_{12} against brookite under UV illumination is important for photocatalytic activity improvement.

The light source for this experiment is Hg-Xe lamp which mainly contains UV light and some visible light. When visible light excitation for PW_{12} was cut, the decomposition rate was not significantly different from the decomposition rate under all light illumination. This result indicates that O_2 reduction could occur at LUMO level of PW_{12}. Additionally, the degree of improvement depends on the film stacking order. Their photocatalytic activity was the highest when PW_{12} was arranged on the film's topmost surface.

Chapter 3

In this chapter, a comparative study of photocatalytic decomposition activity and photoinduced hydrophilicity for the films was conducted using gaseous 2-propanol (IPA) decomposition and sessile drop method. The TTP ($TiO_2/TiO_2/PW_{12}$) film exhibited better photocatalytic activity on the decomposition of gaseous IPA than that of the TT (TiO_2/TiO_2) film. Moreover, the TTP film provided a higher hydrophilization rate under UV illumination, and provided better sustainability of the hydrophilicity in the dark than the TT film did. The sustainability was also atmospheric dependence. The hydrophobicizing rate on TTP was extremely slow when lacking of oxygen atom on the atmosphere. The generation of PW_{12}^- by electron transfer from TiO_2 to PW_{12} was inferred as a key factor underpinning the overall performance of wettability conversion before and after UV illumination on this hybrid film.

Chapter 4

Two tungsten-based Keggin-type heteropolyacids (PW_{12}: ($[PW_{12}O_{40}]^{3-}$) and SiW_{12}: ($[SiW_{12}O_{40}]^{4-}$)) were hybridized with brookite-type TiO_2. Then photocatalytic

decomposition activity, photoinduced hydrophilicity, and sustainability of the hydrophilicity in the dark were evaluated using gaseous 2-propanol (IPA) decomposition and sessile drop method. Both hybrid films exhibited higher photocatalytic decomposition activity and had higher photoinduced hydrophilicizing rates than pure brookite films under UV illumination. The PW_{12}/TiO_2 film exhibited better photocatalytic performance than the SiW_{12}/TiO_2 film did. Atmosphere dependence, XPS analysis, and electrochemical experiments indicated the cause of these two films' different levels of sustainability of hydrophilicity to be differences in their electron storage capability. Results show that the electron scavenger capability and reoxidation efficiency of the heteropolyacid are key factors affecting the overall performance of wettability conversion of this hybrid film system before and after UV illumination.

5.2. Key success of TiO_2/PW_{12} hybrid material

Photocatalyst

The IPA degradation rate of the PW_{12}/TiO_2 hybrid film was considerably higher than that of either TiO_2 or PW_{12} film. Charge separation occurs because PW_{12} acts as an electron pool. Oxidation by hole is the primary process for organic decomposition **[1, 2]**. Apparently, one electron reoxidation of $(PW_{12}O_{40})^{4-}$ by O_2 is difficult. Furthermore, secondary excitation is necessary for promotion of $(PW_{12}O_{40})^{4-}$ to $(PW_{12}O_{40})^{4-*}$, which has higher reduction potential for its reoxidation **[3, 4]**. However, in this current case, TiO_2 acts as an electron supplier for LUMO of PW_{12}. Therefore, multi-electron reductions are feasible at the LUMO band. From future investigations, the reoxidation of PW_{12} is extremely influential on the reaction rate. The reaction field of oxidation and

reduction was also optimized. Their photocatalytic activity was highest when PW_{12} was arranged on the film's topmost surface. Although it is a smaller material amount, the IPA decomposition rate of the PW_{12} top most is equivalent to that of alternative PW_{12}/TiO_2 layered film.

Surface wettability conversion

Water contact angle (WCA) conversion on PW_{12}/TiO_2 film under low-intensity UV illumination was enhanced by the charge separation effect. It is particularly interesting that during dark storage, the sustainability of hydrophilicity on PW_{12}/TiO_2 film was longer than that on the TiO_2 film. In HPAs, because of impurities and lattice defects caused by heteroatom and counter cation, trap states are provided during the O → M LMCT energy gap. Trapped electrons can be released by thermal stimulation (heat) and optical stimulation (photon). Under dark conditions, if the trap depth (ΔE) is greater than kT, then electrons released by thermal stimulation are negligible. In this case, trapped electrons are in metastable stage **[5]**. Water is dipolar. Therefore, it can be affected by an electric field **[6]**. Future investigations must examine electrons collected by heat-treated PW_{12} to assess their effects on the surface potential of the film, causing the longer hydrophilic stage.

Although PW_{12}/TiO_2 electron storage photocatalyst has been reported **[7, 8]**, the present report is the first report describing PW_{12} effects on wettability on TiO_2. It enhances the photoinduced hydrophilic conversion rate because of charge separation. It also lowers the hydrophobicizing rate under dark storage. As described in chapter 3, the rate of hydrophilicization under UV illumination and sustained hydrophilicity in the dark are improved by hybridization of SiO_2 with TiO_2. However, the TiO_2–SiO_2

combination decreases the surface area ratio (commonly 30–40%) of TiO_2 for photocatalytic decomposition while PW_{12}/TiO_2 improved both the photocatalytic activity and wettability of TiO_2. Additionally, this hydrophilic sustainability is quite limited for only PW_{12}/TiO_2 hybrid film. When the LUMO level of HPA was shifted slightly by changing heteroatom of HPA (from PW_{12} to SiW_{12}), this property could not be observed. The P and Si atoms have different electronegativity resulting in their different behavior on electron acceptors and donors.

Electric effects on water tension have been reported **[9]**. However, PW_{12}/TiO_2 can generate electron–hole pair by itself under UV illumination. In addition, under dark condition, a certain period (1–2 days) is necessary for the increase of WCA to 10° and several days (at least 7 days depending on temperature and relative humidity) are necessary for recovery of the PW_{12}/TiO_2 film surface characteristics. In other words, no other electronic circuit is necessary for this system. Therefore, PW_{12}/TiO_2 is flexible for use in many applications.

The PW_{12}/TiO_2 film has additional benefits. First, it is transparent in the visible wavelength range. Second, because it is prepared using the LBL process, it is a potentially useful material for coating on a complexly shaped substrates and altered substrates. Third, because of the hydrophilic sustainability results from the collected electron in PW_{12}, various means exist to control the sustainability period via controlling amount of collected electron by PW_{12} or reoxidation rate of PW_{12}. The collected electron amount might be controlled by PW_{12} concentration, UV intensity, and illumination time. Especially, the oxygen content in the atmosphere strongly affects the PW_{12} reoxidation rate. Additionally, temperature can affect the reoxidation rate.

References

[1] Y. Tamaki, A. Furube, M. Murai, K. Hara, R. Katoh, M. Tachiya, *Phys. Chem. Chem. Phys*., , 9, 1453–1460 (2007)

[2] Y. Tamaki, A. Furube, M. Murai, K. Hara, R. Katoh, M. Tachiya, *J. Am. Chem. Soc*., 128 (2), 416–4177 (2006)

[3] S. Yanagida, A. Nakajima, T. Sasaki, Y. Kameshima, K. Okada, *Chem. Mater*., 20, 3757-3764 (2008).

[4] S. Yanagida, A. Nakajima, T. Sasaki, T. Isobe, Y. Kameshima, K. Okada., *Appl. Catal. A: Gen.*, 366, 148-153 (2009).

[5] T. Yamase, *Chem. Rev*., 98, 307-325 (1998)

[6] S.T. Bramwell, *Nature*, 397, 212-213 (1999)

[7] P. Ngaotrakanwiwat, S. Saitoh, Y. Ohko, T. Tatsuma, A. Fujishima, *J. Electrochem. Soc*., 150 (11), A1405-A1407 (2003).

[8] P. Ngaotrakanwiwat, T. Tatsuma, *J. Electroanal. Chem*., 573, 263–269 (2004).

[9] A. Bateni, S. S. Susnar, A. Amirfazli, A. W. Neumann, *Langmuir*, 20, 7589-7597 (2004)

List of Publications

(1) "Photocatalytic Activity and Its Stacking Order Dependence of Transparent 12 Tungsto(VI) Phosphoric Acid-Brookite Hybrid Films"

K. Pruethiarenun, T. Isobe, S. Matsushita, A. Nakajima,

Appl. Catal. A Gen., 399[1–2], 22-27 (2011).

(Related to CHAPTER 2)

(2) "Photocatalytic Activity and Photoinduced Hydrophilicity of Brookite-Heteropolyacid Hybrid Films"

K. Pruethiarenun, T. Isobe, S. Matsushita, A. Nakajima,

Appl. Catal. A Gen., 445–446, 274–279 (2012).

(Related to CHAPTER 3)

(3) "Comparative study of photoinduced wettability conversion between $[PW_{12}O_{40}]^{3-}$ /brookite and $[SiW_{12}O_{40}]^{4-}$ /brookite hybrid films"

K. Pruethiarenun, T. Isobe, S. Matsushita, J. Ye, A. Nakajima,

Mater. Chem. Phys., 144, 3, 327-334 (2014)

(Relate to CHAPTER 4)

(4) “Recent studies of Heteropolyacid(HPA)/TiO2 Hybrid Photocatalysts”

K. Pruethiarenun, A. Nakajima,

J. Jpn. Soc. Colour Mater., 87, 7, 227-234 (2014)

(Relate to CHAPTER 1)

Acknowledgements

This thesis would not have been possible without the many kindnesses received from the following people. First, I am grateful to Prof. Etsuo Sakai, Prof. Akira Nakajima, Assoc. Prof. Masahiro Miyauchi, Assoc. Prof. Toshiyuki Ikoma and Assoc. Prof. Sachiko Matsushita for their careful reviewing of this thesis. I am heartily very grateful to my supervisor and teacher, Prof. Akira Nakajima, whose thoughtful encouragement, precise guidance and support from the initial to the final level enabled me to complete this study. I also would like to show my grateful to Assoc. Prof. Sachiko Matsushita and Assistant Prof. Toshihiro Isobe for their fruitful discussion, support, suggestion and encouragement. I am also grateful to Assistant Prof. Sayaka Yanagida, an important person for my research. Because of her previous systematical and effective studies, my research could be progress fast. I would like to give a special thanks to Assoc. Prof. Masahiro Miyauchi for his discussion and help in various ways and I also thanks to Assistant Prof. Ken-ichi Katsumata. I would also express my acknowledgement to Prof. Jinhua Ye in Environmental Remediation Materials Unit, Environment and Energy Materials Division, National Institute for Materials Science (NIMS) and the members for their warm welcome and helps during my internship. I am grateful to Ms. Mariko Kurihara who supported office work. Last but not least, I would like to express my deep thanks for many corporation and encouragement from all colleagues of the Nakajima-Matsushita-Laboratory especially, Mr. T. Furuta, Mr. T. Koike, Ms. A. Ooyama, Ms. M. Shimitsu, Ms. M. Nakanome, Mr. S. Uchiyama, Mr. K. Okudaira., Mr. L. Lui, Ms. K. Yasui, Mr. N. Yamamoto, Mr. T. Miyamoto, Mr. T. Kobayashi, Mr. S. Sato, Mr. T. Nogawa, Mr. Y. Tsuruki. and Mr. T. Tatsuno.

It is an honor to show my gratitude on Japanese Government and Tokyo Institute of Technology for providing me a scholarship under the Japanese Government (Monbukagakusho) Scholarship program.

During research conducted at Tokyo Institute of Technology: I would like to express my special thanks for much helps, humor, happiness and friendship from senior, friends, and juniors in the laboratory and also from Thai students in Tokyo Institute of Technology especially “the little cow gang”. I also would like to show my appreciative to Student support division and International student support division in Tokyo Institute of Technology.

It is a pleasure to show my grateful to my previous teachers, for their inspiration; Assistant Prof. Pornnapa Sujaridworakun and Assoc. Prof. Sirithan Jiemsirilers of Chulalongkorn University. I devote to my parent, aunts, sisters and brothers for their endless love, listening-advising and cheering. They never leave me feel alone. With their strong support and motivation, I am being today.

Lastly, I offer my regards and blessings to all of those who supported me in any respect during the completion of the project.

Kunchaya Pruethiarenun
June, 2014